

Structural and Functional Characterization of Human Coagulation Factor XIII

Dissertation

Sneha Singh

Structural and Functional Characterization of Human Coagulation Factor XIII

D I S S E R T A T I O N

zur
Erlangung des Doktorgrades (Dr. rer. nat.)
der
Mathematisch-Naturwissenschaftlichen Fakultät
der
Rheinischen Friedrich-Wilhelms-Universität Bonn

vorgelegt von

Sneha Singh

Aus

Neu Delhi, Indien

Bonn, 2019

**Aus dem Institut für experimentelle Hämatologie
und Transfusionsmedizin der Rheinischen
Friedrich-Wilhelms Universität Bonn**

Angefertigt mit Genehmigung der Mathematisch-Naturwissenschaftlichen
Fakultät der Rheinischen Friedrich-Wilhelms

Universität Bonn

1. Gutachter: Prof. Dr. med. Johannes Oldenburg

2. Gutachter: Prof. Dr. Diana Imhof

Tag der mündlichen Prüfung: 27.02.2020

Erscheinungsjahr: 2020

Betreffend die vorgelegte Dissertation:

Structural and Functional Characterization of Human Coagulation Factor XIII

hiermit versichere ich an Eides Statt:

dass die Dissertation von mir selbständig und ohne unzulässige fremde Hilfe angefertigt und verfasst wurde und andere Hilfsmittel als die in der Dissertation angegeben nicht benutzt habe; insbesondere, dass wörtlich und sinngemäß aus Veröffentlichungen entnommene Stellen als solche kenntlich gemacht worden sind.

Desweiteren Versichere ich, dass ich mich bis zu diesem Tag noch keiner Doktorprüfung unterzogen habe bzw. hat die von mir vorgelegte Dissertation noch keiner anderen Fakultät vorgelegen.

Zudem versichere ich, dass weder ein Dienststraf- noch ein Ehrengerichtsverfahren gegen mich vorliegt.

Bonn, Juli 2019

Sneha Singh

And once the storm is over, you won't remember how you made it through, how you managed to survive. You won't even be sure, whether the storm is really over. But one thing is certain. When you come out of the storm, you won't be the same person who walked in. That's what this storm is all about.

Haruki Murakami

Dedicated to my family... "The Guptas & The Singhs"

Abstract

The formation of a fibrin clot in blood plasma is a two-step event which involves formation of a “primary clot” comprising of fibrin polymers formed by fibrin monomers under the action of thrombin and subsequently the development of this primary clot into a stronger, insoluble, network structure that plugs the wound and thus prevents bleeding. The second step of this process is mediated by coagulation Factor XIII (FXIII), a pro-transglutaminase circulating in the plasma that covalently crosslinks the aforementioned “primary clot” (within itself and to fibrinolytic inhibitors) thereby preventing premature fibrinolysis of the “primary clot” under the action of fibrinolytic enzymes leading to fatal bleeding eventualities. FXIII, circulates in plasma in the form of non-covalently associated hetero-tetrameric FXIII-A₂B₂ complex comprising of the catalytic dimeric subunits A (FXIII-A₂) combined with the protective/regulatory dimeric subunit B (FXIII-B₂). The catalytic FXIII-A₂ subunit belongs to a class of enzyme called Transglutaminase (TG; protein-glutamine:amine γ -glutamyltransferase, EC 2.3.2.13), and is responsible for the formation of $\epsilon(\gamma\text{-glutamyl})\text{lysyl}$ crosslinks between the two polypeptide chains. The FXIII-B₂ subunit is a protective partner towards the FXIII-A₂ subunit dimer in the heterotetramer but more recently regulatory roles for this subunit have also come to light. The zymogenic FXIII-A₂B₂ complex is activated in the plasma by combination of proteolytic cleavage (thrombin) of an N-terminal region of the FXIII-A₂ subunit called the activation peptide followed by binding of Calcium ions to three Calcium binding sites on the FXIII-A₂ subunit that result in conformational changes resulting into dissociation of FXIII-B₂ subunit from complex, and opening of the FXIII-A molecule to an open activated FXIII-A form (FXIII-Aa). The current thesis picks up from aspects of this hetero-tetrameric complex that are not known i.e. about the individual subunits or the complete complex itself. Then it proceeds in a stepwise manner unravelling these aspects using lab investigations driven by hypotheses generated *in silico*. Naturally, therefore the start of thesis involves primarily *in silico* chemo-informatics work that delves into activation path of the FXIII-A₂ subunit and the major structural (like the N-terminal activation peptide of the FXIII-A₂ subunit) and physiological partners contributing to it (i.e. cationic ligand like Calcium, and partner FXIII-B₂). This work revealed some major insights into these aspects which were a) the importance of the activation peptide in the dimeric stability of

the FXIII-A₂ subunit b) the importance of cross-talk within the Ca binding sites of FXIII-A₂ subunit for its activation c) the regulatory role of the FXIII-B₂ in accelerating the activation of the FXIII-A₂ subunit d) plausible after-events in life cycle of FXIII-A₂ subunit post-activation and finally e) the dynamics of assembly and dissociation of the heterotetrameric FXIII-A₂B₂ complex . However, since most of these insights were at a hypothetical level, the next step was to verify them on the bench. While some of the insights from these early investigations were substantiated by bench work done by other groups (like the importance of activation peptide), most of the other investigations and their follow-ups form the core of this thesis. Therefore subsequent to this early investigation, this thesis delves into a) characterizing the role of Calcium binding sites on activation of FXIII-A₂ subunit b) characterizing the structure-functional aspects of the FXIII-B₂ subunit by adopting a combined disulfide-bond mutating approach c) running preliminary investigations into possibilities of pleiotropic roles for the FXIII-B₂ and finally d) the thesis concludes by presenting a structural all-atom model of the FXIII-A₂B₂ complex combined with a look into thermodynamic patterns emerging from the assembly and dissociation of this complex, describing how the complex interface could be an underlying driver of this rare-bleeding deficiency (FXIII deficiency).

The characterization of the three major Calcium binding sites in the FXIII-A₂ subunit involved a series of *in silico* exercises probing the relative conservation, cross-talk and interaction with other ions in the physiological system which is combined with mutating the binding sites themselves to corroborate the effect they would have on the activation of this subunit. With this work this thesis drives home the point that a) there is an antagonistic equilibrium between the first and the second-third Calcium binding sites at play that regulates the speed and rate of FXIII-A₂ activation b) the thermodynamics underlying FXIII-A₂ activation upon Calcium binding favors the formation of a monomeric and not dimeric activated FXIII-A (FXIII-Aa) species and c) the presence of ions regardless of whether they actually co-ordinate with the FXIII-A₂ subunit or not can influence the activation status of FXIII-A₂ subunit by altering its surface electrostatic properties. Moving onto the structural functional aspects of the FXIII-B₂ subunit, this thesis provides insights into how the disruption of structural disulfide bonds lead to functional implications for the development of FXIII deficiency. This study involves a combination of in-silico modelling based approaches, accompanied by the in-vitro characterization of FXIII-B subunits bearing ablated disulfides, that are a consistent feature of

the FXIII-B₂ subunit. By investigating the functional aspects of these disulfide mutated variants combined with the structural perspective, this thesis was able to define structure-functional correlations for this subunit in a manner not touched upon so far. This thesis also investigated the possibility of the FXIII-B₂ subunit having pleiotropic roles in the complement system (because of its high homology to some proteins from the complement system) by using a host of mixing as well as pull-down assays. However, the thesis clearly determined that physiologically the FXIII-B₂ has no role in the complement system. Finally, the thesis takes a detailed structural and functional look at the FXIII-A₂B₂ complex itself. Here, the Mass spectrometry based chemical cross-linking data from FXIII-A₂B₂ complex (isolated from the plasma FXIII concentrate FibrogamminP) is used, along with high resolution atomic force microscopy, in order to model the first all-atom model of this complex. Therefore, this thesis for the first time provides a structural perspective of entire complex. In addition, an intensive investigation into the association and dissociation of this complex was conducted on an Isothermal titration calorimetry(ITC) platform that yielded a) the first K_d (dissociation constants) values for the FXIII-A₂ and FXIII-B₂ subunit established in a non-labelled setting, *in solution* b) the cooperative mode of association followed by these two subunits. Therefore, to sum up, this cumulative thesis begins by asking fundamental questions about the complex and its subunits and ends by presenting major insights into the structural and functional aspects of both the complex and its subunits.

To conclude, this thesis presents a) Structure-functional basis of FXIII complex activation, and roles of its individual subunits; b) A combinatorial approach for dissection of structure-function aspects of complex derived from plasma, here Factor XIII; c) Potential druggable sites for the generation of new anti-coagulants targeting either FXIII-A calcium binding sites, FXIII-B sushi domains, and most importantly FXIII complex interfaces, which may lead to development of new FXIII inhibitors, or more regulated forms of FXIII, which is a major contributor towards maintaining balance between thrombosis and bleeding.

TABLE OF CONTENTS

| | |
|--|-----------|
| ABSTRACT | I |
| TABLE OF CONTENTS..... | IV |
| 1 CHAPTER 1: INTRODUCTION | 1 |
| 1.1 BLOOD COAGULATION CASCADE..... | 1 |
| 1.2 FIBRINOGEN, THE FIBRIN CLOT FORMATION AND STABILIZATION..... | 2 |
| 1.3 COAGULATION FACTOR XIII: DISCOVERY AND EARLY CLINICAL FINDINGS | 3 |
| 1.3.1 COAGULATION FACTOR XIII GENE | 4 |
| 1.3.2 COAGULATION FACTOR XIII SOURCE | 3 |
| 1.3.3 COAGULATION FACTOR XIII PROTEIN STRUCTURE..... | 3 |
| 1.3.4 ACTIVATION, MECHANISM OF ACTION AND REGULATION OF FXIII ACTIVITY | 7 |
| 1.3.5 FXIII A PROTEIN WITH MULTIPLE SUBSTRATES AND PLEIOTROPIC FUNCTIONS..... | 9 |
| 1.3.6 FXIII DEFICIENCY | 9 |
| 1.3.7 INHIBITORS FOR FXIII..... | 12 |
| 1.4 PRINCIPLES UNDERLYING METHODS/STRATEGIES USED IN THIS THESIS..... | 12 |
| 1.4.1 IN-SILICO METHODS | 12 |
| 1.4.2 BENCH METHODS | 16 |
| AIM AND OUTLINE | 21 |
| BIBLIOGRAPHY | 22 |
| ACKNOWLEDGEMENT | 29 |
| <i>FOLLOWING CHAPTERS INCLUDE A BRIEF SYNOPSIS FOLLOWED BY PUBLISHED ARTICLES</i> | |
| 2 CHAPTER 2: (SYNOPSIS) | |
| REVISITING THE MECHANISM OF COAGULATION FACTOR XIII ACTIVATION AND REGULATION FROM A STRUCTURE/FUNCTIONAL PERSPECTIVE..... | 31 |
| <i>ARTICLE</i> | 32 |
| 3 CHAPTER 3: (SYNOPSIS) | |
| STRUCTURE-FUNCTIONAL INSIGHTS INTO CALCIUM INDUCED ACTIVATION OF FACTOR XIII-A MOLECULE..... | 48 |
| <i>ARTICLE</i> | 49 |
| 4 CHAPTER 4: (SYNOPSIS) | |
| 4A: IDENTIFICATION OF POTENTIAL NOVEL INTERACTING PARTNERS FOR COAGULATION FACTOR XIII B SUBUNIT, A PROTEIN ASSOCIATED WITH A RARE BLEEDING DISORDER..... | 67 |
| 4B: EXPLORING THE STRUCTURAL SIMILARITY YET FUNCTIONAL DISTINCTION BETWEEN COAGULATION FACTOR XIII-B AND COMPLEMENT FACTOR H SUSHI DOMAINS. | 67 |
| <i>ARTICLE</i> | 68 |
| 5 CHAPTER 5: (SYNOPSIS) | |
| DISRUPTION OF STRUCTURAL DISULFIDES OF COAGULATION FXIII-B SUBUNIT; FUNCTIONAL IMPLICATIONS FOR A RARE BLEEDING DISORDER. | 88 |
| <i>ARTICLE</i> | 89 |
| 6 CHAPTER 6: (SYNOPSIS) | |
| THE PLASMA FACTOR XIII HETEROTETRAMERIC COMPLEX STRUCTURE: UNEXPECTED UNEQUAL PAIRING WITHIN A SYMMETRIC COMPLEX | 106 |
| <i>ARTICLE</i> | 107 |

Chapter 1: Introduction

1.1 The Blood Coagulation Cascade

Blood coagulation system is a molecular machinery involving roles of several negatively charged glycoproteins (coagulation factors) that undergo maturation, and upon activation induce generation of downstream enzymes ultimately forming fibrin clot which plugs the wound and stops bleeding. Under physiologically normal circumstances, hemodynamics is favored, and system is balanced in favor of anticoagulation. However, under hemodynamic stress which involves bleeding (blood loss, if not controlled may lead to hypovolemic shock), coagulation pathway is activated which works in favor of fibrin clot formation and its stability, in order to arrest bleeding (hemostasis). This process of formation of insoluble strong fibrin clot to arrest bleeding is termed as blood coagulation, and the pathway it follows is termed as the coagulation cascade. Hence regulation of dynamic blood flow in a vertebrate depends on the fine balance between bleeding and thrombosis (or hemodynamics and hemostasis) (Figure 1). This balance is

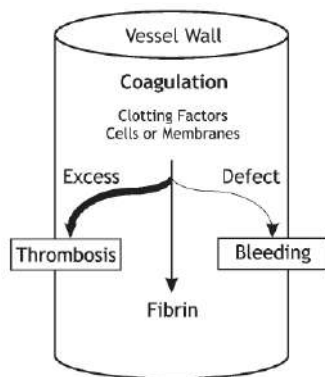
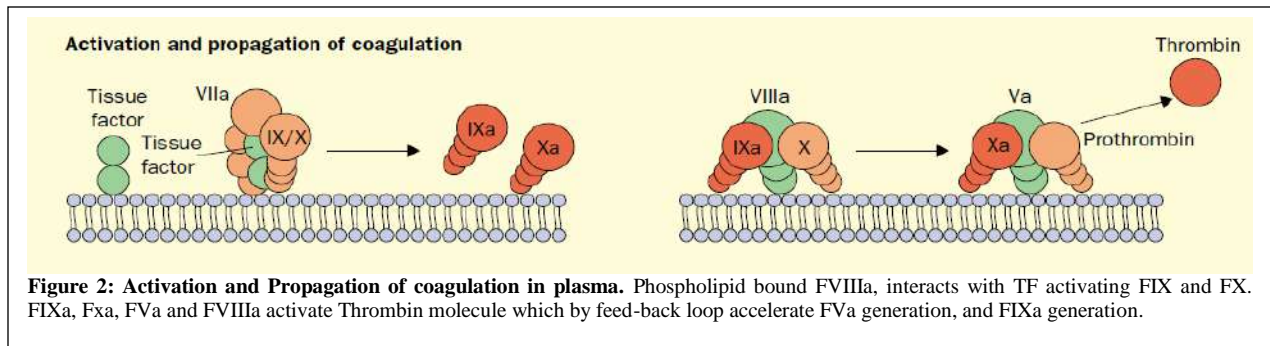


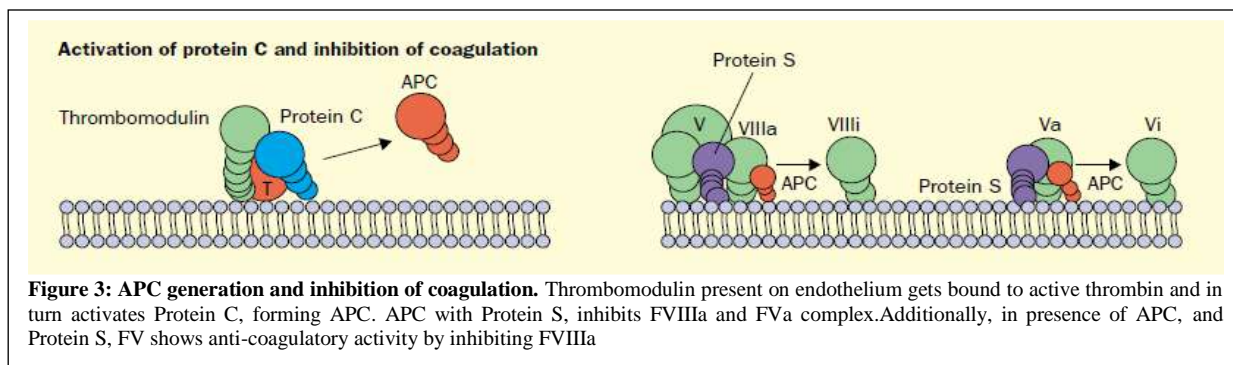
Figure 1: Schematic representation of Dynamic blood flow.

governed by the intricate regulation of coagulation factors which upon activation enables fibrin clot formation.¹ Any defect/deficiency in these coagulation factors may lead to reduced clot formation, i.e. bleeding predisposition. Similarly, over activation or lack or regulation of these factors may lead to unwanted clots, i.e. Thrombosis. Coagulation pathway involves the quorum assembly of substrates, which in turn are also active enzymes, and protein factors, along with Calcium ions on phospholipid membrane which further reduces the bleeding by clot

formation. Coagulation pathways are broadly divided into two types, i.e. extrinsic pathway and intrinsic pathway depending on the source of origin of each pathway.² Both pathways eventually lead to a common path which results in the precise and balanced generation of Thrombin at the site of vascular injury in the form of the prothrombinase complex that converts the fibrin monomers to the first formed or “primary fibrin clot”. In the extrinsic pathway, tissue factor present at the subendothelium binds both zymogen and activated forms of factor VII (factor VIIa). FVIIa binding to TF in turn triggers coagulation by converting factors IX and X to their active forms (IXa and Xa). Feedback amplification is achieved when factor VII bound to TF is activated by factors VIIa, IXa, and Xa (Figure 2). Factors IXa and Xa may remain associated with the tissue-factor-bearing cell or diffuse into the blood and bind to the surface of nearby activated platelets, which have formed the primary platelet plug (by intrinsic pathway). Parallely, prothrombin is activated to thrombin by the phospholipid bound, FXa and FVa. Also, FXa and thrombin activate FV, and Thrombin activates FXI which forms FIXa. This feedback enables rapid and increased activation of FVa, FVIII and FIX. The FVIII complexes with vWF,



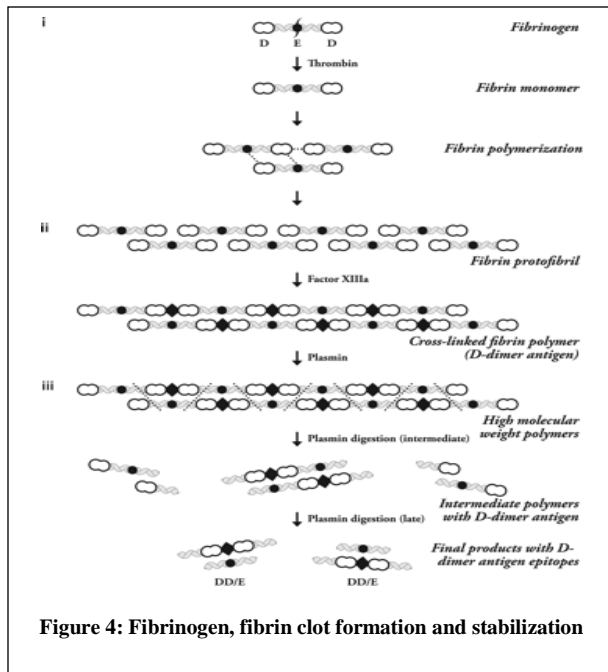
however upon activation FVIIIa forms complex with FIXa, subsequently activating FX (by so-called Tenase complex). Hence, rapid and activation of FX, FV, to generate more Thrombin (FIIa), which is the key effector enzyme of coagulation cascade, is the sole-aim of coagulation factors.³ Subsequently, a) thrombin cleaves fibrinogen to form fibrin monomers, b) thrombin activates coagulation FXIII to form FXIII-Aa, c) activates FXIII-Aa, by covalently crosslinks preformed fibrin monomers, stabilizing the clot, d) Thrombin activates Thrombin-activatable fibrinolysis inhibitor (TAFI), stabilizing the clot. This explains why Thrombin generation occurs after the formation of fibrin clot.⁴ Also, during these proteolytic cleavages of coagulation factor



zymogens to active factors, Calcium ions (Ca) play a major role, which are released in abundance by dense platelet granules upon platelet activation.⁵ In turn, there are several natural anticoagulants in the body which ensure clot dissolution to avoid unwanted thrombosis, or embolism. This includes Antithrombin (thrombin inhibitor), TAFI, Protein S, Protein C (which forms activated Protein C by action of thrombin, and inhibits FVa and FVIIIa), Thrombomodulin etc.⁶ Hence, mechanism of coagulation can be divided into four major parts; Initiation, amplification, propagation and stabilization of the clot. (Figure 3)

1.2 Fibrinogen, the Fibrin Clot formation and Stabilization

Fibrinogen is the last substrate in coagulation pathway which gets cleaved by thrombin to form fibrin clot, i.e. the end product of clotting cascade. Fibrinogen is produced in hepatocyte and is released in circulation after maturation & assembly of all the chains. Limited proteolytic cleavage of Fibrinogen by Thrombin molecules (forming fibrin monomers), releases Fibrinopeptides A & B, results in a dramatic transformation: fibrin monomers assemble



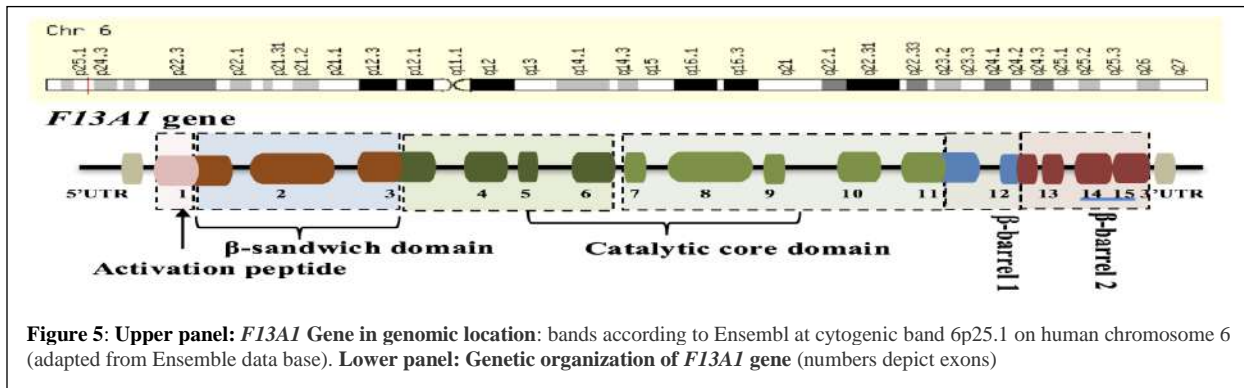
spontaneously forming aggregates/fibrin clots. The unique structure of fibrinogen governs the specificity of its interaction with its activator (thrombin), stabilizer (FXIII) and degrader (Plasmin). Structurally, Fibrinogen is composed of $A\alpha$, $B\beta$ and γ chains, associated by disulphide bonds. A mature fibrinogen molecule is hexamer of dimers of these three chains, i.e., $(A\alpha B\beta\gamma)_2$. Thrombin mediates the conversion of Fibrinogen to Fibrin monomer by removal of N terminal-Fibrinopeptides. The release of these negatively charged fibrinopeptides, decreases the electrostatic repulsion between the molecule and the molecules tend to aggregate, forming Fibrin protofibrils. However, these associations are non-covalent in nature. Covalent crosslinking of aggregated Fibrin polymers is facilitated by Coagulation factor XIII, which by its

transglutaminase activity⁷ induces formation of $\epsilon(\gamma\text{-glutamyl})\text{lysyl}$ bond, covalently crosslinking the fibrin protofibrils. FXIII mediated fibrin cross-linking forms $\gamma\text{-}\gamma$ dimers, and α -polymers. Formation of $\gamma\text{-}\gamma$ dimers is a rapid process compared to the latter. The α -chain crosslinks confer final stability to the clot by providing strength, rigidity and resistance to clot dissolution; whereas $\gamma\text{-}\gamma$ dimers contribute to clot stiffness, providing it mechanical strength.^{8,9} (Figure 4)

1.3 Coagulation Factor XIII: Discovery and early clinical findings

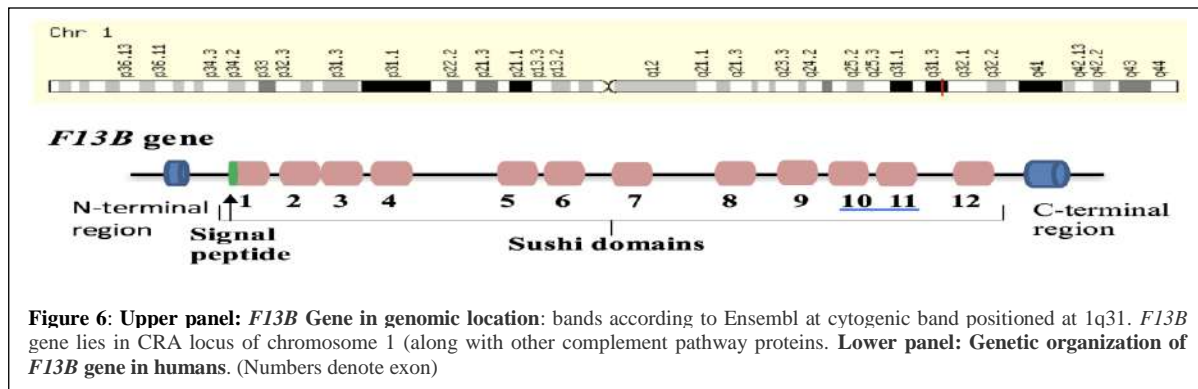
Coagulation Factor XIII (FXIII), also known as the Laki-lorand factor, or fibrin-stabilizing factor (earlier times also known as the serum-factor), is the terminal-transglutaminase responsible for covalent crosslinking of pre-formed fibrin clots. The evidence for the existence of this component came early in 1920s from Barkan and Gaspar who reported that clots formed in oxalated plasma were insoluble in 0.02% NaOH, compared to those formed in non-oxalated plasma.¹⁰ In 1944, Robbins made an important observation demonstrating that when clotted with Thrombin, solutions of purified Fibrinogen formed Fibrin soluble in weak acids even in the presence of Ca; and when a small drop of serum is added to this system the resulting fibrin was insoluble.¹¹ This finding directed to a hint that some component from serum along with both Calcium and Thrombin are influencing the clot stability, and its solubility in Urea and weak acids. Later Laki (1948)¹², and Lorand (1950)¹³, demonstrated that this plasma component is a protein that stabilizes fibrin polymers; hence it was known as fibrin stabilising factor (FSF), but its mode of action was still unclear. Enzyme kinetics performed by Buluk (1961)¹⁴, showed this factor to be a pro-enzyme, which is activated in the presence of Thrombin and Ca. In 1960s a swiss group led by Duckert, encountered a patient with severe bleeding disorder, yet with normal levels of other factors in plasma as demonstrated by normal values for hemostatic parameters.¹⁵ Sub-microscopic analysis revealed that it was the lack of Laki-Lorand factor or FSF that affects the cross-striation of fibrin fibres.¹⁶ The disappearance of cross-striation from fibrin surface following urea treatment was further studied in patient plasma, compared to normal and EDTA plasma with thrombin. In the absence of this serum factor, or Ca, association of fibrin fibrils was loosened, and dissociated into protofibrils faster compared to normal plasma. In 1964, the Laki-

Lorand factor was renamed as Coagulation Factor XIII. This factor was determined to be a zymogenic, pro-transglutaminase, that when activated formed irreversible, covalent cross-links within pre-formed fibrin protofibrils, generating a denser stronger fibrin network. FXIII in plasma is present as a heterotetramer (FXIII-A₂B₂), with dimeric subunits of each catalytic FXIII-A, and carrier FXIII-B subunits (associated non-covalently). The catalytic FXIII-A subunits perform transglutaminase activity by the formation of ε(γ-glutamyl) lysyl crosslinks between two fibrin polymers. FXIII-B subunits primarily perform carrier functions, by avoiding undue activation of catalytic FXIII-A subunit in plasma.^{17–21}

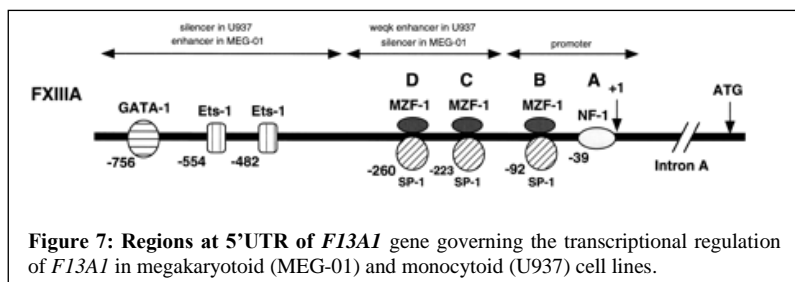


1.3.1 Coagulation FXIII gene

The gene encoding for human FXIII-A subunit (*F13A1*) is present on human chromosome 6, location 6p24-6p25. *F13A1* gene houses 15 exons and 14 introns.¹¹ This gene is transcribed to 3.9kb mRNA, with an 84-bp 3'UTR, 2.2-kb ORF and 1.6-kb 5'UTR. Figure 5 depicts the



regions on *F13A1* responsible for encoding the respective domains on the mature FXIII-A protein. The transcriptional regulation of *F13A* gene demonstrated by Ichinose, revealed that a 5'-fragment was sufficient to support the basal expression in monocytoid (U937) and megakaryocytoid (MEG-01) cell lines. GATA-1 element was found to be responsible for the enhancer activity. Promoter regions for MZF-1, NF-1 and SP-1 are important for the basal expression levels of FXIII-A in the cell (Figure 7).²² FXIII-A is processed in the cytoplasm and it



complexes with FXIII-B in the cytoplasm. The mechanism underlying FXIII-A export out of the cells is not yet clear. The gene encoding for the human non-catalytic FXIII-B subunit is *F13B* gene located at chromosome 1, at position 1q31-32.1. It is a 28-kb long

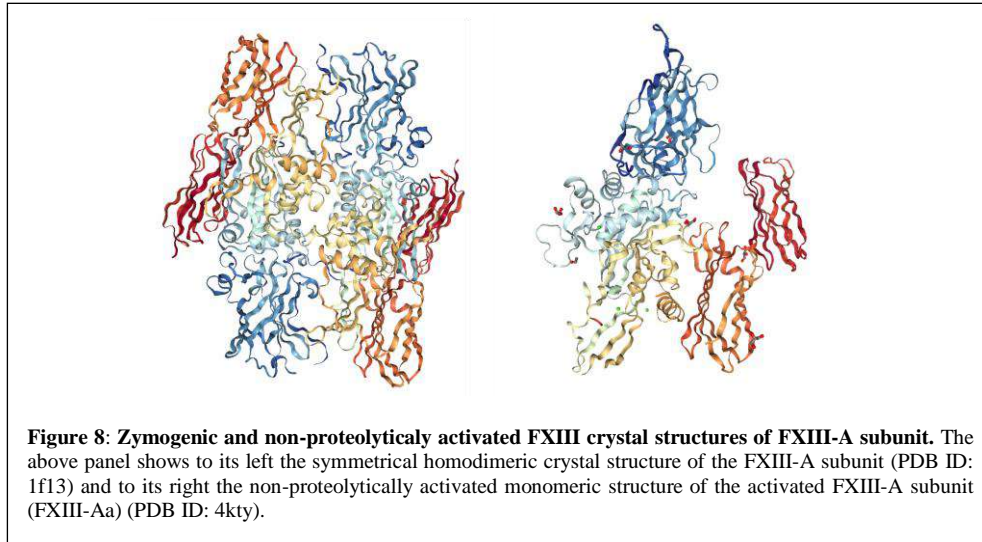
| Nucleotide Variation | Amino Acid Variation | Allele Frequency | | | |
|----------------------|----------------------|------------------|-------------|-------------|-------------|
| | | CEU | YRI | JPT | HCB |
| F13A1 | | | | | |
| c.103G>T | p.V34L | 0.767/0.233 | 0.883/0.117 | 1 | 1 |
| c.514A>T | p.Y204F | 0.983/0.017 | 1 | 1 | 1 |
| c.986A>C | p.P331P | 0.853/0.147 | 0.933/0.067 | 1 | 0.989/0.011 |
| c.1652C>T | p.T550I | 1 | 0.992/0.008 | 1 | 1 |
| c.1694C>T | p.P564L | 0.756/0.242 | 0.864/0.136 | 0.705/0.295 | 0.733/0.267 |
| c.1704A>G | p.L567E | 0.890/0.110* | 0.991/0.009 | 1 | 1 |
| c.1886T>A | p.L588G | 0.875/0.025 | 1 | 1 | 1 |
| c.1951G>A | p.V650I | 0.950/0.050 | 0.942/0.058 | 0.909/0.091 | 0.911/0.089 |
| c.1954G>C | p.E651D | 0.775/0.225 | 0.742/0.258 | 0.909/0.091 | 0.911/0.089 |
| F13B | | | | | |
| c.344G>A | p.R95H | 0.075/0.925 | 0.725/0.275 | 0.034/0.966 | 0.044/0.956 |
| c.456G>A | p.T132T | 0.925/0.075 | 0.307/0.693 | 1 | 1 |
| c.765C>T | p.C235C | 1 | 0.983/0.017 | 1 | 1 |
| c.1049A>G | p.H330R | 1 | 0.933/0.067 | 0.989/0.011 | 0.989/0.011 |
| c.1707T>G | p.D549E | 1 | 0.906/0.092 | 0.966/0.034 | 0.956/0.044 |
| c.1606T>C | p.N562N | 0.492/0.508 | 0.642/0.358 | 0.244/0.756 | 0.169/0.831 |
| c.1952 + 144 C>G | - | 0.65/0.35 | 0.96/0.04 | 0.42/0.58 | 0.35/0.65 |

Table 1: Racial variations of the polymorphisms in FXIII-A and FXIII-B subunit genes

polynucleotide bearing 12 exons which are transcribed to 2.2-kb mRNA. (Figure 6) It has 11 introns. At the N-terminus lies a 20aa long signal sequence which is characteristic of secretory proteins (leader sequence).²² Each of the exon codes for sushi domain which gene duplication and exon shuffling during evolution from complement pathway. FXIII-B protein is expressed in liver by hepatocytes under control of transcription factors HNF1 α and HNF4 α .²³ There are several polymorphisms reported for *F13A* and *F13B* genes globally. According to the HapMap project database, there is a considerable racial variation in polymorphism of *F13A* and *F13B* genes among Asian, Caucasian, and African populations (As listed in Table 1). The well-known and well characterized *Val34Leu* polymorphism in *F13A1* gene increases the rate of FXIII-A activation and influences the clot stability, and its effect on fibrin clot architecture was found to be dependent on fibrinogen levels in plasma.²⁴ In case of *F13B* gene, three major polymorphisms are found *F13B1*, *F13B2* and *F13B3*; from the European, Caucasian and Asian populations. These polymorphisms are not influencing FXIII-A, FXIII-B or pFXIII antigen levels.

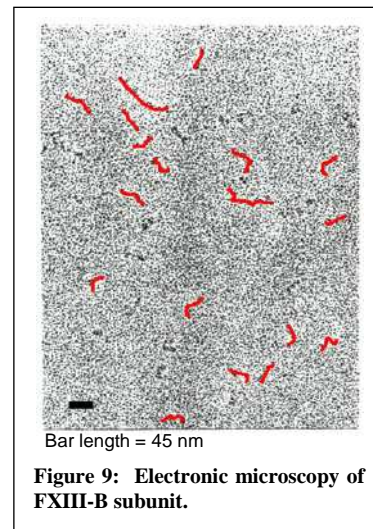
1.3.2 Coagulation FXIII source

The FXIII-A subunit protein is majorly expressed in platelets.²⁴ It is estimated that FXIII-A corresponds to 3% of total platelet protein. (Also, the concentration of FXIII-A is higher in platelet cytoplasm compared to plasma). Although platelets are like bombs of FXIII, the FXIII involved in hemostasis is not of platelet origin.²⁵ Other than platelets, FXIII-A is also expressed in megakaryocytes²⁶, monocytes, macrophages²⁷, osteocytes^{28 29}, and placenta³⁰, and lymphoblasts.³¹ Intracellularly non-proteolytic, reversible activation of FXIII-A, can be attained in the presence of high intracellular Calcium ion concentration.³² However, sporadic evidence also suggests that the trapped platelets in the fibrin clot, generate very low levels of FXIII-A molecules which contribute to clot stability by exposing onto the surface of activated platelets by virtue of increased cytoplasmic Calcium ion concentration.³³ In contrast to the FXIII-A subunit, FXIII-B is by and large expressed from hepatocytes.²³ The two subunits meet in the plasma to form the heterotetramer. The FXIII-B subunit is expressed almost in twice the amount of FXIII-A subunit in the plasma, therefore while there exists both free and bound FXIII-B subunits in the plasma, practically negligible to no free FXIII-A subunit is found in plasma.³⁴



1.3.3 Coagulation FXIII protein structure

Several structural studies conducted in past three decades have reported several crystal structures for the FXIII-A subunits. These have been zymogenic dimeric structures both ion bound (PDB ID: 1ggt³⁵, 1ggu, 1qrk and 1ggy)³⁶ and unbound (PDB ID: 1f13³⁷) as well as a Thrombin activated form (PDB ID: 1fie³⁸) which looks similar to the zymogenic form. FXIII-A belongs to class of enzymes called transglutaminase and the domain organization of FXIII-A is similar to tissue transglutaminase type-2 (TGM2).³⁹ A domain organization of FXIII-A subunit consists of an N-terminal activation peptide (1-37), β -sandwich domain (38-184), catalytic core domain (185-515), barrel-1 (516-628) and barrel-2 (629-731) domains. The catalytic activity resides in a catalytic triad that is composed of a central catalytic nucleophilic Cysteine Cys314 and includes two more supporting His373 and Asp396 residues. In the zymogenic dimeric structures, the catalytic triads are buried deep in the structure with no access to potential substrates. The sandwich and the barrel domains primarily have beta-sheeted structures. More recently the crystal structure of the non-proteolytically activated (with high levels of Calcium) bound to an irreversible inhibitor (PDB ID: 4kty) and Calcium to three of its Calcium binding sites was disclosed.³⁷ (Figure 8) This structure apart from being a monomer in comparison to the dimeric zymogen also shows remarkable differences in conformation with the barrel domains turned around exposing the catalytic triad of this enzyme to substrate access.⁴⁰⁻⁴² Compared to FXIII-A subunit, FXIII-B subunit is not structurally well characterized. Although electronic microscopic images taken years back show it to be a filamentous protein (Figure 9), no biophysically determined all atom structure exists for this subunit.⁴³ Gel filtration analysis showed this subunit to be a dimer and homology to proteins like Complement Factor H suggest that a monomer of this subunit is composed of ten repetitive round sushi domain or Complement control module, called as such owing to their preponderance in some complement system proteins.⁴⁴⁻⁴⁷ Very little is known about how these two subunits interact with binding affinity values differing that vary from



10^{-6} to 10^{-10} depending on the technique used to evaluate it.⁴⁸ Recently partial evidence suggests that the first two sushi domains of the FXIII-B subunit might interact with the FXIII-A subunit.³⁴ However, no all atom structure exists for the FXIII-A₂B₂ complex as well.

1.3.4 Activation, Mechanism of Action and Regulation of FXIII Activity

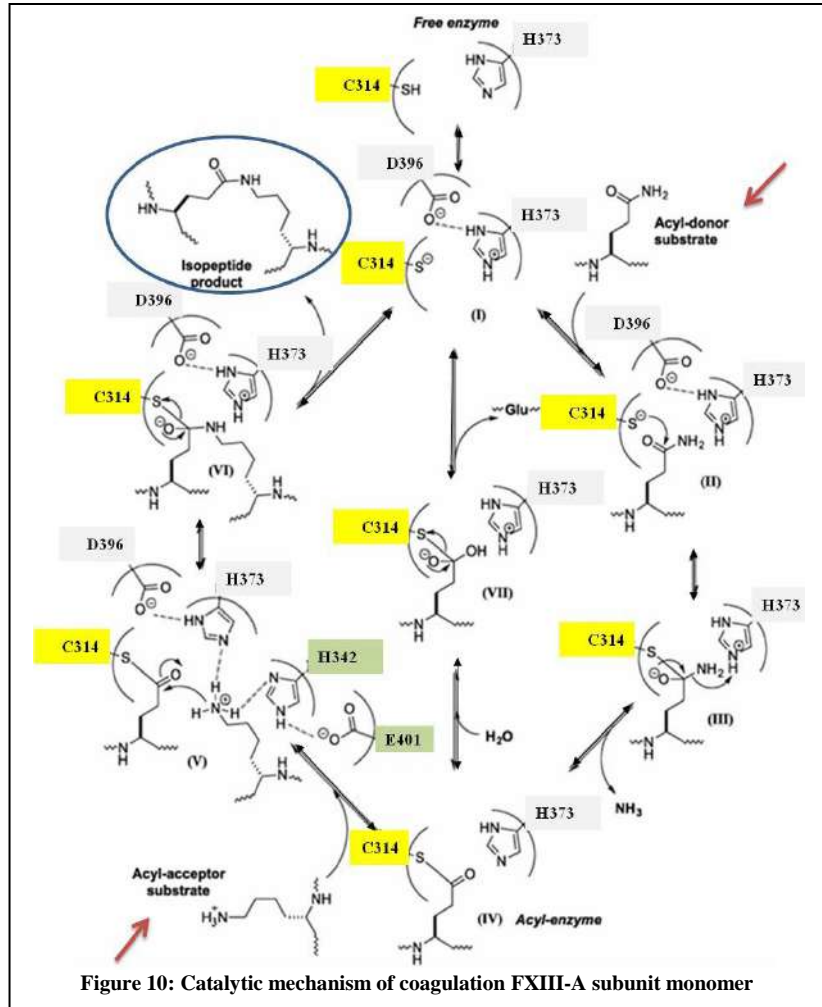
Activation

As the catalytic component of FXIII, i.e FXIII-A, is present both intracellularly (majorly in platelets), as well as in plasma complexed with FXIII-B subunit forming FXIII complex. In both the compartments, this molecule has different mechanism of activation as well as regulation. Cellular FXIII-A₂, dimer is sensitive to intracellular Calcium ion concentration. In resting platelets, intracellular Calcium ion concentration is 10^{-7} M. Upon platelet activation, Calcium ions are released from intracellular storage compartments as well as from extracellular channels. Levels of Calcium > 50 mM can fully activate rFXIII-A even in the absence of thrombin. Since this is a non-proteolytic mode of activation, the molecule can revert back to its zymogenic state if the Calcium is chelated out of the system and attains the ability to get re-activated/reversibly activated. Activation following proteolytic cleavage is common for both the allosteric and catalytic proteins of the blood coagulation cascade including pFXIII. In the well-defined zymogenic crystal structures of FXIII (PDB ID's: 1F13, 4KTY, 1GGU), FXIII-A molecule has a primary Calcium ion binding site (Cab1) with $\sim K_d$ of 10^{-7} M. However, ⁴³Ca NMR studies on rFXIII, rFXIII-A*, and rFXIII-A^o (zymogenic, non-proteolytically activated and proteolytically activated forms) suggested presence of additional low affinity Calcium binding sites (Cab2, Cab3).^{36,49,50} The disclosure of the non-proteolytically activated FXIII A crystal structure (PDB ID: 4kty) showed the existence of these two other Calcium binding sites.³⁷ These Calcium ion binding sites are proposed to be responsible of inducing structural changes in the molecule, leading to complete activation. In the plasma, FXIII-A molecule undergoes proteolytic activation, involving the cleavage by the protease Thrombin. Thrombin cleaves FXIII-A molecule at the 37th Arginine residue, releasing a 37 amino acid long activation peptide.^{37,41,51} The release of activation peptide pushes the molecule towards the activated state and further activation is governed by the binding of Calcium ions to the three Calcium binding sites.

Mechanism of Action

Coagulation FXIII, as discussed earlier is a transglutaminase that covalently crosslinks proteins forming a covalent ϵ -(γ -glutamyl) lysine cross-link between the γ -carboxy-amine group of a glutamine (amine acceptor) and the ϵ -amino group of a lysine residue presenting the amine donor.^{48,52} This catalytic process involves 3 major steps: Transamidation (removal of CONH₂ group from substrate 1, esterification, and hydrolysis).^{53,54} Transglutaminase catalytic mechanism is often termed as the ping-pong mechanism, as the enzyme reacts with both the substrates

sequentially. The first substrate for FXIII-A is peptide-bound glutamine donor and the second substrate is a primary amine. Activation of FXIII molecule involves thrombin mediated cleavage of the N-terminal activation peptide, as well as Calcium binding. Calcium binding to FXIII-A molecule gives rise to conformational changes which ultimately result in a charge-relay system. This charge relay system is responsible for partial deprotonation of catalytic Cysteine that forms a reactive center nucleophilic cysteine. The reactive Cysteine further attacks the amide carbon of the first acyl-donor substrate (Glutamine), forming first acyl-enzyme intermediate, which is stabilized by removal of ammonia as a virtue of charge relay (deamidation), which embarks the first process of transglutaminase mediated catalysis. Additionally, if the second substrate is water, the bound substrate is released as a deamidation product. When the second substrate of FXIII-A, is a peptide bound Lysine that acts as acyl-acceptor and attacks the acyl-enzyme intermediate. This access is by virtue of formation of a hydrophobic tunnel, which stabilizes acyl-donor at its base and acyl acceptor lysine on the other side (by the help of catalytic diad). The electrophilic amine centre of Lysine attacks the nucleophilic centre of acyl-enzyme intermediate, releasing the isopeptide product and recovering the enzyme for next catalyses.



Additionally, if the second substrate is water, the bound substrate is released as a deamidation product. When the second substrate of FXIII-A, is a peptide bound Lysine that acts as acyl-acceptor and attacks the acyl-enzyme intermediate. This access is by virtue of formation of a hydrophobic tunnel, which stabilizes acyl-donor at its base and acyl acceptor lysine on the other side (by the help of catalytic diad). The electrophilic amine centre of Lysine attacks the nucleophilic centre of acyl-enzyme intermediate, releasing the isopeptide product and recovering the enzyme for next catalyses.^{37,55} (Figure 10)

Regulation of FXIII activity

Several theories have been reported for the regulation of coagulation FXIII activity. As the rate of activation of FXIII-A molecule is majorly driven by Calcium ions, its regulation is kept under radar by growing fibrin clot.^{52,56-60} Interestingly once cross linking of 40% of fibrin γ -chains occurs the effect of fibrin on FXIII-A activation is lost giving fibrin cross-linking down regulatory functions for FXIII-A activation. Certain enzymes like Polymorphonuclear proteases have been shown to downregulate activated FXIII-A (FXIII-Aa) within the fibrin clot.⁶¹ More recently it was quite conclusively shown that the primary event initiating downregulation of activated FXIII-A (FXIII-Aa) is cleavage by Plasmin at the cleavage site identified by mass spectrometry to be between K468 and Q469 in the activated form of FXIII-A.⁶²

1.3.5 FXIII a protein with multiple substrates and pleiotropic functions

Other than its well characterized role and involvement in maintenance of clot, FXIII has been found to be associated with other physiological and pathological states, suggesting pleiotropic roles outside the coagulation pathway. Over past few decades several research groups with different backgrounds have studied FXIII and have unveiled putative novel functions for FXIII. FXIII is now recognized as a multifunctional protein involved in regulatory mechanisms and construction and repair processes beyond hemostasis with possible implications in many areas of medicine.⁶³⁻⁶⁵ Such a wide dominion of influence suggests that FXIII has multiple substrates. Currently close to 30 substrates are known for FXIII reported in the TRANSDAB database.⁶⁶⁻⁶⁸ In plasma FXIII interacts with Fibrinogen/Fibrin; Factor V & thrombospondin; α 2-PI; Collagen type I, II, III, V & fibronectin; vWF; pro-carboxypeptidase TAFI, and plasmin activator inhibitor-2 (PAI-2); Vitronectin; α 2-Macroglobulin; Myosin, Actin, Vinculin and Filamin; angiotensin type 1 receptor (AT1R), VEGFR2 and integrin α V β 3. Consequently, FXIII is known to be involved in wound healing, immunity, formation of intracellular networks, embryo implantation, osteogenesis and more recently diabetes (adipocyte maturation) and arthritis.^{18,69-95} (Figure 11)⁶⁴

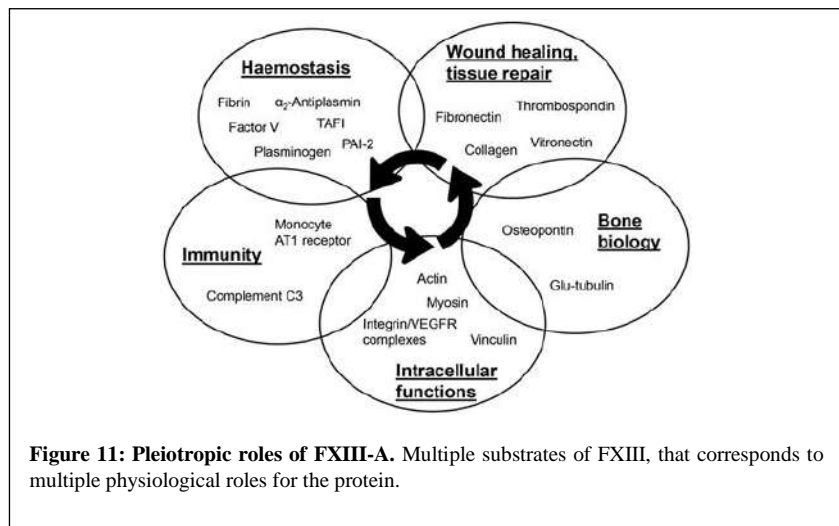
1.3.6 FXIII deficiency

In comparison to other coagulation factors FXIII exists in plasma in lower concentrations of approximately 21.6 μ g/ml. Any discrepancies in the normal plasma levels of either of the FXIII subunits, either due to genetic defects (homozygous/heterozygous), or due to presence of auto-antibodies against FXIII, causes a bleeding predisposition collectively known as FXIII deficiency.

This deficiency is characterized by diverse but distinct signs, symptoms that could include either one or of combination of following:

- a. Umbilical stump bleeding
- b. Intracranial bleeding
- c. Easy bruising
- d. Recurrent pregnancy loss
- e. Menorrhagia, delayed wound healing.

In case of FXIII deficiency, routine coagulation tests are within range, Hence the deficiency is diagnosed on the basis of Clot solubility assay, clot assessment by ROTEM, plasma FXIII activity assay, and plasma FXIII antigen quantification.^{96,97} While Umbilical cord bleeding seen in new-borns is the most commonly observed symptom for inherited FXIII deficiency, intracranial bleeding is the cause of highest mortality in FXIII deficiency.⁹⁶



Acquired FXIII deficiency

Acquired FXIII deficiency is mainly caused by:

- a. Hyperconsumption, hyposynthesis or rare by autoantibody development causing a more mild (plasma FXIII levels between 30-70%) up to severe phenotype (below 30%).
- b. Decreased production of FXIII-B (Hepatitis or acute liver failure) or increased consumption of FXIII subunits as cause of primary diseases like leukaemia, inflammatory bowel disease (crohn's disease or ulcerative colitis), Henoch schoenlein purpura, systemic lupus erythematosus, disseminated intravascular coagulation, pulmonary embolism, liver disease, sepsis, stroke, surgery, trauma are related with more mild decrease requiring rarely replacement therapy.
- c. Impaired synthesis in patients suffering from rheumatoid arthritis treated with anti-interleukin-6-receptor monoclonal antibody (tocilizumab).
- d. Development of autoantibodies (mostly IgG) against FXIII-A (most) and FXIII-B (rare) subunits with neutralizing or non-neutralizing effect which was reported in 83 cases worldwide mostly found in elderly patients around 70 years.^{96,98-102}

Inherited severe FXIII deficiency

Deficiency of FXIII can result in a bleeding predisposition and can have acquired or inherited causes. Patients with severe inherited FXIII deficiency (due to complete absence or loss of function) suffer from severe bleeding tendencies.⁹⁷ The global disease burden of inherited severe FXIII deficiency is not very high and approximately 1-4 out of a million individuals are affected making it a rare autosomal disorder. A total of 112 distinct FXIII mutations from *F13A1* and *F13B* (FXIII-A and FXIII-B subunits) genes have been identified in patients with a broad spectrum of pathological phenotype severity that include post-operative prolonged bleeding, delayed re-bleeding and spontaneous abortion during the first trimester of pregnancy due to placental dysfunction. Over 500 cases of severe FXIII deficiency have been reported worldwide. Typically, inherited severe FXIII deficiency caused by homozygous/compound heterozygous mutations in FXIII gene manifests itself as a severe bleeding diathesis with the rare exception when the mutations occur in the carrier/regulatory FXIII-B subunit in which case the bleeding symptoms are mild to moderate.^{97,103-106}

Inherited mild or isolated heterozygous deficiency

In the past decade, cases reporting insufficiency of active FXIII have been reported, that are different from the inherited severe form of FXIII deficiency both at the genotype and phenotype level. This is the mild heterozygous FXIII deficiency (residual FXIII activity approximately 20-60%) resulting from mutation in only one allele of either the *F13A1* or *F13B* gene. Patients with such deficiency normally do not bleed spontaneously but may have delayed bleeding upon provocation for example after surgery (e.g. tonsillectomy). The first evidence of existence of this deficiency came from Egbring in 1980s. Careful exploration of the medical history of heterozygous members of affected families done by Egbring did reveal a significant bleeding tendency, also there was no clinical correlation observed between the measured FXIII levels and clinical symptoms in these "apparently healthy" individuals. After two decades of no activity on this front, a number of publications from the German-Caucasian population, drew conclusions that support further investigation of heterozygous mild FXIII deficiency through a broader

patient screening approach leading to diagnosis of more afflicted patients. In this cohort were found a surprisingly large number (n=32) of heterozygotes for FXIII deficiency among a cohort of 186 patients suspected of mild FXIII deficiency (FXIII activity levels 20-60%) upon genetic screening of *F13A1* and *F13B* genes between the years 2004-2014. Mutation screening revealed 23 novel missense mutations in these mild carriers (16 in *F13A1* and 7 in *F13B*). Interestingly, a lower skewed ratio between *F13A1* (FXIII-A₂ subunit) and *F13B* (FXIII-B₂ subunit) gene mutations in mild heterozygous FXIII deficiency (2:1 ratio) was observed which is unusual considering that in severe homozygous/compound heterozygous FXIII deficiency >95% mutations occur in the *F13A1* mutations (almost a ratio of 1:20).¹⁰⁷

Diagnosis

FXIII deficiency is hard to detect because normal standard global coagulation tests like the prothrombin time (PT) or activated partial thromboplastin time (aPTT) are not influenced by FXIII deficiency. Special specific tests are required to diagnose the FXIII deficiency. Clot solubility assays which evaluate the effect Urea has on a clot has been traditionally used to detect FXIII deficiency. However, it is a non-quantitative test and can detect this deficiency only in cases where FXIII levels are very low i.e. <3%. Quantitative photometric and incorporation assays are now used as functional tests are to determine the FXIII activity (some more details are presented in a later method sub-section of the introduction). According to current ISTH joint SSC committee guidelines for the diagnosis of inherited FXIII deficiency, the standard protocol involves first to measure FXIII activity in plasma with a quantitative assay when the individual presents itself with symptoms identified with this deficiency. If FXIII activity is observed to be low, then an quantitative antigenic assessment (like an ELISA) of the FXIII heterotetrameric FXIII-A₂B₂ needs to be done. Following this individual quantitative antigenic assessment of individual subunits are to be performed to identify which subunit is the cause of defect. Finally, as the last step of screening, genetic screening of *F13A1* or *F13B* genes is suggested, to detect the mutation underlying this defect. Diagnosis and rapid detection of the acquired form of this deficiency is a subject in development with many new suggestions being made currently to characterize the autoantibodies generated in this form.¹⁰⁶

Replacement therapies

The only available treatment modality for FXIII deficient patient, which is widely used is Cryo-precipitates from healthy donor, commercialized as FibrogamminP by CSL Behring in Europe (described above).¹⁰⁸ The product is administered intravenously and is thus immediately bioavailable resulting in a plasma concentration corresponding to the applied dose (which usually is an initial dose of 40U/kg body weight). No implications as a result of FibrogamminP overdose have been reported. The half-life of FXIII is the longest among coagulation factors (11–14 days). According to more recent analyses, a level higher than 10% is needed to reduce the occurrence of bleedings significantly, but still leaving 10% of patients with cutaneous bleeding (EN-RBD; <http://www.rbdd.eu>). FibrogamminP, is available for prophylaxis in a recommended dosage of 10–20 U/kg once every 4–6 weeks. In major surgery, 20–30 U/kg per day should be administered to achieve a level above 5% until healing is complete; in minor surgery, a dose of 10–20 U/kg per day for 2–3 days is recommended, whereas in spontaneous bleeding, the treatment varies from 10–20 to 20–30 U/kg per day, depending on the severity of bleeding, until bleeding stops. Replacement therapy throughout pregnancy is essential for the prevention of abortion and pregnancy loss in severe FXIII-deficient women.¹⁰⁹ A new human recombinant FXIII-A₂ (rFXIII-A₂) (Tretten, Novo Nordisk, Bagsvaerd, Denmark) product has

been developed for FXIII substitution therapy. Safety and pharmacokinetics of a single administration of rFXIII was investigated in a phase I escalating-dose study. No serious adverse event and no development of specific autoantibodies were observed during the study. The rFXIII-A formed a complex with endogenous FXIII-B and the half-life of administered reconstituted FXIII was similar to that of the native FXIII heterotetramer. It was effective in restoring clot strength and resistance to fibrinolysis.^{98,99,110,111}

1.3.7 Inhibitors for FXIII

Recent investigations suggest that that FXIII-A activity is a major determinant of both clot RBC content and clot size. Wolberg et al, have demonstrated that FXIII-A crosslinking of fibrin α -chains mediates RBC retention in venous thrombi, and consequently, thrombus size.^{33,112} Therefore, FXIII and more specifically the activated form (FXIII-Aa) is an attractive therapeutic target in Thrombotic conditions. Over years many inhibitors have been developed against the catalytic FXIII-A subunit, which include peptide inhibitors as well as biological proteins. Some of the major inhibitors against FXIII-A subunit are:

Tridegin: Tridegin is a potent and highly specific inhibitor of FXIII-A, which has earlier been isolated from Amazon Leech (*Haementeria ghilianii*). Originally, Tridegin is a 66-amino acid long polypeptide. It is also perhaps the only known synthetic inhibitor known so far outside the human body.¹¹³

ZED1301 Ac-(D)-Asp-MA-Nle-Nle-Leu-Pro-Trp-Pro-OH: Is the site-specific irreversible inhibitor of FXIII-A molecule, containing electrophilic Michael-acceptor warhead (to covalently modify the catalytic cysteine at the active center). ZED1301 shows 30-fold selectivity for FXIII-A (IC₅₀ 100nM) compared to tissue transglutaminase (IC₅₀ 3000nM), making it highly selective.³⁷

Transglutaminase inhibitors: These are imidazolium-based drugs, which are not very specific towards FXIII-A inhibition but also block other Transglutaminases. (IC₅₀ for both 0.35uM). e.g. 1,3-Dimethyl-2-(2-oxopropylthio)-4,5-diphenyl-1H-imidazol-3-ium trifluoromethanesulfonate, and 1,3,4,5-Tetramethyl-2-[(2-oxopropyl)thio]imidazolium chloride.^{113,114}

1.4 Principles underlying methods/strategies used in this thesis

1.4.1 *In silico* methods

In silico methods have been used in this thesis for two purposes: 1) to generate experimentally testable hypothesis and 2) to support or verify certain structure functional mechanisms interpolated from biochemical observations at the bench. Very briefly the following methods have been used in this thesis:

Molecular Modeling

Molecular modeling involves the prediction of tertiary structure of a protein based on its primary sequence. Based on if the modelling is^{115,116} performed based on a “template” or “template-independent” it is called “comparative” or “*de novo*” modelling respectively. Comparative protein modelling uses previously solved structures as starting points, or templates. This is effective because it appears that although the number of actual proteins is vast, there is a limited set of tertiary structural motifs to which most proteins belong.¹¹⁷⁻¹²⁰ Comparative modelling itself can be of two types:

- a. *Homology modeling*: This type of modelling heavily relies on the protein and its templates having high degree of homology or sequence identity (coupled with sequence coverage). Because a protein's fold is more evolutionarily conserved than its amino acid sequence, a target sequence can be modelled with reasonable accuracy on a very distantly related template, provided that the relationship between target and template can be discerned through sequence alignment. It is most accurate when the target and template have similar sequences which is the reason why it is not very effective when they show sequence identity <25%.¹²¹
- b. *Protein threading*: This type of comparative modelling determines a protein's template based on several biophysical features i.e. secondary structure, relative surface exposure etc. to generate what are known as threaded alignments of target template sequences. Therefore, it is also effective in cases where high sequence identity (unlike homology modelling) has not been observed but protein folds of the target template are similar.
- c. *De novo* modelling: This type of modelling is completely template independent and relies more on the basic biophysical principles underlying protein folding to generate/predict structure. Since protein folding itself can be modulated by other proteins like chaperone, such methods are limited by not only computational power but also by the size of the protein. Smaller proteins/peptides (<100 amino acids) are more amenable to these techniques since they usually do not rely on chaperones.

A number of open source software's such as Modeller as well as free to use high quality academic servers like Swiss-model and ITASSER are available for the automated or in cases where some helpful information is already available (like knowledge of possible template structures) to perform molecular modelling.¹¹⁹ An improvised alternative to full length protein modelling is to first model smaller domains of the protein that are easier to model and later assemble them into a full-length molecule using domain joining servers like AIDA.¹²⁰ These methods work better when the smaller domain models have higher quality and when some experimental data is available to guide the domain joining. In our thesis we have used a combination of these servers/software's. However, the quality of the eventual model lies in the skill of the modeller who has to combine known information as well as biophysical laws governing folding to predict which of the multiple models arrived at is the closest to the native form of the protein in question. Post modelling the models are also now required to be validated on model validation servers that check the stereo-chemical quality of the models to rank them with respect to other known crystal/biophysical structures of similar sizes.

Molecular docking

Molecular docking is a tool extensively used to model the interaction between two proteins/subunits or between protein and a ligand. Molecular docking by characterizing the binding pockets to an atomistic level helps us to understand the functional relationships underlying these interactions. When docking is performed without any pre-existing knowledge of the interaction between the participating partners it is known as "Blind docking" while when limited experimental knowledge is introduced to guide the docking it is called "Constrained docking". Also based on the flexibility of the participating structures, if they are rigid when the search for conformation fit between the two is conducted the type of docking is called "Rigid body docking". However, if one or both of the participating structures (the receptor or ligand) are considered flexible i.e. docking is performed on an ensemble of structures representing the flexible form of the structure itself the docking is called "Flexible docking". While Flexible

docking is always preferable, the computational cost can be very high especially for larger structures, therefore a combinatorial approach is usually adopted when docking relatively large structures i.e. protein vs protein. A number of academic servers/software like Z-Dock, MZ-dock, Autodock, VINA can serve to make quick “Rigid body” docking calculations to yield primary docking poses in a first screen.^{116,117} However, final screening of the docking poses or the final determination of a binding pocket is best conducted on server/software that can conduct Flexible docking and when also done with guided experimental constraints. One such server is the HADDOCK server.¹¹⁵ This webserver drives a constraint dependent docking of proteins. the constraint is information generated from experiments such as mutagenesis, NMR, chemical shifts, mass-spectrometry etc. This information is introduced as Ambiguous Interaction Restraints (AIRs) to drive the docking process. An AIR is defined as an ambiguous distance between all residues shown to be involved in the interaction. We have used a combination of these docking servers/software in this thesis very extensively to define a number of inter-subunit and protein-ligand interactions.^{116,117,122–124}

Molecular dynamic simulations

A biological function performed by a biomolecule is a result of a collective dynamic of intrinsically accessible global motions within the molecule. A fundamental appreciation for how biological macromolecules work requires knowledge of structure and dynamics. Molecular dynamic simulations (MD Simulations) is a computer-based approach which gives the fluctuations in the relative positions of the atoms in a protein or in DNA as a function of time. The availability of FXIII structural information makes it important to analyse the transition states, or the dynamic of the molecule which ultimately activate a zymogenic FXIII-A. Molecular dynamic simulation provide links between structure and dynamics by enabling the exploration of the conformational energy landscape accessible to protein molecules. For molecular simulations unlike geometrical simulations, Newtonian physics is used to create the motion of atoms, using empirically derived potentials to describe attributes such as bonds, angles, torsions, dihedrals, van der Waals radii, and electrostatics. These potentials are called “force fields”. A Force field is used to remove steric clashes and improve rotamer geometry of the submitted structure (structural refinement). As the dynamics of any atom in a molecule is governed by the kinetic and potential forces on it as a function of interaction at a given course of time, force field is an important parameter in any MD simulation. By definition, a force field is a mathematical expression describing the dependence of the energy of a system on the coordinates of its particles. In a classical MD simulation force field parameterization is necessary for whichever aim. In addition, MD is conducted in a simulation cell (which is defined space for allowing the thermal motion of the structure) with specific boundary (periodic or wall) and pressure, temperature conditions. The cell is usually filled up with relevant solvent like water molecules or specific ions to create the native environment of the structure. The two major categories of MD simulation are Classical MD simulation and Steered MD simulation (SMD). In classical MD simulations, the molecule of interest is allowed to simulate in a given force field for a range of time (that depends on the computational power at hand as well the question being asked and can range for from a few nanoseconds to several microseconds). However, before the production phase of simulation (in which the MD generates conformational data) the structure in question has to be equilibrated i.e. it has to be subjected to a round of MD that will energy minimize bringing it to a near native conformation from which it will differ only to the extent of its normal thermal motion and also adapt it o it surrounding solvent. This round of structural refinement or equilibration MD prevents the generation of structural artefacts in the production

phase MD. In steered MD simulation, a defined external force is applied to one or more atoms/ion/interacting partner; the opposing partner can be kept fixed or free. Such SMD's help us to get information on the binding of two partners (protein-protein or protein-ligand) by looking at the process of unbinding. We have used MD simulation very extensively in this thesis to look at protein-protein/protein –ligand interactions as well as to inspect the stability of our modelled structures.

Conformational ensemble

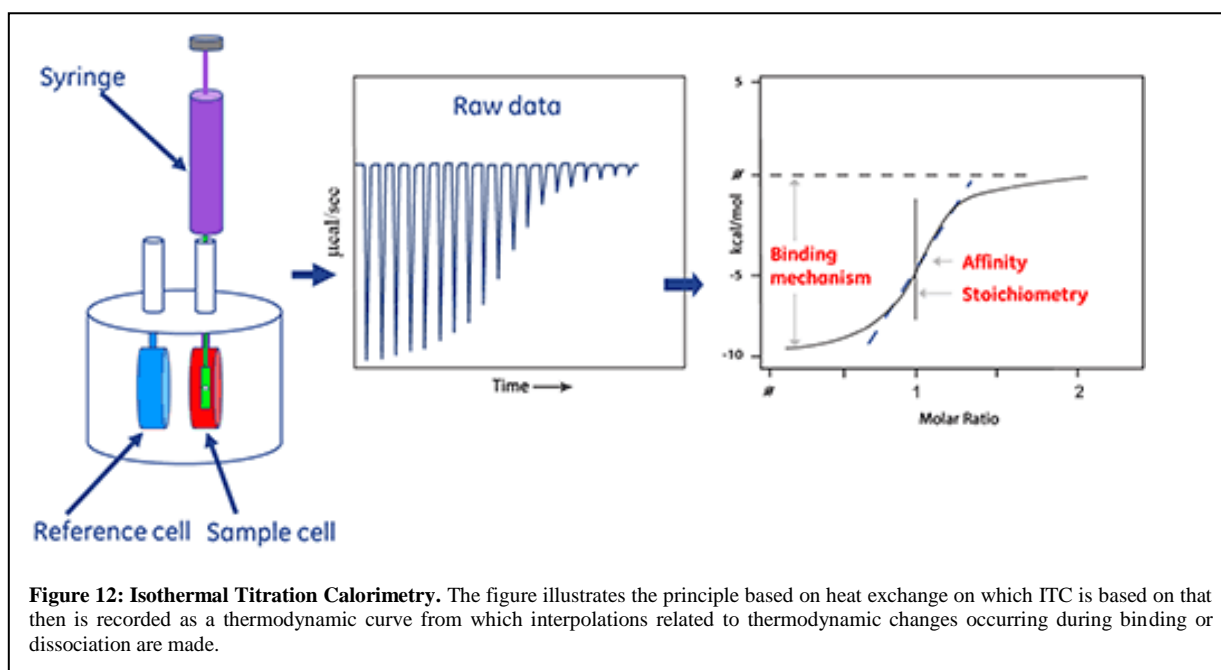
An alternate and less computationally expensive approach to understand the conformation landscape of a structure is to generate conformational ensembles. Recent advances in the performance of simulation algorithms, including specific strategies to increase the conformational sampling, have popularized this concept as the alternative to the analysis of PDB's single structures or run microseconds of MD to mimic actual biochemical reactions. Ensembles can be analysed to derive thermodynamic properties of the system, like entropy or free energy. If properly built, ensembles can also be used to reconstruct complex conformational transitions or even folding events. In our thesis we have realized this concept to generate transition state intermediate structures between zymogenic and activated forms of our proteins in question using the ANMPServer. This server uses a coarse-grained modeling approach to construct a two-state potential calculated by combining two elastic network models (ENMs) representative of the experimental structures representing the beginning and end points of the simulation. Intermediate structures are extracted as snapshots along continuous steepest descent pathways generated for the protein atomic coordinates during the transition from beginning to end point structures.¹²⁴

1.4.2 Bench methods

a. Isothermal Titration Calorimetry

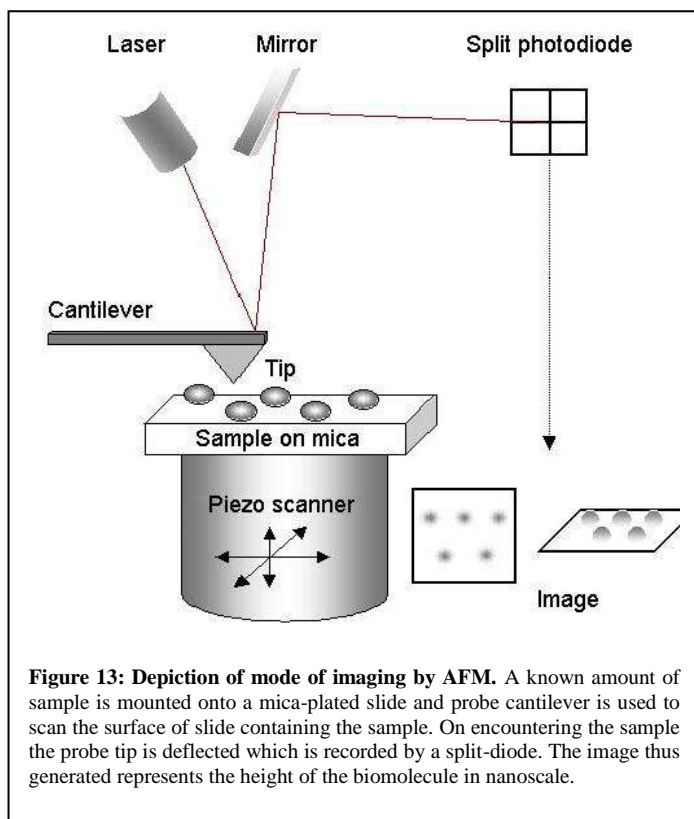
Isothermal titration calorimetry (ITC) is considered the gold-standard tool for studying protein-protein interaction since it's a label free and completely in solution technique. Ligand binding, protein/subunit/small molecule interactions or tertiary structural changes within a protein results change of potential energy of residues to kinetic energy of molecule (causing movements/structural alterations). These energy changes either liberate or absorb heat leaving behind the “thermodynamic signatures” (that may be alteration in enthalpy, entropy, affinity, and/or stoichiometry of protein or biomolecule). An ITC system is composed of an adiabatic jacket, which ensures no escape of heat outside of cell. A thermocouple circuit measures the temperature difference between the sample cell (with biomolecule and ligand), and reference cell (control). A feedback loop system ensures that the temperature difference remains zero and the heat either gained (endothermic) or lost (exothermic) by interacting molecules inside the sample cell is compensated by the feedback control. During an ITC experiment, known amount of ligand is injected to the sample cell containing the protein, ensuring gradual increase in concentration of ligand (in syringe) inside the sample cell with every injection, which causes heat to be either taken up or evolved (depending on the nature of the interaction). Measurements consist of the time-dependent input of power required to maintain equal temperatures between the sample and reference cells. (Figure 12) Every heat injection, generates a heat pulse (power needed to maintain $\delta T=0$), which are integrated with respect to time ($\delta H/\delta T$). The pattern of these heat effects as a function of the molar ratio (concentration of ligand/concentration of receptor), gives the thermodynamic parameters for the interaction. According to the formula:

$$\Delta G = \Delta H - T\Delta S = RT \ln K_a$$



(Where, ΔG = Gibbs Free energy change, ΔH is enthalpy change, ΔS is entropy change, K_a is binding affinity, n is stoichiometry, R is the gas constant and T is absolute temperature). The kinetic and thermodynamic trajectory (the ITC thermodynamic curve) formed during the course of activation explains in depth the heat contributions as a result of huge entropic changes (hydrophobic interactions and conformational changes), or enthalpic changes (due to association/dissociations).^{125,126} (Figure 12) This curve is also used to calculate extremely accurate K_d (dissociation constants) which are a quantitative measure of the binding affinity between two proteins or a protein and a ligand. We have used this tool in this thesis to explain the thermodynamic events underlying binding of individual FXIII subunits to each other and to cations like Calcium and Sodium.

b. Atomic Force Microscopy



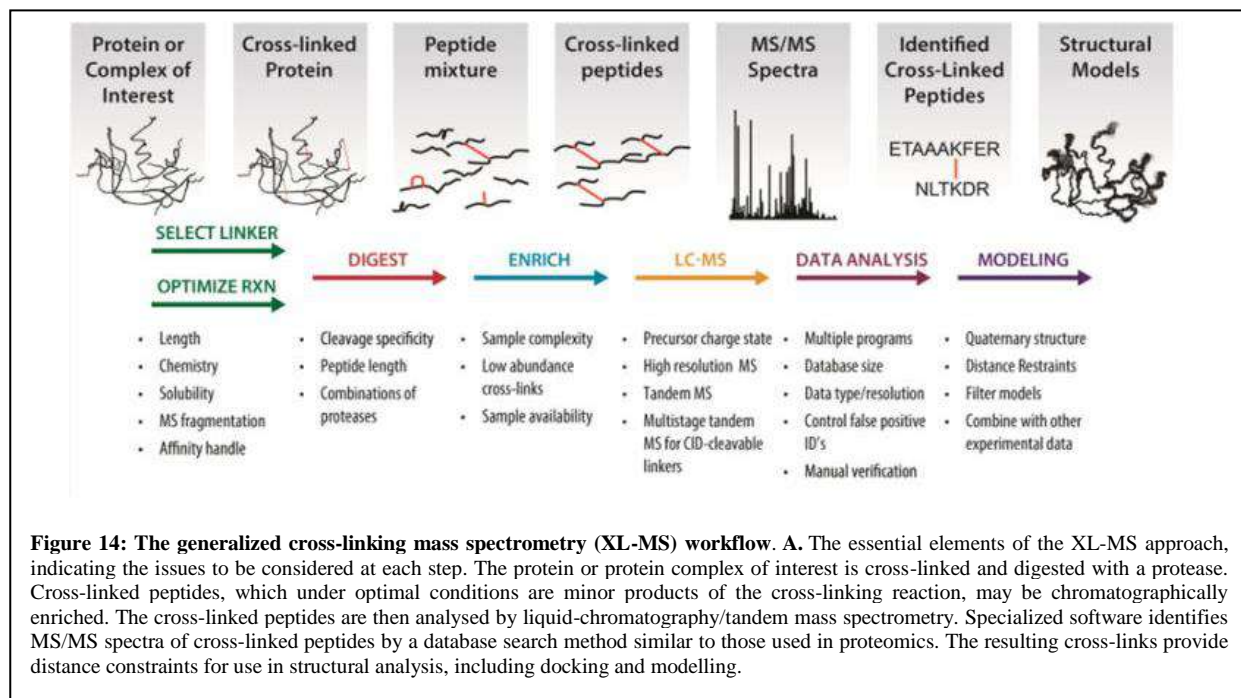
Atomic force microscopy (AFM) allows for the visualizing of individual proteins, DNA molecules, protein-protein complexes, and DNA-protein complexes. It is one kind of scanning probe microscopes (SPM). SPMs are designed to measure local properties, such as height, friction, magnetism, with a probe. To acquire an image, the SPM raster-scans the probe over a small area of the sample, measuring the local property simultaneously. In contact mode AFM the sample (protein complexes for eg.) are coated onto a mica surface which is scanned by the probe. AFMs operate by measuring force between a probe and the sample. Normally, the probe is a sharp tip, which is a 3-6 μm tall pyramid with 15-40nm end radius. Though the lateral resolution of AFM is low ($\sim 30\text{nm}$) due to the convolution, the vertical resolution can be up to 0.1nm. To acquire the image resolution, AFMs can generally measure

the vertical and lateral deflections of the cantilever by using the optical lever. The optical lever operates by reflecting a laser beam off the cantilever. The reflected laser beam strikes a position-sensitive photo-detector consisting of four-segment photo-detector. The differences between the segments of photo-detector of signals indicate the position of the laser spot on the detector and thus the angular deflections of the cantilever. (Figure 13) Piezo-ceramics position the tip with high resolution. Piezoelectric ceramics are a class of materials that expand or contract when in the presence of a voltage gradient. Piezo-ceramics make it possible to create three-dimensional positioning devices of arbitrarily high precision. In contact mode, AFMs use feedback to regulate the force on the sample. The AFM not only measures the force on the sample but also regulates it, allowing acquisition of images at very low forces. The feedback loop consists of the tube scanner that controls the height of the tip; the cantilever and optical lever, which measures the local height of the sample; and a feedback circuit that attempts to keep the cantilever deflection

constant by adjusting the voltage applied to the scanner. In the event that actual structures or modeled structures of the protein.¹²⁷ In this thesis, Atomic Force Microscopy was used to obtain structural information of FXIII up to high-resolution (nano-scale) by scanning the surface of FXIII-A₂B₂, FXIII-A₂ and FXIII-B₂ with a sharp-ended cantilever.

d. Chemical cross-linking followed by Mass Spectrometry (XL-MS)

Non-covalent interactions are one of the major key-players determining the overall shape, fold and orientation of a biomolecule as well as that of a bio-molecular complex. Accurate determination of these interactions is a key to understanding the structure and function of biological complexes. Native mass spectroscopy of intact proteins offers an excellent tool for structural biologists as it reveals the stoichiometry, topology, and composition. Recent advances also enable determination of the conformation/interaction on the basis of ion mobility on MS. This strategy employs the combination of Native MS and Chemical crosslinking (also known as XL-MS). Mass-spectrometry based chemical cross-linking involves covalently bridging the non-covalently bound residues by using a chemical cross-linking reagent. A very frequently used cross-linker is the Disuccinylamide Suberate (DSS) that belongs to the class of N-hydroxysuccinimide (NHS) esters and cross-links proximal Lysine side chains. The DSS-crosslinking may result into different products which may include intra-molecular, inter-molecular crosslinks or mono-link and loop-links. Each of these cross-links that can later be accurately identified has its own information content depending in which context it is to be used.



As depicted in the figure, after chemical crosslinking by DSS, the crosslinked complex is subjected to proteolysis which fragments the sequences leaving the crosslinks intact. Crosslinked peptides are enriched by Size-exclusion chromatography (SEC). The enriched peptides are then analysed by LC-MS analyses.^{128,129} (Figure 14) The length of the linker determines the precision of the distance restraint implied by an observed crosslink. The linker length of the DSS is ~ 12 Å,

corresponding to an eight-carbon aliphatic chain. However, side chain flexibility on either side can add another $\sim 12 \text{ \AA}$ to this calculation bringing the actual implied distance restraint possibility to approximately $\sim 24 \text{ \AA}$. The distance constraints can be realized within modeling strategies to either dock participating structures to generate a complex or to assemble a multipartite structure into a full-length form. We have used this technique in this thesis to generate full length model of the FXIII-B subunit as well as to model the FXIII-A₂B₂ complex structure.

d. Activity analyses of catalytic Factor XIII-A subunit

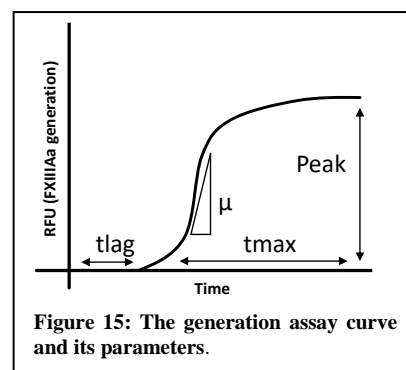
i) End point FXIII activity assays

Since this thesis involved the generation of a large number of FXIII mutant variants, the activity status of these mutants was evaluated by a number of *biochemical, end-point assays* which had variable underlying principles, as follows:

- Photometric FXIII activity assay:** It is based on chromogenic detection of a crosslinked product by the action of FXIII-A transglutaminase activity. Release of ammonia as a by-product of deamidation reaction is utilised in oxidation of NADPH, which is indicator reaction. In the indicator reaction the amount of released ammonia is monitored in a glutamate dehydrogenase catalysed NADPH-dependent reaction. The consumption of NADPH is measured spectrophotometrically by the decrease of absorbance at 340 nm. Within a time window the decrease of absorbance is directly proportional to the FXIII activity.
- Pentylamine incorporation assay:** This is a colorimetric incorporation assay for detection of FXIII activity based on incorporation of 5-(biotinamido) pentylamine (BAPA) into immobilized fibrin/fibrinogen.¹³⁰
- alpha-2-antiplasmin incorporation assay:** Similar to Pentylamine incorporation, the amount of Fibrin crosslinked alpha 2 antiplasmin was calculated by peroxidase conjugated anti-plasmin inhibitor antibody. The end product was hence detected by indicator o-phenylenediamine dihydrochloride, at O.D. 405nm.¹³¹

ii) Generation assay for continuous monitoring of activated FXIII-A (FXIII-Aa)

The real-time monitoring of FXIII-Aa generation for some of the *F13A1* mutated variants, i.e. generation of active FXIII-A molecules was monitored by **FXIII generation assay**.¹³² This is a very physiological assay since unlike the end point assays which employs excess Thrombin as a direct activator, here, the extrinsic pathway of coagulation is initiated by addition of TF/PL, which furthermore activates thrombin required for FXIII-A activation. The assay is performed in a FXIII deficient plasma background with which the recombinant or the plasma sample to be tested is reconstituted based on the investigation being conducted. The continuous generation of FXIII-Aa is monitored with the help of fluorogenic substrate that is highly specific for only the FXIII-Aa molecule and not the zymogenic FXIII-A. This substrate is linked to a quencher which



is split off by the isopeptidase activity of FXIII when it binds the catalytic site of the FXIII-Aa, thereby releasing fluorescence signal, which are further recorded as a continuous FXIII-Aa generation curve.¹³² (Figure 15) Analysis of the curve itself yields a number of parameters. The major parameters derived from FXIII generation assay are: t_{lag} , μ , A , and t_{max} . T_{lag} is the time lag from the TF/PL introduction to the plasma ($t=0$), to the generation of first fluorescent signal ($t=t_{lag}$). An increased t_{lag} , compared to standard plasma explains that the FXIII-A molecule is slowly activating, or has a stronger zymogenic constraint. μ explains the rate of generation of active species, hence is defining the acceleration of the reaction (RFU/time²). An increased μ explains growth rate/slope of the generation curve hence the rate of activation of FXIII-Aa molecules. A is the area under the curve, which explains the availability of active open, catalytic triads of FXIII-A molecule, a downward slope reflects deceleration and probable degeneration of FXIII-A molecule. T_{max} defines the time to peak to maximum number of activated FXIII-Aa species. This may also be proportional to lesser available crude unmodified substrate during the course of reaction. (as the fluorescence signal is imparted by substrate modification, a fast activating FXIII-A will convert the substrate to the end-product in a shorter time compared to a slow active one. Hence a fast activating FXIII-A will either have a shorter t_{lag} , t_{max} , a larger μ and A .

Aim & Outline

Since its discovery as a critical coagulation factor in early 1940s, coagulation Factor XIII has been the subject of clinical and fundamental research for researchers working on coagulation. The last two decades particularly have witnessed an explosion of insights related to this protein especially since the realization that it is in fact a multifunctional protein with roles beyond hemostasis. However, in spite of multiple research groups around the world working on this protein, several structural and functional aspects of this protein remain unknown. These are the aspects that this thesis sets out to resolve.

The first **Aim 1** or **Chapter 2** of this thesis was to generate testable hypothesis that would extend the understanding of FXIII activation, based on what is known so far structurally, functionally and phylogenetically regarding the FXIII. The aim was to generate not only interesting insights into unknown aspects of the protein by in-silico approaches; but also, to provide experimentally testable hypothesis to direct the rest of the objectives of this thesis. Therefore, this thesis provides interesting insights into major structural aspects of FXIII such as activation peptide, calcium binding sites and its activation profile especially in context of both the catalytic FXIII-A and protective/regulatory FXIII-B subunit that the protein is composed.

The second **Aim 2** or **Chapter 3** of the thesis was to investigate the structural and phylogenetic importance of the three Calcium binding sites of FXIII-A subunit that are critical to its activation. In addition, we also delve into how the crosstalk between these binding sites influences FXIII-A activation especially in a thermodynamic sense.

The third **Aim 3** or **Chapter 4** of the thesis focusses on finding pleiotropic roles especially in context of the complement system, for the protective/regulatory FXIII-B subunit since unlike the FXIII-A subunit nothing is known so far for this subunit. The idea was to conduct a preliminary investigation to see if any subsequent leads turned up.

The fourth **Aim 4** or **Chapter 5** of the thesis also focusses on the FXIII-B subunit. In this Chapter we investigate the roles of structural disulfides present on FXIII-B subunit sushi domains, and how individually disrupting the 20 disulfides is affecting the protein's stability, secretion and oligomerization. This Chapter gives us major insights into the functional patterns underlying the structurally repetitive sushi domains of the FXIII-B subunit.

The fifth and last **Aim 5** or **Chapter 6** finally concludes the thesis by looking at the structural and functional aspects of the complete FXIII-A₂B₂ heterotetrameric complex. In this chapter we detail the creation and functional features of a structural model of the FXIII-A₂B₂ heterotetrameric complex based on a boot-strapped integrative hybrid approach. The chapter aims at delineating the structural features of this complex as found in plasma, and how these features are responsible for a timed activation and regulation of FXIII in plasma. Additionally, this chapter also investigate the thermodynamic patterns underlying the assembly,

and activation of FXIII and how the complex interface may be a potential underlying driver of unexplained heterozygous FXIII mutations observed in mild FXIII deficiency.

Bibliography

1. Spronk, H. M. H., Govers-Riemslog, J. W. P. & Cate, H. ten. The blood coagulation system as a molecular machine. *BioEssays : news and reviews in molecular, cellular and developmental biology* **25**, 1220–1228; 10.1002/bies.10360 (2003).
2. Lippi, G., Favaloro, E. J., Franchini, M. & Guidi, G. C. Milestones and perspectives in coagulation and hemostasis. *Semin Thromb Hemost*, 9–22 (2009).
3. Dahlbäck, B. Blood coagulation. *Lancet (London, England)* **355**, 1627–1632; 10.1016/S0140-6736(00)02225-X (2000).
4. Mann, K. G., van't Veer, C., Cawthorn, K. & Butenas, S. The role of the tissue factor pathway in initiation of coagulation. *Blood coagulation & fibrinolysis : an international journal in haemostasis and thrombosis* **9 Suppl 1**, S3-7 (1998).
5. Lewis, B. A., Freyssinet, J. M. & Holbrook, J. J. An equilibrium study of metal ion binding to human plasma coagulation factor XIII. *The Biochemical journal* **169**, 397–402; 10.1042/bj1690397 (1978).
6. Nesheim, M. *et al.* Thrombin, thrombomodulin and TAFI in the molecular link between coagulation and fibrinolysis. *Thrombosis and haemostasis* **78**, 386–391 (1997).
7. Adány, R. & Bárdos, H. Factor XIII subunit A as an intracellular transglutaminase. *Cellular and molecular life sciences : CMLS* **60**, 1049–1060; 10.1007/s00018-003-2178-9 (2003).
8. Helms, C. C., Ariëns, R. A. S., Uitte de Willige, S., Standeven, K. F. & Guthold, M. α - α Cross-links increase fibrin fiber elasticity and stiffness. *Biophysical journal* **102**, 168–175; 10.1016/j.bpj.2011.11.4016 (2012).
9. Francis, R. T., McDonagh, J. & Mann, K. G. Factor V is a substrate for the transamidase factor XIIIa. *The Journal of biological chemistry* **261**, 9787–9792 (1986).
10. Barkan, G., and Gaspar, A. Zur Frage der reversibilitat der Fibringerinung II. *Biochem. Ztschr.*, 291–301 (1923).
11. Robbins, K. C. A study on the conversion of Fibrinogen to fibrin. *Amer.J.Physiol.*, 581–588 (1944).
12. Laki, K. & Lóránd, L. On the Solubility of Fibrin Clots. *Science (New York, N.Y.)* **108**, 280; 10.1126/science.108.2802.280 (1948).
13. Lorand, L. Fibrin Clots. some properties on the "serum factor". *Nature*, 694–696 (1950).
14. BULUK, K., JANUSZKO, T. & OLBROMSKI, J. Conversion of Fibrin to Desmofibrin. *Nature* **191**, 1093–1094; 10.1038/1911093b0 (1961).
15. Duckert, F. Le Facteur XIII et la proteine XIII. *Nouv. Rev. Franc. Hematol.* **10**, 685–690 (1970).
16. Fuller, G.M., and Doolittle, R.F. The formtion of crosslinked fibrins: evidence for the involvement of lysine e-amino groups. *Biochem.Biophys.Res.Commun.* **25**, 694–700 (1966).
17. Lorand, L., KONISHI, K. & JACOBSEN, A. Transpeptidation mechanism in blood clotting. *Nature* **194**, 1148–1149; 10.1038/1941148a0 (1962).
18. Takagi, J. *et al.* Identification of factor-XIIIa-reactive glutaminy residues in the propolypeptide of bovine von Willebrand factor. *European journal of biochemistry* **232**, 773–777 (1995).
19. Bohn H, Haupt, H. and Kranz, T. Die molekulare strukture der fibrinstabilisierenden faktoren des menschen. *Blood* **25**, 235–248 (1972).
20. Schwartz, M.L., Pizzo, s.V., Hill, R.L., and McKee, P.A. Human factor XIII from plasma and platemets. molecular weights, subunit structures, proteolytic activation and cross-linking of fibrinogen and fibrin. *J. biol.chem.* **248**, 1395–1407 (1973).
21. Muszbek, L., Bereczky, Z., Bagoly, Z., Komáromi, I. & Katona, É. Factor XIII: a coagulation factor with multiple plasmatic and cellular functions. *Physiological reviews* **91**, 931–972; 10.1152/physrev.00016.2010 (2011).
22. Kida, M., Souri, M., Yamamoto, M., Saito, H. & Ichinose, A. Transcriptional regulation of cell type-specific expression of the TATA-less A subunit gene

- for human coagulation factor XIII. *The Journal of biological chemistry* **274**, 6138–6147; 10.1074/jbc.274.10.6138 (1999).
23. Inoue, Y., Peters, L. L., Yim, S. H., Inoue, J. & Gonzalez, F. J. Role of hepatocyte nuclear factor 4alpha in control of blood coagulation factor gene expression. *Journal of molecular medicine (Berlin, Germany)* **84**, 334–344; 10.1007/s00109-005-0013-5 (2006).
 24. Muszbek, L., Bagoly, Z., Cairo, A. & Peyvandi, F. Novel aspects of factor XIII deficiency. *Current opinion in hematology* **18**, 366–372; 10.1097/MOH.0b013e3283497e3e (2011).
 25. Mitchell, J. L. & Mutch, N. J. Novel aspects of platelet factor XIII function. *Thrombosis research* **141 Suppl 2**, S17-21; 10.1016/S0049-3848(16)30356-5 (2016).
 26. Kiesselbach, T. H. & Wagner, R. H. Demonstration of factor XIII in human megakaryocytes by a fluorescent antibody technique. *Annals of the New York Academy of Sciences* **202**, 318–328; 10.1111/j.1749-6632.1972.tb16344.x (1972).
 27. Cordell, P. A. *et al.* Association of coagulation factor XIII-A with Golgi proteins within monocyte-macrophages: implications for subcellular trafficking and secretion. *Blood* **115**, 2674–2681; 10.1182/blood-2009-08-231316 (2010).
 28. Cohen, I., Blankenberg, T. A., Borden, D., Kahn, D. R. & Veis, A. Factor XIIIa-catalyzed cross-linking of platelet and muscle actin. Regulation by nucleotides. *Biochimica et biophysica acta* **628**, 365–375; 10.1016/0304-4165(80)90386-4 (1980).
 29. Nakano, Y., Al-Jallad, H. F., Mousa, A. & Kaartinen, M. T. Expression and localization of plasma transglutaminase factor XIIIa in bone. *The journal of histochemistry and cytochemistry : official journal of the Histochemistry Society* **55**, 675–685; 10.1369/jhc.6A7091.2007 (2007).
 30. Backer-Royer, C. de, Traoré, F. & Meunier, J. C. Purification and properties of factor XIII from human placenta. *The International journal of biochemistry* **24**, 91–97 (1992).
 31. Kiss, F. *et al.* Leukemic lymphoblasts, a novel expression site of coagulation factor XIII subunit A. *Thrombosis and haemostasis* **96**, 176–182 (2006).
 32. Kristiansen, G. K. & Andersen, M. D. Reversible activation of cellular factor XIII by calcium. *The Journal of biological chemistry* **286**, 9833–9839; 10.1074/jbc.M110.174128 (2011).
 33. Wolberg, A. S. Plasma factor XIII: understanding the 99%. *Blood* **123**, 1623–1624; 10.1182/blood-2014-01-549683 (2014).
 34. Katona, E. *et al.* Interaction of factor XIII subunits. *Blood* **123**, 1757–1763; 10.1182/blood-2013-10-533596 (2014).
 35. Yee, V. C. *et al.* Three-dimensional structure of a transglutaminase: human blood coagulation factor XIII. *Proceedings of the National Academy of Sciences of the United States of America* **91**, 7296–7300; 10.1073/pnas.91.15.7296 (1994).
 36. Fox, B.A., Yee, V.C., Pedersen, L.C., Le Trong, I., Bishop, P.D., Stenkamp, R.E., Teller, D.C. Human Factor XIII with Yttrebiun bound in the ion site. *J Biol Chem* **274**, 4917–4923 (1999).
 37. Stieler, M. *et al.* Structure of active coagulation factor XIII triggered by calcium binding: basis for the design of next-generation anticoagulants. *Angewandte Chemie (International ed. in English)* **52**, 11930–11934; 10.1002/anie.201305133 (2013).
 38. Yee, V. C., Pedersen, L. C., Bishop, P. d., Stenkamp, R. E. & Teller, D. C. Structural evidence that the activation peptide is not released upon thrombin cleavage of factor XIII. *Thrombosis research* **78**, 389–397; 10.1016/0049-3848(95)00072-Y (1995).
 39. Takahashi, N. Structure and function of blood coagulation factor XIII (transglutaminase). *Tanpakushitsu kakusan koso. Protein, nucleic acid, enzyme* **32**, 1041–1059 (1987).
 40. Lorand, L. Factor XIII: structure, activation, and interactions with fibrinogen and fibrin. *Annals of the New York Academy of Sciences* **936**, 291–311; 10.1111/j.1749-6632.2001.tb03516.x (2001).
 41. Gupta, S. *et al.* Revisiting the mechanism of coagulation factor XIII activation and regulation from a structure/functional perspective. *Scientific reports* **6**, 30105; 10.1038/srep30105 (2016).
 42. Muszbek, L., Yee, V. C. & Hevessy, Z. Blood coagulation factor XIII: structure and function. *Thrombosis research* **94**, 271–305 (1999).
 43. Carrell, N. A., Erickson, H. P. & McDonagh, J. Electron microscopy and hydrodynamic properties of factor XIII subunits. *The Journal of biological chemistry* **264**, 551–556 (1989).
 44. Skerka, C., Chen, Q., Fremeaux-Bacchi, V. & Roumenina, L. T. Complement factor H related proteins (CFHRs). *Molecular immunology* **56**, 170–180; 10.1016/j.molimm.2013.06.001 (2013).

45. Sourì, M., Koseki-Kuno, S., Takeda, N., Degen, J. L. & Ichinose, A. Administration of factor XIII B subunit increased plasma factor XIII A subunit levels in factor XIII B subunit knock-out mice. *International journal of hematology* **87**, 60–68; 10.1007/s12185-007-0005-z (2008).
46. Sourì, M., Kaetsu, H. & Ichinose, A. Sushi domains in the B subunit of factor XIII responsible for oligomer assembly. *Biochemistry* **47**, 8656–8664; 10.1021/bi8006143 (2008).
47. Patthy, L. Detecting homology of distantly related proteins with consensus sequences. *Journal of molecular biology* **198**, 567–577; 10.1016/0022-2836(87)90200-2 (1987).
48. Komáromi, I., Bagoly, Z. & Muszbek, L. Factor XIII: novel structural and functional aspects. *Journal of thrombosis and haemostasis : JTH* **9**, 9–20; 10.1111/j.1538-7836.2010.04070.x (2011).
49. Fox, B. A. *et al.* Identification of the calcium binding site and a novel ytterbium site in blood coagulation factor XIII by x-ray crystallography. *The Journal of biological chemistry* **274**, 4917–4923; 10.1074/jbc.274.8.4917 (1999).
50. Ambrus, A. *et al.* Calcium binding of transglutaminases: a ⁴³Ca NMR study combined with surface polarity analysis. *Journal of biomolecular structure & dynamics* **19**, 59–74; 10.1080/07391102.2001.10506720 (2001).
51. Handrkova, H., Schroeder, V. & Kohler, H. P. The activation peptide of coagulation factor XIII is vital for its expression and stability. *Journal of thrombosis and haemostasis : JTH* **13**, 1449–1458; 10.1111/jth.13035 (2015).
52. Lorand, L. Factor XIII and the clotting of fibrinogen: from basic research to medicine. *Journal of thrombosis and haemostasis : JTH* **3**, 1337–1348; 10.1111/j.1538-7836.2005.01213.x (2005).
53. Keillor, J. W., Clouthier, C. M., Apperley, K. Y. P., Akbar, A. & Mulani, A. Acyl transfer mechanisms of tissue transglutaminase. *Bioorganic chemistry* **57**, 186–197; 10.1016/j.bioorg.2014.06.003 (2014).
54. Folk, J. E. Mechanism of action of guinea pig liver transglutaminase. VI. Order of substrate addition. *The Journal of biological chemistry* **244**, 3707–3713 (1969).
55. Hitomi K, Kojima S, Fesus L. *Transglutaminase: Multiple functional modifiers and targets for new drug discovery.* (Springer, 2017).
56. Shen, L. & Lorand, L. Contribution of fibrin stabilization to clot strength. Supplementation of factor XIII-deficient plasma with the purified zymogen. *The Journal of clinical investigation* **71**, 1336–1341; 10.1172/jci110885 (1983).
57. Greenberg, C. S. & Shuman, M. A. The zymogen forms of blood coagulation factor XIII bind specifically to fibrinogen. *The Journal of biological chemistry* **257**, 6096–6101 (1982).
58. Greenberg, C. S., Enghild, J. J., Mary, A., Dobson, J. V. & Achyuthan, K. E. Isolation of a fibrin-binding fragment from blood coagulation factor XIII capable of cross-linking fibrin(ogen). *The Biochemical journal* **256**, 1013–1019; 10.1042/bj2561013 (1988).
59. Ariëns, R. A. S., Lai, T.-S., Weisel, J. W., Greenberg, C. S. & Grant, P. J. Role of factor XIII in fibrin clot formation and effects of genetic polymorphisms. *Blood* **100**, 743–754; 10.1182/blood.v100.3.743 (2002).
60. Byrnes JR, Duval C, Wang Y, Hansen CE, Ahn B, Mooberry MJ, Clark MA, Johnsen JM, Lord ST, Lam WA, Meijers JC, Ni H, Ariëns RA, Wolberg AS. Factor XIIIa-dependent retention of red blood cells in clots is mediated by fibrin a-chain crosslinking. *Blood* **126(16)**, 1940–1948 (2015).
61. Bagoly, Z., Haramura, G. & Muszbek, L. Down-regulation of activated factor XIII by polymorphonuclear granulocyte proteases within fibrin clot. *Thrombosis and haemostasis* **98**, 359–367 (2007).
62. Hur, W. S. *et al.* Coagulation factor XIIIa is inactivated by plasmin. *Blood* **126**, 2329–2337; 10.1182/blood-2015-07-650713 (2015).
63. Dickneite, G. *et al.* Coagulation factor XIII: a multifunctional transglutaminase with clinical potential in a range of conditions. *Thrombosis and haemostasis* **113**, 686–697; 10.1160/TH14-07-0625 (2015).
64. Schroeder, V. & Kohler, H. P. Factor XIII: Structure and Function. *Seminars in thrombosis and hemostasis* **42**, 422–428; 10.1055/s-0036-1571341 (2016).
65. Tsujimoto, I., Moriya, K., Sakai, K., Dickneite, G. & Sakai, T. Critical role of factor XIII in the initial stages of carbon tetrachloride-induced adult liver remodeling. *The American journal of pathology* **179**, 3011–3019; 10.1016/j.ajpath.2011.08.037 (2011).
66. Hardes, K., Zouhir Hammamy, M. & Steinmetzer, T. Synthesis and characterization of novel fluorogenic

- substrates of coagulation factor XIII-A. *Analytical biochemistry* **442**, 223–230; 10.1016/j.ab.2013.07.043 (2013).
67. Nikolajsen, C. L., Dyrlund, T. F., Poulsen, E. T., Enghild, J. J. & Scavenius, C. Coagulation factor XIIIa substrates in human plasma: identification and incorporation into the clot. *The Journal of biological chemistry* **289**, 6526–6534; 10.1074/jbc.M113.517904 (2014).
68. Csoz, E., Meskó, B. & Fésüs, L. Transdab wiki: the interactive transglutaminase substrate database on web 2.0 surface. *Amino acids* **36**, 615–617; 10.1007/s00726-008-0121-y (2009).
69. Töröcsik, D. *et al.* Detection of factor XIII-A is a valuable tool for distinguishing dendritic cells and tissue macrophages in granuloma annulare and necrobiosis lipoidica. *Journal of the European Academy of Dermatology and Venereology : JEADV* **28**, 1087–1096; 10.1111/jdv.12290 (2014).
70. Nickoloff, B. & Griffiths, C. Factor XIIIa-expressing dermal dendrocytes in AIDS-associated cutaneous Kaposi's sarcomas. *Science* **243**, 1736–1737; 10.1126/science.2564703 (1989).
71. Deguchi, M., Aiba, S., Ohtani, H., Nagura, H. & Tagami, H. Comparison of the distribution and numbers of antigen-presenting cells among T-lymphocyte-mediated dermatoses: CD1a+, factor XIIIa+, and CD68+ cells in eczematous dermatitis, psoriasis, lichen planus and graft-versus-host disease. *Archives of dermatological research* **294**, 297–302; 10.1007/s00403-002-0334-y (2002).
72. Gemmati, D. *et al.* Factor XIII-A dynamics in acute myocardial infarction: a novel prognostic biomarker? *Thrombosis and haemostasis* **114**, 123–132; 10.1160/TH14-11-0952 (2015).
73. Kimura, S. & Aoki, N. Cross-linking site in fibrinogen for alpha 2-plasmin inhibitor. *The Journal of biological chemistry* **261**, 15591–15595 (1986).
74. Valnickova, Z. & Enghild, J. J. Human procarboxypeptidase U, or thrombin-activable fibrinolysis inhibitor, is a substrate for transglutaminases. Evidence for transglutaminase-catalyzed cross-linking to fibrin. *The Journal of biological chemistry* **273**, 27220–27224; 10.1074/jbc.273.42.27220 (1998).
75. Sane, D. C. *et al.* Vitronectin is a substrate for transglutaminases. *Biochemical and biophysical research communications* **157**, 115–120; 10.1016/s0006-291x(88)80020-2 (1988).
76. Podor, T. J. *et al.* Type 1 plasminogen activator inhibitor binds to fibrin via vitronectin. *The Journal of biological chemistry* **275**, 19788–19794; 10.1074/jbc.M908079199 (2000).
77. Jensen, P. H. *et al.* A unique interhelical insertion in plasminogen activator inhibitor-2 contains three glutamines, Gln83, Gln84, Gln86, essential for transglutaminase-mediated cross-linking. *The Journal of biological chemistry* **269**, 15394–15398 (1994).
78. Harpel, P. C. Alpha2-plasmin inhibitor and alpha2-macroglobulin-plasmin complexes in plasma. Quantitation by an enzyme-linked differential antibody immunosorbent assay. *The Journal of clinical investigation* **68**, 46–55; 10.1172/jci110253 (1981).
79. Wassmann, S. *et al.* Inhibition of diet-induced atherosclerosis and endothelial dysfunction in apolipoprotein E/angiotensin II type 1A receptor double-knockout mice. *Circulation* **110**, 3062–3067; 10.1161/01.CIR.0000137970.47771.AF (2004).
80. AbdAlla, S., Lothar, H., Langer, A., el Faramawy, Y. & Quitterer, U. Factor XIIIa transglutaminase crosslinks AT1 receptor dimers of monocytes at the onset of atherosclerosis. *Cell* **119**, 343–354; 10.1016/j.cell.2004.10.006 (2004).
81. Dardik, R. *et al.* Novel proangiogenic effect of factor XIII associated with suppression of thrombospondin 1 expression. *Arteriosclerosis, thrombosis, and vascular biology* **23**, 1472–1477; 10.1161/01.ATV.0000081636.25235.C6 (2003).
82. Dardik, R., Loscalzo, J. & Inbal, A. Factor XIII (FXIII) and angiogenesis. *Journal of thrombosis and haemostasis : JTH* **4**, 19–25; 10.1111/j.1538-7836.2005.01473.x (2006).
83. Dale, G. L. *et al.* Stimulated platelets use serotonin to enhance their retention of procoagulant proteins on the cell surface. *Nature* **415**, 175–179; 10.1038/415175a (2002).
84. Sadler, J. E. Biochemistry and genetics of von Willebrand factor. *Annual review of biochemistry* **67**, 395–424; 10.1146/annurev.biochem.67.1.395 (1998).
85. Mosher, D. F. Cross-linking of fibronectin to collagenous proteins. *Molecular and cellular biochemistry* **58**, 63–68 (1984).
86. Brotchie, H. & Wakefield, D. Fibronectin: structure, function and significance in wound healing. *The*

- Australasian journal of dermatology* **31**, 47–56 (1990).
87. Bale, M. D., Westrick, L. G. & Mosher, D. F. Incorporation of thrombospondin into fibrin clots. *The Journal of biological chemistry* **260**, 7502–7508 (1985).
 88. Roberts, W., Magwenzi, S., Aburima, A. & Naseem, K. M. Thrombospondin-1 induces platelet activation through CD36-dependent inhibition of the cAMP/protein kinase A signaling cascade. *Blood* **116**, 4297–4306; 10.1182/blood-2010-01-265561 (2010).
 89. Huh, M. M., Schick, B. P., Schick, P. K. & Colman, R. W. Covalent crosslinking of human coagulation factor V by activated factor XIII from guinea pig megakaryocytes and human plasma. *Blood* **71**, 1693–1702 (1988).
 90. Mutch, N. J. *et al.* Model thrombi formed under flow reveal the role of factor XIII-mediated cross-linking in resistance to fibrinolysis. *Journal of thrombosis and haemostasis : JTH* **8**, 2017–2024; 10.1111/j.1538-7836.2010.03963.x (2010).
 91. Hada, M., Kaminski, M., Bockenstedt, P. & McDonagh, J. Covalent crosslinking of von Willebrand factor to fibrin. *Blood* **68**, 95–101 (1986).
 92. Francis, J. L. *Fibrinogen, fibrin stabilisation and fibrinolysis. Clinical, biochemical and laboratory aspects* (VCH; Ellis Horwood, Weinheim, Chichester, 1988).
 93. Myneni, V. D., Hitomi, K. & Kaartinen, M. T. Factor XIII-A transglutaminase acts as a switch between preadipocyte proliferation and differentiation. *Blood* **124**, 1344–1353; 10.1182/blood-2013-12-543223 (2014).
 94. Piercy-Kotb, S. A. *et al.* Factor XIIIa transglutaminase expression and secretion by osteoblasts is regulated by extracellular matrix collagen and the MAP kinase signaling pathway. *Journal of cellular physiology* **227**, 2936–2946; 10.1002/jcp.23040 (2012).
 95. Richardson, V. R., Cordell, P., Standeven, K. F. & Carter, A. M. Substrates of Factor XIII-A: roles in thrombosis and wound healing. *Clinical science (London, England : 1979)* **124**, 123–137; 10.1042/CS20120233 (2013).
 96. Tahlan, A. & Ahluwalia, J. Factor XIII: congenital deficiency factor XIII, acquired deficiency, factor XIII A-subunit, and factor XIII B-subunit. *Archives of pathology & laboratory medicine* **138**, 278–281; 10.5858/arpa.2012-0639-RS (2014).
 97. Biswas, A., Ivaskevicius, V., Seitz, R., Thomas, A. & Oldenburg, J. An update of the mutation profile of Factor 13 A and B genes. *Blood reviews* **25**, 193–204; 10.1016/j.blre.2011.03.001 (2011).
 98. Franchini, M., Frattini, F., Crestani, S. & Bonfanti, C. Acquired FXIII inhibitors: a systematic review. *Journal of thrombosis and thrombolysis* **36**, 109–114; 10.1007/s11239-012-0818-3 (2013).
 99. Ichinose, A. Hemorrhagic acquired factor XIII (13) deficiency and acquired hemorrhophilia 13 revisited. *Seminars in thrombosis and hemostasis* **37**, 382–388; 10.1055/s-0031-1276587 (2011).
 100. Ichinose, A. Inhibitors of Factor XIII/13 in Older Patients. *Semin Thromb Hemost* **40**, 704–711; 10.1055/s-0034-1390151 (2014).
 101. Souri, M. *et al.* Non-autoimmune combined factor XIII A and B subunit deficiencies in rheumatoid arthritis patients treated with anti-interleukin-6 receptor monoclonal antibody (tocilizumab). *Thrombosis research* **140**, 100–105; 10.1016/j.thromres.2016.02.026 (2016).
 102. Péntzes, K. *et al.* Alloantibody developed in a factor XIII A subunit deficient patient during substitution therapy; characterization of the antibody. *Haemophilia* **22**, 268–275; 10.1111/hae.12786 (2016).
 103. Thomas, A., Biswas, A., Ivaskevicius, V. & Oldenburg, J. Structural and functional influences of coagulation factor XIII subunit B heterozygous missense mutants. *Molecular genetics & genomic medicine* **3**, 258–271; 10.1002/mgg3.138 (2015).
 104. Ivaskevicius, V. *et al.* Mutations affecting disulphide bonds contribute to a fairly common prevalence of F13B gene defects: results of a genetic study in 14 families with factor XIII B deficiency. *Haemophilia : the official journal of the World Federation of Hemophilia* **16**, 675–682; 10.1111/j.1365-2516.2010.02207.x (2010).
 105. Biswas, A., Thomas, A., Bevans, C. G., Ivaskevicius, V. & Oldenburg, J. In vitro secretion deficits are common among human coagulation factor XIII subunit B missense mutants: correlations with patient phenotypes and molecular models. *Human mutation* **34**, 1490–1500; 10.1002/humu.22391 (2013).
 106. Biswas, A., Ivaskevicius, V., Thomas, A. & Oldenburg, J. Coagulation factor XIII deficiency.

- Diagnosis, prevalence and management of inherited and acquired forms. *Hamostaseologie* **34**, 160–166; 10.5482/HAMO-13-08-0046 (2014).
107. Biswas, A. *et al.* Eight novel F13A1 gene missense mutations in patients with mild FXIII deficiency: in silico analysis suggests changes in FXIII-A subunit structure/function. *Annals of hematology* **93**, 1665–1676; 10.1007/s00277-014-2102-4 (2014).
 108. Nugent, D. Corifact™/Fibrogammin® P in the prophylactic treatment of hereditary factor XIII deficiency: results of a prospective, multicenter, open-label study. *Thrombosis research* **130 Suppl 2**, S12-4; 10.1016/S0049-3848(13)70005-7 (2012).
 109. Abdel-Samad, N. Treatment with Recombinant Factor XIII (Tretten) in a Pregnant Woman with Factor XIII Deficiency. *The American journal of case reports* **18**, 436–439; 10.12659/ajcr.901502 (2017).
 110. Kattula, S. *et al.* Factor XIII in plasma, but not in platelets, mediates red blood cell retention in clots and venous thrombus size in mice. *Blood advances* **2**, 25–35; 10.1182/bloodadvances.2017011890 (2018).
 111. Solomon, C. *et al.* Safety of Factor XIII Concentrate: Analysis of More than 20 Years of Pharmacovigilance Data. *Transfusion medicine and hemotherapy : offzielles Organ der Deutschen Gesellschaft fur Transfusionsmedizin und Immunhamatologie* **43**, 365–373; 10.1159/000446813 (2016).
 112. Aleman, M. M. *et al.* Factor XIII activity mediates red blood cell retention in venous thrombi. *The Journal of clinical investigation* **124**, 3590–3600; 10.1172/JCI75386 (2014).
 113. Lorand, L., Stern, A. M. & Velasco, P. T. Novel inhibitors against the transglutaminase-catalysed crosslinking of lens proteins. *Experimental eye research* **66**, 531–536; 10.1006/exer.1997.0463 (1998).
 114. Barsigian, C., Stern, A. M. & Martinez, J. Tissue (type II) transglutaminase covalently incorporates itself, fibrinogen, or fibronectin into high molecular weight complexes on the extracellular surface of isolated hepatocytes. Use of 2-(2-oxopropyl)thio imidazolium derivatives as cellular transglutaminase inactivators. *The Journal of biological chemistry* **266**, 22501–22509 (1991).
 115. van Zundert, G. C. P. & Bonvin, A. M. J. J. Modeling protein-protein complexes using the HADDOCK webserver "modeling protein complexes with HADDOCK". *Methods in molecular biology (Clifton, N.J.)* **1137**, 163–179; 10.1007/978-1-4939-0366-5_12 (2014).
 116. Vakser, I. A. Protein-protein docking: from interaction to interactome. *Biophysical journal* **107**, 1785–1793; 10.1016/j.bpj.2014.08.033 (2014).
 117. Huang, S.-Y. Exploring the potential of global protein-protein docking: an overview and critical assessment of current programs for automatic ab initio docking. *Drug discovery today* **20**, 969–977; 10.1016/j.drudis.2015.03.007 (2015).
 118. Kreiger E. *The last mile of protein folding problem: A pilgrim's staff and skid-proof boots.* YASARA. (2004).
 119. Yang, J. & Zhang, Y. Protein Structure and Function Prediction Using I-TASSER. *Current protocols in bioinformatics* **52**, 5.8.1-15; 10.1002/0471250953.bi0508s52 (2015).
 120. Xu, D., Jaroszewski, L., Li, Z. & Godzik, A. AIDA: ab initio domain assembly server. *Nucleic acids research* **42**, W308-13; 10.1093/nar/gku369 (2014).
 121. Wieman, H., Tøndel, K., Anderssen, E. & Drabløs, F. Homology-based modelling of targets for rational drug design. *Mini reviews in medicinal chemistry* **4**, 793–804 (2004).
 122. Śledź, P. & Caflisch, A. Protein structure-based drug design: from docking to molecular dynamics. *Current opinion in structural biology* **48**, 93–102; 10.1016/j.sbi.2017.10.010 (2018).
 123. Muratcioglu, S., Guven-Maiorov, E., Keskin, Ö. & Gursoy, A. Advances in template-based protein docking by utilizing interfaces towards completing structural interactome. *Current opinion in structural biology* **35**, 87–92; 10.1016/j.sbi.2015.10.001 (2015).
 124. Amaro, R. E. *et al.* Ensemble Docking in Drug Discovery. *Biophysical journal* **114**, 2271–2278; 10.1016/j.bpj.2018.02.038 (2018).
 125. Johnson, R. A., Manley, O. M., Spuches, A. M. & Grosseohme, N. E. Dissecting ITC data of metal ions binding to ligands and proteins. *Biochimica et biophysica acta* **1860**, 892–901; 10.1016/j.bbagen.2015.08.018 (2016).
 126. Falconer, R. J. Applications of isothermal titration calorimetry - the research and technical

- developments from 2011 to 2015. *Journal of molecular recognition : JMR* **29**, 504–515; 10.1002/jmr.2550 (2016).
127. Pleshakova TO, Bukharina NS, Archakov AI, Ivanov YD. Atomic Force Microscopy for Protein Detection and Their Physicochemical Characterization. *Int J Mol Sci.* **19(4)**, pii: E1142 (2018).
128. Merkley, E. D., Cort, J. R. & Adkins, J. N. Cross-linking and mass spectrometry methodologies to facilitate structural biology: finding a path through the maze. *Journal of structural and functional genomics* **14**, 77–90; 10.1007/s10969-013-9160-z (2013).
129. Leitner, A., Faini, M., Stengel, F. & Aebersold, R. Crosslinking and Mass Spectrometry: An Integrated Technology to Understand the Structure and Function of Molecular Machines. *Trends in biochemical sciences* **41**, 20–32; 10.1016/j.tibs.2015.10.008 (2016).
130. Philippou, H. *et al.* Roles of low specificity and cofactor interaction sites on thrombin during factor XIII activation. Competition for cofactor sites on thrombin determines its fate. *The Journal of biological chemistry* **278**, 32020–32026; 10.1074/jbc.M305364200 (2003).
131. Dunn, E. J., Philippou, H., Ariëns, R. A. S. & Grant, P. J. Molecular mechanisms involved in the resistance of fibrin to clot lysis by plasmin in subjects with type 2 diabetes mellitus. *Diabetologia* **49**, 1071–1080; 10.1007/s00125-006-0197-4 (2006).
132. Dodt, J., Volkers, P. & Seitz, R. Factor XIIIa generation assay: a tool for studying factor XIII function in plasma. *Analytical biochemistry* **439**, 145–151; 10.1016/j.ab.2013.04.012 (2013).

Acknowledgement

My PhD has been a very special part of my life. These “almost five years”, were like a whirlpool pushing me into the depression currents and throwing me out in the air of satisfaction at the same time. After years of wait and struggle a PhD student waits to write this page, and I must say that today I am overwhelmed, emotional, satisfied, proud and thankful for witnessing this very thesis coming to an end. I thank you for giving importance to this page and reading it. If at all, I miss out mentioning someone here, trust me that you are counted even if you are not mentioned here.

This thesis wouldn't have been feasible by the kind support, and guidance of my principle investigator Prof. Dr. med. Johannes Oldenburg. He is the one who always trusted me and encouraged me. His passion towards research, care towards hemophiliacs and never-dying positive attitude has inspired me a lot, and helped me developing into a better person than what I was before. It's a great honor being a part of your research team sir.

Next, I would like to mention my sincere gratitude towards my mentor, group-leader, and very good friend PD Dr. Arijit Biswas, for keeping faith in me, and helping me sail-out through this right from the beginning. He proposed the project, designed the thesis and has been a great help in writing down this work. I especially thank you for the *in silico* support. This thesis is possible today only due to his efforts, help and not-to-forget, his criticism that improved me on a daily basis. His support, scientific discussions, networks, collaborative and managerial skills inspired me, and I am sure will help me in the coming future. I thank you for trusting me, and giving me freedom to design and perform experiments at my own. You have indeed been the “cool-boss”.

I would also like to express my gratitude towards my second supervisor Prof Dr. Diana Imhof, who constantly motivated me. I am thankful for her support, critical analyses of my PhD work, and mind-storming discussions. Your encouragement and support has made me more strong and confident, as a researcher and a woman. I thank AG Imhof (especially Ms. Charlotte Bäuml), for support and fun-times we shared together while working at the Pharmacy institute.

I thank Prof. Dr. Dr. Hartmut Micheal, the GPCR group and every member of Department of Molecular Membrane Biology (MPI-Biophysics, Frankfurt), who made my stay easy in Frankfurt, where I stayed for first two years of my PhD. A special thanks to my great friends and mentors, Dr. Christoph Reinhart and Dr. Christoph Krettl, who taught me almost every concept of Protein biochemistry. I would like to thank Ms. Gabi Mauel and Ms Sabine Buschmann for support.

I thank PD Dr. Johannes Dodt for his excellent support with FXIII generation assays, at Langen. I thank Prof Dr. Helen Philippou and Prof Dr. Laszlo Muszbek, who are pioneers of the FXIII

community, for encouraging my work. I thank the working group of Prof Dr. Eva-Maria Mandelkow at the CAESER Forschungszentrum Bonn, for providing me access to Atomic Force microscopy and Akta facilities. A special mention of Dr. SenthilVelrajan Kaniyappan, whose expertise in AFM has helped me in resolving the structure of FXIII complex.

At my institute I would like to thank all my co-workers for a friendly and supportive yet competitive atmosphere with positive energy which helped me perform the best all throughout these years. I thank Dr Hamideh Yadegari for being a great friend and troubleshooting my difficulties in the lab with her expertise. I thank PD Dr med Vytatus Ivaskevicius for FXIII clinical support. I thank all the former students of my group, who stayed for any length of the time during these years. The time was wonderful with all of you (Dr Anne Thomas, Dr Mohd Suhail Akhter, Dr Amit Sharma, Nadia Mir-Montzeri, Isabelle Patricia Claus, Sakthi Swaminathan). Thanks for giving a homely experience. I express my gratitude towards Mr. Mohd Ahmer Jamil, for a supportive and productive office atmosphere. I would like to thank the German transport services, for smooth commutes in between the labs these four years (Bonn-Frankfurt-Bonn).

No words are ever enough for the constant support, motivation and encouragement I have been getting from my friends. A special mention of Dr Monu Kaushik and Dr Hundeeep Kaur; from Frankfurt, who have always been there to ease out my jitters, in my ups-and-downs, professionally as well as personally. Thanks for keeping up with me and being my person. I would also like to mention my other friends, Lakshmi, Wenxia, Sandra, Maria, Ruth, Abha and many more who helped me sail through my toughest times away from home.

I am falling short of words on expressing my gratitude towards my family, which has been my back-bone ever since. A special thanks to my life-support-system, my husband Prahlad, who was patient, understanding and supportive all through-out since the time I moved out of India for PhD. I guess I owe him a life-time acknowledgement for this. My parents who never slept a single night without talking to me. Your great advises helped me during the tough times. My brother, Dr Abhinav Agrahari, who patiently handled all my mood-loops, de-loops, frustrations and just stopped me from giving-up whenever I was at the verge of losing it all. My Parents-in-laws, who are proud of me and who never stop encouraging me. Thank you for your support. My brother-in-law(s) for their constant fun-talks, the laughter we shared has made this a little easier.

In the end, I would like to thank the almighty, for helping me fulfill my dream, my way.

Thank you, Germany!

Chapter 2

Published Article

Revisiting the mechanism of coagulation factor XIII activation and regulation from a structure/functional perspective

Sneha Gupta, Arijit Biswas, Mohammad Suhail Akhter, Christoph Krettler, Christoph Reinhart, Johannes Dodt, Andreas Reuter, Helen Philippou, Vytautas Ivaskevicius & Johannes Oldenburg

A brief synopsis:

The human Coagulation Factor XIII plasma transglutaminase complex, is responsible for covalent crosslinking of pre-formed fibrin clots, providing clot stability as well as resistance to premature fibrinolysis of clot. There are several studies performed in the last three decades explaining the roles of the catalytic (FXIII-A) and carrier (FXIII-B) subunits which are part of the FXIII complex. However, a detailed structure-functional view of the activation of A-subunits and role of B-subunits is missing. This chapter starts with collective analyses of information known so far about Factor XIII (structure, sequence, phylogeny, activation, regulation); to derive a) How the subtle macromolecular changes at calcium binding sites of FXIII-A, are responsible for driving the molecule from its zymogenic to activated state; b) Antagonistic roles of calcium binding sites, during this course of transition from zymogen to activated FXIII-A*; c) A structural outlook of FXIII complex assembly and disassembly, and; d) Regulatory roles of FXIII-B subunits. Although the studies performed in this chapter were majorly in-silico, but they aided in generation of testable hypothesis for the future (most of which are part of the thesis in itself); and also brought to us first structural insights into the mechanism of FXIII-A activation.

Scientific Reports / 6:30105 / DOI: 10.1038/srep30105

SCIENTIFIC REPORTS



OPEN

Revisiting the mechanism of coagulation factor XIII activation and regulation from a structure/functional perspective

received: 08 October 2015

accepted: 27 June 2016

Published: 25 July 2016

Sneha Gupta^{1,*}, Arijit Biswas^{1,*}, Mohammad Suhail Akhter¹, Christoph Krettler², Christoph Reinhart², Johannes Dodt³, Andreas Reuter³, Helen Philippou⁴, Vytautas Ivaskevicius¹ & Johannes Oldenburg¹

The activation and regulation of coagulation Factor XIII (FXIII) protein has been the subject of active research for the past three decades. Although discrete evidence exists on various aspects of FXIII activation and regulation a combinatorial structure/functional view in this regard is lacking. In this study, we present results of a structure/function study of the functional chain of events for FXIII. Our study shows how subtle chronological submolecular changes within calcium binding sites can bring about the detailed transformation of the zymogenic FXIII to its activated form especially in the context of FXIIIA and FXIIIB subunit interactions. We demonstrate what aspects of FXIII are important for the stabilization (first calcium binding site) of its zymogenic form and the possible modes of deactivation (thrombin mediated secondary cleavage) of the activated form. Our study for the first time provides a structural outlook of the FXIIIA₂B₂ heterotetramer assembly, its association and dissociation. The FXIIIB subunits regulatory role in the overall process has also been elaborated upon. In summary, this study provides detailed structural insight into the mechanisms of FXIII activation and regulation that can be used as a template for the development of future highly specific therapeutic inhibitors targeting FXIII in pathological conditions like thrombosis.

The fibrin stabilizing factor or coagulation factor XIII (FXIII) is a heterotetrameric protein complex, circulating in the plasma as a 320 kDa molecule consisting of a dimer of A subunits (FXIIIA₂, 83 kDa) and a dimer of B subunits (FXIIIB₂, 80 kDa)^{1–3}. FXIII belongs to the transglutaminase family of enzymes (EC 2.3.2.13)⁴. The catalytic FXIIIA₂ subunit possesses transglutaminase activity that covalently crosslinks fibrin polymers to confer resistance against premature fibrinolysis⁵. Deficiency of FXIII can result in a bleeding predisposition from acquired or inherited causes^{6,7}. Patients with severe inherited FXIII deficiency (complete absence or loss of function) suffer from severe bleeding tendencies. Inherited severe FXIII deficiency is a rare autosomal disorder with a global average of approximately 1–4 out of a million individuals being affected⁶. However, a more frequently inherited form of FXIII deficiency is the heterozygous form that is usually associated with a mild or even asymptomatic phenotype^{6,7,8–11}. This form is difficult to detect and, therefore is currently under-reported and poorly characterized. The past few decades of research have shown FXIII to have multiple pleiotropic functions¹². It is known to play roles in maintaining vascular permeability, in development of extracellular matrix in bone and cartilage, in fostering cardioprotective effects, as a first line of defense against invading pathogens and, as recently reported, in pre-adipocyte differentiation and arthritis^{13–18}. Identification and cloning of the *F13A1* and *F13B* genes, along with the recombinant expression of the FXIIIA₂ and B₂ subunits^{19–21}, was followed by high-resolution structural determination of the FXIIIA₂ dimer in zymogenic forms^{22–25}. Recently the structure of calcium-activated and inhibitor-stabilized FXIIIA subunit (FXIIIAa) was solved which shows remarkable differences from the zymogenic form²⁶. Structurally, the FXIIIA subunit is composed of four sequentially arranged structural units: the beta

¹Institute of Experimental Haematology and Transfusion Medicine, University Clinic Bonn, 53127 Bonn, Germany.

²Department of Molecular Membrane Biology, Max Planck Institute of Biophysics, 60439 Frankfurt, Germany. ³Paul Ehrlich Institute, 63225 Langen, Germany. ⁴Leeds Institute for Cardiovascular and Metabolic Medicine, University of Leeds, Leeds, UK. *These authors contributed equally to this work. Correspondence and requests for materials should be addressed to A.B. (email: arijit.biswas@ukb.uni-bonn.de) or J.O. (email: johannes.oldenburg@ukb.uni-bonn.de)

sandwich, core, barrel-1 and barrel-2 domains. Unique to the FXIIIa subunit in the transglutaminase family is the presence of a 37 amino acid N-terminal activation peptide (FXIII-AP) which is cleaved by thrombin during FXIII activation. Despite early achievements investigating secondary structural elements and structural domains of FXIIIB^{21,26}, progress in structure/function studies of this non-catalytic subunit have been slow and there are no high-resolution X-ray crystallographic or NMR structures for FXIIIB monomers, putative dimers, or for the FXIIIa₂-bound conformation in FXIIIa₂B₂ tetramer. High primary sequence homologies with proteins from the complement system suggest that the monomeric FXIIIB subunit is composed of ten Sushi domains, each comprising ~60 amino acid residues^{21,27,28}. Limited information exists on the interaction between FXIIIa and FXIIIB subunits and on FXIIIB₂ dimerization^{29,30}. The FXIIIB subunit is known to have a protective role, although more recently a regulatory role has also come to light^{31,32}. The FXIIIa subunit has been a potential target for developing therapeutic inhibitors against thrombotic conditions. Earlier, the primary targeted region for developing therapeutic inhibitors was the thrombin cleavage site and the catalytic triad in the zymogenic form of the FXIIIa subunit^{33–38}. With emerging details of structural changes taking place during FXIII activation, the activated form (FXIIIa) is being considered as a good potential target^{26,38}. The activation of the FXIIIa₂B₂ heterotetramer in plasma is an elaborate process involving the cleavage of FXIII-AP by thrombin combined with calcium binding which causes large-scale conformational changes in the FXIIIa subunit structure and also results in the dissociation of the FXIIIB subunits^{26,39}. Although a number of studies by various groups have shed light on different aspects of this complicated process, however a comprehensive understanding of the complete activation process is lacking. In the current study we present a structure/function study of the chain of events comprising FXIII heterotetramer dissociation, FXIIIa subunit activation and subsequent down-regulation. We use computational analysis to elucidate structure/function associations that relate various stages of the entire FXIII pathway. Complimentary to this, we performed gel filtration analysis to characterize the dissociation of the FXIIIa₂B₂ heterotetrameric complex in different local biochemical conditions. In addition, we have tried to offer an alternative explanation for the regulatory role of FXIIIB subunit on FXIIIa activation *in vitro*. Finally, we compare observations and conclusions from the present study with results and conclusions derived from past literature.

Materials and Methods

Simulation and comparison of FXIIIa₂ and Transglutaminase-2 structures. In order to understand the inter-residue relationships within the different parts of FXIIIa subunit and tissue transglutaminase-2 (TG2) plain molecular dynamics (MD) simulation was performed on the zymogenic human FXIIIa₂ crystal structure (PDB ID: 1f13; 2.1 Å resolution)²⁴ and the zymogenic TG2 structure (PDB ID: 1kv3; *H. Sapiens* species; 2.1 Å resolution)⁴⁰ using the YASARA Structure package version 13.11.1^{41,42}. Gaps or unresolved regions within the crystal structure(s) were modeled them on the FREAD loop modeling server (<http://opig.stats.ox.ac.uk/webapps/fread/php/>; accessed on 05.10.2014)⁴³. For e.g. the PDB file 1f13 that is unresolved at the thrombin cleavage site Arg37-Gly38 was submitted to the server under default parameters. The final structurally resolved structure was chosen based on scores that were a combination of all backbone atom anchor match RMSD (corresponds to the base structure) and all backbone atom loop match RMSD (corresponds to the loop structure). The PDB files were initially subjected to 500 ps of refinement MD simulation using YAMBER3 force field parameters in YASARA in order to remove steric clashes and improve rotamer geometry⁴¹. The file with the lowest energy in the simulation trajectory was chosen for conducting further simulations. In order to simulate the structures, a simulation cell with periodic boundaries and 20 Å minimum distances to protein atoms was employed with explicit solvent. The AMBER03 force field, NPT ensemble was used with long range PME potential and a cut-off of 7.86 Å⁴⁴. Hydrogen bond networks were optimized using the method of Hooft and co-workers⁴⁵. The simulation cell was filled with water at a density of 0.997 g/mL and a maximum sum of all bumps per water of 1.0 Å. The simulation cell net charge was neutralized with a final 0.9% (wt/vol) NaCl concentration. The entire system was energy minimized by steepest descent to remove conformation stress within the structure, followed by simulated annealing minimization until convergence was achieved. The MD simulation was performed at three different temperatures i.e. 298 K, 340 K and 370 K. Simulations for both structures were run for 100 ns (nanoseconds). Structural image visualization, analysis and rendering were done with YASARA 13.11.1 and Chimera version 1.10.2^{42,46}. Solvation energies for initial crystal structures as well as for simulation trajectory snapshots were calculated by submitting trajectory converted PDB-formatted files to the PDBePISA server (<http://www.ebi.ac.uk/pdbe/pisa/pistart.html>; accessed on 05.01.2015)⁴⁷. Electrostatic surface potential was calculated and graphically depicted using the Adaptive Poisson-Boltzmann Solver integrated within YASARA⁴⁸. The extent of correlated motion calculated in YASARA for all simulations is represented by C(i, j). It is collected in matrix form and displayed as a three-dimensional dynamic cross-correlation map (DCCM). The time scale is implicit in the C(i, j) values. The cross correlation was calculated as average over the time period of the entire trajectory. Positively correlated residues move in the same direction, whereas (negatively) anti-correlated residues move in the opposite direction. A completely correlated or anti-correlated motion, C(i, j) = 1 or C(i, j) = -1, means that the motions have the same phase and period. Blue color represent value 1 and yellow -1, all intermediate values are depicted by shades which are semi-proportionate mix of these two colors. The color code is represented as an inset diagram for all matrices.

Removal of bound calcium from zymogenic FXIII crystal structures using steered molecular dynamic simulation. Steered molecular dynamics (SMD) simulation was performed on the monomer (A chain) of the calcium-bound (at Ala457, Cab1) human FXIIIa subunit zymogenic structure (PDB ID: 1gg; 2.1 Å resolution)²⁵ to simulate relocation of bound Ca²⁺ ions into the bulk solvent. The PDB file was passed through a refinement simulation protocol (described before) to generate an energy minimized structure before conducting the SMD⁴¹. The SMD simulation was conducted in two steps: 1) An initial 10 ns classical MD simulation with parameters as described above (for files 1f13 and 1kv3) followed by 2) a steered simulation during the production phase in which steering potentials were applied on the complex. After 10 ns of classical MD run, a steering force

with an acceleration of 1000 pm/ps^2 (picometre/picosecond square) was imposed on the bound ligand Calcium. The direction of the force was applied from the geometric center of the receptor to the geometric center of the ligand. The steered simulation was halted and analyzed at the point at which the Ca^{2+} ion was displaced into and completely surrounded by hydrated counter ions. No part of the whole system was restrained during the production phase SMD or the initial MD. Upon reaching the simulation end point, the resulting protein models and the simulation averaged structures were compared to the starting crystallographic structures and scored for backbone alpha-carbon (or side chain atom) Root mean squared displacement (RMSD). The simulation trajectory was also analyzed for variations in RMSD and Root mean square fluctuations (RMSF). A plain MD simulation with parameters similar to those described for 1f13 and 1kv3 in the earlier section was also run with two PDB files: 1) the simulation refined 1 ggu file with calcium bound at the first calcium binding site 2) a simulation refined 1 ggu file but with the calcium manually removed from its first calcium binding site. These simulations were run for 100 ns each at 298 K, 340 K and 370 K and the simulation end point structures and simulation averaged structures were compared with each other by structural alignment (results shown in main images correspond only to simulation run at 298 K).

Steered molecular dynamic simulation of zymogenic FXIII structures with and without the activation peptide. A similar SMD methodology to the one applied for calcium removal from zymogenic FXIII_A was employed for simulating dissociation of individual monomers from two separate homodimeric FXIII_A₂ structures: one a zymogenic human Factor XIII_A₂ structure including the activation peptide (PDB ID: 1f13; 2.1 Å resolution) and the other with N-terminal FXIII-AP residues through Pro39 deleted. Like before both structures were initially minimized using a structure refinement protocol⁴¹. A steering force with an acceleration of 100 pm/ps^2 was then applied to displace monomer chain B from monomer chain A. No part of the whole system was restrained during the SMD or the initial MD to allow freedom of movement for residues being influenced by the separation of the monomers. The SMD was analyzed to the point at which no intermolecular contacts were observed between the FXIII_A monomers and/or the atoms started crossing the periodic boundaries.

Modeling all-atom factor XIII activation pathway intermediates. To generate FXIII activation pathway intermediate structural models, we used two crystal structures of FXIII_A₂: the starting zymogenic FXIII_A₂ crystal structure (PDB ID: 1f13; 2.1 Å resolution) and the non-proteolytically (high Ca^{2+} concentration) activated FXIII_A_A crystal structure (PDB ID: 4kty; 1.8 Å resolution)^{24,26}. The intermediates were generated by submitting these two structures as end-state structures to the ANMPATHWAY server (<http://anmpathway.lcrn.ac.uk/anmpathway.cgi>; accessed on 08.11.2014), which uses a coarse-grained modeling approach to construct a two-state potential calculated by combining two elastic network models (ENMs) representative of the experimental structures representing the beginning and end points of the simulation⁴⁹. Intermediate structures are extracted as snapshots along continuous steepest descent pathways generated for the protein atomic coordinates during the transition from beginning to end point structures. Since the server requires the beginning and end states to be similar in terms of molecular content, all atoms and molecules not common to both input structural coordinate files were deleted, missing/unresolved residues were modeled by modeling them (as described before), and only monomeric chains from each file were submitted. The ANMPATHWAY server replaces amino acid side-chain atoms with a single representative vdW shell and returns alpha-carbon backbone traces without explicit side chain atoms as results. Once a large number of coarse grained intermediates were generated, eight were finally selected which differed from each other by at least $>2 \text{ Å}$ RMSD (of the alpha carbons of the backbone trace). The side chains of these intermediates were modeled using the PD2 ca2main server (http://www.sbg.bio.ic.ac.uk/~phyre2/PD2_ca2main; accessed on 25.11.2014) to generate the corresponding full atom models⁵⁰. Full atom models were then subjected to a structure refinement protocol as described before⁴¹. Lowest energy models were selected from the simulation trajectory and analyzed. All the transition intermediate as well as end state models have been deposited in the protein modeling database (<https://bioinformatics.cineca.it/PMDB/main.php>) (PMDBID: PM0080129-PM0080136).

An all-atoms partial heterotetrameric model of FXIII_A₂B₂. In order to generate a partial model of the FXIII_A₂B₂ heterotetramer, we used a step-wise approach to first generate a dimeric modeled structure of FXIII_B₂, followed by a constrained docking of a limited number of contiguous Sushi domains on the zymogenic FXIII_A₂ subunit crystal structure. A threaded model of a monomeric FXIII_B subunit was at first generated on the I-TASSER server (<http://zhanglab.ccmb.med.umich.edu/I-TASSER/>; accessed on 11.12.2014) with distance constraints applied for the known disulfide bonded cysteine's within each Sushi domain of the FXIII_B subunit⁵¹. Since the auto generated structure had certain flaws i.e. absence of specific disulfide bond, presence of disordered structures in ordered (predicted) areas etc., all ten individual sushi domains of this threaded model were replaced with previously modeled structures of these domains while keeping the linker regions of the threaded monomeric FXIII_B subunit model²⁸. The linker region of the automated structure was not touched in order to retain the backbone properties of this earlier model. The modified monomeric FXIII_B model was subjected to a round of model refinement simulation protocol as described before and the final energetic minimum monomeric structure was chosen from the trajectory⁴¹. The modified monomeric FXIII_B model was symmetrically dimerized using the M-ZDOCK docking server (<http://zlab.umassmed.edu/m-zdock/>; accessed on 12.01.2015), to generate a dimeric structure⁵². The ZDOCK server searches the translational and rotational space between the two proteins for all possible binding modes and evaluates and ranks each pose using an energy-based scoring function. The M-ZDOCK is an adapted from the ZDOCKing algorithm to predict structures of symmetric or cyclically symmetric multimers. The server generated (based on its scores) top ten docking poses, only one of which showed a head to tail (antiparallel) orientation with close proximity between the Sushi domains 4 and 9 on adjacent chains (with oppositely charged electrostatic patches) and this was chosen as the final model for the FXIII_B₂ structure

(based on current experimental data; see Supplementary methods for more details)^{29,53}. The docking pose was energy minimized with a 100 ns long classical MD simulation with parameters as described before i.e. simulation of PDB files 1f13 and 1kv3 (trajectory details i.e. RMSD/energy values can be made available on request). The lowest energy conformers from these simulations were subjected to a model refining simulation protocol as described earlier⁴¹. The lowest energy structure from this simulation trajectory was chosen as the final FXIIIB₂ subunit dimeric model. In the absence of adequate experimental data to enable co-operative docking of the FXIIIB₂ subunit Sushi domains on the FXIIIA₂ subunit, we performed blind docking of only a symmetrically identical end component of the FXIIIB₂ dimer model (consisting of Sushi domains 1, 2, 3 and 4 of one monomer and Sushi domains 8, 9 and 10 of the opposite monomer) onto a monomeric chain of FXIIIA₂ zymogenic crystal structure using the Z-dock server (<http://zdock.umassmed.edu/>; accessed on 21.01.2015). The model with closest proximity between Sushi domains 1 and 2 (as per what is currently known for FXIIIA: FXIIIB subunit interactions) and the monomeric FXIIIA was chosen as the final model. This model was subjected to rounds of energy minimizing classical MD simulation followed by refining simulation protocol as applied for the B₂ subunit. The lowest energy structure from the final refinement protocol was once again chosen as the final model. The docked FXIIIA-FXIIIB (S1–S4 antiparallel S8–S10) model was then converted into a partial heterotetramer by dimerizing it using the M-ZDOCK server as described above. In this specific docking, all known non-interface residues (identified from the PDB file: 1f13 using PDBePISA) of the FXIIIA₂ dimer were used as a negative constraint. This gave us a final partial heterotetrameric model of FXIIIA₂B₂ (S1–S4 antiparallel S8–S10). This final model was not subjected to any more rounds of classical MD simulation but minimized directly by refining it with the previously described 500 ps refinement protocol. However, in order to test for the stability of this docked complex it was subjected to 100 ns of classical MD simulation post the refinement simulation, following parameters described for the simulation of PDB files 1f13 and 1kv3. The primary FXIIIA₂B₂ heterotetrameric partial model has been deposited in the protein modeling database (<https://bioinformatics.cineca.it/PMDB/main.php>) (PMDBID: PM0080128).

Dissociation of FXIIIB (S1–S4 antiparallel S8–S10) subunit component from the partial FXIIIB heterodimer by steered molecular dynamic simulation. A similar methodology to the one applied for dissociating bound calcium from the zymogenic FXIIIA molecule was employed for dissociating the FXIIIB partial subunit component from the previously modeled partial FXIIIB heterodimer [*i.e.*, consisting of one half of the previously generated partial heterotetrameric FXIIIA₂B₂ (S1–S4 antiparallel S8–S10) model]. A steering force with an acceleration of 200 pm/ps² was applied on the FXIIIB subunit component. No part of the whole system was restrained during the SMD or the initial MD to allow freedom of movement for residues being influenced by the separation of the individual subunits. The steered simulation was analyzed to the point at which no intermolecular contacts were observed between the individual subunits and/or the atoms started crossing the periodic boundaries.

Gel filtration analysis of the activation of FXIII A₂B₂ heterotetramer. Plasma concentrate *Fibrogammin P* (CSL Behring), was used as a source of human Factor XIII heterotetramer. FXIII was purified using gel filtration chromatography on a Superdex 200 10/300 GL column (GE Healthcare). Briefly, the column was equilibrated with running buffer (30 mM Tris, 150 mM NaCl, pH 7.4), *Fibrogammin P* was loaded and fractions were eluted. Fractions corresponding to the molecular weight of FXIII heterotetramer (~320 kDa), were collected and sequentially re-purified thrice until a single, homogenous, monodispersed peak was observed. For each set of *in vitro* activation experiments, 25 µg of purified FXIIIA₂B₂ dissolved in 20 mM Tris, 120 mM NaCl, pH 7.4 buffer was incubated with 46.2 U/mL of thrombin (Sigma, USA), at different concentrations of calcium chloride (0 mM, 1 mM, 2 mM, 5 mM, 10 mM and 25 mM), for 60 minutes at 30 degrees. Reaction product was filtered and resolved using a Superdex 200 PC 3.2/30 (GE Healthcare) analytical column. Peaks from samples loaded at different calcium ion concentrations were collected and analyzed on Native PAGE (Life technologies, Germany). The observed bands were analyzed and confirmed for the presence of FXIIIA and FXIIIB by Mass Spectrometry (see Supplementary Data).

Spiking FXIIIB during activated FXIIIA (FXIIIAa) generation. FXIIIAa generation was triggered by tissue factor/phospholipids (TF/PL) and FXIIIA isopeptidase activity was measured using the fluorogenic substrate A101 (Zedira, Darmstadt, Germany) in a Safire microtiter plate reader (Tecan, Crailsheim, Germany)⁵⁴. Twenty five microliters human standard plasma (Siemens Healthcare, Marburg, Germany) or FXIII-deficient plasma (deficient for FXIIIA₂ and FXIIIB₂; Haemochrom Diagnostica GmbH, Essen, Germany) spiked with rFXIII-A₂ (1 IU/mL) or a mixture FXIIIA₂ (1 IU/mL) (Purified *in-house*, see Supplementary data) and rFXIIIB₂ (10 µg/mL) (Zedira, Darmstadt, Germany) were incubated with 35 µL reagent solution (5 µL 100 mM glycine methyl ester, 5 µL 2 mM fluorogenic FXIIIA substrate, 10 µL Innovin (recombinant TF; Dade Behring, Liederbach, Germany) diluted 1:2800 in phospholipids (PTT reagent kit, Roche, Mannheim, Germany) and 15 µL HBS (20 mM Hepes, 150 mM NaCl)/0.1% serum albumin pH 7.5. After pre-incubation of the mixture for 5 minutes, the reaction was started with 40 µL 25 mM CaCl₂ pH 7.5. Fluorescence was measured over 1 h at λ_{ex} = 330 nm and λ_{em} = 430 nm in kinetic mode 2 times per minute. The curve data was evaluated according to a bi-exponential model with first order absorption and elimination. Data were fitted to the equation:

$$C(t) = c \cdot ka / (ka - kb) \cdot (\exp(-kb \cdot (t - tlag)) - \exp(-ka \cdot (t - tlag)))$$

where ka – constant of absorption which describes the development of FXIIIA and kb – elimination constant. The parameters area under the curve (AUC), peak FXIIIA concentration (CP), and time to peak (TTP) were also evaluated.

Results

Simulation and comparison of FXIII_{A2} and TG2 models: Structure/sequence differences between FXIII_{A2} and TG2 account for their respective functional evolution. The FXIII_A (monomeric chain A) and TG2 zymogenic structures show perfect alignment of the respective domains except for the absence of the FXIII-AP region in TG2 (Figure S1). TG2 is known to bind 6 calcium ions of which 5 non-canonical sites have been characterized by mutagenesis¹³. The monomeric chain of the FXIII_A subunit possesses only 3 calcium binding sites (Cab1–3), but with similar spatial correlation to homologous TG2 sites. The RMSD graphs during the simulation run for both these structures at different temperatures are shown in Figure S1. The simulation for both FXIII_{A2} and TG2 PDB files stabilized around ~2–2.5 Å RMSD after 10 and 40 ns respectively (total energy of the systems $\sim -37 \times 10^6$ kJ/mol and -29×10^6 kJ/mol respectively). For the FXIII_{A2} and TG2 structures we observed a positive correlation (DCCM) between the residues of the separate calcium binding sites (TG2 mean $C(i, j) = 0.462$; FXIII_{A2} mean $C(i, j) = 0.186$) (Figure S3). The TG2 redox switch¹⁴, which consists of two vicinal disulfide bonded cysteine's, lies in a highly conserved region of FXIII_{A2}, although one of the cysteine's is substituted by an arginine in FXIII_{A2} which precludes the possibility of formation of an allosteric disulfide bond in FXIII_{A2}. The GTP/GDP binding site¹⁵ (Arg478/Ser482) of TG2 is not conserved in the FXIII_{A2} dimer (Figure S1). Instead, the region aligns with a sequence of the FXIII_A subunit that forms a secondary thrombin cleavage site (Figure S2, Lys513/Ser514)⁵.

A constitutively bound calcium at Cab1 stabilizes the zymogenic form of FXIII_{A2}. Applying simulated dissociative force (using SMD) on calcium to remove it from the constitutively bound site at Cab1 of FXIII_A results in significant change of structure (>2 Å RMSD) around the FXIII-AP cleavage site (Fig. 1). Prior to MD simulation to displace bound calcium, this region was part of an ordered beta sheet (the regions between residue numbers 27–31 and 168–172 constitute two antiparallel beta strands stabilized by means of 4 hydrogen bonds). During simulation, these 4 hydrogen bonds that stabilize the sheet were lost and the antiparallel beta strands assumed a disordered random coils conformation for most of the simulation time. Interestingly, this region is spatially distant (>10 Å) from the calcium binding site, therefore the observed modeled structural change is most likely consistent with an allosterically mediated calcium binding effect. The plain MD simulation of calcium bound 1 ggu file did not show any remarkable differences in secondary structure post 100 ns of simulation in this region around the thrombin cleavage site [the Fig. 1 Panel A clearly shows that even post 100 ns of simulation this region is represented by a beta sheet (green colored)]. However when we simulated the 1 ggu PDB file after manually removing the bound calcium for 100 ns, we observed the loss of ordered secondary structure (see Fig. 1 Panel A; the red and blue backbone structures corresponding to this region in the shaded areas are disordered) in the region around the cleavage site as observed during the SMD in which calcium was pulled out. Unusually high RMSF values were observed in simulation averaged structures of the plain MD run for 1 ggu without calcium as well as for the SMD, but none for the plain MD run for 1 ggu with bound calcium (Fig. 1 Panel D; spikes 1 and 2; results correspond to simulations done at 298 K only although similar observations were registered for 340 and 370 K as well). The RMSD graphs for plain simulations run on the PDB files of 1 ggu with and without calcium are depicted in Figures S4. These figures show that both structures are relatively stable with or without calcium, although the PDB file without calcium achieves its RMSD plateau ~ 0.2 Å higher than with calcium which might be attributed to RMSD changes occurring around the thrombin cleavage site. Structural alignment of the simulation averaged structures from both simulations shows little overall structural difference (average RMSD: 1.342 Å). However a significantly higher average RMSD of 5.6 Å was observed between the thrombin cleavage site and neighboring residues (considering the P1–P4 and P1'–P4' residues) of the two simulation averaged structures. This indicates local changes in structure (and hence of accessibility) around the thrombin cleavage site sessile bond following the removal of calcium.

The activation peptide is the major contributor to the dimeric interface of the zymogenic Factor XIII_{A2}, and its cleavage weakens the dimer interaction. The SMD simulation to dissociate the individual monomers of FXIII_{A2}, with and without the FXIII-AP sequence, revealed that the structure without FXIII-AP becomes dissociated in less time (30 ns) at a constant separation force than the dimer with the intact activation peptides (60 ns) (Fig. 2, Panel A). The absence of FXIII-AP also results in a weaker interaction between non-FXIII-AP residues within the dimeric interface. The mean solvation energies of the residues on these interfaces (estimated from the simulations) are lower, exemplified by greater negative calculated values for the structure without FXIII-AP (Fig. 2, Panel B). Also, the residues that become separated by the end of the simulation are responsible for FXIII-AP/core domain interactions as judged by comparison with the starting crystallographic structure. The activation peptide residues show positive correlation [mean $C(i, j) = 0.762$] with respect to the rest of the dimeric interface residues (during the SMD of the zymogenic FXIII_A with FXIII-AP) (Fig. 2, Panel C). We observe that the interaction of two neighboring Arg residues on FXIII-AP, Arg11 and Arg12 with Asp343 and Glu401, respectively, on the core domain of the opposing monomer may be critical to the dimeric stability of the FXIII_A subunit structure since as observed, these interactions were last to be separated during simulation of subunit dissociation. The mean correlation value for these four residues with the rest of the dimeric interface is negative [mean $C(i, j) = -0.647$] indicating that they are displaced from their starting positions in a manner consistent with opposition to the dissociative forces experienced during the overall simulation.

MD simulation suggests large conformational changes upon activation of FXIII_A is affected by calcium binding at three sites in a temporal manner. The end state models of the activation path intermediates show overall similarity in secondary structure although the complete backbone moves to a large extent (Figure S5). Comparison of models in the series suggests major changes in secondary structure in the region between residues 450 and 650 (intermediates 2 through 5) which is affected by local changes in calcium

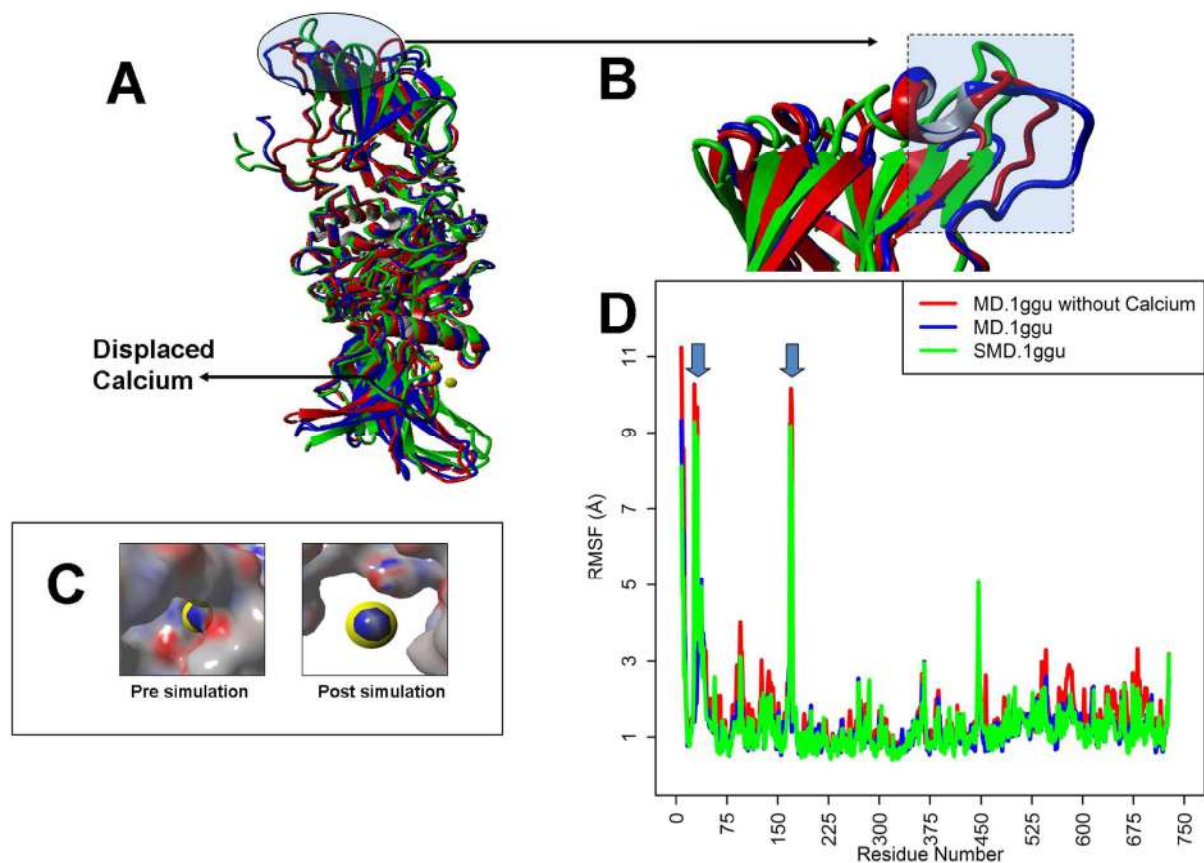


Figure 1. Steered Molecular Dynamic (SMD) simulation to dissociate bound calcium from FXIIIa models. (Panel A) The structural alignment of three simulation snapshots (one simulation end point structure for the SMD performed on 1 ggu colored blue; one a post 100 ns simulation snapshot of the 1 ggu file deprived of calcium at Cab1 colored red; one a post 100 ns simulation snapshot of the original 1 ggu file colored green) from one monomer (chain A) of the zymogenic FXIIIa₂ structure (PDB ID: 1 ggu). Backbone structures are depicted in ribbons. Bound calcium is represented as a yellow ball. Shaded regions show maximum amount of displacement in secondary structure alpha-carbon backbone ($>2 \text{ \AA}$ RMSD). (Panel B) Close up view of the structural alignment depicted in (Panel A) focusing on the region around the FXIII-AP cleavage site. Ribbon colors as for (Panel A). (Panel C) Molecular surface view of the calcium binding site pre- (left side) and post-SMD (right side) simulation. Red, negative potential; blue, positive potential; calcium ion, yellow ball. The electrostatic surface potential was calculated using YASARA. (Panel D) A RMSF (Root mean square fluctuation) graph comparing the average RMSF per residue for the plain simulation run on the PDB file 1 ggu with and without calcium and also of the SMD run on 1 ggu. Spikes in RMSF exclusively for the SMD run on 1 ggu and 1 ggu file without bound calcium are shown with downward pointing arrows.

binding at Cab1 and Cab2 (Fig. 3). Changes in backbone structure during the simulation are initially observed around the beta sandwich region and parts of core and barrel-1 domains (Fig. 3, RMSD graphs). Structural changes shift to core domain, barrel-1 and barrel-2 in successive intermediates and translate to and/or rotate the two barrel domains with respect to each other and with respect to the core domain. Finally, backbone conformational changes appear to alternate between the barrel-1 and barrel-2 domains during the course of the transition, which results in movement of the barrel domains across their common plane of symmetry, thereby twisting the final molecule three dimensionally while causing the FXIIIa subunit to unfold like a jackknife (Fig. 3). During the simulation, the first calcium binding site (Cab1) becomes disrupted as the second calcium binding site (Cab2) is unmasked and coordinates a Ca^{2+} ion. The distance between Glu401 and His342 residues (referred as catalytic diad), which are distant in the zymogenic form, decreases through the early intermediates 1–4 (Fig. 4, Panel A, sections i, ii). This simulated movement appears to be a consequence of intermittent switching between beta strand and coil forms for the backbones of both Glu401 and His342 those results in a flapping movement of these residues close and then subsequently away from each other. A hydrophobic pocket, whose base is occupied by the catalytic Cys314 residue, emerges along with a hydrophobic tunnel formed by the movement of the planar rings Trp370 and Trp279 (also as a result of Cab2 coordination), which are finally stabilized by aromatic stacking interactions (Fig. 4, Panels A, B). On one side of this tunnel is the K substrate (Lysine substrate) entrance site and the other side is the His342/Glu401 diad known to guide the Q substrate (Glutamine substrate) to the base of the hydrophobic pocket where a positively charged oxyanion hole, formed by electronegative backbone carbonyl

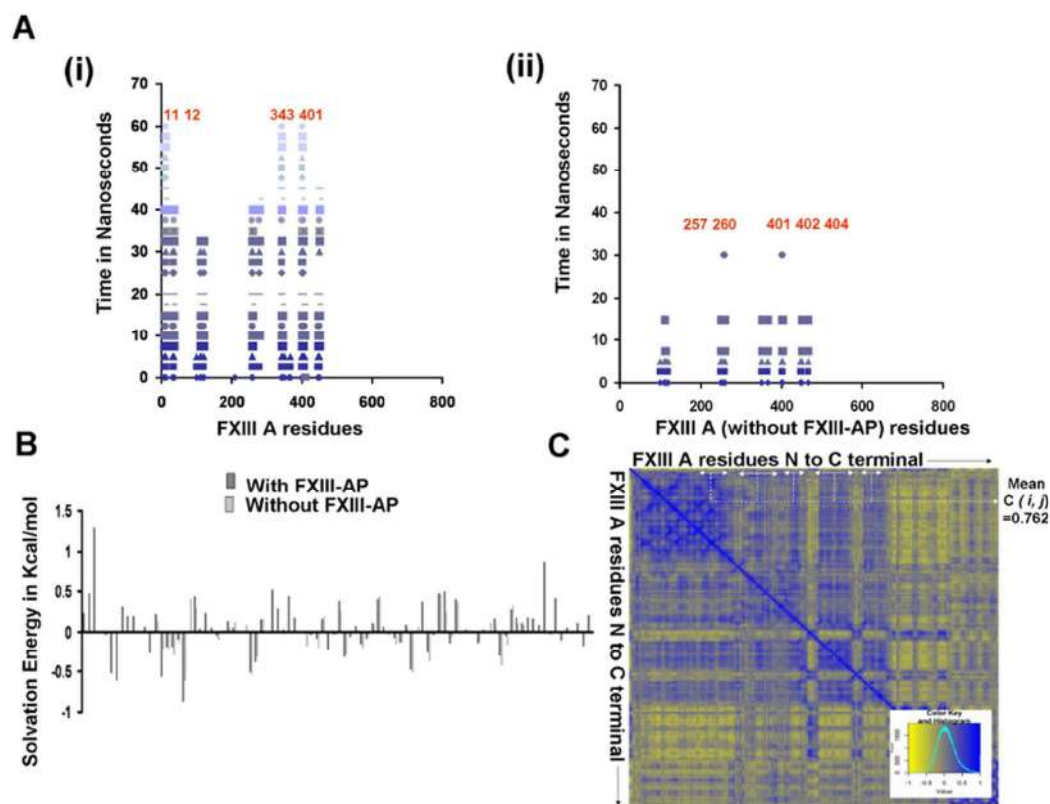


Figure 2. Steered molecular dynamic simulation of FXIII A2 dimer dissociation into separated monomers.

(Panel A) Separation plots showing physical interactions (each spot represents an interaction observed in a specific snapshot; the spots are colored in different shades of blue and spots from the same simulation snapshot have the same shade) for residues N to C terminal (x-axis) of one FXIII A monomer at the dimeric interface over the progress time (y-axis) of the SMD (in picoseconds). (i) Interactions for the zymogenic FXIII A structure (with FXIII-AP); (ii) interactions for the zymogenic structure without FXIII-AP (residue numbering for both plots according to the complete zymogen primary sequence). The main interacting partners in FXIII A monomer, forming the dimeric interfaces in the both the cases, are labelled in red. (Panel B) Post-simulation mean solvation energies (y-axis) for the FXIII A subunit dimeric interface residues (x-axis). Black bars, zymogenic FXIII A₂ with FXIII-AP, Grey, without FXIII-AP. (Panel C) Calculated DCCM (dynamic cross correlation matrix) values for the 60 ns SMD simulation of FXIII A monomer dissociation from zymogenic FXIII A₂ dimer with FXIII-AP. Color key shown as inset: yellow, negative correlation; blue, positive correlation. The bidirectional white arrows represent the positively correlated region between the FXIII-AP residues and the corresponding FXIII A dimeric interface residues (not including the FXIII-AP).

groups of both Cys314 and Trp279, is located. This oxyanion hole stabilizes the substrate-enzyme intermediate (Fig. 4, Panel B).

The all-atoms partial heterotetrameric model of FXIII A₂ B (S1–S4 S8–S10)₂ suggests that bound FXIII B subunits mediate regulation of FXIII activation. A flowchart for the generation of the FXIII A₂ B partial heterotetrameric model is presented in Figure S6. The FXIII B₂ subunit dimeric model is symmetric, long and filamentous as has been suggested from electron microscopy based studies (approximately 21.5 nm end to end)²⁷. The first two N terminal Glu residues for this model were skipped from the final structure owing to conformational equilibrium purposes. This model had regions around sushi domains 4 and 9 interacting with each other on the opposite chains in a head to toe manner and therefore the overall structure was symmetrical. The regions around sushi domains 4 and 9 were observed to have oppositely charged surface electrostatic potential (Figure S7) which adequately fitted into each other. The final all-atoms partial heterotetrameric model was a symmetric fitting of the B subunit fragments around the A subunit. While the A subunit retained its former non-associated structure, the B subunit (fragments) appears to undergo significant rearrangement to wrap around one side of the A subunit. This partial model for the FXIII A₂ B₂ complex was quite stable as can be seen from the plain simulation runs performed at 298 K in which it hits an equilibrated RMSD plateau around the 2.5 Å mark (c-α backbone RMSD)(Figure S8). Plain simulations performed at 370 K showed significantly higher RMSDs approaching the 3.5 and 4.5 Å respectively mark at 100 ns of runtime which is not unusual for a non covalently associated complex plus this model is lacking in possible binding contributory domains. The all-atoms partial heterotetrameric model of FXIII A₂ B₂ (Fig. 5, Panel A) suggests an interaction between the variable length loop region of FXIII B Sushi domain 1 (Residues Tyr18-Pro28) with the N-terminal residues (Thr6-Asp25) of the

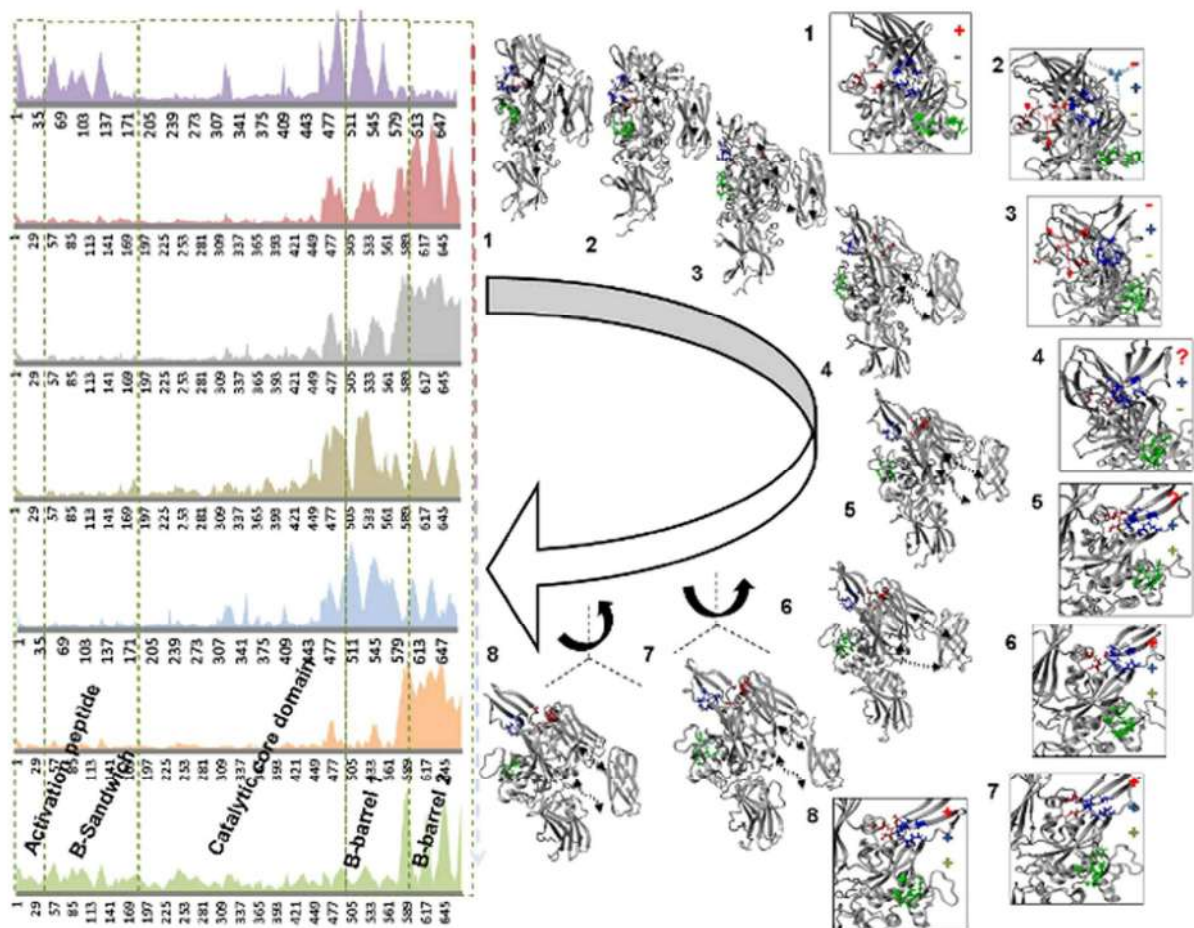


Figure 3. Domain displacements and structural changes in calcium binding sites for the simulated transition state intermediate models. Domain displacements and structural changes in calcium binding sites observed within transition state intermediate models ($n = 8$). RMSD values per backbone alpha-carbon for each residue of FXIII A (left side). Y-axis values are normalized RMSD in Å, x-axis denotes the backbone alpha Carbon (N to C terminal), with domains specified. Next to arced open arrow (middle) are models of the 8 transition state intermediate (grey). Calcium binding sites are Cab1 (red), Cab2 (blue) and Cab3 (green). Direction of motions of domains due to calcium binding is shown with small black dashed double-headed arrows. The direction and relative magnitude of twisting motions are depicted next to intermediates 6–8 (straight dashed lines indicate x-, y- and z-axes for an arbitrary reference frame representing the orientation of each intermediate as shown). The boxed images (right) are close up views showing the location, formation and/or disruption of three calcium binding sites for the 8 intermediates. The coordination states of the calcium binding sites are indicated either with bound calcium (+) or with no calcium bound (-). Arrows indicate simulated movements of Ca^{2+} ions relative to each binding site. Residues forming the calcium binding sites are shown in stick format.

FXIII A subunit activation peptide (Fig. 5, Panel C). The interaction appears to be primarily hydrophobic since although the activation peptide region bears a strong positive electrostatic potential, the variable length loop of Sushi domain 1 is electrostatically neutral. Other regions of interaction are defined in Fig. 5, Panel B. In this model, the Cab1 site is always exposed and therefore occupied by a calcium ion, Cab2 is occluded by the FXIII B S1/FXIII-AP interaction surface, while the third Cab3 is partially occluded by the FXIII A₂ dimeric interface, but, more significantly, by the FXIII B₂ subunit Sushi 1/Sushi 2 domains from apposing monomers.

Intermediate partial FXIII A₂B (S1–S4 S8–S10)₂ complex models generated during SMD simulated activation suggest successive weakening of intersubunit interactions. Simulated dissociation of the modeled partial monomeric component of the FXIII B subunit from the monomeric FXIII A structure using our SMD method resulted in a sharp change in estimated solvation energy for residues which spatially surround the three calcium binding sites (Fig. 6, Panel C). From a calculated dynamic cross correlation matrix (DCCM) for the simulation we infer that the three calcium binding site residues show a negative correlation with beta sandwich domain residues of FXIII A subunit interacting with the FXIII B subunit (Fig. 6; Panel A). In contrast, the residues from the other C-terminal domains (Barrel domains) of the FXIII A subunit that interact with the FXIII B

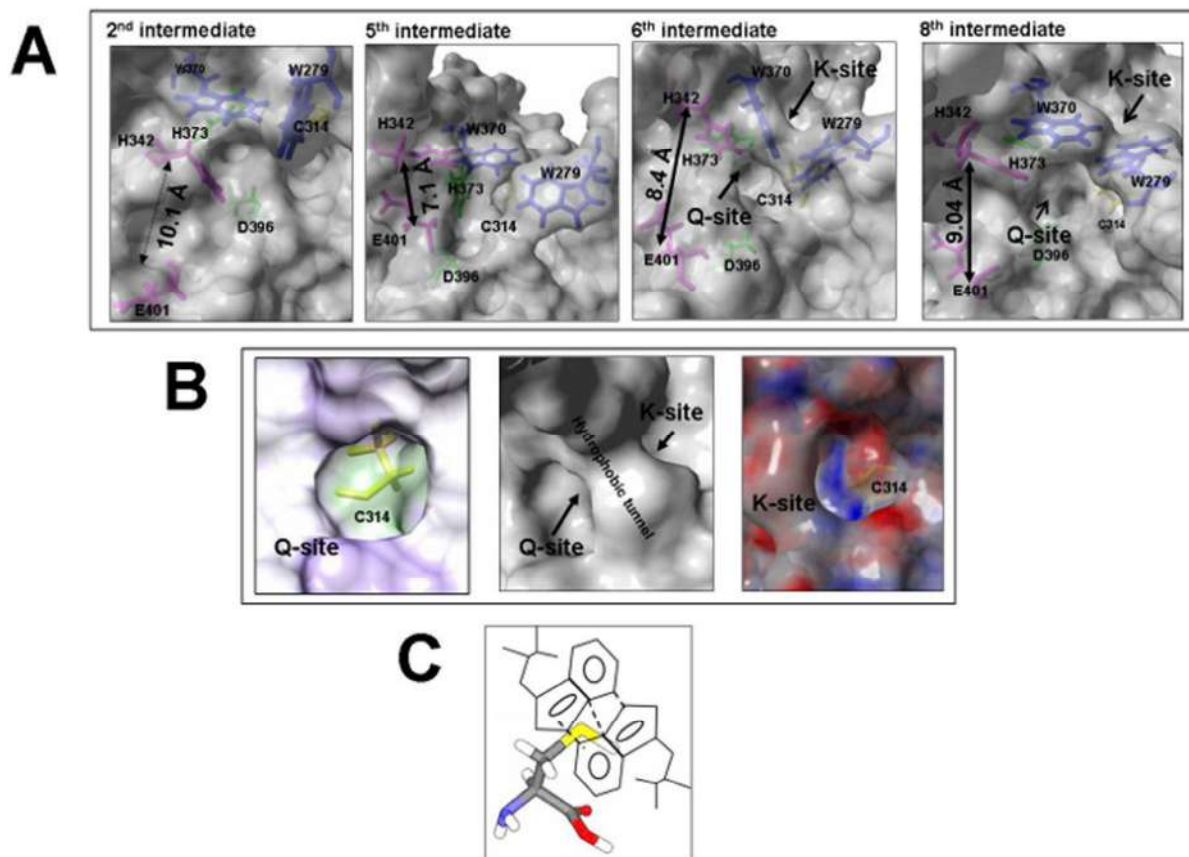


Figure 4. Detailed views of transition state intermediate models. (Panel A) Molecular surface representations of transition intermediate models 2, 5, 6 and 8 (left to right, respectively). The molecular surfaces (grey); key residues including catalytic triad (green), substrate guiding diads (magenta), and aromatic residues lining the hydrophobic tunnel (blue) shown as stick representations. (Panel B) Views of the FXIIIa subunit catalytic site in its fully activated (FXIIIa) form as molecular surface representations (grey surfaces). Shown are entry of vestibule for the Q substrate binding site (i) relative hydrophobicity: minimum (purple) to maximum (green)), hydrophobic tunnel (ii), and entry point of vestibule for the K substrate binding site (iii; electrostatic surface potentials: negative (red), positive (blue)); catalytic C314 (panels i and iii, yellow stick representation); molecular schematic representation of pi-stacking interactions (dashed lines) that stabilize the hydrophobic tunnel (iv). The electrostatic surface potential was calculated with YASARA. (Panel C) This is cartoonist illustration of the hydrophobic tunnel formed by the planar interaction of the Trp rings. The reactive cysteine is shown as a stick model at the bottom with sulphur atom colored yellow.

subunit show a strong positive correlation. This indicates that the motions influenced by calcium binding at the N- and C-terminals are opposite to each other, suggesting that the entire FXIIIa molecule will tend to twist. This twisting movement of the FXIIIa subunit suggests a mode for weakening FXIIIa: FXIIIb subunit interactions within the heterotetramer. The last FXIIIa subunit residues to lose contacts with the FXIIIb subunit during this simulation are Asn175, Asp297 and Lys677 (Fig. 6, Panel B). Interestingly, simulated dissociation of the FXIIIb subunit from the FXIIIa subunit also distorts the region around the FXIII-AP cleavage site lowering the accessibility around the Arg37-Gly38 sessile bond (Fig. 5, Panel D).

Presence of the FXIIIb subunits accelerates the rate of *in vitro* activation of FXIIIa₂. Results of the *in vitro* FXIIIa activation assay (see Supplementary Methods)⁵² revealed that, in the absence of FXIIIb, the rate of generation of FXIIIa is lower ($k_a = 0.145$, where k_a is constant which describes the absorption of FXIIIa development in a one compartment model) than when FXIIIb is present ($k_a = 0.485$). The lag time in FXIIIa generation assay was shortened by 9.45 minutes when rFXIIIb (Zedira, Darmstadt, Germany) was added to rFXIIIa in FXIII-deficient plasma (Figure S9). The time course for FXIIIa generation for rFXIIIa in the presence of added rFXIIIb subunit resembled that of normal pooled plasma.

The FXIIIb subunits separate from the FXIII heterotetramer at high calcium ion concentration in the *in vitro* activation assay. Gel filtration analysis (Fig. 7) revealed that only at very high calcium ion concentration (25 mM) during activation, measured *in vitro* concentrations of FXIIIb subunit suggest that it completely dissociates from the initial FXIIIa₂B₂ complex (peak separation starts at *in vitro* calcium ion concentration: 5 mM/activation reaction mixture of 50 μ l). The first eluted peak corresponded to the tetrameric FXIIIa₂B₂

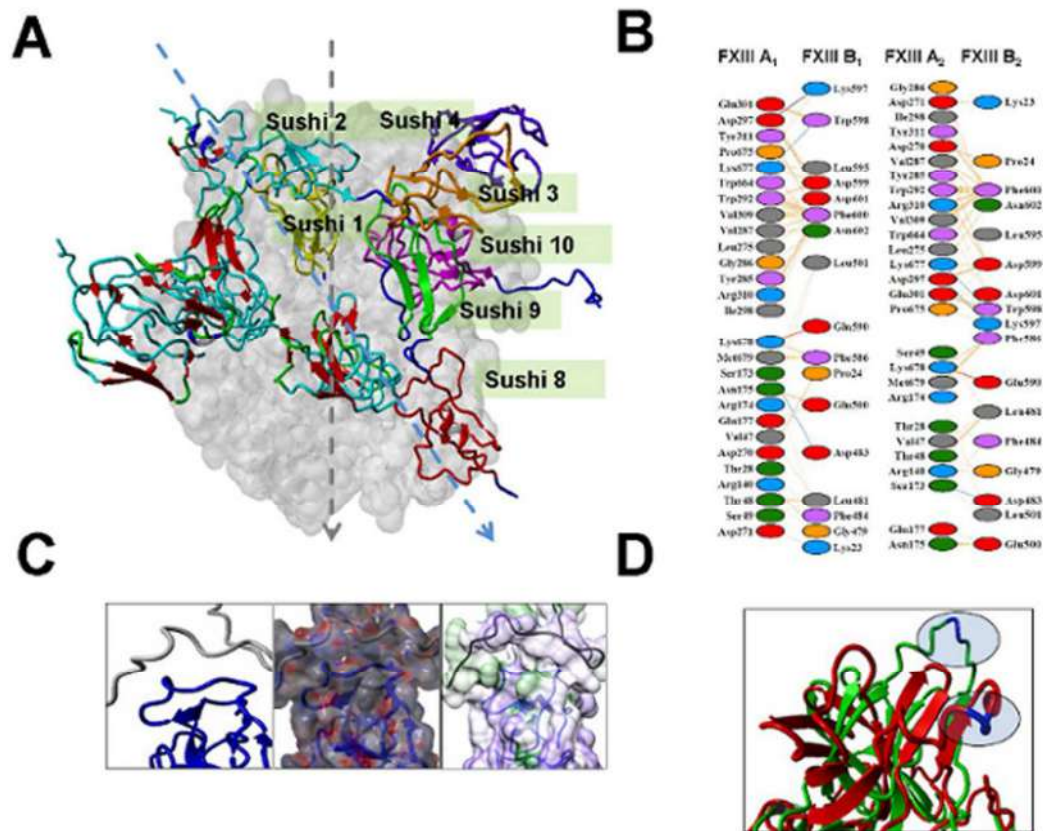


Figure 5. All-atoms partial heterotetrameric FXIII A₂B (S1–S4 S8–S10)₂ model. (Panel A) Heterotetrameric FXIII A₂B (S1–S4 antiparallel S8–S10)₂ model. FXIII A subunit shown as molecular surface rendering (grey); Sushi domains from apposed FXIII B monomers shown in alpha-carbon trace (ribbons) format. (colored according to secondary structure: beta-strand (red), extended loop (cyan), random coil (green), alpha-helix (blue)); dashed arrow marks the mirror symmetry of both FXIII A (grey) and FXIII B (cyan) subunits. (Panel B) Schematic diagram of putative interface residues forming physical contacts between the FXIII A and FXIII B subunits of the heterotetrameric FXIII A₂B (S1–S4 antiparallel S8–S10)₂ model. The dashed lines represent inter-residue contacts while the multiple colored oval structures represent the participating residues. (Panel C) FXIII B S1 Sushi domain interaction with the FXIII-AP N-terminal region. Backbone alpha-carbon trace (left panel, ribbons: S1 domain, blue; FXIII-AP, grey). Middle panel shows electrostatic potential (negative, red; positive, blue) superimposed on molecular surface view for same domains depicted in left panel. The electrostatic surface potential was calculated and graphically depicted using Adaptive Poisson-Boltzmann Solver (integrated within YASARA). Right panel shows hydrophobicity (minimum, purple; maximum, green) for the same molecular view as in left and middle panels. (Panel D) Close up view of aligned models from simulation snapshots. Pre- (green) and post-SMD (red) alpha-carbon backbone traces (ribbons) from 80 ns simulation of FXIII B dissociation from FXIII A in the vicinity of FXIII-AP.

complex as determined by mass spectrometry, while the second peak contained only FXIII B₂ (Figure S10). No dissociated FXIII A₂ or activated FXIII A_a was observed in any of the eluted peaks. The second peak corresponding to FXIII B appeared distinctively when the concentration of calcium ions exceeded 5 mM in the reaction mix applied to the column. In the absence of thrombin cleavage, however, no separation of subunits was observed irrespective of calcium ion concentration (0–25 mM). The resolved FXIII A₂ B₂ and FXIII B₂ peaks at different calcium concentrations exhibited different elution times (Fig. 7).

Discussion

The activation of FXIII *in vivo* follows a sequence of events that is initiated by proteolytic cleavage, calcium binding and ensuing conformational changes. In the present report we attempt to rationalize the complete train of molecular events with an eye on plausible sub-molecular conformational changes that may take place during this process. The structural and sequence alignment of FXIII A subunit to the better characterized homologous TG2 transglutaminase suggests a few insightful observations. Firstly, both enzymes share identical domain organization except for an additional activation peptide (FXIII-AP) absent in TG2 and which is cleaved by thrombin in the first step of *in vivo* FXIII activation. *In vivo*, TG2 remains inactive until binding of GTP/GDP at low intracellular calcium levels⁵⁵. At relatively higher extracellular calcium concentration and low concentration of GTP/GDP, a redox switch involving two vicinal cysteine's (Cys408–Cys409) regulates TG2 activation⁵⁶. The homologous region

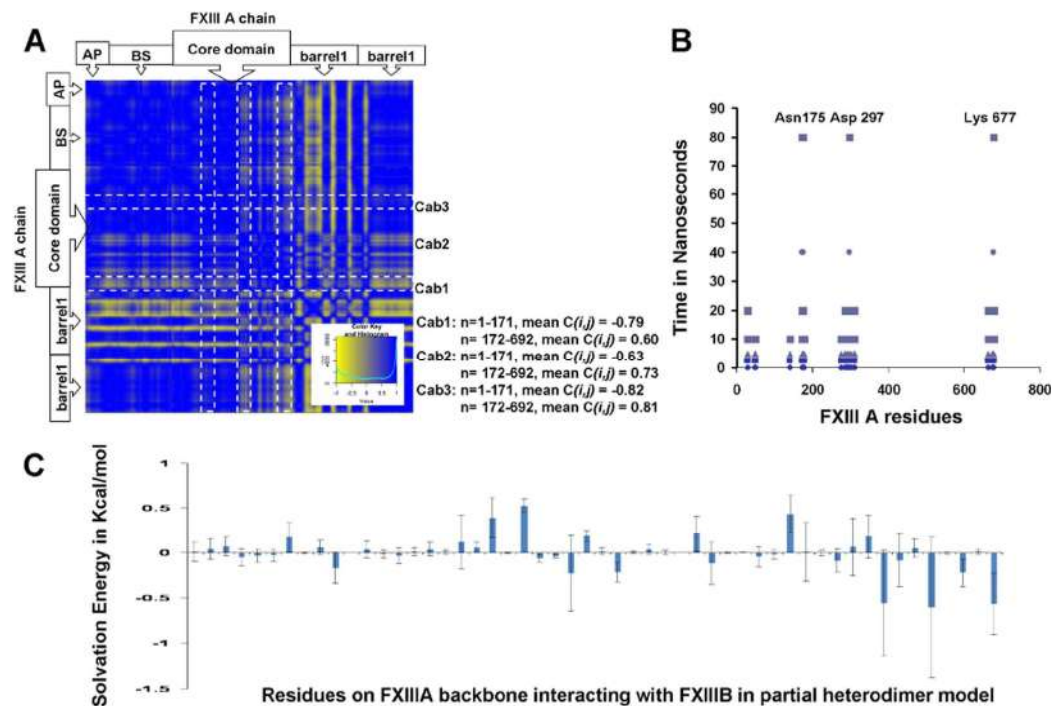


Figure 6. SMD simulation results for FXIII B subunit dissociation from FXIII A subunit. (Panel A) Inter-residue displacement (DCCM) correlation calculated for the 80 ns SMD simulation of FXIII B dissociating from FXIII A for the all atom partial heterotetrameric FXIII A₂B (S1–S4 S8–S10)₂ model. (Negative correlation, yellow; and positive correlation, blue). The DCCM map is shown only for the FXIII A residues. Mean correlation (DCCM) values for FXIII A residues on the FXIII A: FXIII B interface comprising the three calcium binding sites are tabulated on the right for two regions; residues 1–171 (N-terminal beta sandwich domain) and residues 172–692 (the remaining C-terminal domains). (Panel B) Separation plots showing physical interactions (blue spots represent interaction at each simulation snapshot; same shade represent interactions at the same snapshot) for residues (x-axis) of one FXIII A monomer at the FXIII B (S1–S4 antiparallel S8–S9) interface over the progress time (y-axis) of the SMD (residue numbering for both plots according to the complete zymogen primary sequence). (Panel C) Change in mean estimated solvation energies for FXIII A residues at the FXIII A: FXIII B heterodimeric interface during the 80 ns SMD simulation run. The error bars represent standard deviation.

of FXIII A, where the vicinal cysteine's are substituted by Arg408-Cys409 of FXIII A, forms the central core of the dimeric interface of FXIII A₂ and is also part of the buried Cab3 site in the zymogenic FXIII A subunit structure. Therefore, this homologous region of FXIII A appears to have evolved as part of a regulatory mechanism (instead of a redox switch) that stabilizes the dimeric interface, occluding the solvent access to the Cab3 binding site. Residues involved in GTP/GDP binding of TG2 (Arg478/Ser482) align with a secondary thrombin cleavage site (Lys513/Ser514) of FXIII A which suggests that this region interacts with the FXIII B subunit, instead of GTP/GDP, to prevent secondary cleavage of zymogenic FXIII A (Figure S1). Therefore, these two homologous regions apparently have regulatory functions in protecting/maintaining the zymogenic form of either protein, although the biochemical nature of the binding partner is different for the two transglutaminases.

Our results suggest that the calcium binding sites of TG2 and FXIII A serve to coordinate and stabilize conformational changes during a multistep activation process that directs a global change in the respective protein folds and leads to exposure of enzymatically competent active sites. We observed a mean positive dynamic correlation between the movement of different calcium binding site residues with respect to each other when simulating activation of the zymogenic TG2 and the FXIII A structures. This suggests mutual interdependence and possibly cooperativity between these calcium binding sites during the activation of both structures (Figure S2). Interestingly though, unlike TG2 in which all individual cross-correlations between individual calcium binding sites were positive, in FXIII A the individual cross-correlation of Cab1 with Cab2 and Cab3 [$C(i,j) = -0.127$ and -0.199] each were negative values which was compensated by a high positive correlation [$C(i,j) = 0.886$] between Cab2 and Cab3 value resulting in a positive mean correlation value [$C(i,j) = 0.186$] (Figure S2). Therefore unlike TG2, the saturation of calcium binding sites for FXIII A may be a sequentially ordered set of events which is also consistent with conclusions drawn from our transition state intermediate model analysis (Fig. 5). In fact, the constitutively calcium-occupied Cab1 site of FXIII A may impart a stabilizing influence on the zymogen structure, similar to the effect of GTP/GDP binding on TG2 intracellularly⁵⁵. We observed that when we simulated dissociation of this calcium, there appeared to be an allosteric effect on the region around the FXIII-AP that suggests it may change conformation to a random coil from an ordered beta sheet. The same distortion was

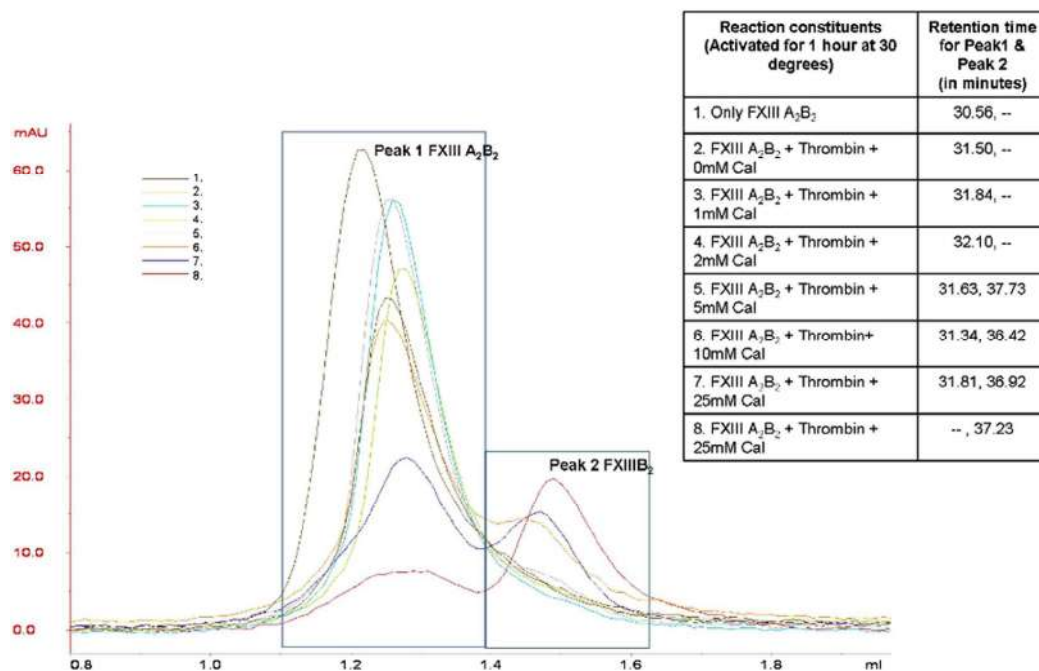


Figure 7. *In vitro* dissociation of the FXIII A₂B₂ heterotetramer observed by gel filtration. Gel filtration elution profiles for purified heterotetramer FXIII A₂B₂, at various calcium & thrombin concentrations in local environment during *in-vitro* activation. The color key (with number) depicts the different treatment conditions during activation (number corresponds to the table on right). X-axis shows the retention volume of peak; y-axis shows the amount of protein in mAU. The table also details the retention time of the peaks corresponding to FXIII A₂B₂ (peak 1) and FXIIIB₂ (peak 2), at different conditions, respectively. Protein identities eluted at peak maxima confirmed by mass spectrometry (Supplementary Figure S10).

also observed in a plain simulation of the FXIII A subunit 1 ggu file deprived of its bound calcium. On the other hand a plain simulation of the original calcium bound structure did not show the breakdown of the ordered secondary structure clearly indicating that the reason for the loss of order in the region around the activation peptide (even when the rest of the structure does not change much) is the absence of calcium at Cab1. Such a loss of secondary structure would tend to render it more susceptible to proteolytic attack (Fig. 1). This data explains an earlier observation in the literature, which reports that mutating the Cab1 binding site residues results in faster proteolysis of the zymogenic FXIII A⁵⁷.

Post thrombin cleavage, the Cab1-mediated zymogenic constraint is apparently lost when the Cab2 binding site becomes exposed and coordinates a calcium ion. The first four of a simulated temporal series of eight transition state intermediate models suggest that the co-ordination of the first two calcium binding sites may be antagonistic to each other (*i.e.*, the bound calcium occupancy at Cab2 transiently destabilizes the Cab1 site) (Fig. 3). The cleavage of FXIII-AP may serve multiple roles. Firstly, it may expose Cab2 as discussed above. Secondly, SMD simulated dissociation of the subunits of the zymogenic FXIII A₂ dimer (with or without N-terminal FXIII-AP sequence) suggested that the absence of FXIII-AP results in a weakened dimeric interface (Fig. 2). A similar, supportive experimental observation was recently reported by Schroeder *et al.*³² using mutated FXIII-AP variants⁵⁸. Lastly, the removal of FXIII-AP, according to our simulation analysis, may result in overall tendency towards heterotetramer dissociation, as supported by analysis of our partial heterotetramer model (Fig. 5). Our simulation analysis also suggests that the ionic co-ordination of Cab2 and Cab3 imparts a conformational change through forces on the peptide backbone that propagates N- to C-terminal, finally enabling the barrel-1 and barrel-2 domains to rotate/translate and convert the apoenzyme to the active form. The calcium coordination of the Cab2 site also conformationally alters residue conformations at the Cab3 site. Stieler *et al.* (2013) hypothesized that this rearrangement of the loop is critical for access of the K substrate (Lysine substrate) that enters the catalytic hydrophobic pocket from this direction²⁶. We observed in our partial heterotetramer model that this region is masked partly by portions of the FXIIIB subunit. The rearrangements in the Cab3 site would potentially also weaken the FXIII A: FXIIIB interactions, thereby increasing access of calcium in the aqueous milieu to the Cab3 site. With our transition state intermediate models we were able to reproduce and observe the calcium binding changes postulated by Stieler *et al.* (2013), but in an all-atoms dynamic representation across a short temporal window²⁶. Furthermore, we were able to observe the formation of a hydrophobic catalytic pocket in which the acylenzyme Q substrate (Glutamine substrate) intermediate could be formed. The formation of a hydrophobic tunnel and the oxyanion hole that retains and stabilizes this intermediate was also observed in later stage transition intermediates (Fig. 4B). Such oxyanion holes have been reported not only for FXIII, but also in other transglutaminases as well as cysteine proteases that comprise a family of enzymes from which transglutaminases are thought to have evolved⁵⁹. Movement of the His342-Glu401 diad residues towards each other in the early

stage simulation intermediates, and then away from each other in the final stages, was also observed in this study (Fig. 4A). Maurer *et al.* (2004 and 2007) observed that FXIIIa residues 513–522 showed decreased surface accessibility post-activation for both proteolytic and non-proteolytic activation pathways^{60,61}. Among our simulated transition state intermediates, we observed that residue patch 501–522 in the zymogenic FXIIIa forms a V with an angle of 122° that closes upon itself in subsequent activation intermediates, thereby occluding access to residues 513–522. This would explain the decreased surface accessibility. Similarly, Maurer *et al.* (2004 and 2007) also showed that residues 523–546 also exhibited decreased accessibility only during non-proteolytic activation^{60,61}. We believe that during non-proteolytic activation, the presence of FXIII-AP serves to retain the activated form of FXIIIa as a weak dimer, unlike in proteolytic activation where it apparently dissociates into monomers. We observed that, on application of simulated forces to separate the FXIIIa subunits, the dimer remains associated only through a few residues (Arg11, Arg12, Asp343 and Glu410) that form interactions between the FXIII-AP and the core domain. Our dissociation simulation results suggest that these associations will have the effect of rotating each monomer relative to the other during activation. As a result, residues 526–546 of one monomer would end up opposed to the analogous residues on the opposite monomer, effectively forming a rearranged interface for the weakened dimer and concomitantly preventing local solvent accessibility (Figure S11). This is also consistent with non-proteolytic activation of FXIIIa being reversible⁶².

When we simulated dissociation of the FXIIIB subunit from the FXIIIa subunit in the partially modeled heterodimer, we observed that structural rearrangements in the interface regions between FXIIIa and FXIIIB showed a strong correlation with rearrangements in the three calcium binding sites along with large variations in estimated solvation energies (Fig. 6). These two relationships in distant structural rearrangements suggest the interdependence of the rearrangements (*i.e.*, the binding of calcium at Cab2 also contributes to weakening of the FXIIIa:FXIIIB interface and also causes local rearrangements at the Cab3 site). The final residues to dissociate in the FXIIIa dimer are from the core domain (Asn 175, Asp297) and barrel-2 domain, (Lys677) indicating that dissociation of at least a portion of the FXIIIB subunit is crucial to full exposure of the catalytic site as well as to the final movements of the barrel domains.

Our simulation suggests that saturation of calcium binding at Cab3 is likely the last molecular event leading to dissociation at the FXIIIa:FXIIIB interface. This is in agreement with our *in vitro* dissociation results observed by gel filtration when higher calcium concentrations resulted in increased dissociation of FXIIIB₂ dimer from the primary heterotetramer FXIIIa₂B₂ (Fig. 7). The absence of FXIIIa_a, as a resolved peak in our gel filtration results could be the result of subsequent inactivation or instability of FXIIIa_a. This instability of FXIIIa_a may be due to dissociation of FXIIIB subunits that would expose the secondary thrombin cleavage site of FXIIIa_a 515–516⁶³. Interestingly, when we analyzed the exposed surface area of activated FXIIIa_a compared to that of the zymogenic form in our simulations, we identified a number of putative sites within additional surface exposed locations that would theoretically be susceptible to protease activity (Figure S12). The FXIIIa zymogenic form, as well as the activated form, has been shown in the literature to be susceptible to cleavage by proteases other than thrombin^{2,64}. Also, cleavage by polymorphonuclear granulocyte proteases (PMN) has been suggested to be one of a number of possible down-regulation mechanisms for inactivating FXIIIa_a within the fibrin clot⁶⁵. We expect that activated FXIIIa_a in the absence of bound FXIIIB is down-regulated *in vivo* primarily by sequential proteolytic degradation that might be initiated by thrombin. This also explains reports of its short circulating activity half-life in literature and in results of this study as well⁶⁶. This aspect of down-regulation of FXIIIa requires further investigation, however, as we could not identify evidence of proteolyzed FXIIIa following the two major protein elution peaks observed in the present gel filtration experiments. Interestingly a very recent article suggests that Thrombin cleavage could be a means of FXIIIa_a downregulation but only after primary cleavage by Plasmin⁶⁷. The fact that our simulation results suggested that the FXIIIB subunit dissociates from FXIIIa only after the calcium binding site Cab3 becomes saturated is experimentally supported by the results of our gel filtration experiments. Specifically, the amount of FXIII heterotetramer resolved significantly decreased with increasing calcium concentration, but also appeared at different retention times which suggest that the complex structure undergoes some conformational transformation as a loose/weakened heterotetramer without the dissociation of FXIIIB subunit.

A secondary observation in this study, which has also recently been reported by two other groups^{35,36}, was the influence of FXIIIB subunit on the activation of FXIIIa. We observed in FXIII generation assays (which mimic the physiological conditions) that addition of rFXIIIB₂ to rFXIIIa₂ accelerates activation (Figure S5). Ichinose *et al.*³¹ explained their similar observation by the interaction of FXIIIB₂ subunit with fibrinogen³⁵. However, in the same article they also elaborate that differences in the FXIIIB₂ C-terminus (interaction site for Fibrinogen) as observed between FXIIIB subunit isoforms FXIIIB*1 and FXIIIB*3 do not affect fibrinogen binding and that there might be other contributing factors to this observation. We suggest an explanation for this observation using simulation result based on our partial heterodimeric model of FXIIIa₂B. Specifically, our results suggest that Sushi domain 1 may dock onto a hydrophobic fold formed by the N-terminal part of the activation peptide (Fig. 5). Also, our simulation results suggest that dissociation of FXIIIB may cause the FXIII-AP sessile bond to be less accessible. We suggest that the putative hydrophobic interactions between the FXIIIB Sushi S1 domain and the FXIII-AP may allow increased efficiency in proximal thrombin cleavage. This is evident also from our FXIIIB subunit spiked FXIII generation assay, results where in the presence of FXIIIB accelerates the activation of FXIIIa. This combined with the data from activation peptide, suggests that the interactions of activation peptide with the opposite monomer of FXIIIa and the FXIIIB subunit maintain the region around the activation peptide in a spatial location ideal for insertion and cleavage by thrombin at the right time and place *i.e.* they both contribute to a perfect cleavage (neither too early nor delayed).

The entire simulated sequence of activation events described in our article would be expected to take place in the plasma (Concentration of calcium: Free ions 1.18 mmol/L, protein bound 1.14 mmol/liter, total 2.48 mmol/liter)⁶⁸. The question then arises: What is the sequence of events involving activation for intracellular FXIIIa₂? We assume that the dimeric FXIIIa₂ molecule exists intracellularly as an ion regulated equilibrium between its

activated and zymogenic state. Since the intracellular levels of calcium are lower than in plasma, the occluding effects of FXIII-AP and FXIIIB binding on the Cab2 and Cab3 calcium binding sites would not be expected to be consequential *in vivo* in cells. At low levels of calcium, only the Cab1 site would be occupied and, hence, a dynamic equilibrium shift towards the zymogenic state is expected. A change in this equilibrium might be caused by intracellular calcium influx under conditions when activation of intracellular FXIII_{A2} is required. Therefore, saturation of Cab2 and Cab3 with calcium could occur without FXIII-AP cleavage, resulting in a reversible form of activation of FXIII_{A2} possibly in a manner similar to our simulated results. Interestingly, it has been reported that FXIII_{A2} can also be activated without thrombin cleavage and at low calcium concentration, but only on a very long time scale⁶⁹. Thus, our results further suggest that all three calcium binding sites are occupied during the activation of FXIII irrespective of the type of activation.

To briefly summarize our work, this study provides some major insights into the activation and regulation mechanism of FXIII. In a stepwise manner we have shown how calcium binding regulates both the zymogenic and activated forms of FXIII. The information contained in the subtle structural changes observed in the various intermediates models can be used to design high efficiency inhibitors against FXIII. Additionally, for the first time our study lends a hypothetical structure functional perspective/account of FXIII: FXIIIB interactions during the dissociation of the FXIII_{A2}B₂ complex. Information in this regard would further contribute to the final elucidation of the FXIII_{A2}B₂ complex structure and its dynamics during assembly or dissociation.

References

- Lorand, L., Losowsky, M. S. & Miloszewski, K. J. Human factor XIII: fibrin-stabilizing factor. *Prog Hemost Thromb.* **5**, 245–290 (1980).
- Schwartz, M. L., Pizzo, S. V., Hill, R. L. & McKee, P. A. Human Factor XIII from plasma and platelets. Molecular weights, subunit structures, proteolytic activation, and cross-linking of fibrinogen and fibrin. *J Biol Chem.* **248**, 1395–1407 (1973).
- Muszbeek, L., Ariens, R. A. & Ichinose, A. & Isth Ssc Subcommittee On Factor, X. Factor XIII: recommended terms and abbreviations. *J Thromb Haemost.* **5**, 181–183 (2007).
- Lorand, L. & Graham, R. M. Transglutaminases: crosslinking enzymes with pleiotropic functions. *Nat Rev Mol Cell Biol.* **4**, 140–156 (2003).
- Klock, C. & Khosla, C. Regulation of the activities of the mammalian transglutaminase family of enzymes. *Protein Sci.* **21**, 1781–1791 (2012).
- Biswas, A., Ivaskevicius, V., Seitz, R., Thomas, A. & Oldenburg, J. An update of the mutation profile of Factor 13 A and B genes. *Blood Rev.* **25**, 193–204 (2011).
- Biswas, A., Ivaskevicius, V., Thomas, A. & Oldenburg, J. Coagulation factor XIII deficiency. Diagnosis, prevalence and management of inherited and acquired forms. *Hamostaseologie.* **34**, 160–166 (2014).
- Biswas, A. *et al.* Eight novel F13A1 gene missense mutations in patients with mild FXIII deficiency: in silico analysis suggests changes in FXIII-A subunit structure/function. *Ann Hematol.* **93**, 1665–1676 (2014).
- Ivaskevicius, V. *et al.* A common F13A1 intron 1 variant IVS1 + 12(A) is associated with mild FXIII deficiency in Caucasian population. *Ann Hematol.* **92**, 975–979 (2013).
- Ivaskevicius, V. *et al.* Mutations affecting disulphide bonds contribute to a fairly common prevalence of F13B gene defects: results of a genetic study in 14 families with factor XIII B deficiency. *Haemophilia.* **16**, 675–682 (2010).
- Ivaskevicius, V. *et al.* Identification of eight novel coagulation factor XIII subunit A mutations: implied consequences for structure and function. *Haematologica.* **95**, 956–962 (2010).
- Muszbeek, L., Bereczky, Z., Bagoly, Z., Komaromi, I. & Katona, E. Factor XIII: a coagulation factor with multiple plasmatic and cellular functions. *Physiol Rev* **91**, 931–972 (2011).
- Myneni, V. D., Hitomi, K. & Kaartinen, M. T. Factor XIII-A transglutaminase acts as a switch between preadipocyte proliferation and differentiation. *Blood.* **124**, 1344–1353 (2014).
- Malara, A. *et al.* Megakaryocyte-matrix interaction within bone marrow: new roles for fibronectin and factor XIII-A. *Blood.* **117**, 2476–2483 (2011).
- Gemmati, D. *et al.* Factor XIII-A dynamics in acute myocardial infarction: a novel prognostic biomarker? *Thromb Haemost.* **114**, 123–132 (2015).
- Wang, Z. *et al.* Pathogen entrapment by transglutaminase—a conserved early innate immune mechanism. *PLoS Pathog.* **6**(29), e1000763 (2010).
- Aeschlimann, D. & Thomazy, V. Protein crosslinking in assembly and remodelling of extracellular matrices: the role of transglutaminases. *Connect Tissue Res.* **41**, 1–27 (2000).
- Raghu, H. *et al.* Transglutaminase factor XIII promotes arthritis through mechanisms linked to inflammation and bone erosion. *Blood.* **125**, 427–437 (2015).
- Grundmann, U., Amann, E., Zettlmeissl, G. & Kupper, H. A. Characterization of cDNA coding for human factor XIIIa. *Proc Natl Acad Sci.* **83**, 8024–8028 (1986).
- Ichinose, A., Hendrickson, L. E., Fujikawa, K. & Davie, E. W. Amino acid sequence of the a subunit of human factor XIII. *Biochemistry.* **25**, 6900–6906 (1986).
- Ichinose, A., McMullen, B. A., Fujikawa, K. & Davie, E. W. Amino acid sequence of the b subunit of human factor XIII, a protein composed of ten repetitive segments. *Biochemistry.* **25**, 4633–4638 (1986).
- Yee, V. C. *et al.* Three-dimensional structure of a transglutaminase: human blood coagulation factor XIII. *Proc Natl Acad Sci.* **91**, 7296–7300 (1994).
- Yee, V. C., Pedersen, L. C., Bishop, P. D., Stenkamp, R. E. & Teller, D. C. Structural evidence that the activation peptide is not released upon thrombin cleavage of factor XIII. *Thromb Res.* **78**, 389–397 (1995).
- Weiss, M. S., Metzner, H. J. & Hilgenfeld, R. Two non-proline cis peptide bonds may be important for factor XIII function. *FEBS Lett.* **423**, 291–296 (1998).
- Fox, B. A. *et al.* Identification of the calcium binding site and a novel ytterbium site in blood coagulation factor XIII by x-ray crystallography. *J Biol Chem* **274**, 4917–4923 (1999).
- Stieler, M. *et al.* Structure of active coagulation factor XIII triggered by calcium binding: basis for the design of next-generation anticoagulants. *Angew Chem Int Ed Engl.* **52**, 11930–11934 (2013).
- Carrell, N. A., Erickson, H. P. & McDonagh, J. Electron microscopy and hydrodynamic properties of factor XIII subunits. *J Biol Chem.* **264**, 551–556 (1989).
- Biswas, A., Thomas, A., Bevans, C. G., Ivaskevicius, V. & Oldenburg, J. *In vitro* secretion deficits are common among human coagulation factor XIII subunit B missense mutants: correlations with patient phenotypes and molecular models. *Hum Mutat.* **34**, 1490–1500 (2013).
- Souri, M., Kaetsu, H. & Ichinose, A. Sushi domains in the B subunit of factor XIII responsible for oligomer assembly. *Biochemistry.* **47**, 8656–8664 (2008).

30. Katona, E. *et al.* Interaction of factor XIII subunits. *Blood*. **123**, 1757–1763 (2014).
31. Souri, M., Osaki, T. & Ichinose, A. The Non-catalytic B Subunit of Coagulation Factor XIII Accelerates Fibrin Cross-linking. *J Biol Chem*. **290**, 12027–12039 (2015).
32. Schroeder, V., Handrkova, H., Dodt, J. & Kohler, H. P. Free factor XIII activation peptide affects factor XIII function. *Br J Haematol*. **168**, 757–759 (2015).
33. Leung-Toung, R. *et al.* 3-Substituted imidazo[1,2-d][1,2,4]-thiadiazoles: a novel class of factor XIIIa inhibitors. *J Med Chem*. **48**, 2266–2269 (2005).
34. Lorand, J. B., Pilkington, T. R. & Lorand, L. Inhibitors of fibrin cross-linking: relevance for thrombolysis. *Nature*. **210**, 1273–1274 (1966).
35. Lorand, L., Chou, C. H. & Simpson, I. Thiolester substrates for transamidating enzymes: studies on fibrinoligase. *Proc Natl Acad Sci*. **69**, 2645–2648 (1972).
36. Finney, S., Seale, L., Sawyer, R. T. & Wallis, R. B. Tridegin, a new peptidic inhibitor of factor XIIIa, from the blood-sucking leech *Haementeria ghilianii*. *Biochem J*. **324** (Pt 3), 797–805 (1997).
37. Tymiak, A. A., Tuttle, J. G., Kimball, S. D., Wang, T. & Lee, V. G. A simple and rapid screen for inhibitors of factor XIIIa. *J Antibiot (Tokyo)*. **46**, 204–206 (1993).
38. Heil, A., Weber, J., Buchold, C., Pasternack, R. & Hils, M. Differences in the inhibition of coagulation factor XIII-A from animal species revealed by Michael Acceptor- and thioimidazol based blockers. *Thromb Res*. **131**, e214–e222 (2013).
39. Komaromi, I., Bagoly, Z. & Muszbek, L. Factor XIII: novel structural and functional aspects. *J Thromb Haemost*. **9**, 9–20 (2011).
40. Liu, S., Cerione, R. A. & Clardy, J. Structural basis for the guanine nucleotide-binding activity of tissue transglutaminase and its regulation of transamidation activity. *Proc Natl Acad Sci*. **99**, 2743–2747 (2002).
41. Krieger, E., Koraimann, G. & Vriend, G. Increasing the precision of comparative models with YASARA NOVA—a self-parameterizing force field. *Proteins*. **47**, 393–402 (2002).
42. Krieger, E. & Vriend, G. YASARA View - molecular graphics for all devices - from smartphones to workstations. *Bioinformatics*. **30**, 2981–2982 (2014).
43. Choi, Y. & Deane, C. M. FREAD Revisited: Accurate loop structure prediction using a database search algorithm. *Proteins*, **78**, 1431–1440 (2009).
44. Case, D. A. *et al.* The Amber biomolecular simulation programs. *J Comput Chem*. **26**, 1668–1688 (2005).
45. Hooft, R. W., Vriend, G., Sander, C. & Abola, E. E. Errors in protein structures. *Nature* **381**, 272 (1996).
46. Pettersen, E. F. *et al.* UCSF Chimera—a visualization system for exploratory research and analysis. *J Comput Chem*. **25**, 1605–1612 (2004).
47. Krissinel, E. & Henrick, K. Inference of macromolecular assemblies from crystalline state. *J Mol Biol*. **372**, 774–797 (2007).
48. Baker, N. A., Sept, D., Joseph, S., Holst, M. J. & McCammon, J. A. Electrostatics of nanosystems: application to microtubules and the ribosome. *Proc Natl Acad Sci*. **98**, 10037–10041 (2001).
49. Das, A. *et al.* Exploring the conformational transitions of biomolecular systems using a simple two-state anisotropic network model. *PLoS Comput Biol*. **10**, e1003521 (2014).
50. Moore, B. L., Kelley, L. A., Barber, J., Murray, J. W. & MacDonald, J. T. High-quality protein backbone reconstruction from alpha carbons using Gaussian mixture models. *J Comput Chem*. **34**, 1881–1889 (2013).
51. Roy, A., Kucukural, A. & Zhang, Y. I-TASSER: a unified platform for automated protein structure and function prediction. *Nat Protoc*. **5**, 725–738 (2010).
52. Pierce, B., Tong, W. & Weng, Z. M-ZDOCK: a grid-based approach for Cn symmetric multimer docking. *Bioinformatics*. **21**, 1472–1478 (2005).
53. Soares, D. C., Gerloff, D. L., Syme, N. R., Coulson, A. F., Parkinson, J. & Barlow, P. N. Large-scale modelling as a route to multiple surface comparisons of the CCP module family. *Protein Eng Des Sel*. **18**, 379–388 (2005).
54. Dodt, J., Volkars, P. & Seitz, R. Factor XIIIa generation assay: a tool for studying factor XIII function in plasma. *Anal Biochem*. **439**, 145–151 (2013).
55. Jang, T. H. *et al.* Crystal structure of transglutaminase 2 with GTP complex and amino acid sequence evidence of evolution of GTP binding site. *PLoS One* **9**, e107005 (2014).
56. Stammaes, J., Pinkas, D. M., Fleckenstein, B., Khosla, C. & Sollid, L. M. Redox regulation of transglutaminase 2 activity. *J Biol Chem*. **285**, 25402–25409 (2010).
57. Lai, T. S., Slaughter, T. F., Peoples, K. A. & Greenberg, C. S. Site-directed mutagenesis of the calcium-binding site of blood coagulation factor XIIIa. *J Biol Chem*. **274**, 24953–24958 (1999).
58. Handrkova, H., Schroeder, V. & Kohler, H. P. The activation peptide of coagulation factor XIII is vital for its expression and stability. *J Thromb Haemost*. **13**, 1449–1458 (2015).
59. Simón, L. & Goodman, J. M. Enzyme catalysis by hydrogen bonds: the balance between transition state binding and substrate binding in oxyanion holes. *J Org Chem*. **75**(6), 1831–1840 (2010).
60. Turner, B. T. Jr., Sabo, T. M., Wilding, D. & Maurer, M. C. Mapping of factor XIII solvent accessibility as a function of activation state using chemical modification methods. *Biochemistry*. **43**, 9755–9765 (2004).
61. Sabo, T. M., Brasher, P. B. & Maurer, M. C. Perturbations in factor XIII resulting from activation and inhibition examined by solution based methods and detected by MALDI-TOF MS. *Biochemistry*. **46**, 10089–10101 (2007).
62. Kristiansen, G. K. & Andersen, M. D. Reversible activation of cellular factor XIII by calcium. *J Biol Chem*. **286**, 9833–9839 (2011).
63. Mary, A., Achyuthan, K. E. & Greenberg, C. S. b-chains prevent the proteolytic inactivation of the a-chains of plasma factor XIII. *Biochim Biophys Acta*. **8:966**(3), 328–335 (1988).
64. Curtis, C. G. *et al.* Calcium-dependent unmasking of active center cysteine during activation of fibrin stabilizing factor. *Biochemistry*. **13**(18), 3774–3780 (1974).
65. Bagoly, Z., Haramura, G. & Muszbek, L. Down-regulation of activated factor XIII by polymorphonuclear granulocyte proteases within fibrin clot. *Thromb Haemost*. **98**, 359–367 (2007).
66. Robinson, B. R., Houg, A. K. & Reed, G. L. Catalytic life of activated factor XIII in thrombi. Implications for fibrinolytic resistance and thrombus aging. *Circulation*. **5:102**(10), 1151–1157 (2000).
67. Hur, W. S. *et al.* Coagulation factor XIIIa is inactivated by plasmin. *Blood*. **126**(20), 2329–2337 (2015).
68. Baker, S. B. & Worthley, L. I. The essentials of calcium, magnesium and phosphate metabolism: part I. *Physiology. Crit Care Resusc*. **4**(4), 301–306 (2002).
69. Polgar, J., Hidasi, V. & Muszbek, L. Non-proteolytic activation of cellular protransglutaminase (placenta macrophage factor XIII). *Biochem J*. **267**, 557–560 (1990).

Acknowledgements

The authors would like to acknowledge Prof. Dr. Hartmut Michel (Max Planck Institute for Biophysics, Frankfurt) for providing the infrastructure for performing gel filtration analysis. Mohammad Ahmar Jamil (IHT, Bonn) and Peter Volkars (PEI, Langen) for the heat map generation and biostatistical analysis. Dorothea Hausleithner (PEI, Langen) for help with the FXIII generation assay. Sophie Lyonga (IHT, Bonn) for technical help. The authors would like to acknowledge CSL Behring for funding research on Factor XIII.

Author Contributions

A.B. and J.O. are the principle investigators of the study. S.G., C.K., C.R. and M.S.A. performed the gel filtration analysis, recombinant FXIIIa production and purification of FXIIIa₂B₂ from Fibrogamin. A.B. performed the *in silico* work. J.D. and A.R. contributed with the FXIIIa generation assays and MS analysis. A.B. and S.G. analyzed the data. A.B. and S.G. co-wrote the article. J.O., H.P. and V.I. edited and contributed to the intellectual content of the article. A.B. designed and supervised the study.

Additional Information

Supplementary information accompanies this paper at <http://www.nature.com/srep>

Competing financial interests: The authors declare no competing financial interests.

How to cite this article: Gupta, S. *et al.* Revisiting the mechanism of coagulation factor XIII activation and regulation from a structure/functional perspective. *Sci. Rep.* **6**, 30105; doi: 10.1038/srep30105 (2016).



This work is licensed under a Creative Commons Attribution 4.0 International License. The images or other third party material in this article are included in the article's Creative Commons license, unless indicated otherwise in the credit line; if the material is not included under the Creative Commons license, users will need to obtain permission from the license holder to reproduce the material. To view a copy of this license, visit <http://creativecommons.org/licenses/by/4.0/>

© The Author(s) 2016

Chapter 3

Published article

Structure-functional insights into calcium induced activation of factor XIII-A molecule.

Sneha Singh, Johannes Dodt, Peter Volkers, Emma Hethershaw, Helen Philippou, Vytautas Ivaskevicius, Diana Imhof, Johannes Oldenburg, & Arijit Biswas

A brief synopsis:

Based on the hypothesis generated in chapter 1, this chapter proceeds with analyzing the roles of individual calcium binding sites on overall activation of FXIII-A molecule. In order to achieve that we performed point mutations at the calcium binding site residues, that derived structural mutants that were expected to bear differential activation states as compared to wild-type FXIII-A (based on hypothesis). A detailed phylogenetic, structural and functional characterization of eight such mutants, combined with in-silico experiments, further concluded that; a) Calcium binding sites on FXIII-A molecule are rather conserved sites and their saturation influences the substrate specificity of FXIII-A; b) Saturation of Cab1 (first calcium binding site) act as zymogenic constraint towards FXIII activation; c) other than Calcium, ancillary ions also support in bringing the FXIII-A molecule to a pre-activated state; and, d) Energetically, FXIII-A activation is a step-wise process which ultimately leads to formation of a calcium saturated, open, active-monomeric FXIII-A* molecule. The conclusions from this chapter lies in agreement with the recent studies performed by several other FXIII-research groups as well. Collectively, this chapter presents a new set of targetable sites on FXIII-A molecule (calcium binding sites), that may lead to generation of inhibitors against FXIII-A, or recombinant FXIII-A species with altered substrate specificity and/or rate of activation.

Sci Rep. 2019; 9: 11324. Published online 2019 Aug 5. doi: 10.1038/s41598-019-47815-z

open **Structure functional insights into calcium binding during the activation of coagulation factor Xiii A**

Sneha Singh¹, Johannes Dodt^{1,2}, peter Volkers², emma Hethershaw^{1,3}, Helen philippou^{1,3}, Vytautas ivaskevicius¹, Diana imhof^{1,4}, Johannes oldenburg¹ & Arijit Biswas¹

the dimeric fXiii-A₂, a pro-transglutaminase is the catalytic part of the heterotetrameric coagulation fXiii-A₂B₂ complex that upon activation by calcium binding/thrombin cleavage covalently cross-links preformed fibrin clots protecting them from premature fibrinolysis. Our study characterizes the recently disclosed three calcium binding sites of fXiii-A concerning evolution, mutual crosstalk, thermodynamic activation profile, substrate binding, and interaction with other similarly charged ions. We demonstrate unique structural aspects within FXIII-A calcium binding sites that give rise to functional differences making FXIII unique from other transglutaminases. The first calcium binding site showed an antagonistic relationship towards the other two. The thermodynamic profile of calcium/thrombin-induced FXIII-A activation explains the role of bulk solvent in transitioning its zymogenic dimeric form to an activated monomeric form. We also explain the indirect effect of solvent ion concentration on FXIII-A activation. Our study suggests FXIII-A calcium binding sites could be putative pharmacologically targetable regions.

Calcium ions (Ca²⁺) play a major role in the tight regulation of coagulation cascade that is paramount in the maintenance of hemostasis^{1,2}. Other than platelet activation, calcium ions are responsible for complete activation of several coagulation factors, including coagulation Factor XIII (FXIII)³. FXIII is responsible for covalently cross-linking preformed fibrin clots preventing their premature fibrinolysis, by maintaining the clot architecture and strength. FXIII circulates in plasma as a heterotetrameric pro-transglutaminase (pFXIII), complex FXIII-A₂B₂ composed of dimeric subunits of catalytic FXIII-A and protective/regulatory FXIII-B⁴⁻⁷. Although the catalytic FXIII-A subunit bears several structural and sequence similarities with other transglutaminases, it is also unique in specific aspects⁸. Unlike other members of the transglutaminase family, FXIII-A is the only molecule activated by a combination of calcium binding and proteolytic thrombin cleavage of an N-terminal 37-amino acid region [activation peptide (FXIII-AP)]. Additionally, it is also the only transglutaminase whose functional molecule is a complex, unlike other transglutaminases that are monomeric. FXIII-A, like all other transglutaminases belongs to a category of calcium-binding proteins that lacks EF-hand motif, a typical structural helix-loop-helix topology commonly found in calcium binding proteins⁹. Transglutaminases are believed to have evolved from an ancient cysteine protease in bacteria¹⁰. The microbial transglutaminase though has evolved divergently from the eukaryotic transglutaminases¹¹. Although calcium-binding is common to the activation pathway of all transglutaminases, different members of the transglutaminase family show additional regulatory/functional features in their activation mechanisms, despite sharing a structural and sequential similarity. For instance, Transglutaminase 2 (TG2) has multiple regulatory features in addition to calcium binding like vicinal disulfide bonds and GTP/GDP binding which in combination control the activity status of the protein at different ionic conditions⁹. The FXIII-A subunit is a structurally well-characterized protein with several zymogenic crystal structures, in ion-bound (to different cations; PDB IDs: 1ggg, 1ggy, 1qrk) and unbound states (PDB ID: 1fie, 1f13) present in the protein structure database¹²⁻¹⁴. The recent disclosure of the non-proteolytically activated form of FXIII-A (FXIII-A*) (PDB ID: 4kty) has shown the presence of three calcium binding sites in FXIII-A¹⁵. The first FXIII-A calcium binding site (Cab1) involves the residues Ala457, Asn 436, Glu 485 and Glu 490, the

¹Institute of Experimental Hematology and Transfusion medicine, University Hospital of Bonn, Bonn, 53127, Germany. ²Paul-Ehrlich Institute, Langen, 63225, Germany. ³Discovery and Translational Science Department, University of Leeds, Leeds, LS29JT, United Kingdom. ⁴Pharmaceutical Biochemistry and Bioanalytics, Pharmaceutical Institute, University of Bonn, An der Immenburg 4, Bonn, 53121, Germany. Correspondence and requests for materials should be addressed to A.B. (email: arijit.biswas@ukb.uni-bonn.de)

Received: 12 October 2018

Accepted: 24 July 2019

Published online: 05 August 2019

second calcium binding site (Cab2) uses the residues Asp 351, Gln 459, Asn 347, Asp 349, and Asp 343 and the third calcium binding site (Cab3) coordinates the residues Asp 271, Asn 267, Asp 270 and Ala 264¹⁵. In our earlier study, while explaining the concerted model of FXIII activation we had demonstrated *in silico* that the first calcium binding site (Cab1) that is usually observed constitutively coordinated in specific zymogenic FXIII-A crystal structures (E.g. PDB ID: 1ggu), actually lays a stabilizing influence on the zymogenic form^{12,16}. We also showed that its transient disruption upon thrombin-mediated FXIII-AP cleavage and simultaneous coordination of the other two calcium binding sites (Cab2, Cab3) is essential for the conformational activation of zymogenic FXIII-A. Cellular FXIII (cFXIII) that is inaccessible to plasma thrombin requires high supra-physiological levels of calcium or a combination of high sodium and physiological calcium for non-proteolytic activation. Hence, Cab1 as a zymogenic constraint acts antagonistically to the other two calcium binding sites keeping the molecule inactive intracellularly in the absence of thrombin unless provoked by high ion concentrations¹⁶.

In continuation of our preliminary work and observations, our current study takes a deeper look into the calcium binding sites of FXIII-A. We investigate how these sites contribute to the functional evolution of FXIII molecule as a unique protein in the transglutaminase family. We characterize the three FXIII-A calcium binding sites concerning their evolution, mutual crosstalk, and effect on FXIII-A thermodynamic profile, substrate binding and interaction with other similarly charged ions. The FXIII-A calcium binding sites show a high degree of conservation within transglutaminases, but at the same time, they also possess unique spatial and structural features that differentiate FXIII-A as a unique molecule amongst transglutaminases. Our results confirm that saturation of the first calcium-binding site lays a zymogenic constraint that resists the activation of FXIII-A, as was hypothesized in our earlier work¹⁶. The thermodynamic profile of FXIII-A activation observed during increased calcium binding reiterates recent observations that calcium binding to FXIII-A results in major conformational changes leading up to the dissociation of the FXIII-A₂ dimer during activation to a monomeric activated FXIII-A (FXIII-A*) form. Using all atoms MD simulations of FXIII-A and its core domain under different ionic concentrations we show that apart from coordination with charged residues, the mere presence of cations can also bring about subtle changes in the structure of FXIII-A by altering the surface electrostatics. The alteration of FXIII-A subunit's surface electrostatics can, in the long term, influence the activation status of the molecule in different ionic conditions.

Results

Calcium binding site residues on FXIII-A molecule are highly conserved. Within the multiple alignments of FXIII-A with other known transglutaminases, all three calcium binding site residues showed a high degree of conservation [Average generalized conservation score: 9 (range = 8–9)] (Fig. 1a). However, several variant substitutions observed in the multiple alignments corresponding to these residues, including few (Cab1 residues E485 and E490) in which the substitution was to an oppositely charged residue. These residues occur in a semi-conserved region with the conservation status varying between high to low conservation between alternating residues (Fig. 1b). The structural alignment of the crystal structures of FXIII-A, TG2, TG3 and threaded models of TG1, TG4, TG5, TG6, TG7 shows proper domain-wise alignment with the average RMSD of 1.2 Å (Range: 0.5–1.71 Å) (Fig. 1c). FXIII-A shows the closest structural similarity with TG1 (0.5 Å RMSD) (Fig. 1c,d). The three calcium binding sites were in spatially similar locations in the aligned structures (Fig. 1c). However, the distance between their backbone atoms as well as the orientation of the side chain residues differed between transglutaminases (Fig. 1e).

Biochemical endpoint FXIII activity assays reveal that calcium binding influences the formation of substrate binding pockets on FXIII-A molecule. Biochemical endpoint FXIII activity assays, which primarily evaluate transglutaminase cross-linking function when evaluated for the FXIII-A calcium binding mutants showed most of them lacking in cross-linking ability. The photometric assay, combined with antigenic determination revealed that the specific activity of FXIII-A was reduced in all mutants expressed when compared with the wild type (0.02 ± 0.001 IU/mg/mL). The mutant N347D reported the lowest specific activity (0.00087 ± 0.0001 IU/mg/mL; $p < 0.0001$) (Fig. 2a). Pentylamine incorporation assay also reported low levels of interpolated FXIII-A activity (incorporated/crosslinked substrate in $\mu\text{g/mL}$) in all mutants except N267K (2.17 ± 0.58 $\mu\text{g/mL}$) in which it was non-significantly elevated when compared to the Wild type (1.92 ± 0.31 $\mu\text{g/mL}$; $p = 0.42$) (Fig. 2b). The lowest interpolated FXIII-A concentration was observed for the mutant D271K (0.32 ± 0.04 $\mu\text{g/mL}$; $p < 0.0001$). Similar to the Pentylamine incorporation assay, average interpolated active FXIII-A* concentration from the α -2-antiplasmin incorporation assay using fibrin as a substrate (in $\mu\text{g/mL}$) was also reduced for all mutants when compared with the wild type (8.97 ± 0.83 $\mu\text{g/mL}$), except in mutant A457D which showed non-significantly elevated levels (9.40 ± 0.02 $\mu\text{g/mL}$; $p = 0.09$) (Fig. 2c). One mutation from the Cab3 (D271K) and two from Cab2 (N347D, Q349D) showed no detectable α -2-antiplasmin incorporation (i.e. < 1.25 $\mu\text{g/mL}$). The putative substrate binding regions corresponding to fibrinogen substrate (in cyan) outnumber those of substrates α -2-antiplasmin (in magenta) and BAPA [5-(Biotinamido) pentylamine; PubChem ID: CID 83906] (in yellow) (Fig. 2d). This difference in putative binding sites is expected considering the relative sizes of these substrates, fibrinogen being the largest and BAPA the smallest (Supplementary Fig. 1). While some of these regions lie close to the active site, others are far from it and most likely have an allosteric role in substrate binding. Interestingly, fibrinogen substrate binding regions cover almost all calcium binding sites, but those of α -2-antiplasmin appear closer to Cab2 while those of BAPA lie closer to Cab3 (Fig. 2d).

Real-time monitoring of fXiii-A* generation confirms that Cab1 is a zymogenic constraint on FXIII-A. The FXIII-A* generation assay which tracks the rate of FXIII-A* generation real-time reported differences from the endpoint assay for the calcium binding site mutants in several of the parameters derived from

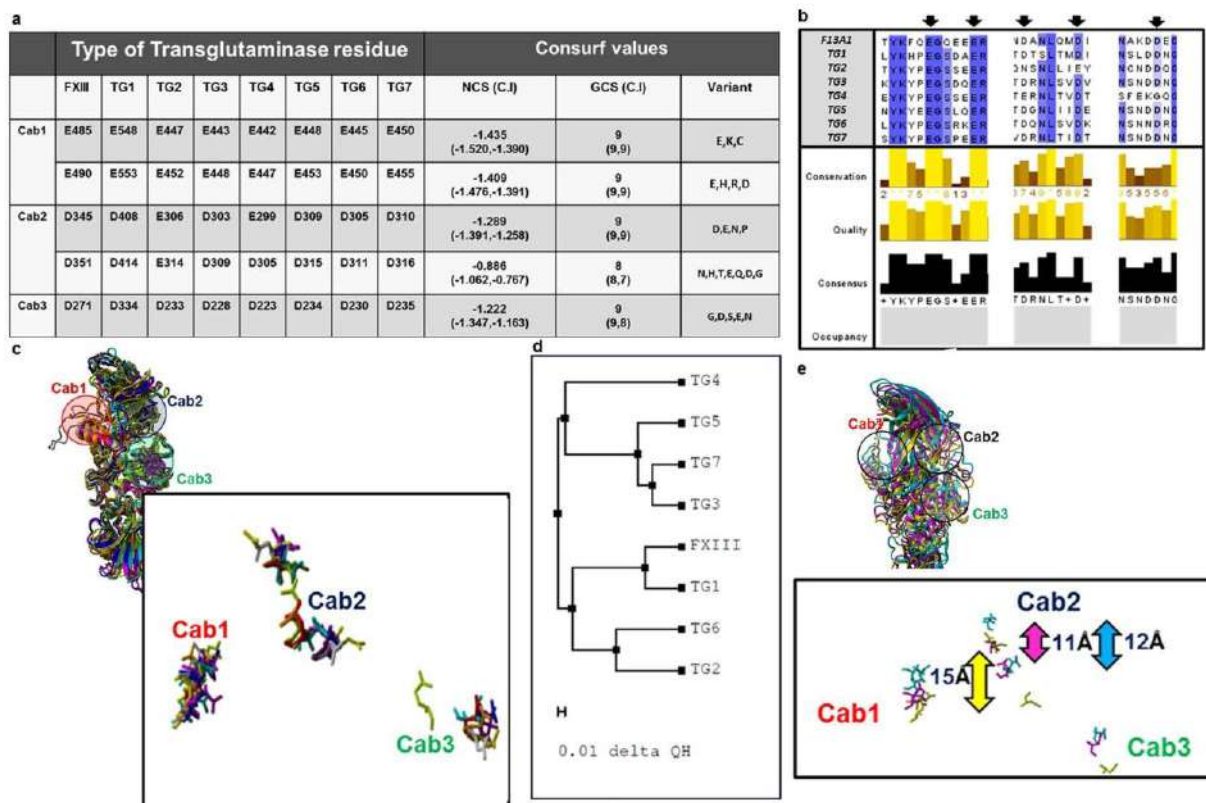


Figure 1. Conservation of calcium binding sites in Transglutaminases with respect to FXIII-A. Panel a tabulates the conservation results generated for the FXIII-A amino acid sequence input (Uniprot ID: P00488; F13A_HUMAN) on the *Consurf* server. Abbreviations: NCS: Normalized conservation score, GCS: Generalized conservation score. Panel b illustrates the actual alignment generated as output on the *Consurf* server for the FXIII-A subunit sequence input. The highly conserved residues are shaded in blue. Arrows indicate the binding site residues mutated in this study. Panel c shows a structural alignment of all seven human Transglutaminases i.e. of three crystal structures TG2, TG3 and FXIII-A and threaded models for the remaining four transglutaminases. The structures are depicted in ribbon format. The inset image shows the spatial alignment of the calcium binding site residues of all transglutaminases as stick models. The different transglutaminases are colored differently. Panel d shows a structural similarity tree generated from the structural alignment on Panel c. The distances on the tree represented by the delta QH value is proportional to the dissimilarity between two structures i.e. the farther two structures are there on the tree, the more structurally unlike they are. Panel e shows the structural alignment of only three human Transglutaminases with biophysical crystal structures i.e. TG2, TG3 and FXIII-A. The inset diagram the spatial alignment of the calcium binding site residues as stick models of the three human transglutaminases. The structures are depicted in ribbon format with TG2, TG3 and FXIII colored yellow, magenta and cyan respectively. The bidirectional arrows represent the C- α backbone atom distances between the D345 and D351 residue (FXIII; cyan), E306 and E314 residue (TG2; yellow), and D303 and D309 residue (TG3; magenta).

its curve (Fig. 3, Supplementary Fig. 2). The calcium binding site mutations have been designed keeping in mind our earlier formulated and reported hypothesis that making the Cab1 more positive will result in acceleration of FXIII-A activation while doing the same to Cab2 and Cab3 will impede activation and vice-versa (Fig. 3a)¹⁶. The Cab1 mutant E490K reported an almost ~2.5x times higher rate of FXIII-A* generation (μ) (217.36 ± 54.74 R.F.U./min) than the wild type rFXIII-A (83.17 ± 21.88 R.F.U./min) (Fig. 3b). The other Cab1 mutant A457D reported a lower rate of FXIII-A* generation but not significantly, so (64.34 ± 21.36 R.F.U./min). One mutation from the Cab3 (D271K) and two from Cab2 (N347D, Q349D) revealed a highly significant decrease in the rate of FXIII-A* generation/activation (Fig. 3b). The parameter t_{max} (time taken to reach the maximal rate μ) revealed a good inverse correlation with the rate of FXIII-A* generation or μ , with the lowest value for t_{max} consistent with the highest μ observed for Cab1 mutant E490K (Fig. 3c). The parameter t_{lag} (time required for the activation of FXIII-A by thrombin) was elevated for all mutants when compared to the wild type rFXIII-A except for the Cab2 mutant Q349D, which reported lower but non-significant values (6.90 ± 2.69 min) (Fig. 3d). The thrombin resistant mutant FXIII-A-R38A showed an exponential increase in the rate of FXIII-A* generation when the assay was performed with increasing levels of calcium concentration (Supplementary Fig. 3). However, it is noticeable that the exponential trend-line is a better fit at levels above 20 mM calcium, suggesting that this concentration might be rate-limiting for non-proteolytic activation of FXIII-A. The maximal rate of FXIII-A* generation of the corresponding standard plasma was observed to be 158.8 R.F.U./min.

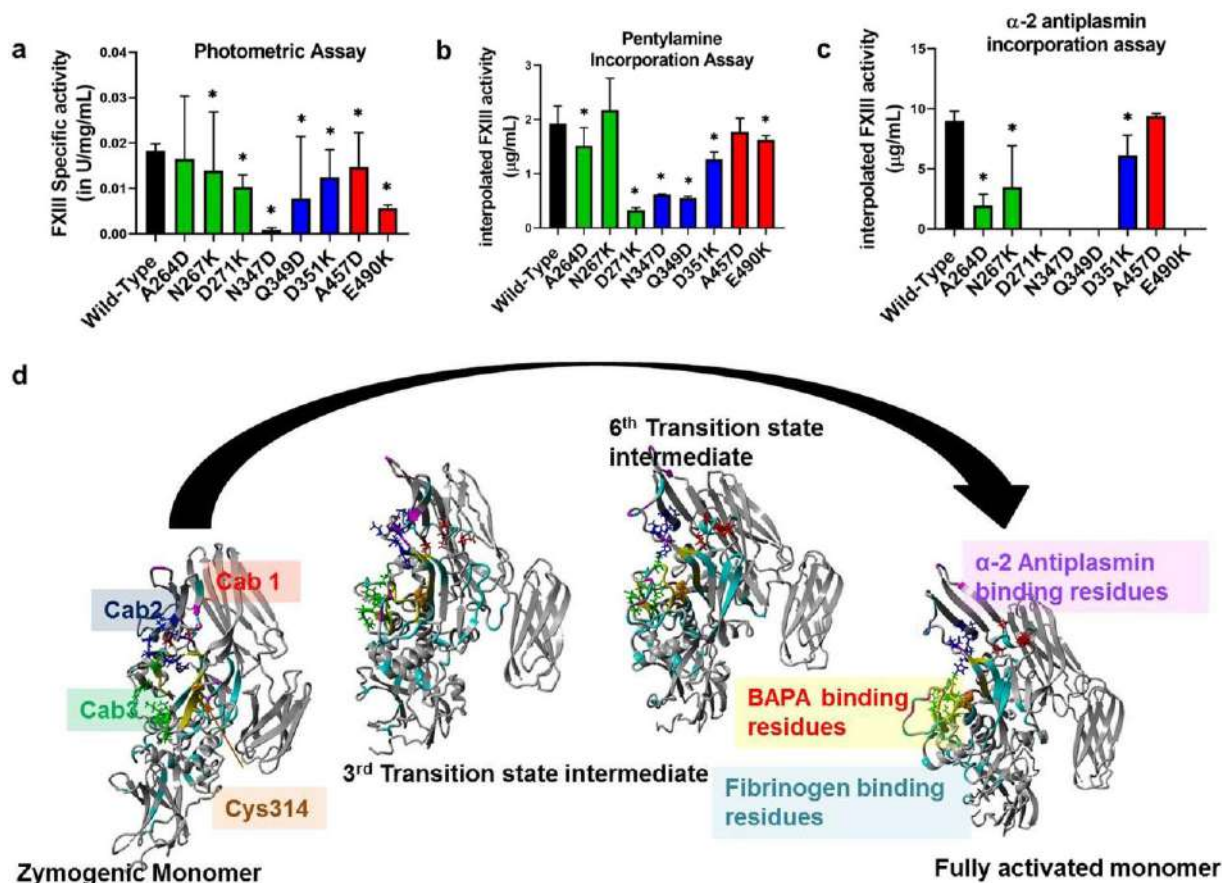


Figure 2. Effect of rFXIII-A calcium binding site mutants on its specific activity and substrate specificity. Panels a, b and c represent comparative bar graphs for specific activity of intracellular lysates (wild type and variant) based on photometric assay, interpolated FXIII-A activity based on Pentylamine incorporation assay and α -2 antiplasmin incorporation assay, respectively. In the event a variant is significantly different than the wild type, it is marked with a star (*) sign on top of the corresponding bar. Statistical significance is set at $p < 0.05$. Experiments were performed in duplicates, thrice ($N = 6$). Panel d shows the putative fibrinogen, α -2 antiplasmin and BAPA binding site residues on zymogenic FXIII-A monomeric and activated monomeric FXIII-A* structures along with two intermediate transition state structures. The structure backbone is depicted in grey colored ribbon format. The putative binding site region backbones are colored cyan for fibrinogen, yellow for BAPA and magenta for α -2 antiplasmin. The three calcium binding sites are also depicted on all four structures as stick models colored red (Cab1), blue (Cab2) and green (Cab3) respectively.

Simulation of FXIII-A at different ionic concentrations reveals that ancillary ions play a role in bringing the molecule to a pre-activated state by altering surface electrostatics. Molecular dynamic simulations of FXIII-A and its core domain performed under different concentrations of calcium and sodium shed some light into the activation behavior of FXIII-A when exposed to binding (calcium) as well as non-binding (ancillary; sodium) ions. Simulations for the full zymogenic FXIII-A crystal structure (source PDB ID: 1f13) equilibrated close to the 30 ns time point between 1–1.5 Å RMSDs for both physiological and high sodium ion concentrations. The core domain simulations, on the other hand, equilibrated faster closer to 20 ns and between 1.5–3.5 Å RMSDs, depending on the calcium ion concentration of the simulation (Supplementary Fig. 4). All simulation trajectories in the production phase i.e., only post equilibrations were considered relevant and analyzed. Simulations performed at different ion concentrations for both the full zymogenic FXIII-A subunit as well as the core domain did not demonstrate any drastic changes in overall structure post equilibration (Fig. 4a). The lack of any significant differences in overall structure is expected owing to the relative short time scale of simulation (100 ns; consistent conformational changes on a large scale i.e., $>5 \text{ \AA}$ will require runs close to microseconds which considering the size of our simulations, i.e., 85,000–500,000 atoms would be computationally too expensive for this study). However, a noticeable change in the surface electrostatic pattern/distribution was observed (Fig. 4b). Increasing cation concentrations in different simulations resulted in an increasing spread of positive potential over the surface of the simulated structures (Fig. 4b). This change was also coupled to change in RINs within these structures (Fig. 4a,b). The overall impact was that the changes in RINs within these structures were bringing about a change in their secondary structure profile. However, the changes in the secondary structure profile were very subtle and not amply visible on the secondary structure profile, most likely owing to the shortness of the simulation runs.

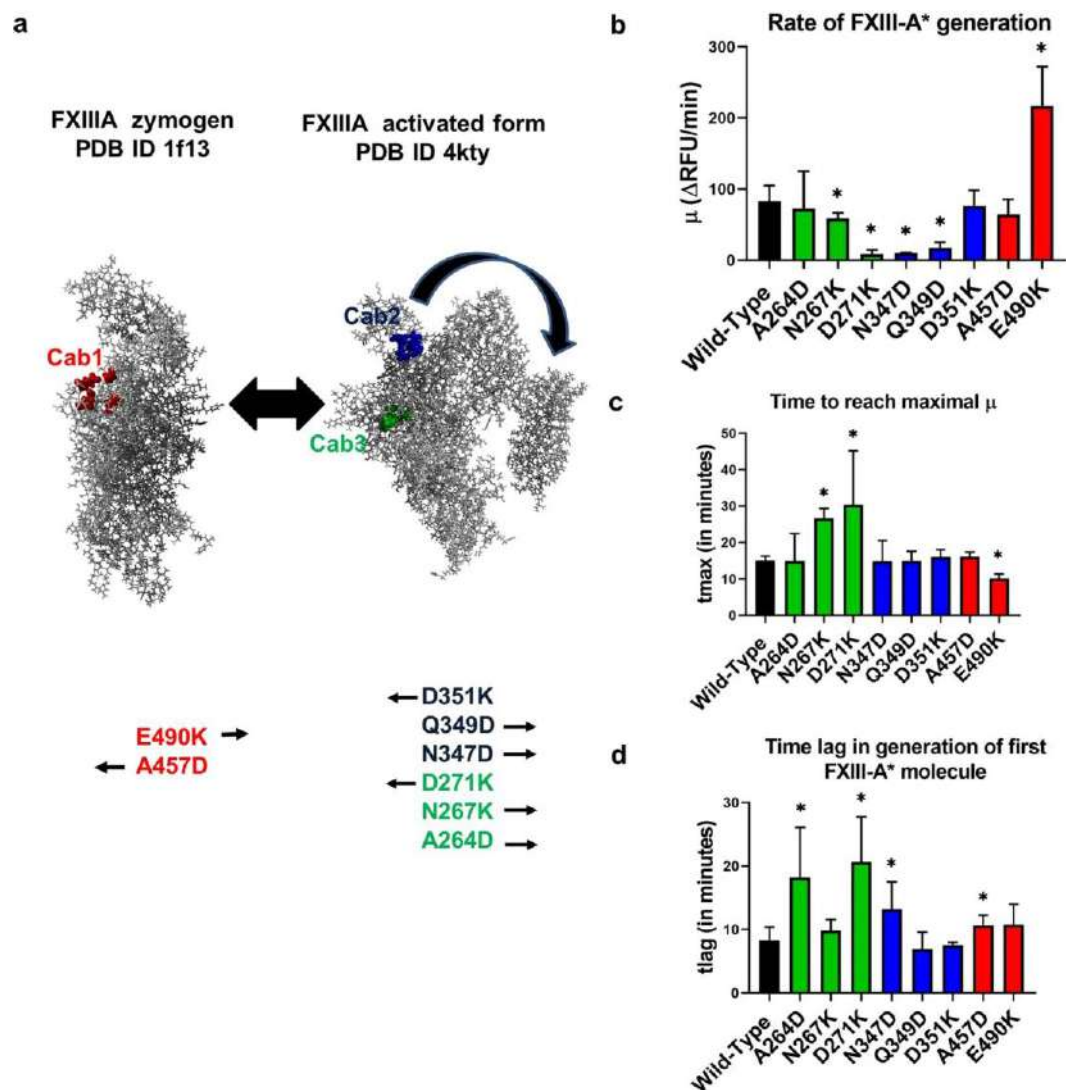


Figure 3. Results of FXIII-A* generation assay for rFXIII-A calcium binding site mutants. Panel a explains the principle underlying different rFXIII-A calcium binding site mutants generated in this study. It depicts the conformational transformation between the zymogenic and activated FXIII-A crystal structures. Both structures are depicted as grey ball and stick models. The first calcium binding site (Cab1) residues are depicted as red ball models on the zymogenic FXIII-A crystal structure because the coordination of this site is a zymogenic constraint. The second and third calcium binding site (Cab2 and Cab3) are depicted as blue and green ball models respectively on the activated FXIII-A* crystal structure. Below both these structures, the mutants generated for this study are listed with arrows indicating the anticipated structure favored by each of this mutant as per our hypothesis. Panels b, c and d depict the comparative bar graphs corresponding to three major parameters (μ , t_{max} and t_{lag}) obtained from the FXIII-A* generation assay. In the event a variant is significantly different than the wild type, it is marked with a star (*) sign on top of the corresponding bar. Statistical significance is set at $p < 0.05$. Experiments were performed in duplicates, thrice ($N = 6$). Please note, FXIII-A* generation data for the mutants D271K and N347D show very low activity and a fit of the data to the model revealed no valid estimates.

thermodynamic analyses of calcium binding to fxiii-A suggests that fxiii-A activation is a stepwise process resulting in its monomerization upon activation. Our ITC thermodynamic profiles suggest that at varying c -values [i.e., ratio of the concentration of ligand in the injection (calcium) to the concentration of macromolecule in the cell (rFXIII-A₂)]; the binding profile of calcium to rFXIII-A₂ is different. Our thermodynamic profiles reveal that the binding of calcium is not a simple protein-ligand association; rather, it is a complicated mechanism involving conformational changes coupled with domain movement and subunit dissociation taking place simultaneously. Amongst a range of c -values tested, a c -value of 20 yielded an interesting thermodynamic profile representative of all aspects of calcium binding and subsequent rFXIII-A activation (Fig. 5). Other c -values either yielded no binding or were low on informational content (Supplementary Figs 5 and 6, for c -value 25,000). Fitting exercises performed in *Affinimeter*, following a custom model binding approach (see Method section). The thermodynamic activation profile is divided into three events. The titrations involving

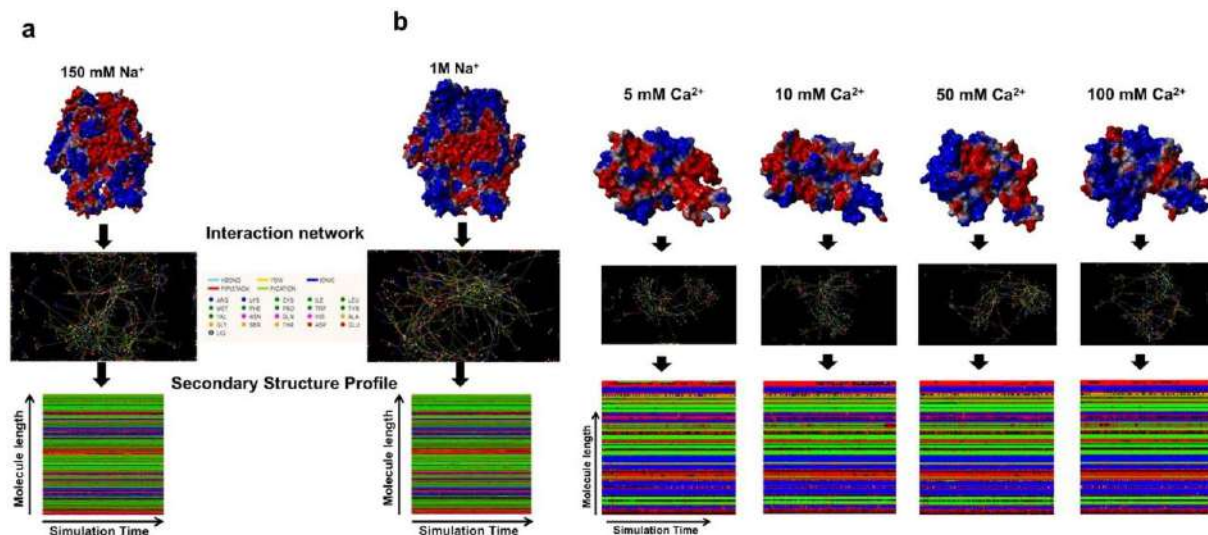


Figure 4. Effect of calcium and sodium on the structure of FXIII-A. Upper parts of panels a and b represent the simulation snapshots of full length FXIII-A molecule and FXIII-A core domain post 100ns of simulation in different sodium and calcium concentrations respectively as indicated. The simulation snapshot structures are depicted by their molecular surface view with the electrostatic potential (Red: Negative, Blue: Positive) superimposed on it. Below the simulation snapshots in both panels are the Residue interaction network (RIN) or the inter-residue interaction chart extracted from the Ring 2.0 server by submitting to it the post 100ns simulation snapshot as a PDB file under default server conditions. Lowermost section of both panels is the Secondary structure profile for the entire 100ns of simulation plotted for the entire length of the molecule. The colour code for the secondary structure profile is the following: Coil: Red, Strand: Green, Helix: Blue, Turn: Black.

c-value = 20 (1.25 mM rFXIII-A₂ (sample cell) and 25 mM calcium (syringe: CaCl₂)), showed endothermic values with $\Delta H = 1.35$ kJ/mol for the first binding event ($M1 + A1 \leftrightarrow M1A1$, $k_{D1} 100 \mu\text{M}$)¹⁷. In the second binding event ($M1A1 + A1 \leftrightarrow M1A2$, $k_{D2} 2.7$ mM), calcium binding affinity was lower with $\Delta H = -3.58 \pm 0.08$ kJ/mol (exothermic). The third and final binding event ($M1A2 + A1 \leftrightarrow M1A3$, $k_{D3} = 72.5$ mM), calcium affinity was also low with $\Delta H = -41.84$ kJ/mol (exothermic) (Global- $\chi^2 = 0.11$). The overall analysis suggests that all three reaction components involve entropy changes (see thermal footprints, Fig. 5d) with $\Delta\Delta S$ (change in entropy) getting more positive with the binding event taking place. All the three events were spontaneous ($\Delta G < 0$) at given conditions (temperature $T = 30^\circ\text{C}$). The first event involving the saturation of Cab2 and transient disruption of Cab1 following its binding is an entropy-driven event. The second event involving saturation of Cab2 and solvent exposure of the dimeric interface is also driven by entropy. The third event i.e., the saturation of Cab3 resulting in dimer disruption, is an enthalpy-driven event different than the first two events. The contribution of individual species towards the thermogram (Fig. 5c), suggests that the intermediate M1A1 (Cab1 saturated rFXIII-A₂ with FXIII-AP cleaved), is high energy unstable intermediate which undergoes heat absorption (endothermic). For data evaluation, a proper fit was achieved in *Affinimeter*. The data fitting depicted in Fig. 5b represents the raw data and fitting based on the sequential binding site model of Origin software (with fixed parameter K_d and ΔH) (also see Supplementary Fig. 5, for fitting curves obtained from *Affinimeter*). Blank measurements were made for thrombin and FXIII-A in the cell, against buffer to rule out the heat changes due to ion hydration. The absence of any heat changes in the blank ITC experiment overrides the possibility that the interpretations made here may be an effect of the heat of dilution. The data obtained after fitting exercises in *Affinimeter* following the stoichiometric equilibria model suggests significant enthalpy-entropy compensation involved in the binding of calcium to rFXIII-A₂, to reach full saturation (thermal footprints, Fig. 5d, range of $\Delta\Delta G$ is much smaller than their associated changes in $\Delta\Delta H$ & $\Delta\Delta S$)^{18,19}.

Discussion

the structural and functional conservation of calcium binding sites within the transglutaminase family. Allosteric changes resulting from ion coordination of amino acid side chains often have fascinating functional implications²⁰. Such coordination when they result in changes crucial to the catalytic cycle of a protein becomes a conserved trait across the evolutionary chain. The binding of calcium to FXIII and its paralogues and orthologues across the phylogenetic tree is a property that not only initiates the events of their catalytic cycle but in effect is responsible for all downstream changes. That includes dictating the rate of generation of the activated species, exposure of the catalytic triad, to the formation of substrate binding pockets and eventually (in the case of FXIII) formation of a monomeric activated form^{16,21}. A closer look into the multiple sequence alignment of calcium binding site residues reveals that the negatively charged amino acids capable of side chain coordination are highly conserved (Fig. 1a). These residues usually occur in a neighborhood cluster of similarly charged amino acids which offsets the potentially deleterious effect of any unfavorable substitution

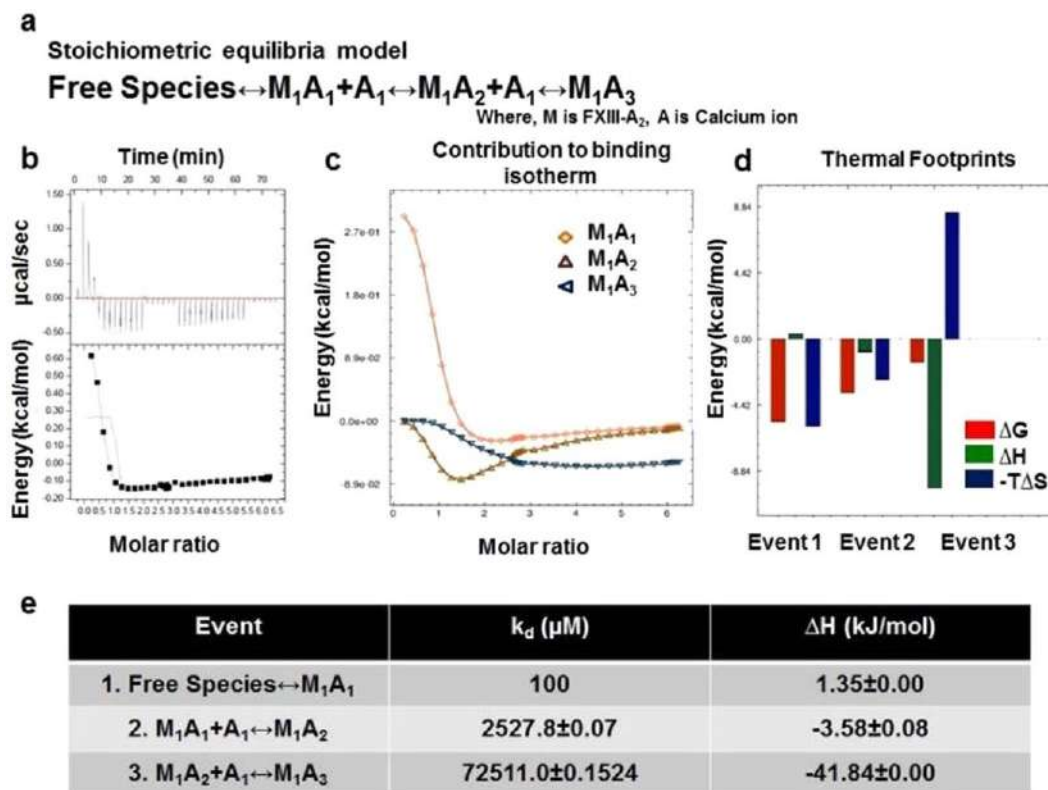


Figure 5. Calcium binding to rFXIII-A₂ studied by ITC. Panel a. Equation depicting the stoichiometric binding equilibrium model, followed for the analysis of data derived from ITC (Model was generated in *Affinimeter* using model builder approach). Panel b. Titration of 1.25 mM rFXIII-A₂ with 25 mM CaCl₂ (c-value = 20). Upper image of this panel is the raw data depicting the heat change upon each injection; lower image in this panel is the normalized data, with integrated heat change plotted against the concentration ratio of calcium vs rFXIII-A₂. Solid black line represents the corresponding fit obtained in Origin software using sequential binding mode, with n = 3. All heat changes are plotted after subtraction of reference titration (no rFXIII-A₂ in sample cell vs. 25 mM CaCl₂ in the presence of thrombin, at same conditions). Panels c, d and e are based on evaluation performed on *Affinimeter* (see Supplementary Fig. 5 for corresponding fit curves). Panel c depicts the contribution of individual species, generated during a sequential binding of calcium to FXIII-A (based on earlier observations¹⁹ and as participants of the Stoichiometric equilibria here (Panel A)), towards the binding isotherm. Panel d is the comparative heat signatures, or the thermal footprints obtained at each binding event following the equation $\Delta G = \Delta H - T\Delta S$ (2nd Law of Thermodynamics); explaining the three thermodynamic events, and their corresponding changes in free energy (ΔG), entropy ($-T\Delta S$) and enthalpy (ΔH) (for the corresponding data obtained at c-value = 25,000 please refer to the Supplementary Fig. 6). Panel e is table representing event-wise changes in enthalpy (ΔH), in kJ/mol, and corresponding change in binding affinity of calcium ions towards FXIII-A in all three corresponding events as per the stoichiometric equilibria model.

at the coordinated residue by overtaking its coordination function (Fig. 1b). Therefore in spite of the high degree of conservation amongst calcium binding site residue, substituted variants including substitution to positively charged residues are observed in the conservation-related multiple sequence alignment. The existing literature indicates that amongst transglutaminases (EC 2.3.2.13) there can be as many as six high to low-affinity calcium binding sites. However, multiple alignments of a fairly large cohort of non-redundant sequences across the transglutaminase enzyme family indicate that at least in eukaryotic transglutaminases, three of these are of almost universal occurrence²². Unavailability of detailed structural information and the evolution of a compensatory regulatory motif might be the reason why some of these sites are not yet reported or not present in a few members of transglutaminase (TGase) family²³. Amongst the structurally best-characterized transglutaminases, i.e., TG2, FXIII-A, and TG3; TG2 has additional regulatory mechanism²³. These are the GTP/GDP switch (effective intracellular, at low calcium levels) and the vicinal disulfide bonds (effective extracellular, at high calcium levels). These additional regulatory mechanisms explain the need of six calcium binding sites in TG2 to induce the conformational pull needed for overall activation of the molecule (which therefore would be higher than FXIII or TG3). The enzymes, FXIII and TG3 differ from TG2 concerning calcium binding (Fig. 1c) because unlike TG2, both proteins have one constitutively bound calcium which confers their zymogenic forms stability while the other two sites are structurally shielded in the zymogenic state till they are functionally required. The TG3 is an inactive 77 kDa zymogen that must be cleaved into a 50 kDa N-terminal fragment containing the active site and a 27 kDa C-terminal fragment, which remains associated with the mature enzyme²⁴. The zymogen binds a single

calcium ion with high affinity ($K_d = 0.3 \mu\text{M}$)²⁵. Upon cleavage, two additional ion binding sites with an average dissociation constant of $4 \mu\text{M}$ become available. Calcium coordination by Asp324 induces the movement of a loop region, enabling substrate access to the active site. The FXIII-A molecule, similar to TG1, has been reported in certain crystal structures to be bound constitutively to a single calcium ion at Cab1¹². The activation events initiated by thrombin-mediated cleavage of its N-terminal activation peptide expose the other two calcium binding sites to coordinate, resulting in a series of conformational changes involving the formation of substrate binding pockets and ultimately exposing the catalytic triad¹⁶. Therefore, while retaining these three highly conserved calcium binding sites, these enzymes have functionally evolved differently to use these sites in a way that is best suited to their physiological milieu. Amongst FXIII-A and TG3, the one calcium binding site that imparts the zymogenic restraint differs. Sequence-wise and structurally, the constitutively bound zymogenic calcium binding site in FXIII-A (Cab1) effectively aligns with the activating/regulatory calcium binding site in TG3 (Cab3 in TG3) and vice versa. The spatial position of all three calcium binding sites in all transglutaminase structures is similar (Fig. 1c). However, the orientation of the binding site residue side chains varies along with their inter-atomic distance, between transglutaminases. As an example, the distance between the C- α backbone atoms of the Cab2 binding site residues (FXIII-A calcium binding site nomenclature) is shown in Fig. 1e. The C- α backbone inter-atomic distances are similar for TG3 and FXIII-A (11 and 12 Å respectively) with TG2 (15 Å) being different. The difference in inter-atomic distances is reflected in the similarity of the coordination pattern, as mentioned earlier for these proteins. Based on a structural relationship tree, we find that TG1 is more similar to FXIII-A than any other transglutaminase, which also is true evolutionarily since these two proteins are closely related (Fig. 1d). The overall structural similarity is reflected in similarity in calcium binding sites as well since the binding site residues align better between FXIII-A and TG1 than with TG7 which is far away on the structural tree from FXIII (Fig. 1d; Supplementary Fig. 7). Transglutaminases at a prokaryotic level have evolved from ancient cysteine proteases (*papain-like thiol proteases*); and several microbial transglutaminases, as well as cysteine proteases, show a dependency on calcium for the regulation of activity. Therefore one might assume that the mammalian FXIII calcium-binding sites have evolved from ancestral calcium binding sites in microbial transglutaminases and cysteine proteases²². However, microbial transglutaminases themselves have evolved divergently to eukaryotic transglutaminases. The only structurally fully characterized primitive transglutaminase from *Streptovorticillum mobaraense* (PDB ID: 1iu4) does not even show calcium dependence. Also the structural alignment of microbial cysteine protease that do show calcium dependence/binding like LapG (*Legionella pneumophila*) with the core domain of FXIII-A subunit shows no similarity in the spatial location of the calcium binding sites, even though the two structures align well with respect to sharing the conserved 4-sheet one-helix fold (Supplementary Fig. 8) of transglutaminases. All the above observations lead us to conclude that calcium binding sites in eukaryotic transglutaminases including FXIII have evolved divergently and have no evolutionary connection to the calcium binding sites in microbial transglutaminases or ancestral cysteine proteases.

cross-talk of fxiii calcium binding sites and their importance in the development of substrate binding pockets.

In our earlier *in silico* study, we had presented the possibility that coordination of Cab1 of FXIII-A molecule stabilizes the zymogenic form of FXIII-A¹⁶. Our results from the generation assay support our hypothesis that the Cab1 binding site is a zymogenic constraint and that its transient disruption caused by calcium coordination at Cab2 post thrombin-mediated FXIII-AP cleavage is the rate determining step for FXIII-A activation (Fig. 3). The unique role of Cab1 is confirmed by the accelerated rate of activation of the molecule upon disrupting the calcium coordinating shells of Cab1 (E490K), disengaging calcium binding to Cab1, in the presence of an intact Cab2 (Fig. 3). The mutation (E490K) which introduces an additional positive charge within Cab1 has the same effect as the coordination at Cab2 i.e., it prevents the calcium binding at Cab1 thereby releasing this variant molecule from the zymogenic constraint imposed by Cab1, and it is then reflected in a significantly higher rate of FXIII-A* generation than the wild type as well as the other Cab variants (Fig. 3b). The endpoint assays, however, record lower activity of this mutant compared to the wild type (Fig. 2a–c), which re-emphasizes the fact that the rate of activation of the enzyme and the direct substrate turn-over are independent properties of the FXIII mediated catalysis especially when it comes to mutations/variants close to substrate binding or active site. The strong differences between the generation assay parameters and the endpoint assays (like photometric assay) indicate that the isopeptidase activity on which the generation assay is based²⁶ and the transglutaminase crosslinking activity should not be considered synonymous especially when dealing with mutants. Our study is in close agreement with an earlier report that suggests that by mutating hydrophobic residues around the active site it is possible to have transglutaminase variants that are deficient in crosslinking activity but have normal or raised isopeptidase activity²⁴. Certain calcium binding mutants (like E490K) therefore influence cross-linking activity negatively by altering the substrate binding sites of the acceptor or donor (cross-linking activity as also mentioned in the methods section is a two-step ping pong reaction). However, this same mutation shows a raised isopeptidase activity because by releasing the zymogenic constraint (of Cab1) the one-step conversion of FXIII-A to FXIII-A* (and the isopeptidase cleavage since no acceptor-donor cross-linked intermediate formation is required in this type of reaction) is facilitated. These observations present an interesting pharmaceutical possibility of engineering enzymes with multiple but quantitatively varying enzymatic capacities. Since FXIII-A possesses a transglutaminase, isopeptidase and also protein disulfide isomerase activity, it can serve as a model protein to generate variants with higher enzymatic efficiency than normal in one aspect but neutralized concerning the other activities^{27,28}. A higher lag observed for some calcium-binding mutants in the FXIII-A* generation assay is a representation of slow generation of the first active FXIII-A* species that can be attributed not just to thrombin cleavage but also to the underlying events which are responsible for the accessibility of active site cysteine (opening of molecule) for incoming substrate molecule (Fig. 3c). Therefore, the calcium binding site residues critically govern the structural integrity of the core domain with a possible distal allosteric effect on FXIII-AP. Whether these variants alter the binding affinity of FXIII-A to thrombin or directly impede the cleavage reaction cannot

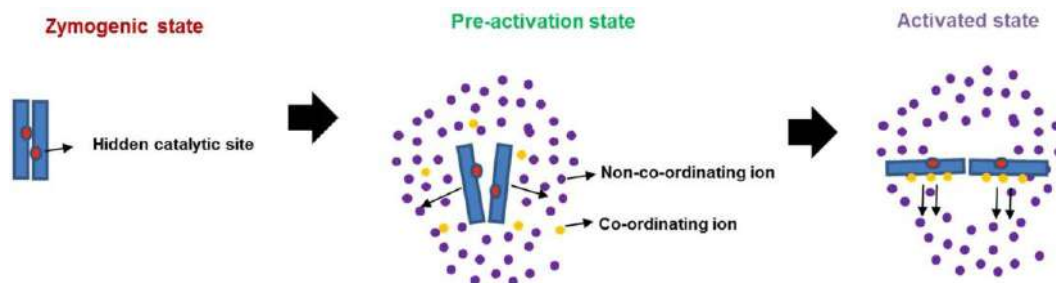


Figure 6. Effect of ancillary sodium ions towards generation of a pre-activation state of FXIII-A molecule. A cartoonist impression of the FXIII-A zymogenic state where no ions are influencing the structure followed by pre-activation state where the both the non-coordinating (assumed to be sodium in purple) as well as later coordinating ions (assumed to be calcium in yellow) influence the structure and conformation of FXIII-A molecule by altering its surface electrostatic properties. The last part of the figure depicts the fully activated molecule which is the final outcome of the coordination of the coordinating ions to its binding sites in a FXIII-A molecule that has already been moved from its zymogenic to a pre-activation state.

be ascertained from our data. The different endpoint-based assays between themselves revealed consistency only to a limited extent, i.e., all mutants reported consistently lower or similar activity status when compared to the wild type in all endpoint assays. However, quantitatively, these assays also revealed relative differences from one another for the mutants. For example, one mutation from Cab3 (D271K) and two from Cab2 (N347D, Q349D), reported consistently low levels in all these assays, indicating that the mutations distorted the substrate binding site (Fig. 2a–c). However, the extent of decrease in each assay was different, i.e., for the α 2-antiplasmin assay all three mutants reported to have non-detectable levels, but for the other two assays variable detectable levels were observed which can be attributed to the fact that calcium binding sites spatially surround the catalytic site and are also proximal to the putative substrate binding sites. Their coordination subsequently plays a major role in the correct orientation of the substrate binding sites as can be seen in the transition state intermediate models¹⁷. Since the three assays are related to three different substrates, the relative impact on substrate affinity would depend on the extent to which each mutation affects the substrate binding site. As mentioned at the beginning of this paragraph, the disruption of Cab1 is also the rate-limiting step in FXIII-A activation which is highlighted by the increased response of the thrombin resistant FXIII-A subunit mutant (FXIII-A-R38A) in the generation assay to increased concentrations of calcium (Supplementary Fig. 3). The 20 mM calcium concentration appears to be the concentration barrier threshold above which calcium can coordinate Cab2 and Cab3 that eventually overpowers the zymogenic constraint associated with a coordinated Cab1. After the loss of the zymogenic constraint above this concentration, the rate of FXIII-A* generation follows an uninhibited exponential increase with increasing calcium concentrations (Supplementary Fig. 3).

FXIII conformational changes during activation are effected at the secondary structure level and are governed by ion coordination and its surface electrostatic potential. In several transglutaminases cross-talk between calcium and other ions (depending on the physiological milieu) influences the activity status of the protein. In TGM3, calcium ion coordination induces the movement of a loop region that enables substrate access to the active site. Tighter coordination with magnesium ion instead of calcium keeps the loop in its inactive configuration. Therefore, the relative concentrations of calcium and magnesium act as a regulatory switch for transglutaminase activity in TGM3²⁹. FXIII-A protein which can be activated non-proteolytically by calcium only in the presence of supra-physiological levels of calcium (> 50 mM) FXIII-A shows an interesting behavior in the presence of sodium (Fig. 4)¹⁷. In the presence of high levels of sodium (~1 M NaCl), the non-proteolytic activation requirement of calcium goes down to physiological levels (2.5 mM). The principle behind the effect of sodium on the non-proteolytic calcium-induced activation of FXIII-A is very much different from that observed for TGM3 in the case of magnesium and calcium since unlike in TGM3, where binding of both magnesium and calcium is observed, in FXIII-A there is no actual coordination of sodium. Our MD simulations performed on FXIII-A monomer at physiological versus high concentration (supra-physiological) of sodium ions in the simulation cell reveals that higher levels of sodium without actual binding (or coordination) to FXIII, alters the FXIII-A surface electrostatic distribution (Fig. 4a). This event most likely disturbs the pKa (ionization constant) of internal buried residues, thereby affecting intra-domain residue interactions and changing the local secondary structure, which results in subtle conformational changes. Very high concentrations of 1 M sodium likely alter the secondary structure of FXIII to the extent of overcoming the primary restraint induced by Cab1 bringing the molecule to the tipping point of activation but not activating it (Fig. 6). At this point, even physiological levels of calcium are adequate to non-proteolytically drive it from its zymogenic to activated conformation (heterotopic, the sequential and positive allosteric effect of sodium & calcium towards FXIII activation) (Fig. 6). Therefore, the extent and influence of calcium coordination on FXIII conformation also depends on the surface electrostatic state that in turn, is determined by the ionic strength/pH of FXIII's solvent. The fact that ionic coordination alone does not influence protein conformation at the secondary structure level is further strengthened from our MD simulations in which we subjected only the core domain of the FXIII-A subunit to increasing concentrations of calcium (Fig. 4a). Again, as with high sodium concentrations, we observed a change in surface electrostatic potential with increasing calcium concentration (even though in the period of simulation,

no actual coordination was observed for calcium as well). Therefore, the activity status of FXIII-A is not only the result of the coordination of calcium ions to its three binding sites; it is the net impact of calcium coordination as well as the response to ancillary solvent ion concentration surrounding the molecule. Even physiologically FXIII-A exists in different solvent environments with differing ionic concentrations. Intracellularly FXIII-A is present as a dimer, and since thrombin is accessible intracellularly, any enzymatic role, e.g., crosslinking of cytoskeletal proteins like actin/myosin is possible only through non-proteolytic activation^{30–34}. Intracellular non-proteolytic FXIII activation could be achieved either through sudden ion fluxes like calcium release from endoplasmic reticulum that might alter the levels of calcium to supra-physiological levels fit for non-proteolytic activation¹⁷. The other option might involve an increase in sodium concentration, which, as mentioned earlier, will support non-proteolytic activation even at low concentrations of calcium. FXIII-A has been reported in various bodily fluids like placental fluid, tears, spinal fluid, etc. where it might have reparative roles^{30,35–38}. If FXIII-A is considered as a therapeutic option for reparative processes related to these body fluids, knowledge of the subtle conformational changes brought about by the combination of ions in these fluids will help design easy to activate FXIII-A and with possibly a high specific activity.

energetic implications of calcium binding to fXiii explains why the activated form of fXiii-A is monomeric.

The FXIII complex assembly and its dissociation in plasma primarily involve the formation and disruption of non-covalent hydrophobic interactions²². Intrinsic ion binding to proteins involves hydration energies, which are entropically driven³⁹. Also, calcium binding to transglutaminases is reported to induce conformational changes, as is observed in the crystal structures of activated forms of FXIII-A as well as TG2^{15,22}. These conformational changes result in a change of hydrophobic surface area while exposing the core domain active site. Therefore, these changes are associated with an increase in entropy as is evident from our thermodynamic profile observed upon the sequential binding of calcium at c -value = 20 (entropy-driven, $\Delta H > 0$ to $\Delta H < 0$) (Fig. 5). This also is evidence of in-cell FXIII-A activation taking place upon calcium binding at these concentrations. Interestingly, the proteins belonging to the family bearing the 'transglutaminase core' including FXIII-A, are not part of the EF-hand superfamily (a superfamily of proteins bearing two EF-hand units, each is made up of two helices connected with calcium binding loop), which characteristically are calcium-binding proteins (SCOPe database; <http://scop.berkeley.edu/>). Calcium binding to proteins lacking an EF-hand motif involves the coordination of distal residues, made possible by changes in secondary structure/conformational changes as well as, major participation of a secondary ligand (like water) when required⁴⁰. In our experiments with thrombin-cleaved rFXIII-A, the first step would be the saturation of Cab1. The ITC data suggest that the initial saturation event is highly spontaneous ($\Delta G < 0$), which is expected owing to the high affinity of FXIII-A towards calcium for Cab1 (100 μM)^{3,17}. The high K_1 for Cab1 would ideally be enthalpically favorable since this strong ion binding would constrict the molecular motions by bringing about an order in the spatial secondary structure^{41–43}. This however is not the case with FXIII-A in which we observe a $\Delta H > 0/\Delta S < 0$ patterns at Cab1 saturation indicating that there is a secondary event, most likely the coordination of Cab2, happening concurrently, that's directed towards the transient disruption of Cab1 resulting in an overall absorption of energy which is reflected in the $\Delta H > 0/\Delta S < 0$ patterns (Fig. 5d). Therefore, the first event cannot be independently thought of as binding of calcium at Cab1 but rather the combined saturation of Cab1 and simultaneous coordination of Cab2 to the point of transient disruption of Cab1. Once the Cab1 is transiently disrupted, the molecule overcomes the zymogenic constraint and moves conformationally towards the open, active structure as a result of a gain of entropy. This part of the activation cycle can be considered as the second binding event where we observe a pattern of $\Delta H < 0/\Delta S < 0$. The gain in entropy (ΔS) for this second event is higher than that observed for the first event, although effectively $\Delta G < 0$, keeping the transformation to the activated form still favorable. At this point of time, the conformational changes taking place in FXIII-A have set into motion another event, which is the disruption of the zymogenic dimeric interface¹⁶. Major hydrophobic and non-covalent interactions between the opposing dimers are lost, resulting in (a) solvent-protected to a solvent-exposed state, and (b) exposure of Cab3. The third event in our thermodynamic cycle is the final coordination and saturation of Cab3, which is occurring simultaneously to the monomerization of the activated FXIII molecule. In this step, we observe a pattern of ($\Delta H < 0$, $\Delta S > 0$) with the increase in entropy ($\Delta S > 0$), and release of heat ($\Delta H < 0$) (Fig. 5d). This major increase itself represents a dissociative event combined with flexible inter-domain movements (of β -barrel domains). This event is aided by a major influx of water molecules in FXIII-A regions which were previously inaccessible to water (owing to the closed structural fold or the dimeric interface). The rise in entropy is the result of the enthalpic contribution of the final Cab3 saturation and dimer dissociation. This also keeps the overall free energy of the system negative ($\Delta G < 0$) favoring the final disruption of the dimeric interface to an open monomeric activated FXIII-A* form. The fast internal dynamics (conformational entropy, as a result of β -barrel domain movements), and slow internal dynamics (disruption of dimeric interface due to loss of hydrophobic interactions), leads to activation of a fully saturated FXIII-A* monomer, as the protein dissociates/solvate to a monomeric calcium saturated form (Fig. 7). One must, of course, remember that these events can occur in two different species, i.e., the dimeric FXIII-A₂/intracellular FXIII-A₂ and the plasma heterotetramer FXIII-A₂B₂ complex. In the latter, there are two dissociative processes in action, i.e., the dissociation of the FXIII-A₂ zymogen to its activated monomeric FXIII-A* form and the dissociation of the FXIII-B₂ molecule from the complex. Our thermodynamic experiments do not involve the FXIII-B subunit since they are performed with rFXIII-A₂ alone. However, both dissociative events most likely run simultaneously each contributing to the success of the other. Both are brought about by conformational changes upon calcium binding and influx of water molecule into previous hydrophobic cores formed by the respective folds of the protein and the pattern in which the zymogenic complex is assembled.

Studies on FXIII-A calcium binding explain the conformational changes occurring in the FXIII-A core domain, but how calcium binding contributes to the movement of the β -barrel domains was still unclear. A recent article shows that the first β -barrel domain protects the active site, and the second one is responsible for exposing

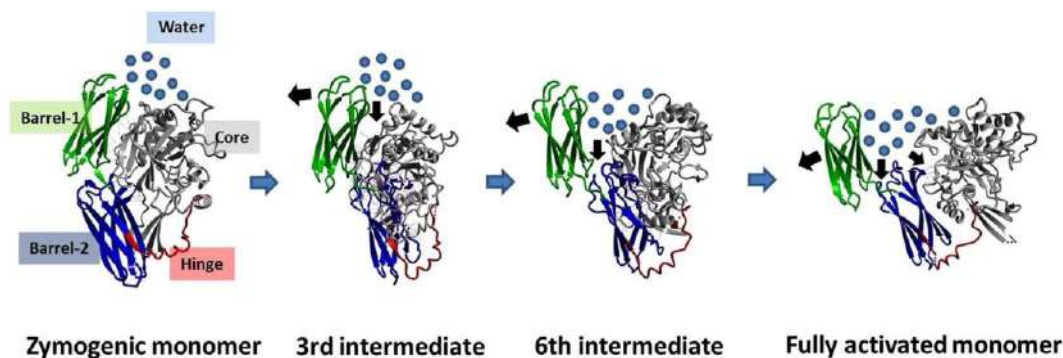


Figure 7. Entry of bulk solvent induces movement of β -barrel domains. Figure illustrates the stepwise conformational changes occurring during the activation of FXIII-A. The figure(s) represent in successive order the zymogenic crystal structure of FXIII-A monomer, the third and sixth transition state intermediate models reported earlier and the fully activated structure of FXIII-A monomer. All structures are depicted in the ribbon format. The N-terminal beta sandwich domain has been hidden for the sake of clarity. The β -barrel 1 and β -barrel 2 domains are coloured in green and blue respectively while the core domain is coloured grey. The hinge region of almost 20 amino acids is coloured red. The water solvation shell is depicted with blue circles. The movement of the β -barrel domains is depicted with black arrows. Contacts between the core and β -barrel domains are depicted with lightly coloured lines.

it⁴². Our data highlights how enthalpy-entropy compensation contributes to the generation and stabilization of a monomeric FXIII-A* activated molecule upon calcium ion binding. Since the final event in the thermodynamic cycle of FXIII-A activation is enthalpically driven instead of entropically (i.e. like the first two events) this suggests that the first two events introduce disorder into the molecule (conformational changes) while the third and last event stabilizes the final molecule resulting from this disorder/conformational change, i.e., dissociation into a monomeric state. Our thermodynamic analysis highlights the role of the influx of bulk solvent that in continuation of the conformational changes induced by calcium binding enables the global domain movements observed during FXIII-A activation. At a structural level, we can observe these changes if we follow the conformation of the transition state models between the activated and zymogenic form of FXIII-A (Fig. 7). The β -1 and β -2 barrel domains in the zymogenic form are stabilized in through non-covalent bonds they form with the core domain that serves to shield the hydrophobic interior. The core domain is linearly linked to the β -barrel-1 domain by a hinge region which is unresolved in certain crystal structures of the zymogenic form like PDB ID: 1f13 because it is disordered and highly flexible. Therefore, barring the non-covalent attachment to the core domain, there is nothing preventing the β -barrel domains from moving flexibly over the hinge region. With the binding of calcium, conformational changes occurring at the core domain disrupt the non-covalent association of core domain with the barrel domains. This primary disruption enables the entry of the solvent molecules to this conformationally shielded region. Water influx further disrupts the β -barrel domain-core domain contacts, causing the β -barrel 2 domain to fall over under its weight, pulling the β -barrel 1 domain along with it in which the connecting hinge region acts as the pivot. This falling over motion appears as the twisting and opening up of the β -barrel domain to expose the catalytic site. We can, therefore, suggest that the formation of active FXIII-A* species involves a thermodynamic process of “conditional conformational switching”²⁹, which involves the essential participation of calcium and water molecules. In other words, the activation of FXIII-A is majorly driven by conformational entropy brought about by calcium binding. Since all reactions follow a common energetic purpose, i.e. to favor the energetically stable complex/conformation, dimeric zymogenic FXIII-A has Cab2 and Cab3 sites hidden which make the dimeric, calcium unbound form more favorable in the zymogenic state (Fig. 8). During activation, since regions previously hidden get exposed, calcium binding alters conformation as well stabilize the final monomeric FXIII-A* molecule by bringing structural order upon coordination and reducing the transiently generated randomness. This explains why a monomeric bound FXIII-A* would be favored over the activated form (Fig. 8). It also explains why the chelation of calcium from a non-proteolytically activated FXIII-A, will shift the equilibrium to reversibly generate the zymogenic-dimeric FXIII-A that can be re-activated. Recent experimental evidence has also shown that the activated form of FXIII-A is, in fact, monomeric and is capable of reversion to its zymogenic dimeric state upon removal of calcium from the medium²¹. Ever since FXIII-A has been recognized as a pharmaceutical candidate for inhibitor development, inhibitors have been designed primarily against the active site or the thrombin cleavage mechanism of this protein⁴⁴⁻⁴⁸. Our results suggest that two other areas of FXIII can potentially serve as regions against which inhibitors can be designed. The regions in and around the calcium binding sites belong to one group of potential candidates since they not only dictate the rate of activation but also the proper orientation of substrate binding sites. The other regions belong to the areas/cavities (next to β -barrel/core domain contacts) which allow the entry of bulk solvent upon the conformational changes induced by calcium binding. Neutralizing either of these candidate regions can potentially result in thermodynamically stabilizing intermediate conformational states of FXIII-A, thereby preventing the full activation of FXIII-A.

As a final commentary to this study, we would like to acknowledge some limitations of our study. Our work focusses on calcium binding without discriminating between proteolytic and non-proteolytic modes of

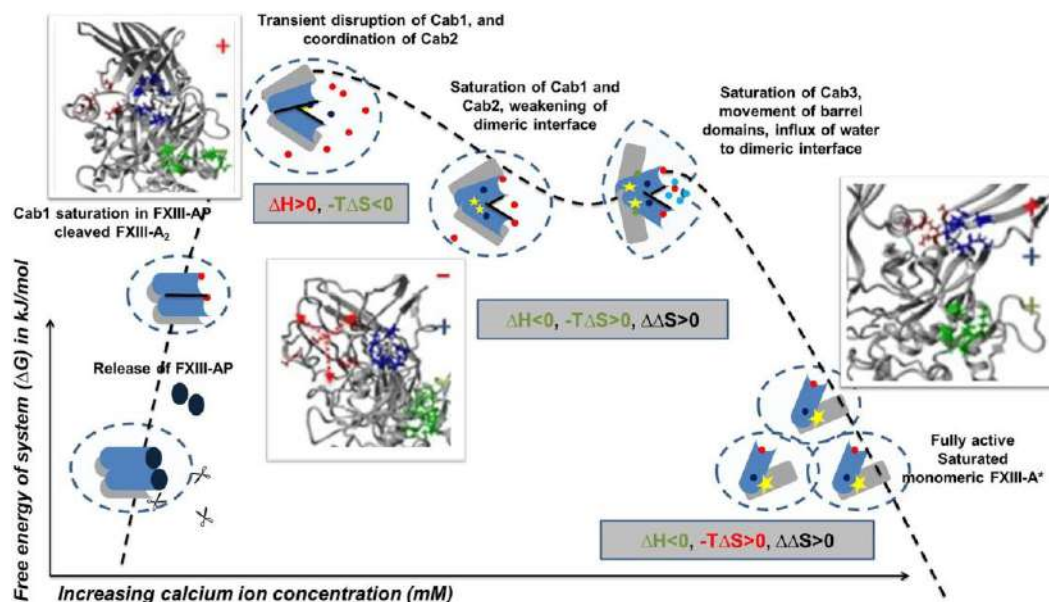


Figure 8. Derived Thermo-chemical Activation Cycle of Coagulation FXIII-A molecule in plasma. The free FXIII-A₂ dimer, when devoid of any calcium possesses intact FXIII-AP and this species represents a low free energy stable form¹⁶. Cleavage of FXIII-AP by thrombin is followed by coordination and subsequent saturation of Cab1 and Cab2. Cab1 being spatially more accessible gets saturated faster and strongly than Cab2 yielding a low-energy, relatively stable state. Subsequently, the Cab2 coordination transiently disrupts Cab1 giving rise to a high-energy, unstable, transient state (event 1). The increasing saturation of Cab2 accompanied by the conformational changes directed by it result in the stabilization of unstable intermediate bringing down free energy. Meanwhile, slow disruption of the dimeric interface proceeds as the molecule proceeds towards full saturation (Cab3 gets exposed with the dimeric interface coming apart) (event 2). As the dimer loosens up, water molecules seep through and expose the dimeric interface further. Sharp movements of β -barrel domains as a consequence of calcium saturation, and movement of water molecules across the dimeric interface raise the entropy of the system, that finally culminate into dimer disruption, giving rise to monomeric, energy minimized, open active FXIII-A* species (event 3). Blue-grey object depicts the N&C terminal of FXIII-A monomer, respectively. Molecule solvation shell is represented by dotted circle. Calcium ion saturation at Cab1, Cab2 and Cab3 is depicted by red, blue and green solid dots respectively. Black rod is the dimeric interface. Yellow star is the catalytic center. The three inset figure(s) demonstrate the secondary structure changes occurring during the course of activation explaining assembly (+) or disassembly (-) of calcium binding sites extracted from the Transition state intermediate models reported earlier¹⁶.

activation¹⁶. A significant part of the work is based on transient transfections and *insilico* analysis performed on modeled structures. Similarly, the thermodynamic analyses are based on custom fitting models which themselves are built around hints from *insilico* experiments. We present this work to the readers as an exploratory characterization of individual calcium ion binding sites of FXIII-A. As future work, we will attempt to purify the mutants explored in this study to characterize them structurally/functionally in a pure, undiluted setting.

Methods

Transient heterologous expression of FXIII wild type and mutant variants. The human HEK293T cell line purchased from DMSZ (German Collection of Microorganisms and Cell Cultures) were cultured in high Glucose DMEM Invitrogen, supplemented with 10% v/v FBS (Invitrogen), 1% v/v Penicillin-Streptomycin antibiotics (Invitrogen) and 0.1% v/v Fungizone (Invitrogen), at 37 degrees in 5% CO₂. All experiments were done on sub-cultured cells in logarithmic phase (below passage 20). Human FXIII-A cDNA, inserted into the cloning site of pDEST26™ vector (Invitrogen) was used as a wild-type construct for all the experiments. Site-directed mutagenesis was performed on the aforementioned construct, using *GeneArt* Site-directed mutagenesis system (Life Technologies). Mutagenesis was performed with the aim of either accelerating calcium ion binding (FXIII-A A264D, FXIII-A N347D, FXIII-A Q349D, FXIII-A A457D), or disrupting calcium ion binding to the respective site (FXIII-A N267K, FXIII-A D271K, FXIII-A D351K, FXIII-A E490K) based on our previous hypothesis¹⁶. One more mutant at the thrombin cleavage site (FXIII-A R38A) was generated to be resistant to thrombin-mediated activation. Although a total of 13 different residues contribute to calcium binding in the three FXIII-A calcium binding sites, we were successful in cloning and expressing only 8 of them. All primers were synthesized by MWG Eurofins (Eurofins genomics). All vector construct clones were completely sequenced and verified for the correct incorporation of mutations *in-house*. Wild-type FXIII-A DNA and mutated DNA were transfected into mammalian HEK293T cells for transient expression. Briefly, 2.7×10^5 cells were transfected with 3 μ g of plasmid DNA along with 6 μ l of transfection reagent lipofectamine 2000 (Invitrogen). Cultures were harvested 48 hours post-transfection, by performing intracellular lysis using mammalian native M-PER reagent (Thermo Fischer

Scientific Inc), containing 25 mM bicine, pH 7.6, supplemented with 0.1 mM PMSF for 10 minutes and centrifuged at 14,000g for 5 minutes at 4 °C. Lysates were stored at -70 °C for later evaluation. Each transfection lot was accompanied with a positive control, i.e., HEK293T cells transfected with expression vector expressing eGFP. This lot helped us evaluate the success of the transfection as well as check for any endogenous FXIII/transglutaminase activity. Results for all assays performed on the transfection lysates were normalized accordingly.

Antigenic estimation of rFXIII-A by FXIII-A Western Blot Analyses. Intracellular lysate derived from transiently transfected HEK293T cells was verified for the antigenic presence of FXIII-A protein by western blot analysis. Intracellular lysate from transfected cells was quantified by BCA estimation (Pierce, Life technologies). The intracellular lysate was separated on 4–16% precast SDS PAGE (Biorad), followed by transfer to PVDF membrane at 60 V for 90 minutes in cold room. The membrane was blocked for 1 hour at room temperature in blocking reagent (3% w/v BSA in PBS with 0.05% Tween-20). Subsequently, after a wash with PBS-Tween (0.05%), the membrane was incubated for 1 h at room temperature in Primary antibody (1 µg/mL) (Rabbit-anti human Factor XIII-A polyclonal antibody, Thermo Fischer Scientific Inc) with mild shaking. After washing thrice in PBS-Tween (0.05%), the membrane was incubated for 1 h at room temperature in HRP tagged Secondary antibody (50 ng/mL) (Anti-Rabbit HRP, Thermo Fischer Scientific Inc). Finally, the membrane was washed thrice in PBS-Tween and PBS, respectively. Chemiluminescent signal quantification, Image acquisition (Chemidoc MP, Bio-Rad) and densitometric evaluation of signal were performed on Image lab Software (Bio-Rad) version 4.1. Using known amounts of recombinant FXIII-A (positive control), the percentage antigenicity and absolute quantity of antigenically active FXIII-A was calculated in transfected samples based on the chemiluminescent intensity of the signal. The antigenic levels determined by densitometry were confirmed with a commercial sandwich ELISA (AssayMax). The antigenic levels were used in combination with activity levels from photometric assay to calculate the specific activity of the individual samples.

FXIII activity determination by biochemical end-point assays. *Photometric assay.* Intracellular lysates (Wild type; Mutants), were 6X concentrated using Amicon filters (30 kDa cut-off) (Merck Millipore) for the evaluation of FXIII activity with a kinetic photometric assay (Berichrom, Siemens, Germany). Briefly, samples were activated in the presence of thrombin and calcium, at 37 °C, transglutaminase activity of FXIII-A was measured indirectly by measuring released indicator, i.e., Ammonia (Abs 340 nm). A decrease in absorbance is directly proportional to FXIII-A transglutaminase activity in the samples⁴⁹. The assay was performed on the Behring Coagulation System[®] (BCS) (Dade Behring, Marburg, Germany). All the experiments were performed in duplicates, with three sets of transfections to ensure reproducibility.

Pentylamine incorporation assay. The activity of intracellular lysates of recombinant factor XIII (rFXIII) Wild type, Mutants and a negative control was determined based on a pentylamine incorporation assay as described previously⁵⁰. Briefly, microtiter plates were coated with 80 µg/mL human fibrinogen (Enzyme Research Laboratories, UK) at 37 °C for 1 hour, then blocked with 1% BSA overnight at 4 °C. Plates were incubated with duplicates of 10 µL lysate, 0.27 µM 5-(Biotinamido) pentylamine (Thermo Fisher Scientific Inc), 1 U/mL human thrombin (Calbiochem, Merck KGaA), 100 µM Dithiothreitol (Sigma), and 1 mM CaCl₂. Incorporation of 5-(Biotinamido) pentylamine was stopped with 133 mM EDTA after 0 or 30 minutes. Cross-linking of the 5-(biotinamido) pentylamine into the fibrin by recombinant FXIII was detected using streptavidin-alkaline phosphatase (Life Technologies) and p-Nitrophenyl phosphate (Sigma). Plates were measured at OD 405 nm in a Powerwave Bio-Tek multiwell plate reader (Winooski, USA). Optical density (OD) values at time 0 were subtracted from the 30-minute readings for each lysate to remove background and a standard curve of known concentrations of FXIII were used to extrapolate activity of rFXIII in each lysate.

Determination of protein activity by α₂-antiplasmin incorporation. The activity of intracellular lysates containing recombinant factor XIII (rFXIII) wild type, mutants, and a negative control was also assayed by α₂-antiplasmin incorporation, based on a method previously described⁵¹. Briefly, microtiter plates were coated with 80 µg/mL human fibrinogen (Enzyme Research Laboratories, UK) at 37 °C for 1 hour, then blocked with 1% BSA overnight at 4 °C. Plates were then treated in duplicate with 10 µL lysate, 10 µg/mL α₂-antiplasmin (Calbiochem), 1 U/mL human thrombin, 0.1 mM DTT, and 10 mM CaCl₂. Incorporation of α₂-antiplasmin was stopped with 133 mM EDTA after 0 or 60 minutes. Cross-linking of the α₂-antiplasmin into the fibrin by rFXIII was detected using goat anti-human α₂-antiplasmin antibody with a horse-radish peroxidase conjugate (Enzyme Research Laboratories) and 1, 2-diaminobenzene *o*-phenylenediamine (OPD; Dako). Plates were measured at 490 nm in a multi-well plate reader (Bio-Tek). OD values at time 0 were subtracted from the 60-minute readings for each lysate to remove background and a standard curve of known concentrations of FXIII were used to extrapolate activity of rFXIII in each lysate.

fXiii activity determination by a continuous fXiii-A* generation assay. Activated FXIII-A (FXIII-A*) generation was triggered by tissue factor/phospholipids (TF/PL), and FXIII-A* isopeptidase activity was measured using the fluorogenic substrate A101 (Zedira, Darmstadt, Germany) in a Safire microtiter plate reader (Tecan, Crailsheim, Germany)²⁶. Twenty-five microliters FXIII-deficient plasma (deficient for FXIII-A₂ and FXIII-B₂; Haemochrom Diagnostica GmbH, Essen, Germany) spiked rFXIII-A₂ mutants (equal amount of crude samples based on antigenicity) were incubated with 35 µL reagent solution (5 µL 100 mM glycine methyl ester, 5 µL 2 mM fluorogenic FXIII-A* substrate, 10 µL Innovin (recombinant TF; Dade Behring, IL, USA) diluted 1:700 in phospholipids (PTT reagent kit, Roche, USA) and 15 µL HBS (20 mM Hepes, 150 mM NaCl)/0.1% serum albumin pH 7.5. The reaction was started with 40 µL HBS pH 7.5 containing 25 mM CaCl₂. For the thrombin resistant mutant FXIII-A-R38A, increasing amounts of calcium (25 mM, 50 mM, 100 mM, and 200 mM) in

HBSpH7.5 were used. Fluorescence was measured over 1 hour at excitation wavelength = 330 nm and emission wavelength = 430 nm in kinetic mode with data acquisition 2 times per minute. All the experiments were performed in duplicates, with three sets of transfections to ensure reproducibility. Human standard plasma (Siemens Healthcare, Erlangen, Germany) was used as an internal assay control.

Three parameters (further explained in the statistical analysis section) were obtained for each variant and the wild type from the FXIII-A* continuous generation curve:

- (A) Rate of FXIII-A* generation/maximal rate (μ ; expressed as $\Delta R.F.U./min$) which represents the rate of conformational change between the zymogenic and activated forms. The transglutaminase crosslinking reaction is a two-step reaction (a ping-pong mechanism), in which two substrates sequentially access the active site to first form intermediates and then get crosslinked to each other^{22,25}. Since the continuous generation assay relies on the isopeptidase activity which involves a singular cleavage/hydrolysis of a quencher attached to the substrate peptide immediately post the formation of the activated FXIII-A*, it is more reflective of the change in conformation between the zymogenic and activated FXIII-A forms than any end-point assays. Theoretically, both continuous-generation assay and end-point activity assay should show correlation, but that might not be the case for mutant variants, especially those that alter substrate binding sites.
- (B) The tlag is the time required for the activation of FXIII-A by thrombin (in plasma background), in the generation assay. Since in generation assay, the activation process is initiated by Innovin, a recombinant tissue factor and which is upstream to the thrombin cleavage of FXIII-A in the coagulation pathway, there is always some time lag before the first signal of activated FXIII-A* can be recorded. Any delay or faster tlag might signify differences in thrombin cleavage of FXIII-A.
- (C) The tmax is the time taken to reach the maximal rate μ .

(Note: An illustration of the generation assay curve along with a small commentary is provided in Supplementary Fig. 2 to help the reader understand the assay better).

Mapping substrate binding sites on FXIII-A subunit activation transition state intermediate models. We used FXIII-A subunit activation transition state intermediate models we had earlier generated and reported, to study the changes in the substrate binding regions as the FXIII-A molecule unfolds from its closed zymogenic state to its open fully activated state during the process of activation¹⁶. Three major putative substrate binding regions i.e. fibrinogen, BAPA and α -2 antiplasmin were considered since the endpoint FXIII activity assays dealt with these substrates. These binding regions had been determined by rigid docking studies we had earlier conducted and reported for fibrinogen and α -2 antiplasmin⁵². The putative BAPA binding region(s) were predicted by docking the structural coordinates of BAPA [5-(Biotinamido) pentylamine; Pubchem ID: CID 83906] that were downloaded from Pubchem database (as an SDF file and later converted to a PDB file on YASARA), onto the activated FXIII-A crystal structure (PDB ID: 4kty) downloaded from the protein database. Semi-flexible docking was performed with the Autodock function embedded in YASARA⁵². Finally these binding regions were mapped and highlighted on the FXIII-A subunit activation transition state intermediate models.

Molecular dynamic simulation of FXIII-A at different ionic concentrations. The effect of increasing ion concentration on the structure of FXIII-A subunit was studied by running plain Molecular dynamics (MD) simulation the zymogenic human FXIII-A2 crystal structure (PDB ID: 1f13; 2.1 Å resolution) and only the core domain of FXIII-A subunit (isolated from the PDB ID: 1f13 and consisting of the amino acids between 183–515 residues) on the YASARA Structure package version 13.11.1 platform^{53,54}. Gaps or unresolved regions within the crystal structure(s) were modelled on the FREAD loop modelling server (<http://opig.stats.ox.ac.uk/webapps/fread/>)⁵⁵, e.g., the PDB file 1f13 that has missing regions at the thrombin cleavage site Arg37-Gly38 was submitted to the server under default parameters and with the starting and ending residue of the missing region specified. The final gap resolved structure was chosen from the output file based on scores that were a combination of all backbone atom anchor match RMSD (corresponds to the base structure) and all backbone atom loop match RMSD (corresponds to the loop structure). The PDB files were initially subjected to a 500 ps refinement MD simulation run that imposes the YAMBER3 force field parameters in YASARA in order to remove steric clashes and improve rotamer geometry⁵³. The file with the lowest energy in the simulation trajectory was chosen for conducting further simulations. Simulations were performed with the md_sim macro embedded in YASARA. The macro was modified for running simulations at different ionic concentrations. Briefly, a simulation cell with periodic boundaries and 20 Å minimum distances to protein atoms was employed with explicit solvent. The AMBER03 force field, NPT ensemble was used with long range PME potential and a cut-off of 7.86 Å⁵⁶. Hydrogen bond networks were optimized using the method of Hooft and co-workers⁵⁷. The simulation cell was filled with water at a density of 0.997 g/mL and a maximum sum of all bumps per water of 1.0 Å. Most importantly, the simulation cell net charge was neutralized with different NaCl and CaCl₂ concentrations. While the full zymogenic dimeric structure was simulated at 150 mM and 1 M NaCl, the core domain was simulated at 5 mM, 10 mM, 50 mM, and 100 mM CaCl₂. The entire system was energy minimized by steepest descent to remove conformation stress within the structure, followed by simulated annealing minimization until convergence was achieved. The MD simulation was performed at 298 K. Simulations for all structures at all concentrations were run for a minimum of 100 ns after equilibration was achieved. Secondary structure content during the MD simulations was visualized using the md_analysecstr macro output embedded in YASARA on R. Structural image visualization, analysis, and rendering were done with YASARA 13.11.1 and Chimera version 1.10.2^{54,58}. Electrostatic surface potential was calculated and graphically depicted using the Adaptive Poisson-Boltzmann Solver integrated within YASARA⁵⁹. The inter-residue interaction or Residue interaction network (RIN) within a structure was visualized

by submitting the PDB file corresponding to that structure (usually the 100ns simulation snapshot for all simulated structures in this study) to the RING 2.0 server (<http://protein.bio.unipd.it/ring/>)⁶⁰. The server identifies covalent and non-covalent bonds in protein structures, including π - π stacking and π -cation interactions using a complex empirical re-parameterization of distance thresholds performed on the entire submitted PDB file. The output is in the form of a colour coded point and connector network pattern. The colour codes are explained in the inset diagram for all network pattern outputs.

Conservation of calcium binding sites within FXIII-A subunit. The conservation of the calcium binding sites residues within the FXIII-A subunit were analyzed on the *ConSurf* server (<http://consurf.tau.ac.il/2016/>)⁶¹ which is a bioinformatics tool for estimating the evolutionary conservation of amino/nucleic acid positions in a protein/DNA/RNA molecule based on the phylogenetic relations between homologous sequences⁶¹. The degree to which an amino (or nucleic) acid position is evolutionarily conserved (i.e., its evolutionary rate) is strongly dependent on its structural and functional importance. The FXIII-A sequence from UniProt (ID: P00488) was submitted to this server under default conditions (Homolog search algorithm: HMMER; E value cut off at 0.0001; Proteins database: UNIREF-90; Alignment method: MAFFT-L-INS-i; Calculation method: Bayesian; Evolutionary substitution model: Best model) but with higher number ($n = 5$) iterations. The resulting alignment output was viewed on the Jalview alignment viewer. The structural conservation of the calcium binding sites was evaluated by structurally aligning all human transglutaminase structures, including FXIII-A subunit using the Multiseq tool embedded in VMD⁶². All biophysical structures for FXIII-A subunit (PDB ID: 1f13), TG2 (PDB ID: 4pyg) and TG3 (PDB ID: 1nuf) that are currently resolved and available were downloaded from the protein database for this purpose^{15,29,63}. The remaining transglutaminases with no known structures were modeled on *I-TASSER* modeling and threading server⁶⁴. The sequences of these transglutaminases (extracted from the Uniprot database) were submitted to the *I-TASSER* server under default conditions. The highest scoring (best C-score) model among the output files was chosen for multiple alignments (Supplementary Fig. 9a-d). Post alignment, a structure-based phylogenetic tree was generated using delta QH values, which is a measure of structural homology. Subjects closer to each other on this tree are structurally similar.

thermodynamic analyses of calcium binding to fXiii-A by isothermal titration calorimetry.

Isothermal titration calorimetry experiments were carried out on a MicroCal200 microcalorimeter (Malvern Panalytical, UK). The reference cell was filled with Autoclaved MiliQ water. The rFXIII-A₂ (expressed in-house in Yeast expression system) in the sample cell was titrated against calcium concentrations. The sample (rFXIII-A₂) was re-suspended in 20 mM Tris pH 8.2 before titration. In principle, the titrations were performed based on the c-value (concentration of calcium in syringe/concentration of sample rFXIII-A₂ in the cell). Since plasma FXIII and calcium ion concentration are 2 mg/L (an effective molar concentration of 0.0125 μ M) and 2.5 mM respectively, the c-value for mimicking a plasmatic environment will be almost 200,000 which is beyond the sensitivity of ITC⁶⁵⁻⁶⁷. Hence, titrations were performed at a high c-value as 25,000; and a standard c-value of 20⁶⁷. For each of the conditions, titrations were performed in the same buffer (20 mM Tris, pH 8.2), unless stated otherwise. For c-value = 20, 1.25 mM of rFXIII-A₂ was titrated against 25 mM CaCl₂ (with 13.8 U thrombin (Sigma) in the sample cell). The titration involved 19 injections ($12 \times 2, 0.4 \times 6$, each injection spaced by 120 s). To ensure complete saturation, the reaction was continued with a further 19 injections ($12 \times 2, 0.4 \times 6$, each injection spaced by 120 s). Both the resulting isotherms were concatenated with CONCAT tool provided with the Origin software (version 7.0) (OriginLab)⁶⁸. For c-value = 25,000; 1×10^{-3} mM rFXIII-A₂, activated by 2 U of thrombin (Sigma) was titrated against 25 mM calcium. The titration was performed for 19 injections 2 μ L each, spaced at 150 s, to reach full saturation, the reaction proceeded with further 19 injections (0.4 μ L each, spaced at 150 s) and the titrations were concatenated with CONCAT tool provided with the Origin software (version 7.0). All the experiments were performed in the same buffer (20 mM Tris, pH 8.2), at 30 degrees with the stirring speed set to 750 rpm, at low feedback. For each experiment, thrombin was added before the start of the reaction; hence rFXIII-A₂ was incubated with thrombin, in the absence of calcium for the period of pre-titration delay. To account for the heat of dilution, we performed blank experiments under the same conditions without rFXIII-A₂ in the sample cell (Thrombin in cell titrated against CaCl₂ in the syringe). Peak integration was done in the software Origin 7.0. For thermodynamic analysis, initially, we used Origin software, for single set of binding model, in order to observe the binding as a global fit. The parameter K_d was approximated around 100 μ M based on earlier reports, was set as non-varying parameter for sequential binding site model with 3 set of binding sites (Even for sequential binding site model, it is advisable to have initial guesses for n , K and ΔH)^{3,69}. (The K_1 was used as a standalone non-varying parameter for the further fitting of data in all fitting exercises). Subsequently, heat capacity changes for each injection were calculated based on the algorithms followed by Origin software, as well as stoichiometric equilibria model (described below) in *Affinimeter* (<https://www.affinimeter.com/>)⁷⁰ and the process was iterated until no further significant improvement in fit were observed. Individual heat-signatures were derived from the energy definitions upon each binding after model fitting also by using *Affinimeter*. The corresponding thermodynamic parameters were calculated according to the equation $\ln(1/K_d) = (\Delta H - T\Delta S)/RT$. Additionally, titrations were performed at 1 μ M and 0.4 μ M FXIII-A₂, with ligand (calcium ion) concentration of 12 μ M and 14 μ M respectively (for c-values 12 and 35) (data not shown), and no binding was observed in these titrations. The titrations were first simulated in *Affinimeter* with the aforementioned c-values & fitting was simulated to the following custom design model, using the model-builder approach on *Affinimeter* app to dissect the contribution of individual species generated during the course of FXIII-A activation, following the hypothetical equation:



where M is FXIII-A₂, A is calcium ion.

The final data was interpreted based on fitting exercises performed using *Affinimeter*.

Statistical analysis. Statistical analysis was performed using R⁶⁹. For endpoint assays, mean values were compared (to the wild type) by Student's two-tailed t-test. In the generation assays, data was analyzed based on growth-curve analyses, with the slope of the curve (μ) representing the growth rate. Data were fit using R-package "Grofit", based on the dose-response relationship⁷¹. Non-parametric spline estimation was done to fit the data, and to obtain the characteristic parameters lag phase (t_{lag}), maximal growth rate (μ), time of maximal growth rate (t_{max}), maximal growth (A) and area under the growth for each single growth curve.

The function follows the following parameterization:

$$y(t) = A^* \exp[-\exp(\mu^* \exp(1)/A^* (\lambda - t) + 1)]$$

Abbreviations: lag phase (t_{lag}): λ maximal growth rate (rate of activation): μ , Area under curve: A, and time of observation: t

Data Availability

The datasets generated during and/or analyzed during the current study are available from the corresponding author on reasonable request.

References

- Varga-Szabo, D., Braun, A. & Nieswandt, B. Calcium signaling in platelets. *Journal of Thrombosis and Haemostasis* **7**, 1057–1066, <https://doi.org/10.1111/j.1538-7836.2009.03455.x> (2009).
- Braun, A., Vogtle, T., Varga-Szabo, D. & Nieswandt, B. STIM and Orai in hemostasis and thrombosis. *Frontiers in bioscience (Landmark edition)* **16**, 2144–2160 (2011).
- Ambrus, A. *et al.* Calcium binding of transglutaminases: a 43Ca NMR study combined with surface polarity analysis. *Journal of biomolecular structure & dynamics* **19**, 59–74, <https://doi.org/10.1080/07391102.2001.10506720> (2001).
- Lorand, L., Losowsky, M. S. & Miloszewski, K. J. Human factor XIII: fibrin-stabilizing factor. *Progress in hemostasis and thrombosis* **5**, 245–290 (1980).
- Schwartz, M. L., Pizzo, S. V., Hill, R. L. & McKee, P. A. Human Factor XIII from plasma and platelets. Molecular weights, subunit structures, proteolytic activation, and cross-linking of fibrinogen and fibrin. *The Journal of biological chemistry* **248**, 1395–1407 (1973).
- Muszbeek, L., Ariens, R. A. & Ichinose, A. Factor XIII: recommended terms and abbreviations. *Journal of thrombosis and haemostasis: JTH* **5**, 181–183, <https://doi.org/10.1111/j.1538-7836.2006.02182.x> (2007).
- Lorand, L. & Graham, R. M. Transglutaminases: crosslinking enzymes with pleiotropic functions. *Nature reviews. Molecular cell biology* **4**, 140–156, <https://doi.org/10.1038/nrm1014> (2003).
- Nemes, Z., Petrovski, G., Csoos, E. & Fesus, L. Structure-function relationships of transglutaminases—a contemporary view. *Progress in experimental tumor research* **38**, 19–36, <https://doi.org/10.1159/000084231> (2005).
- Belkin, A. M. Extracellular TG2: emerging functions and regulation. *FEBS Journal* **278**, 4704–4716, <https://doi.org/10.1111/j.1742-4658.2011.08346.x> (2011).
- Gifford, J. L., Walsh, M. P. & Vogel, H. J. Structures and metal-ion-binding properties of the Ca²⁺-binding helix-loop-helix EF-hand motifs. *The Biochemical journal* **405**, 199–221, <https://doi.org/10.1042/BJ20070255> (2007).
- Makarova, K. S., Aravind, L. & Koonin, E. V. A superfamily of archaeal, bacterial, and eukaryotic proteins homologous to animal transglutaminases. *Protein science: a publication of the Protein Society* **8**, 1714–1719, <https://doi.org/10.1110/ps.8.8.1714> (1999).
- Fox, B. A. *et al.* Identification of the calcium binding site and a novel ytterbium site in blood coagulation factor XIII by x-ray crystallography. *The Journal of biological chemistry* **274**, 4917–4923 (1999).
- Weiss, M. S., Metzner, H. J. & Hilgenfeld, R. Two non-proline cis peptide bonds may be important for factor XIII function. *FEBS letters* **423**, 291–296 (1998).
- Yee, V. C., Pedersen, L. C., Bishop, P. D., Stenkamp, R. E. & Teller, D. C. Structural evidence that the activation peptide is not released upon thrombin cleavage of factor XIII. *Thrombosis research* **78**, 389–397 (1995).
- Stieler, M. *et al.* Structure of active coagulation factor XIII triggered by calcium binding: basis for the design of next-generation anticoagulants. *Angewandte Chemie (International ed. in English)* **52**, 11930–11934, <https://doi.org/10.1002/anie.201305133> (2013).
- Gupta, S. *et al.* Revisiting the mechanism of coagulation factor XIII activation and regulation from a structure/functional perspective. *Scientific reports* **6**, 30105, <https://doi.org/10.1038/srep30105> (2016).
- Kristiansen, G. K. & Andersen, M. D. Reversible activation of cellular factor XIII by calcium. *The Journal of biological chemistry* **286**, 9833–9839, <https://doi.org/10.1074/jbc.M110.174128> (2011).
- Marinelli, F. *et al.* Evidence for an allosteric mechanism of substrate release from membrane-transporter accessory binding proteins. *Proceedings of the National Academy of Sciences of the United States of America* **108**, E1285–92, <https://doi.org/10.1073/pnas.1112534108> (2011).
- Olsson, T. S. G., Ladbury, J. E., Pitt, W. R. & Williams, M. A. Extent of enthalpy-entropy compensation in protein-ligand interactions. *Protein science: a publication of the Protein Society* **20**, 1607–1618, <https://doi.org/10.1002/pro.692> (2011).
- Eisenstein, E., Markby, D. W. & Schachman, H. K. Changes in stability and allosteric properties of aspartate transcarbamoylase resulting from amino acid substitutions in the zinc-binding domain of the regulatory chains. *Proceedings of the National Academy of Sciences of the United States of America* **86**, 3094–3098 (1989).
- Anokhin, B. A., Stribinskis, V., Dean, W. L. & Maurer, M. C. Activation of factor XIII is accompanied by a change in oligomerization state. *The FEBS journal* **284**, 3849–3861, <https://doi.org/10.1111/febs.14272> (2017).
- Kiyotaka, H., Fesus, L. Transglutaminase multiple functional modifiers and targets for new drug discovery. ISBN 978-4-431-55823-1 ISBN 978-4-431-55825-5 (eBook), 10.1007/978-4-431-55825-5; 2017, 1–5; 10.1007/978-4-431-55825-5 (2017).
- Kanchan, K. *et al.* Identification of a specific one amino acid change in recombinant human transglutaminase 2 that regulates its activity and calcium sensitivity. *The Biochemical journal* **455**, 261–272, <https://doi.org/10.1042/BJ20130696> (2013).
- Király, R. *et al.* Isopeptidase activity of human transglutaminase 2: disconnection from transamidation and characterization by kinetic parameters. *Amino acids* **48**, 31–40, <https://doi.org/10.1007/s00726-015-2063-5> (2016).
- Ahvazi, B., Kim, H. C., Kee, S.-H., Nemes, Z. & Steinert, P. M. Three-dimensional structure of the human transglutaminase 3 enzyme: binding of calcium ions changes structure for activation. *The EMBO journal* **21**, 2055–2067, <https://doi.org/10.1093/emboj/21.9.2055> (2002).
- Dotz, J., Volkert, P. & Seitz, R. Factor XIIIa generation assay: a tool for studying factor XIII function in plasma. *Analytical biochemistry* **439**, 145–151, <https://doi.org/10.1016/j.ab.2013.04.012> (2013).
- Lahav, J. *et al.* Coagulation factor XIII serves as protein disulfide isomerase. *Thrombosis and haemostasis* **101**, 840–844 (2009).
- Parameswaran, K. N. *et al.* Hydrolysis of γ -E isopeptides by Cytosolic Transglutaminases and by Coagulation Factor XIIIa. *Journal of Biological Chemistry* **272**, 10311–10317, <https://doi.org/10.1074/jbc.272.15.10311> (1997).

29. Ahvazi, B. *et al.* Structural basis for the coordinated regulation of transglutaminase 3 by guanine nucleotides and calcium/magnesium. *The Journal of biological chemistry* **279**, 7180–7192, <https://doi.org/10.1074/jbc.M312310200> (2004).
30. Komáromi, I., Bagoly, Z. & Muszbek, L. Factor XIII: novel structural and functional aspects. *Journal of thrombosis and haemostasis: JTH* **9**, 9–20, <https://doi.org/10.1111/j.1538-7836.2010.04070.x> (2011).
31. Richardson, V. R., Cordell, P., Standeven, K. F. & Carter, A. M. Substrates of Factor XIII-A: roles in thrombosis and wound healing. *Clinical science (London, England: 1979)* **124**, 123–137, <https://doi.org/10.1042/CS20120233> (2013).
32. Asijee, G. M. *et al.* Platelet vinculin: a substrate of activated factor XIII. *Biochimica et biophysica acta* **954**, 303–308 (1988).
33. Cohen, I., Kahn, D. R. & Drisdell, R. C. Inhibition of platelet factor XIIIa-catalyzed reactions by calmodulin. *Biochimica et biophysica acta* **883**, 265–270 (1986).
34. Kahn, D. R. & Cohen, I. Factor XIIIa-catalyzed coupling of structural proteins. *Biochimica et biophysica acta* **668**, 490–494 (1981).
35. Cohen, I., Young-Bandala, L., Blankenberg, T. A., Siefing, G. E. & Bruner-Lorand, J. Fibrinolytic-catalyzed cross-linking of myosin from platelet and skeletal muscle. *Archives of biochemistry and biophysics* **192**, 100–111 (1979).
36. Muszbek, L., Bereczky, Z., Bagoly, Z., Komáromi, I. & Katona, É. Factor XIII: a coagulation factor with multiple plasmatic and cellular functions. *Physiological reviews* **91**, 931–972, <https://doi.org/10.1152/physrev.00016.2010> (2011).
37. Mitchell, J. L. & Mutch, N. J. Novel aspects of platelet factor XIII function. *Thrombosis research* **141**(Suppl 2), S17–21, [https://doi.org/10.1016/S0049-3848\(16\)30356-5](https://doi.org/10.1016/S0049-3848(16)30356-5) (2016).
38. Orosz, Z. Z., Katona, E., Facskó, A., Berta, A. & Muszbek, L. A highly sensitive chemiluminescence immunoassay for the measurement of coagulation factor XIII subunits and their complex in tears. *Journal of immunological methods* **353**, 87–92, <https://doi.org/10.1016/j.jim.2010.01.001> (2010).
39. Osawa, M. *et al.* Mg²⁺ and Ca²⁺ differentially regulate DNA binding and dimerization of DREAM. *The Journal of biological chemistry* **280**, 18008–18014, <https://doi.org/10.1074/jbc.M500338200> (2005).
40. Wang, X., Kirberger, M., Qiu, F., Chen, G. & Yang, J. J. Towards predicting Ca²⁺-binding sites with different coordination numbers in proteins with atomic resolution. *Proteins* **75**, 787–798, <https://doi.org/10.1002/prot.22285> (2009).
41. Shimokhina, N., Bronowska, A. & Homans, S. W. Contribution of ligand desolvation to binding thermodynamics in a ligand-protein interaction. *Angewandte Chemie (International ed. in English)* **45**, 6374–6376, <https://doi.org/10.1002/anie.200602227> (2006).
42. Amaral, M. *et al.* Protein conformational flexibility modulates kinetics and thermodynamics of drug binding. *Nature communications* **8**, 2276, <https://doi.org/10.1038/s41467-017-02258-w> (2017).
43. Syme, N. R., Dennis, C., Bronowska, A., Paesen, G. C. & Homans, S. W. Comparison of entropic contributions to binding in a “hydrophilic” versus “hydrophobic” ligand-protein interaction. *Journal of the American Chemical Society* **132**, 8682–8689, <https://doi.org/10.1021/ja101362u> (2010).
44. Hethershaw, E. L. *et al.* The role of beta-barrels 1 and 2 in the enzymatic activity of factor XIII A-subunit. *Journal of thrombosis and haemostasis: JTH* **16**, 1391–1401, <https://doi.org/10.1111/jth.14128> (2018).
45. Al-Horani, R. A., Karuturi, R., Lee, M., Afosah, D. K. & Desai, U. R. Allosteric Inhibition of Factor XIIIa. Non-Saccharide Glycosaminoglycan Mimetics, but Not Glycosaminoglycans, Exhibit Promising Inhibition Profile. *PLoS one* **11**, e0160189, <https://doi.org/10.1371/journal.pone.0160189> (2016).
46. Iwata, Y. *et al.* Conformational analysis and docking study of potent factor XIIIa inhibitors having a cyclopropenone ring. *Journal of molecular graphics & modelling* **18**(591-9), 602–4 (2000).
47. Seale, L., Finney, S., Sawyer, R. T. & Wallis, R. B. Tridegin, a novel peptidic inhibitor of factor XIIIa from the leech, *Haementeria ghilianii*, enhances fibrinolysis *in vitro*. *Thrombosis and haemostasis* **77**, 959–963 (1997).
48. Prasa, D. & Sturzebecher, J. Inhibitors of factor XIIIa. *Haemostaseologie* **22**, 43–47 (2002).
49. Lee, K. N., Birkbichler, P. J. & Patterson, M. K. Colorimetric assay of blood coagulation factor XIII in plasma. *Clinical chemistry* **34**, 906–910 (1988).
50. Philippou, H. *et al.* Roles of low specificity and cofactor interaction sites on thrombin during factor XIII activation. Competition for cofactor sites on thrombin determines its fate. *The Journal of biological chemistry* **278**, 32020–32026, <https://doi.org/10.1074/jbc.M305364200> (2003).
51. Dunn, E. J., Philippou, H., Ariens, R. A. S. & Grant, P. J. Molecular mechanisms involved in the resistance of fibrin to clot lysis by plasmin in subjects with type 2 diabetes mellitus. *Diabetologia* **49**, 1071–1080, <https://doi.org/10.1007/s00125-006-0197-4> (2006).
52. Thomas, A. *et al.* Coagulation Factor XIIIa Subunit Missense Mutations Affect Structure and Function at the Various Steps of Factor XIII Action. *Human mutation* **37**, 1030–1041, <https://doi.org/10.1002/humu.23041> (2016).
53. Krieger, E., Koraimann, G. & Vriend, G. Increasing the precision of comparative models with YASARA NOVA—a self-parameterizing force field. *Proteins* **47**, 393–402 (2002).
54. Krieger, E. & Vriend, G. YASARA View - molecular graphics for all devices - from smartphones to workstations. *Bioinformatics (Oxford, England)* **30**, 2981–2982, <https://doi.org/10.1093/bioinformatics/btu426> (2014).
55. Case, D. A. *et al.* The Amber biomolecular simulation programs. *Journal of computational chemistry* **26**, 1668–1688, <https://doi.org/10.1002/jcc.20290> (2005).
56. Hooft, R. W., Vriend, G., Sander, C. & Abola, E. E. Errors in protein structures. *Nature* **381**, 272, <https://doi.org/10.1038/381272a0> (1996).
57. Pettersen, E. F. *et al.* UCSF Chimera—a visualization system for exploratory research and analysis. *Journal of computational chemistry* **25**, 1605–1612, <https://doi.org/10.1002/jcc.20084> (2004).
58. Krissinel, E. & Henrick, K. Inference of macromolecular assemblies from crystalline state. *Journal of molecular biology* **372**, 774–797, <https://doi.org/10.1016/j.jmb.2007.05.022> (2007).
59. Das, A. *et al.* Exploring the conformational transitions of biomolecular systems using a simple two-state anisotropic network model. *PLoS computational biology* **10**, e1003521, <https://doi.org/10.1371/journal.pcbi.1003521> (2014).
60. Piovesan, D., Minervini, G. & Tosatto, S. C. E. The RING 2.0 web server for high quality residue interaction networks. *Nucleic acids research* **44**, W367–74, <https://doi.org/10.1093/nar/gkw315> (2016).
61. Ashkenazy, H. *et al.* ConSurf 2016: an improved methodology to estimate and visualize evolutionary conservation in macromolecules. *Nucleic acids research* **44**, W344–50, <https://doi.org/10.1093/nar/gkw408> (2016).
62. Roberts, E., Eargle, J., Wright, D. & Luthey-Schulten, Z. MultiSeq: unifying sequence and structure data for evolutionary analysis. *BMC bioinformatics* **7**, 382, <https://doi.org/10.1186/1471-2105-7-382> (2006).
63. Jang, T.-H. *et al.* Crystal structure of transglutaminase 2 with GTP complex and amino acid sequence evidence of evolution of GTP binding site. *PLoS one* **9**, e107005, <https://doi.org/10.1371/journal.pone.0107005> (2014).
64. Roy, A., Kucukural, A. & Zhang, Y. I-TASSER: a unified platform for automated protein structure and function prediction. *Nature protocols* **5**, 725–738, <https://doi.org/10.1038/nprot.2010.5> (2010).
65. Muszbek, L., Yee, V. C. & Hevesy, Z. Blood coagulation factor XIII: structure and function. *Thrombosis research* **94**, 271–305 (1999).
66. Lindgärde, F. Potentiometric determination of serum ionized calcium in a normal human population. *Clinica chimica acta; international journal of clinical chemistry* **40**, 477–484 (1972).
67. Broecker, J., Vargas, C. & Keller, S. Revisiting the optimal c value for isothermal titration calorimetry. *Analytical biochemistry* **418**, 307–309, <https://doi.org/10.1016/j.ab.2011.07.027> (2011).
68. Edwards, P. M. Origin 7.0: Scientific Graphing and raw data analysis software. *J. Chem. Inf. Comput. Sci.* **42**(5), 1270–1271 (2002).
69. R Core Team R: A language and environment for statistical computing. R Foundation for Statistical Computing, Vienna, Austria. <https://www.R-project.org/2017> (2017).

70. Herrera, I. & Winnik, M. A. Differential Binding Models for Direct and Reverse Isothermal Titration Calorimetry. *The journal of physical chemistry. B* **120**, 2077–2086, <https://doi.org/10.1021/acs.jpcc.5b09202> (2016).
71. Kahm, M., Hasenbrink, G., Lichtenberg-Frate, H., Ludwig, J. & Kschischo, M. Grofit: Fitting Biological Growth Curves with R. *Journal of Statistical Software*, **33**(7), 1–21, <http://www.jstatsoft.org/v33/i07/2010> (2010).

Acknowledgements

The authors would like to acknowledge funding (consumables and staff salary for S.S.) received from CSL Behring (N-045.0180) towards FXIII research. The authors would like to thank Dr. Agatha Korytowski (Malvern Panalytical), for her valuable inputs and suggestions for the ITC analysis.

Author contributions

A.B. conceived the project. A.B. and S.S. contributed to the design of the project, discussion and interpretation of results. S.S. designed, performed and analyzed site-directed mutagenesis, performed SDS PAGE, Western blots, ELISAs and ITC experiments. H.P. and E.H. performed incorporation assays. J.D. performed FXIII generation assay and P.V. did data analysis for the same. A.B. performed the *in-silico* experiments. S.S., and A.B. co-wrote the manuscript and V.I., D.L., and J.O. read and edited the manuscript. All authors critically reviewed the manuscript.

Additional information

Supplementary information accompanies this paper at <https://doi.org/10.1038/s41598-019-47815-z>.

Competing Interests: The authors declare no competing interests.

Publisher's note: Springer Nature remains neutral with regard to jurisdictional claims in published maps and institutional affiliations.



Open Access This article is licensed under a Creative Commons Attribution 4.0 International License, which permits use, sharing, adaptation, distribution and reproduction in any medium or format, as long as you give appropriate credit to the original author(s) and the source, provide a link to the Creative Commons license, and indicate if changes were made. The images or other third party material in this article are included in the article's Creative Commons license, unless indicated otherwise in a credit line to the material. If material is not included in the article's Creative Commons license and your intended use is not permitted by statutory regulation or exceeds the permitted use, you will need to obtain permission directly from the copyright holder. To view a copy of this license, visit <http://creativecommons.org/licenses/by/4.0/>.

© The Author(s) 2019

Chapter 4

Published Articles

4A: Identification of Potential Novel Interacting Partners for Coagulation Factor XIII B (FXIII-B) Subunit, a Protein Associated with a Rare Bleeding Disorder

Sneha Singh, Mohammad Suhail Akhter, Johannes Dodt, Peter Volkers, Andreas Reuter, Christoph Krettler, Christoph Reinhart, Johannes Oldenburg & Arijit Biswas

A brief synopsis:

Owing to the comparatively unexplored roles of FXIII-B subunits, in this sub-section of chapter 4 we tried to identify novel interacting partners of FXIII-B, that may be characterized further defining new roles of this subunit. Here, we first explored the excipients that exist with FXIII complex in FXIII plasma concentrate and verified it by mass spectrometry. Additionally, owing to the structure and sequential similarity of FXIII-B with Complement factor H, we tested if CFH influences the rate of activation of FXIII-A, like FXIII-B subunit. Furthermore, FXIII-B based pull-down assays revealed more sticking partners of FXIII-B subunits in a FXIII-deficient plasma background. The studies reveal; a) no direct role of CFH on FXIII activation; and, b) α -2 macroglobulin as only common denominator found both in content characterization of plasma concentrate and pull-down assays; future functional investigations will be needed to understand the physiological significance of this association.

Int. J. Mol. Sci. 2019, 20, 2682; doi:10.3390/ijms20112682

4B: Exploring the structural similarity yet functional distinction between coagulation factor XIII-B and complement factor H sushi domains.

Sneha Singh, Mohammad Suhail Akhter, Hamideh Yadegari, Vytautas Ivaskevicius, Johannes Oldenburg & Arijit Biswas

A brief synopsis:

Owing to the structural and sequential homology between complement factor H (CFH) and FXIII-B; we performed a combination of in-silico and ELISA based studies to investigate any potential role of FXIII-B subunit in complement activation. Our investigations show no effect of FXIII-B subunit on the rate of complement activation. Therefore, in this chapter we conclude that at a physiological level, FXIII-B subunit plays no role in the complement system, although a vestigial function in altered pathological states might still exist.

J Thromb Thrombolysis (2019). <https://doi.org/10.1007/s11239-019-01841-w>



Article

Identification of Potential Novel Interacting Partners for Coagulation Factor XIII B (FXIII-B) Subunit, a Protein Associated with a Rare Bleeding Disorder

Sneha Singh ^{1,†}, Mohammad Suhail Akhter ^{1,2,†}, Johannes Dodt ³, Peter Volkers ³,
Andreas Reuter ³, Christoph Reinhart ⁴, Christoph Krettler ⁴, Johannes Oldenburg ¹ and
Arijit Biswas ^{1,*}

¹ Institute of Experimental Hematology and Transfusion Medicine, University Clinic Bonn, 53127 Bonn, Germany; Sneha.Gupta@ukbonn.de (S.S.); suhailaiims@gmail.com (M.S.A.); johannes.oldenburg@ukbonn.de (J.O.)

² College of Applied Medical Sciences, Jazan University, 82911 Jazan, Saudi Arabia

³ Paul-Ehrlich Institute, 63225 Langen, Germany; Johannes.Dodt@pei.de (J.D.); Peter.Volkers@pei.de (P.V.); Andreas.Reuter@pei.de (A.R.)

⁴ Department of Molecular Membrane Biology, Max-Planck Institute for Biophysics, Max-Von Laue Str 3, 60438 Frankfurt am Main, Germany; christoph.reinhart@biophys.mpg.de (C.R.); christoph.krettler@biophys.mpg.de (C.K.)

* Correspondence: arijit.biswas@ukb.uni-bonn.de; Tel.: +49-228-287-19428

† These authors contributed equally to the work.

Received: 10 May 2019; Accepted: 29 May 2019; Published: 31 May 2019



Abstract: Coagulation factor XIII (FXIII) is a plasma-circulating heterotetrameric pro-transglutaminase complex that is composed of two catalytic FXIII-A and two protective/regulatory FXIII-B subunits. FXIII acts by forming covalent cross-links within a preformed fibrin clots to prevent its premature fibrinolysis. The FXIII-A subunit is known to have pleiotropic roles outside coagulation, but the FXIII-B subunit is a relatively unexplored entity, both structurally as well as functionally. Its discovered roles so far are limited to that of the carrier/regulatory protein of its partner FXIII-A subunit. In the present study, we have explored the co-presence of protein excipients in commercial FXIII plasma concentrate FibrogamminP by combination of protein purification and mass spectrometry-based verification. Complement factor H was one of the co-excipients observed in this analysis. This was followed by performing pull down assays from plasma in order to detect the putative novel interacting partners for the FXIII-B subunit. Complement system proteins, like complement C3 and complement C1q, were amongst the proteins that were pulled down. The only protein that was observed in both experimental set ups was alpha-2-macroglobulin, which might therefore be a putative interacting partner of the FXIII/FXIII-B subunit. Future functional investigations will be needed to understand the physiological significance of this association.

Keywords: Factor XIII; FXIII deficiency; excipients; pleiotropy; mass spectrometry; complement system

1. Introduction

Coagulation Factor XIII (FXIII) is plasma-circulating pro-transglutaminase acting at the terminal phase of the coagulation pathway, which is responsible for cross-linking pre-formed fibrin polymers within it and to anti-fibrinolytic inhibitors to prevent its premature fibrinolysis. In plasma, it circulates as a zymogenic heterotetramer composed of dimeric subunits of catalytic FXIII-A and carrier/regulatory FXIII-B bound to each other non-covalently [1]. The inherited form of FXIII deficiency is a rare autosomal disorder with a prevalence of one in three million, with its clinical manifestations ranging

from mild to severe bleeding diathesis [2]. The FXIII deficient patients are presented with severe bleeding tendencies, such as intracranial bleeds, dysmenorrhea, and umbilical cord bleeding, etc. [2]. The catalytic component of FXIII-A₂B₂ complex, i.e., FXIII-A subunit, is a structurally and functionally well characterized protein [3,4]. The FXIII-B subunit, which is the regulatory/protective partner, in comparison is a relatively unexplored entity. Homology studies reveal that FXIII-B bears 10 sushi domains (or Complement Control Protein modules), although no biophysical structures for this subunit exist so far [5,6]. The possibility that it might have pleiotropic roles outside the coagulation pathway exists similar to its partner FXIII-A subunit, which is known to be involved in roles beyond coagulation, like inflammation, angiogenesis, and wound healing, since FXIII-B is present both in complexed (FXIII-A₂B₂) and free form [7]. However, only a select few studies on the FXIII-B subunit have investigated this possibility and have reported mostly negative results [8]. Patients that are severely deficient for FXIII often require a lifelong supplement of plasma derived FXIII concentrates as a majorly available treatment modality in cases of inherited FXIII deficiencies [9]. However, in the case of acquired FXIII deficiency, which may be a secondary effect of immune-mediated inhibition, or defective synthesis and/or consumption of either of FXIII subunits; the treatment involves antifibrinolytic administration, and/or inhibitor eradication, along with replacement therapy [10]. Hence, replenishing the FXIII deficient and/or defective plasma by active and functional FXIII is a leading treatment modality. The two major types of FXIII concentrates that are administered to the patients include virus inactivated fresh frozen plasma (FFP) derived from healthy donors; or the commercially available drug Cortifact (US)/FibrogamminP (Europe & Asia), marketed by CSL Behring [9,11]. These plasma concentrates are suitable for both FXIII-A and FXIII-B subunit deficient states. Recently, a recombinant form of FXIII (Tretten) expressed in yeast has also been commercialized by NovoNordisk and it is only being administered to patients with severe/mild FXIII-A deficiency [12]. The plasma concentrate FibrogamminP is a highly purified, pasteurized, plasma-derived concentrate that has been in use since 1993 and it contains the hetero-tetrameric complex that shows high transglutaminase activity [12]. The other main excipients that are currently indicated in the commercial product are human albumin, glucose, and sodium chloride. In the current study, we performed content characterization of plasma derived FibrogamminP, by gel filtration analyses. Amongst others, we detected complement factor H (CFH) as one of the major proteomic excipients within FibrogamminP. Owing to the structural and sequential complementarity of CFH and FXIII-B [8], we further evaluated whether this co-presence has any functional/physiological implications or not, which is verified by real-time FXIIIa generation assay [13]. However, CFH was not detected in the pull-down assays under the physiological conditions. Additionally, in vitro qualitative assessment of proteins interacting with FXIII-B subunit employing FXIII-B subunits interacting with FXIII-B monoclonal antibodies immobilized to resin, which aided the pull-down of interacting partners in a FXIII deficient background (FXIII-DP) was done. Two complement system proteins i.e., complement C3 and complements C1q were detected in the pull-down assays. When compared to all the detected proteins, only alpha-2-macroglobulin was a common denominator detected in the pull-down assay as well as an excipient in FibrogamminP, which indicates that it might be the true interacting partner of the FXIII/FXIII-B subunit.

2. Results

2.1. Content Characterization of Plasma FXIII Concentrate Reveals Co-Presence of Complement Factor H and Alpha-2-Macroglobulin Along with FXIII Complex

Size exclusion chromatography revealed that the crude fractions of FibrogamminP contain majorly coagulation FXIII-A₂B₂ (MW 320 kDa) (retention at 23.31 min), along with albumin (MW 66 kDa) (at 34.51 min), alpha-2-macroglobulin (MW 725 kDa) (at 19.47 min), and complement Factor H (MW 155 kDa) (at 29.33 min) eluted at different retention times (Figure 1, Figure 2 and Figure S1). The peak corresponding to the molecular weight of FXIII-A₂B₂ was collected and re-run to generate a single monodispersed homogenous peak. Upon analysis, this peak showed the co-presence of

complement Factor H and albumin, in addition to FXIII-A₂B₂ (Figure 1, Figure 2, Figures S1 and S3, and attached MS data files (peptide summary reports) in the Supplementary Information).

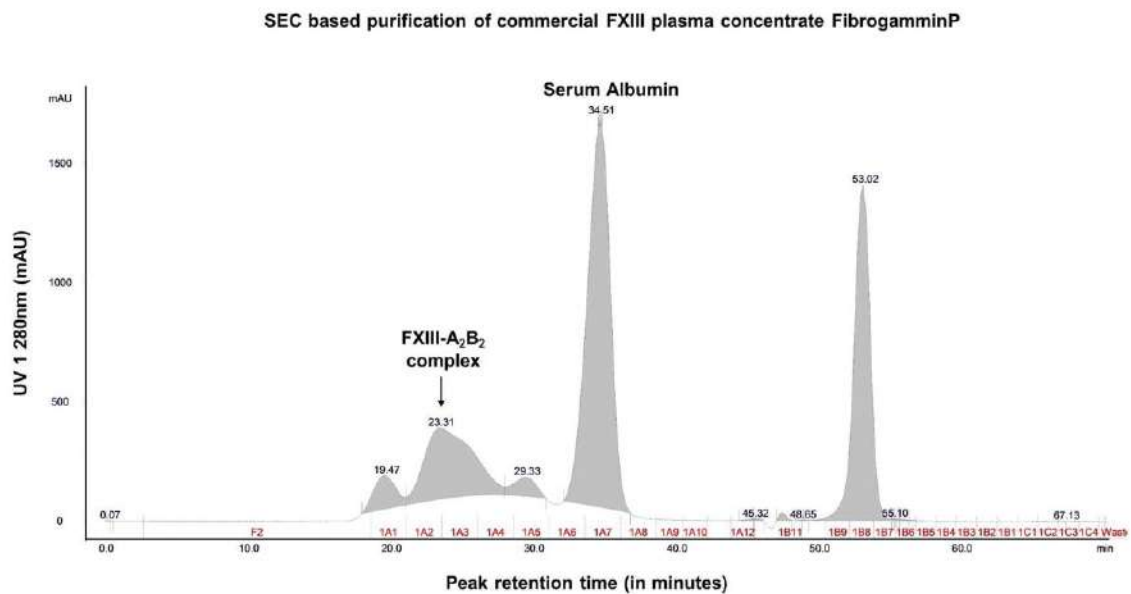


Figure 1. Content characterization of plasma FXIII concentrate (FibrogamminP) by size exclusion chromatography. This image represents the mass-based separation run for commercial plasma FXIII concentrate FibrogamminP on a ÄKTA explorer purifier system. The respective peaks on the chromatograph were detected by UV₂₈₀. The arrow indicates the main peak corresponding to the molecular weight of FXIII-A₂B₂ complex that was further characterized.

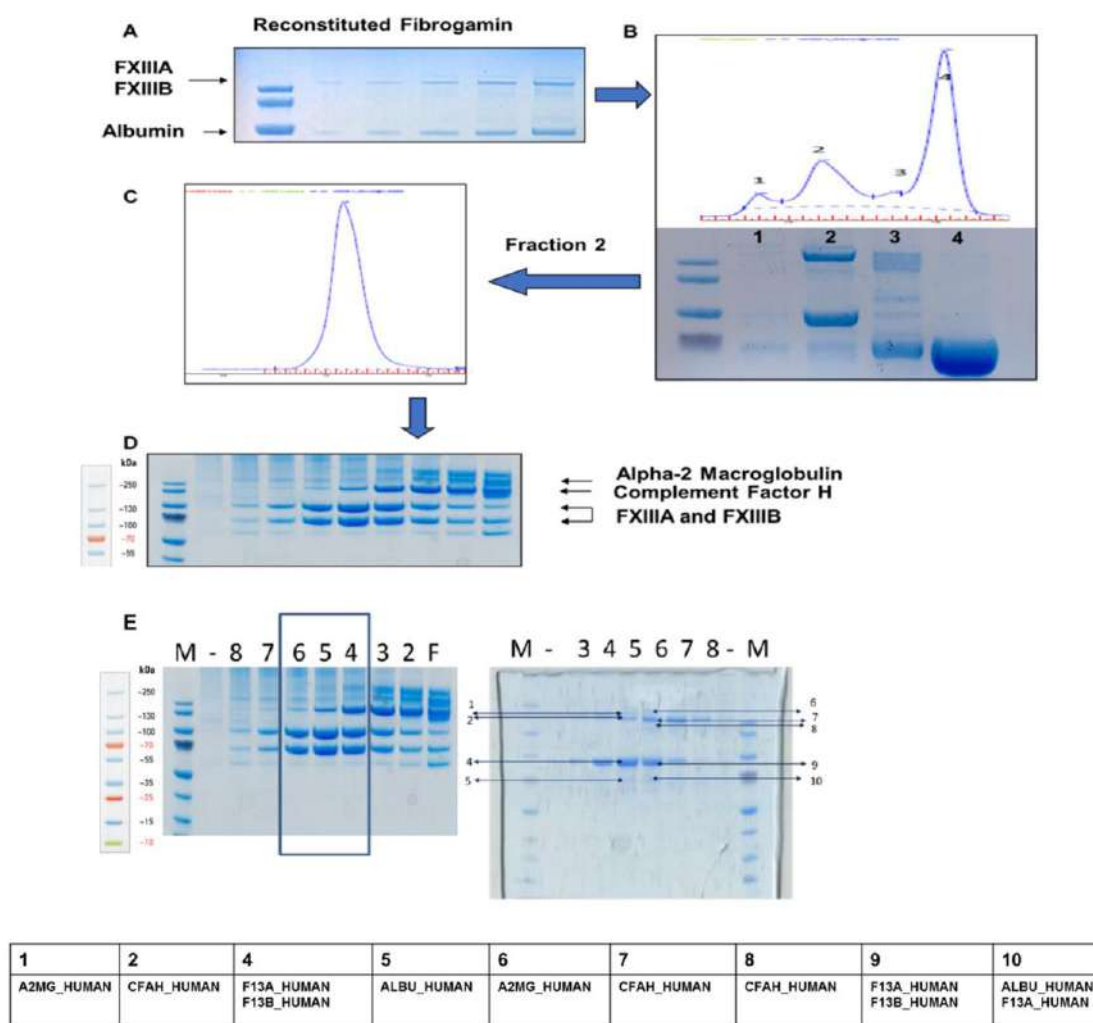


Figure 2. Plasma FXIII concentrate (FibrogamminP) analysis. (A) The preliminary SDS-PAGE gel run of the commercial FXIII plasma concentrate “FibrogamminP” reconstituted in water. The fastest running band corresponds to human serum albumin, which is a known constituent of FibrogamminP. (B) Mass based separation of reconstituted FibrogamminP run on a SEC column (Superdex 200 PC 3.2/30 column, running buffer: 20 mM Tris HCl, pH 7.4; 120 mM NaCl). The four main peaks of interests were collected separately. Peak 4 corresponds to albumin (size-wise). Peak 2 contained majority of FXIII-A₂B₂ heterotetramer complex. The sampled Peak 2 was separately run again, but it still resolved into one peak only shown in (C). This single, monodispersed peak was fractionated, sampled and run on an SDS-PAGE, fraction wise as collected from the SEC; which is shown in (D) The separated bands (see Figure S3) were excised and evaluated with Mass spectrometry. (E) This panel consists of two SDS-PAGE gels, the gel 1 is same as the one in (D) depicting fractions corresponding to FXIII complex (boxed lanes). These three fractions were re-pooled and ran on GFC, with fractions separated on gel 2. Marked bands were analysed by mass spectrometry. The labels at the top of both gels are numbered based on fraction ids from the gel filtration runs not to be confused with lane numbers. The “F” represents the crude fraction of FibrogamminP. Table at the bottom represents the major protein hits corresponding to each band (total nine). For detailed peptide summary report please refer Supplementary Materials (Figure S3).

2.2. No Significant Effect of CFH on FXIII-Aa Activation Observed in the FXIIIa Generation Assay

The FXIIIa generation assay reveals that the rate of activation of FXIII-A is accelerated in the presence of FXIII-B (K_a (FXIII-DP+ FXIII-A) is 0.12 sec^{-1} ; K_a (FXIII-DP+ FXIII-A+FXIII-B) is 0.54 sec^{-1}) (Figure 3 and Supplementary Table S1). However, the rate of depletion of activated species is reduced

in the presence of FXIII-B subunit and a similar effect is observed with CFH. The lag time, which represents thrombin accessibility to FXIII-A molecule, is also mildly influenced (but not significantly so) by both CFH and FXIII-B. However, most of the parameters that were analyzed for these set of experiments showed non-significant association (Figure 3; and Supplementary Table S1).

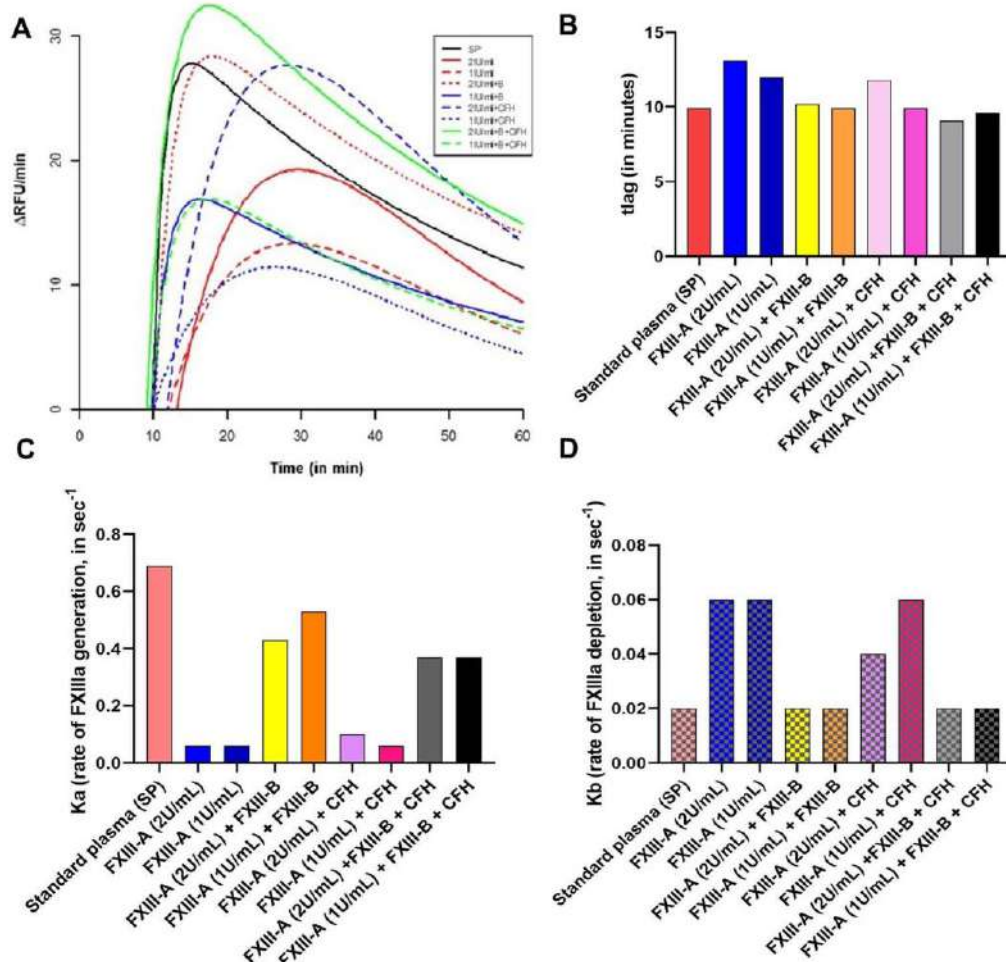


Figure 3. Effect of Complement Factor H (CFH) on FXIIIa generation. FXIIIa generation assay is a real-time, quantitative measurement of generation of active FXIIIa species, in a FXIII deficient background (deficient both for FXIII-A and FXIII-B subunits) [13]. The parameters tlag (time-delay in generation of first signal), Ka (constant of absorption that describes the rate of development of FXIIIa), and Kb (elimination constant) have been represented here. (A) Raw data obtained as growth curves representing the generation of active FXIIIa species. X-axis denotes time in minutes; Y-axis denotes the rate of generation of active FXIII-Aa (RFU/min). (B–D) are comparative bar graph representation of tlag, Ka and Kb observed with different spiking conditions. A tabular representation can be found in Supplementary Information.

2.3. In a FXIII Deficient Background, FXIII-B Pulls Down Fibrinogen, Few Complement Proteins, and Alpha-2-Macroglobulin

The pull down from rFXIII-B bound resin that had been exposed to FXIII-DP had alpha-2-macroglobulin, complement C3, complement C1q, and fibrinogen- α , - β , - γ chains (Figure 4C lists the most relevant proteins; for complete list see Figure S2) in its proteomic content. Resin bound rFXIII-B exposed to rFXIII-A and FXIII-DP also showed similar content in its pull down. No CFH or alpha-2-macroglobulin that was detected earlier in FibrogamminP was detected in any of these pull downs (Figure 4 and Figure S2).

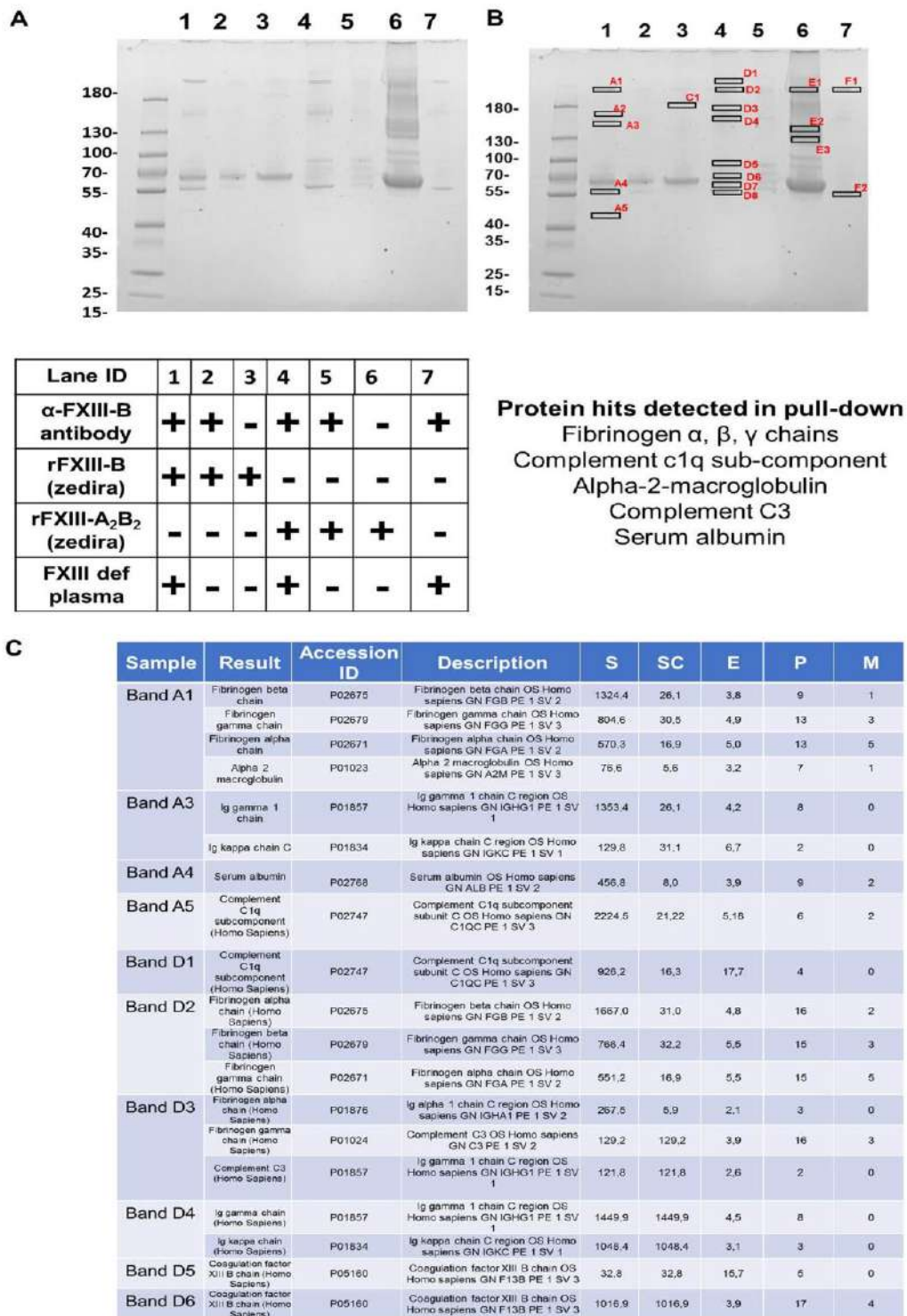


Figure 4. Interactome analysis of FXIII-B in FXIII-DP by Co-immunoprecipitation. (A) Coomassie stained SDS-PAGE gel for the proteins pulled down by resin immobilized FXIII-B (bound through amine-linked monoclonal antibody). Table below shows the experimental conditions. (B) Shows the same SDS-PAGE as in Panel A, but with those bands that were subsequently analysed for proteomic content by mass spectrometry individually marked (data in Supplementary Figure S2). The major hits are listed at the bottom of this panel, as well as in (C). (C) Table representing the majority of protein hits obtained by MS analyses of excised bands indicated in B. For a detailed protein-hit summary refer Supplementary Information. Abbrev: S: Protein Score; SC: Sequence coverage in %, E: Mean mass error in ppm; P: number of identified peptides; M; number of modified peptides interactome analyses.

3. Discussion

Amongst the two FXIII subunits, the FXIII-B₂ dimeric subunit has a unique filamentous structure, with each of its monomers consisting of 10 sushi domains (also known as complement control protein (CCP) modules) that are rich in cysteine bonds and bear specific structure with beta-sandwich arrangement [6,14–16]. Other than FXIII-B, a majority of proteins belonging to the complement pathway have such structural domains [17]. The structural arrangement of sushi domains in FXIII-B bear close resemblance to CFH, which might be the result of the co-evolution of complement and coagulation systems. Based on the sequence and structural homology, our group had earlier reported the homology models for the FXIII-B sushi domains [6,15]. In the current report, we find detectable levels of CFH in plasma-derived factor concentrate of FXIII. The peak corresponding to FXIII-A₂B₂ appears to be homogenous and monodispersed in gel filtration analyses (obtained after re-analyzing the peak corresponding to FXIII, there appears to be a non-stoichiometric association of proteins within this eluted peak, later detected by MS (Supplementary Information)). Such an association might also be suggestive of its association to albumin instead of the main active drug FXIII-A₂B₂. The separated bands of individual fraction, detected by coomassie staining, when evaluated by MS were determined to be FXIII-A₂ and FXIII-B₂ subunits, CFH, and alpha-2-macroglobulin in the order, as indicated in Figure 2D. However, the functional analysis reveals that the presence of CFH does not alter FXIII activity, as observed from the FXIIIa generation assay in which no significant change in variables was observed when CFH was added along with FXIII (Figure 3). Their co-presence in FibrogamminP may be attributed to the very nature of sushi domains and/or the similar size of FXIII heterotetramer (320 kDa) and dimeric CFH (155 kDa monomer), as well as a possible association with albumin. Since only 4–15% of total CFH tends to self-assemble in plasma, forming CFH dimers of ~320 kDa, this may explain the reduced amount of CFH detected in FXIII concentrate. Along with CFH, traces of alpha-2-macroglobulin (homo-tetrameric acute phase protein, MW 163 kDa) were also detected by size-exclusion chromatography, followed by mass spectrometry in FibrogamminP. Since dimeric forms of alpha-2-macroglobulin have also been recently described and these would have a molecular weight that is close to the FXIII heterotetramer, which might also explain their co-presence with FXIII [18,19]. The fact that CFH is merely co-present with FXIII is substantiated by interactome-analysis of FXIII in FXIII-DP (Figure 4). While we found that fibrinogen- α , - β , - γ chains, complement C1q, and complement C3 in the pull downs for both FXIII-B, as well as FXIII-B exposed to FXIII-A, none of the pull downs detected CFH. However, alpha-2-macroglobulin was one protein that was detected in FibrogamminP as well as in the pull-down assays. This suggests that it could be one of the novel proteins interacting with FXIII-B subunit. It is already known that alpha-2-macroglobulin is a substrate for the FXIII-A subunit (although no clear functional role has been discovered in this context), but there are no reports of its direct interaction with the FXIII-B subunit [20]. Alpha-2-macroglobulin is an inhibitor that can inhibit coagulation as well as fibrinolysis by acting on thrombin and plasmin, respectively [18,19]. Interaction with FXIII or FXIII-A/FXIII-B subunit might fine tune its inhibitory roles towards the two different processes. Further functional analysis will be needed to substantiate this idea. The presence of fibrinogen chains (from deficient plasma) in the pull downs of resin bound FXIII-B supports earlier reports that showed that the FXIII-B subunit could be mediating the interaction between FXIII and fibrinogen [21,22]. The presence of complement C1q and complement C3 in the pull-down assays came as a surprise. There has been no report of FXIII or the FXIII-B subunit interacting with complement C1q so far. The complement C3 protein, on the other hand, has been shown to be a substrate for FXIII-A subunit, but again, no interaction with FXIII-B subunit has been reported so far [18]. The interaction possibility of alpha-2-macroglobulin complement C1q and complement C3 with FXIII/FXIII-B subunit, as shown from our study, presents the opportunity to discover newer roles for FXIII/FXIII-B subunit in coagulation, as well as outside the coagulation pathway. These proteins (i.e., alpha-2-macroglobulin, complement C1q and CFH) are related to known physiological and diseased states. Complement C1q deficiency has been known to cause recurrent skin lesions, chronic infections, systemic lupus erythematosus (SLE), and has also been associated with a kidney disease,

known as mesangial proliferative glomerulonephritis [23,24]. Complement C3 deficiency manifests itself into recurrent bacterial infections [25]. Elevated plasma levels of alpha-2-macroglobulin, along with Fibrinogen and albumin levels, is commonly seen in nephrotic syndrome [26–28]. Therefore, FXIII could play an important role in all these aspects by interacting with these proteins. A significant association of FXIII with a complement system had been discussed by Schroeder et al.; describing FXIII mediated covalent cross-linking of fibrin to complement C3 that could have inflammatory roles in pro-thrombotic states [7,29]. Our study demonstrates that there are a number of proteins, some of which are part of the complement system (like complement C3 and complement C1q), and some of which belong to the coagulation pathway itself (alpha-2-macroglobulin) that might interact with the FXIII/FXIII-B subunits. More work will be needed to further investigate whether these interactions have physiological or pathological implications. The complement factor H protein that shares homology with FXIII-B subunit, on the other hand, is merely co-present with FXIII in FibrogamminP and it appears to have no functional interaction with FXIII/FXIII-B subunit.

4. Materials and Methods

4.1. Coagulation Factor XIII Complex and FXIII Subunits

Three separate lots of FibrogamminP (CSL Behring; Marburg, Germany) were used as source, to purify FXIII-A₂B₂ complex. Recombinant FXIII-A and recombinant FXIII-B were purchased from Zedira GmbH (Darmstadt, Germany). Additionally, the FXIII-B subunit was also expressed and purified in house, as per previously reported protocol [30]. Briefly, the human *HEK293t* cell line purchased from DMSZ (German Collection of Microorganisms and Cell Cultures, Braunschweig, Germany) were cultured in high glucose DMEM, supplemented with 10% *v/v* FBS, 1% *v/v* Penicillin-Streptomycin antibiotics and 0.1% *v/v* Fungisone (all cell culture products bought from Invitrogen, Bleiswijk, Netherlands), at 37 °C at 5% CO₂. All of the experiments were done on sub-cultured cells in logarithmic phase (below passage 20). Human FXIII-B cDNA, inserted into the cloning site of pReciever-M01 mammalian expression vector was transfected into *HEK293t* cells, as per previously reported protocol [15]. Briefly, 2.7×10^5 cells were transfected with 3 µg of plasmid DNA along with 6 µl of transfection reagent Lipofectamine 2000 (Invitrogen, Bleiswijk, Netherlands). The cultures were harvested 48 h post-transfection, by collecting extracellular fractions containing the secreted rFXIII-B. The extracellular fraction was centrifuged for five minutes, at 14,000 rpm at 4 °C. A negative control of non-transfected cells was used, whereas a plasmid construct with eGFP cloned in pcDNA mammalian expression vector was the positive control for transfection. Secreted protein harvested post transfection of *HEK293t* cells was concentrated and subjected to immuno-affinity-based purification while using the Thermo Scientific Pierce Co-IP kit (Pierce Biotechnology, Rockford, IL, USA), following the manufacturer's protocol. Briefly, monoclonal antibodies against FXIII-B, raised in mice were immobilized to Amino Link plus coupling resin (Pierce Biotechnology, Rockford, IL, USA) for two hours. The resin was then washed with PBS and incubated with extracellular concentrate overnight in cold-room. The next day, the resin was again washed with PBS and protein bound to anti-FXIII-B antibodies was eluted with acidic elution buffer provided with the kit. The eluted protein was verified on coomassie stained gel. Eluted protein was further subjected to gel filtration chromatography, to ensure the purity and dimeric state of the recombinant protein.

4.2. Separation of the FXIII Plasma Concentrate, FibrogamminP into its Constituents

One vial (from three different lots) of FibrogamminP (CSL Behring; Marburg, Germany) i.e., 250 U, was reconstituted with water, as per the manufacturer's guidelines. The sample was purified in ÄKTA explorer purifier systems (GE Healthcare, Uppsala, Sweden) (all the chromatography experiments were performed in cold-room at 4 °C). Briefly, crude sample was slowly injected (400 µl/min) onto pre-equilibrated column Superdex200 10/300 GL (GE healthcare) (Buffer: 20 mM Tris, 120 mM NaCl, 1 mM EDTA. pH 7.4), and the eluate was collected in 500 µl fractions. SDS-PAGE analyzed the resultant

fractions confirm the success of purification. All the fractions were separately pooled (peak-wise), concentrated, and stored.

4.3. Mass Spectrometric Analysis

Eluates were first analyzed on pre-cast SDS-PAGE gels (Bio-Rad laboratories, Hercules, CA, USA). The protein bands were analyzed by Coomassie staining (Bio-Rad laboratories, USA). Coomassie-stained protein bands were excised and their identity was confirmed while using mass spectrometric analysis, as reported previously [21]. Briefly, peptides were eluted with 25 mM NH_4HCO_3 ; 10% acetonitrile (ACN) and digestion stopped by adding 5% formic acid. The peptides were resolved on a nano-ultra performance LC system coupled to a nano-ESI-MS (nano Acquity UPLC nanoESI Synapt-MS, Waters, Milford, MA, USA) with a 5 μm symmetry 180 μm \times 20 mm C18 pre-column and a 1.7 μm BEH 130 100 μm \times 100 mm C18 separation column. A 30-min gradient (3% ACN to 40% CAN at 500 nL/min) after three minutes of trapping (99% water at 5 $\mu\text{L}/\text{min}$) was applied to separate peptides. The MS was operated in V mode, acquiring MSE data and applying standard parameters. Data analysis was performed using ProteinLynx Global Server version 2.4 (Waters corporation, Milford, MA, US), searching an in-house database consisting of the Uniprot database (September 2016 version, restricted to reviewed entries of *Homo sapiens*; taxon identifier 9606. Proteins hits were accepted at a false positive rate of less than 4%, as reported previously. For analyses of peaks retained from size exclusion chromatography of FibrogamminP (Figure 2C), Mascot search engine was utilized, which is based on the probabilistic scoring algorithm for protein identification (a detailed report can be found in the Supplementary Information section).

4.4. FXIIIa Generation Assay

The rate of activated FXIII (FXIIIa) generation was monitored by FXIIIa Generation Assay [13,21]. Briefly, the generation of active FXIIIa species was monitored in the background of different plasmatic condition. Compared to standard plasma (SP) (ISTH: SCSP FXIII activity 0.76 U/vial; FXIII antigen A_2B_2 0.74 IU/vial), FXIIIa generation was monitored with FXIII-DP (deficient for both FXIII-A and FXIII-B subunits; Haemochrom Diagnostica GmbH, Essen, Germany). Coagulation was triggered by adding tissue factor/phospholipids TF/PI, and FXIII-A (2 IU/mL of plasma) to 25 μl plasma in order to generate active FXIIIa (subsequently detected by FXIII isopeptidase activity on a chromogenic substrate A101 (Zedira GmbH, Darmstadt, Germany)). The reactions spiked with rFXIII-B (20 $\mu\text{g}/\text{mL}$) (Zedira GmbH, Germany), CFH (20 $\mu\text{g}/\text{mL}$), and both rFXIII-B and CFH with respective controls of standard plasma (SP) were incubated with 35 μL reagent solution (5 μL 100 mM glycine methyl ester, 5 μL 2 mM fluorogenic FXIII-A substrate, 10 μL Innovin (recombinant TF; Dade Behring, Liederbach, Germany) diluted 1:2800 in phospholipids (PTT reagent kit, Roche, Mannheim, Germany) and 15 μL HBS (20 mM HEPES, 150 mM NaCl)/0.1% serum albumin pH 7.5. After pre-incubation of the mixture for five minutes, the reaction was started with 40 μL 25 mM CaCl_2 pH 7.5. Fluorescence was measured over 1 h at $\lambda_{\text{ex}} = 330 \text{ nm}$ and $\lambda_{\text{em}} = 430 \text{ nm}$ in kinetic mode two times per minute. The curve data was evaluated according to a bi-exponential model with first order absorption and elimination. The data were fitted to the equation:

$$C(t) = \frac{c_{ka}}{(ka - kb)} (\exp(-kb(t - tlag)) - \exp(-ka(t - tlag))) \quad (1)$$

where k_a : constant of absorption, which describes the development of active FXIIIa and k_b – elimination constant. The parameters area under the curve (AUC), peak FXIII-A concentration (CP), and time to peak (TTP) were also evaluated [13].

4.5. Isolation and Verification of Plasma Sub-Proteome Interacting with FXIII-B by Immunoaffinity Based Pull-Down Assays

The Pierce co-immunoprecipitation kit (ThermoFischer Scientific, Rockford, IL, USA) was used to bind the commercial recombinant FXIII-B (Zedira, Germany) to immobilized anti(α)-FXIII-B monoclonal antibodies (in-house) (similar experiments were also performed with rFXIII-B expressed/purified from HEK293t mammalian cell lines in-house). Briefly, 75 μ l of mouse- α -human-FXIII-B monoclonal antibody (1 mg/mL) (produced in-house) was coupled to amino-link plus coupling resin, according to the manufacturer's protocol. Firstly, 100 μ l of 1mg/mL rFXIII-B (Zedira, Darmstadt, Germany) (or rFXIII-B in-house) was bound to the immobilized antibodies. The following set of experiments followed: (1) the resin bound rFXIII-B was exposed to FXIII-DP; (2) the immobilized α -FXIII-B antibody exposed to FXIII-DP. Additionally, a resin was prepared with α -FXIII-B antibody that was bound to FXIII-A₂B₂ complex purified from FibrogamminP and exposed to FXIII-DP (with a negative control that included a resin support with immobilized-monoclonal FXIII-B antibodies, but with no exposure to either recombinant FXIII-B or FXIII concentrate; to rule out the cross-reactivity of this antibody). The bound complexes were eluted with elution buffer (Primary amine pH 2.8; Pierce, Rockford, IL, USA) and SDS-PAGE analyzed the eluates. The bands observed were characterized by peptide mass fingerprinting, followed by mass spectrometry (Supplementary Materials).

Supplementary Materials: Supplementary materials can be found at <http://www.mdpi.com/1422-0067/20/11/2682/s1>.

Author Contributions: Conceptualization, A.B.; methodology, A.B., S.S., M.S.A. and J.D.; software, A.B.; validation, A.B., S.S., P.V. formal analysis, S.S., M.S.A., C.K., C.R., J.D., P.V. and A.R.; investigation, A.B., S.S. and M.S.A.; resources, A.B. and J.O.; data curation, A.B. and S.S.; writing – original draft preparation, A.B. and S.S.; writing – review and editing, A.B., S.S., M.S.A., J.D. and J.O.; visualization, A.B.; supervision, A.B. and J.O.; project administration, A.B. and J.O.; funding acquisition, A.B. and J.O.

Funding: This research received no external funding.

Conflicts of Interest: The authors declare no conflict of interest.

Abbreviations

| | |
|----------|------------------------------|
| FXIII-DP | Factor XIII deficient plasma |
| CFH | Complement Factor H |
| FXIIIa | Activated FXIII-A |
| SP | Standard Plasma |
| MS | Mass spectrometry |

References

1. Biswas, A.; Ivaskevicius, V.; Thomas, A.; Oldenburg, J. Coagulation factor XIII deficiency. Diagnosis, prevalence and management of inherited and acquired forms. *Hamostaseologie* **2014**, *34*, 160–166. [PubMed]
2. Muszbek, L.; Katona, É. Diagnosis and Management of Congenital and Acquired FXIII Deficiencies. *Semin. Thromb. Hemostasis* **2016**, *42*, 429–439.
3. Fox, B.A.; Yee, V.C.; Pedersen, L.C.; Le Trong, I.; Bishop, P.D.; Stenkamp, R.E.; Teller, D.C. Identification of the calcium binding site and a novel yttrium site in blood coagulation factor XIII by x-ray crystallography. *J. Biol. Chem.* **1999**, *274*, 4917–4923. [CrossRef] [PubMed]
4. Stieler, M.; Weber, J.; Hils, M.; Kolb, P.; Heine, A.; Buchold, C.; Pasternack, R.; Klebe, G. Structure of active coagulation factor XIII triggered by calcium binding: basis for the design of next-generation anticoagulants. *Angew. Chem. Int. Ed. Engl.* **2013**, *52*, 11930–11934. [CrossRef]
5. Souri, M.; Kaetsu, H.; Ichinose, A. Sushi domains in the B subunit of factor XIII responsible for oligomer assembly. *Biochemistry* **2008**, *47*, 8656–8664. [CrossRef] [PubMed]
6. Thomas, A.; Biswas, A.; Ivaskevicius, V.; Oldenburg, J. Structural and functional influences of coagulation factor XIII subunit B heterozygous missense mutants. *Mol. Genet. Genomic Med.* **2015**, *3*, 258–271. [CrossRef]
7. Schroeder, V.; Kohler, H.P. Factor XIII: Structure and Function. *Semin. Thromb. Hemostasis* **2016**, *42*, 422–428.

8. Akhter, M.S.; Singh, S.; Yadegari, H.; Ivaskevicius, V.; Oldenburg, J.; Biswas, A. Exploring the structural similarity yet functional distinction between coagulation factor XIII-B and complement factor H sushi domains. *J. Thromb. Thrombolysis* **2019**. [[CrossRef](#)]
9. Lassila, R. Clinical Use of Factor XIII Concentrates. *Semin. Thromb. Hemostasis* **2016**, *42*, 440–444. [[CrossRef](#)]
10. Yan, M.T.S.; Rydz, N.; Goodyear, D.; Sholzberg, M. Acquired factor XIII deficiency: A review. *Trans. Apheresis Sci.* **2018**, *57*, 724–730. [[CrossRef](#)]
11. Nugent, D. Corifact™/Fibrogammin® P in the prophylactic treatment of hereditary factor XIII deficiency: results of a prospective, multicenter, open-label study. *Thromb. Res.* **2012**, *130*, S12–S14. [[CrossRef](#)]
12. Dreyfus, M.; Barrois, D.; Borg, J.-Y.; Claeysens, S.; Torchet, M.-F.; Arnuti, B.; Pautard, B. Successful long-term replacement therapy with FXIII concentrate (Fibrogammin® P) for severe congenital factor XIII deficiency: a prospective multicentre study. *J. Thromb. Haemostasis* **2011**, *9*, 1264–1266. [[CrossRef](#)]
13. Dodt, J.; Volkers, P.; Seitz, R. Factor XIIIa generation assay: a tool for studying factor XIII function in plasma. *Anal. Biochem.* **2013**, *439*, 145–151. [[CrossRef](#)]
14. Norman, D.G.; Barlow, P.N.; Baron, M.; Day, A.J.; Sim, R.B.; Campbell, I.D. Three-dimensional structure of a complement control protein module in solution. *J. Mol. Biol.* **1991**, *219*, 717–725. [[CrossRef](#)]
15. Biswas, A.; Thomas, A.; Bevans, C.G.; Ivaskevicius, V.; Oldenburg, J. In vitro secretion deficits are common among human coagulation factor XIII subunit B missense mutants: correlations with patient phenotypes and molecular models. *Hum. Mutat.* **2013**, *34*, 1490–1500. [[CrossRef](#)]
16. Perkins, S.J.; Nan, R.; Li, K.; Khan, S.; Miller, A. Complement factor H-ligand interactions: self-association, multivalency and dissociation constants. *Immunobiology* **2012**, *217*, 281–297. [[CrossRef](#)] [[PubMed](#)]
17. Krushkal, J.; Bat, O.; Gigli, I. Evolutionary relationships among proteins encoded by the regulator of complement activation gene cluster. *Mol. Biol. Evol.* **2000**, *17*, 1718–1730. [[CrossRef](#)] [[PubMed](#)]
18. Dodds, A.W.; Law, S.K. The phylogeny and evolution of the thioester bond-containing proteins C3, C4 and alpha 2-macroglobulin. *Immunol. Rev.* **1998**, *166*, 15–26. [[CrossRef](#)] [[PubMed](#)]
19. Armstrong, P.B.; Quigley, J.P. Alpha2-macroglobulin: an evolutionarily conserved arm of the innate immune system. *Dev. Comp. Immunol.* **1999**, *23*, 375–390. [[CrossRef](#)]
20. Nikolajsen, C.L.; Dyrland, T.F.; Poulsen, E.T.; Enghild, J.J.; Scavenius, C. Coagulation factor XIIIa substrates in human plasma: identification and incorporation into the clot. *J. Biol. Chem.* **2014**, *289*, 6526–6534. [[CrossRef](#)]
21. Gupta, S.; Biswas, A.; Akhter, M.S.; Krettler, C.; Reinhart, C.; Dodt, J.; Reuter, A.; Philippou, H.; Ivaskevicius, V.; Oldenburg, J. Revisiting the mechanism of coagulation factor XIII activation and regulation from a structure/functional perspective. *Sci. Rep.* **2016**, *6*, 30105. [[CrossRef](#)] [[PubMed](#)]
22. Souri, M.; Osaki, T.; Ichinose, A. The Non-catalytic B Subunit of Coagulation Factor XIII Accelerates Fibrin Cross-linking. *J. Biol. Chem.* **2015**, *290*, 12027–12039. [[CrossRef](#)] [[PubMed](#)]
23. Liu, G.; Pang, Y.; Liu, X.; Li, Q.-W. Structure, distribution, classification, and function of C1q protein family: a review. *Yi Chuan = Hereditas* **2013**, *35*, 1072–1080. [[CrossRef](#)]
24. Devasahayam, J.; Erode-Singaravelu, G.; Bhat, Z.; Oliver, T.; Chandran, A.; Zeng, X.; Dakshinesh, P.; Pillai, U. C1q Nephropathy: The Unique Underrecognized Pathological Entity. *Anal. Cell. Pathol.* **2015**, *2015*, 490413. [[CrossRef](#)]
25. Rossi, O.; Coward, C.; Goh, Y.S.; Claassens, J.W.C.; MacLennan, C.A.; Verbeek, S.J.; Mastroeni, P. The essential role of complement in antibody-mediated resistance to Salmonella. *Immunology* **2019**, *1*, 69–73. [[CrossRef](#)]
26. De Sain-van der Velden, M.G.; Kaysen, G.A.; de Meer, K.; Stellaard, F.; Voorbij, H.A.; Reijngoud, D.J.; Rabelink, T.J.; Koomans, H.A. Proportionate increase of fibrinogen and albumin synthesis in nephrotic patients: measurements with stable isotopes. *Kidney Int.* **1998**, *53*, 181–188. [[CrossRef](#)] [[PubMed](#)]
27. De Sain-van der Velden, M.G.; Rabelink, T.J.; Reijngoud, D.J.; Gadellaa, M.M.; Voorbij, H.A.; Stellaard, F.; Kaysen, G.A. Plasma alpha 2 macroglobulin is increased in nephrotic patients as a result of increased synthesis alone. *Kidney Int.* **1998**, *54*, 530–535. [[CrossRef](#)]
28. Ritchie, R.F.; Palomaki, G.E.; Neveux, L.M.; Navolotskaia, O.; Ledue, T.B.; Craig, W.Y. Reference distributions for alpha2-macroglobulin: a practical, simple and clinically relevant approach in a large cohort. *J. Clin. Lab. Anal.* **2004**, *18*, 139–147. [[CrossRef](#)] [[PubMed](#)]

29. Richardson, V.R.; Schroeder, V.; Grant, P.J.; Standeven, K.F.; Carter, A.M. Complement C3 is a substrate for activated factor XIII that is cross-linked to fibrin during clot formation. *Br. J. Haematol.* **2013**, *160*, 116–119. [[CrossRef](#)] [[PubMed](#)]
30. Singh, S.; Akhter, M.S.; Dodt, J.; Sharma, A.; Kaniyappan, S.; Yadegari, H.; Ivaskevicius, V.; Oldenburg, J.; Biswas, A. Disruption of Structural Disulfides of Coagulation FXIII-B Subunit; Functional Implications for a Rare Bleeding Disorder. *Int. J. Mol. Sci.* **2019**, *20*, 1956. [[CrossRef](#)]



© 2019 by the authors. Licensee MDPI, Basel, Switzerland. This article is an open access article distributed under the terms and conditions of the Creative Commons Attribution (CC BY) license (<http://creativecommons.org/licenses/by/4.0/>).

Exploring the structural similarity yet functional distinction between coagulation factor XIII-B and complement factor H sushi domains

Mohammad Suhail Akhter^{1,2} · Sneha Singh¹ · Hamideh Yadegari¹ · Vytautas Ivaskevicius¹ · Johannes Oldenburg¹ · Arijit Biswas¹

Abstract

Coagulation factor XIII (FXIII) covalently crosslinks pre-formed fibrin clots preventing their premature fibrinolysis. In plasma, FXIII circulates as a zymogenic heterotetramer composed of catalytic FXIII-A subunits, and carrier/regulatory FXIII-B subunits. FXIII-A is a well characterized component of this complex, and has been associated with several pleiotropic roles outside coagulation as well. In comparison only protective/regulatory roles towards the FXIII-A subunit have been identified for FXIII-B. Strong homology between FXIII-B and complement regulator Complement factor H suggests a putative role of FXIII-B in complement activation. In the current study we have analyzed the similarities and yet functional divergence of these two proteins using in silico sequence alignment and structural analysis. We have evaluated complement activation post reconstitution of FXIII components into FXIII deficient and CFH deficient plasma. We have also transiently expressed FXIII-B in *SH-SY5Y* cell lines and evaluated its effect on the endogenous complement activation. Our investigations show no effect of FXIII-B subunit on the rate of complement activation. Therefore we conclude that at a physiological level, FXIII-B subunit plays no role in the complement system, although a vestigial function in altered pathological states might still exist.

Keywords Factor XIII · Factor XIIIb · Complement system proteins · Complement factor h

Highlights

- The carrier/regulatory coagulation FXIII-B protein has sequence homology with and shares structural similarities with complement factor H.
- Reconstitution assays reveal no significant role for FXIII-B in physiological complement activation.
- In spite of homologous and structural similarity with CFH, FXIII-B does not mimic its functional role in the alternative pathway.
- Although no evidence of involvement of FXIII-B in physiological complement activation was detected in our study the same cannot be said of complement system related pathological states and therefore need further investigation

Mohammad Suhail Akhter and Sneha Singh have contributed equally.

* Arijit Biswas
arijit.biswas@ukb.uni-bonn.de

¹ Institute of Experimental Haematology and Transfusion Medicine, University Clinic Bonn, Sigmund Freud Str. 25, 53127 Bonn, Germany

² College of Applied Medical Sciences, Jazan University, Jazan, Saudi Arabia

Introduction

The complement and coagulation pathways, are proteolytic cascades that act as body defense mechanisms aiding detection, capture, elimination of pathogens, and responsible for conversion of insoluble fibrin to strong fibrin clot disabling blood loss as a consequence of injury, respectively [1–3]. In many pathological scenarios like sepsis, coagulation pathway proteases have been implicated in the activation of

complement system [4, 5]. On the other hand, strong effects of complement components like mannose-associated serine protease 1 (MASP-1), have been reported towards clot formation [6, 7]. In this study we attempt to delineate the interconnections between coagulation factor XIII-B (FXIII-B) (non-catalytic subunit of coagulation FXIII-A₂B₂ complex in plasma), and central complement regulator factor H (CFH), that show significant homology and structural similarity [8–10]. The catalytic component of FXIII-A₂B₂ complex, i.e. FXIII-A, is well characterized with several crystal structures reported for both active/zymogenic states [11]. The FXIII-B subunit, which is the regulatory/protective partner, is not as well characterized. Homology studies reveal that FXIII-B bears 10 sushi domains (or Complement Control Protein modules) [12]. Since FXIII-B is present both in complexed (FXIII-A₂B₂) and free form, it raises the question if it has pleiotropic roles, outside the coagulation pathway similar to its partner FXIII-A subunit [13–17]. CFH is a major player in the alternative complement pathway (AP) at the level of the central C3b component, blocking undue activation of the complement [18]. Homology/threading-based models of FXIII-B subunit sushi domains indicate similarity to CFH in structure/surface electrostatics [9, 10]. Both proteins are coded by genes in the RCA gene cluster (chromosome 1), with liver being the major site of expression [19, 20]. Similarities between FXIII-B and CFH hint towards a putative role for FXIII-B in complement activation. In our current study we explore this possibility by first comparing and contrasting its structural and functional properties CFH. Since the primary mode of action for all sushi domains is to bind and modulate the function of other proteins, we speculated that the sushi domains of FXIII-B might be able to mimic the functional properties of the sushi domain bearing complement proteins, especially in their absence thereby influencing the complement system. Here we investigate this possibility by introducing the FXIII-B subunit in an in vitro condition in which a fully functional complement system is present i.e. *SH-SY5Y* cell lines [21, 22]. Simultaneously we evaluated the status of complement system in plasma that is lacking Factor XIII. We further specifically look into the possibility of the FXIII-B subunit mimicking CFH in plasma deficient in CFH.

Methods

Structural comparison of FXIII-B subunit and CFH

A comparative evaluation of the full length structures of FXIII-B subunit and CFH was done in silico. A number of biophysical structures corresponding to the full length CFH protein deposited in the protein structure database were downloaded i.e. PDB IDs: 1haq, 3gav, 3gaw and

3gau [23, 24]. All four of these structures were characterized using solution-based scattering data and therefore the PDB coordinates were comprised of mostly the C- α backbone. The side chains of these four PDB files were modeled using the PD2 ca2main server (http://www.sbg.bio.ic.ac.uk/~phyre2/PD2_ca2main) to generate the corresponding full atom models [25]. We used high quality models of the ten sushi domains of FXIII-B we had earlier generated and reported to assemble into a full length FXIII-B monomer model [9]. The full length model was assembled and energy minimized from the individual sushi domains on the AIDA domain joining server (<http://aida.godziklab.org/>) using the default server conditions [26]. The FXIII-B model was structurally aligned with the four all-atom structures of CFH using the MUSTANG function embedded in YASARA. Electrostatic surface potential of the structures was calculated and graphically depicted using the Particle Mesh Ewald method integrated within YASARA (force field applied: AMBER03; periodic boundary conditions) [27, 28].

Rate of complement system activation

A semi-quantitative estimation of the rate of complement activation in all subsequent experiments has been done with a commercially available kit (Complement System Screen, Euro Diagnostica, Sweden) which uses a set of activators and inhibitors of complement activation pathways i.e. all pathways separately. The wells of the microtiter strips are coated with specific activators of all the three pathways separately (More details in supplementary methods).

Reconstitution experiments with factor XIII deficient plasma

Reconstitution experiments with FXIII deficient plasma (FXIII-DP) (Affinity Biology, Canada) were performed in five set ups: pooled plasma (PP), only FXIII deficient plasma (FXIII-DP), FXIII-DP reconstituted with recombinant FXIII-A₂ (rFXIII-A₂, 12 μ g/ml), FXIII-DP reconstituted with recombinant FXIII-B₂ (rFXIII-B₂, 12 μ g/ml) and FXIII-DP reconstituted with Factor XIII heterotetramer (FXIII-A₂B₂ 28 μ g/ml) [29, 30]. (rFXIII A₂, rFXIII B₂ and FXIII A₂B₂ purchased from Zedira GmbH, Germany). All these set ups were incubated post reconstitution for a time period of 30 min at 4 °C before evaluating their rate of complement activation using kits as described above. Equal final volumes of all five set ups were evaluated. In another experimental set up we followed the rate of complement activation when increasingly different concentrations of rFXIII-B₂ (5, 10, 20 μ g/ml tested) were spiked into FXIII-DP.

Evaluation of complement activation upon transient expression of FXIII-B subunit in *SH-SY5Y* cell lines

Mammalian expression vector pEZ-MO1 (Genecopia, Rockville, USA) carrying the *F13B* subunit cDNA were transfected into *SH-SY5Y* cell lines (DSMZ German Collection of Microorganisms and Cell Cultures, Braunschweig) [21, 22]. The cells were cultured in with Dulbecco modified Eagles medium (DMEM, Invitrogen, Darmstadt, Germany) supplemented with 10% fetal bovine serum (Invitrogen), 1% penicillin- streptomycin (Invitrogen) and 0.1% Fungizone (Invitrogen) in 5% CO₂. The harvested culture supernatants were tested for FXIII-B secretion 36 h post transfection by western-blotting (supplementary methods), and the rate of complement activation upon transfection using the activation kits as described above. Supernatants from non-transfected cells served as a control for this experiment.

Reconstitution experiment on CFH deficient plasma (CFH-DP)

Reconstitution experiments on CFH deficient plasma (CFH-DP) were performed on the following four set ups: only CFH-DP (Assaypro, Missouri, USA), CFH-DP reconstituted with rFXIII-A₂ (12 µg/ml), CFH-DP reconstituted with rFXIII-B₂ (12 µg/ml), CFH-DP reconstituted with rFXIII-A₂B₂ (28 µg/ml) [29, 30]. All these set ups were incubated post reconstitution for a time period of 30 min at 4 °C before evaluating their rate of AP activation using kits as described above. The endogenous FXIII activity of the commercial CFH-DP was evaluated using a photometric assay [31].

Statistical analyses

Statistical analysis was performed on an R platform. Comparisons of means were performed using a non-parametric Mann–Whitney’s t test. All experiments were performed in duplicates and repeated at least thrice (n = 6).

Results

Structural comparisons between FXIII-B and CFH

A structural alignment of the FXIII-B full length all-atoms structural model with the different structural conformations of CFH, showed alignment limited to specific number of sushi domains. The FXIII-B sushi domains S8, S9 and S10 structurally aligned to sushi domains S17, S18 and S19 when the alignment was done with the structurally resolved all atoms PDB file 1HAQ. In solution based structure PDB file 3GAW, FXIII-B sushi domains S2–S8 aligned with S9–S11, S17 and S18 numbered CFH sushi domains (Fig. 1a). The

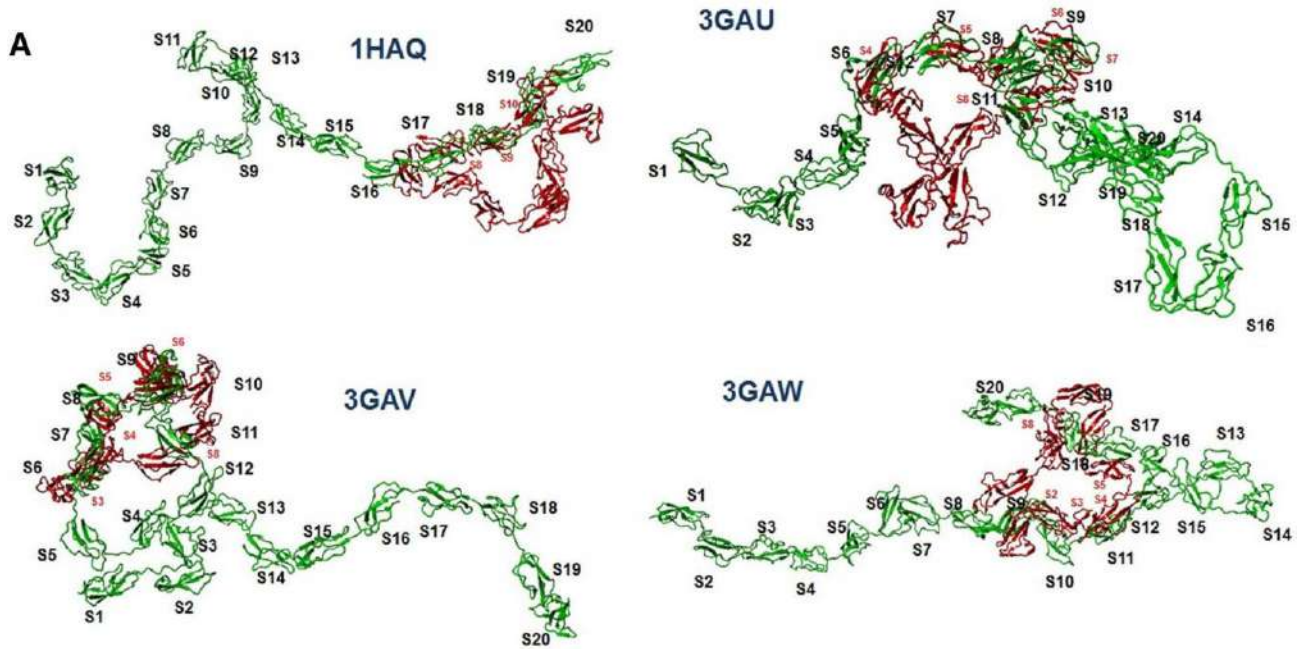
surface electrostatic distribution for CFH at different NaCl concentrations has been represented in Fig. 1a. The FXIII-B sushi domains S3–S7 align with CFH sushi domains that participate in oligomerization (Fig. 1c; shaded Green). The FXIII-B sushi domains S8–S10 align with CFH sushi domains that are protein interaction binding sites (Fig. 1c; shaded Blue). The longest inter-domain linkers for CFH were present between S8/S9 and S19/S20 while for FXIII-B they were between S5/S6 and S8/S9 (Fig. 1d).

Reconstitution experiments with factor XIII deficient plasma, and CFH deficient plasma

No significant differences were observed for the rate of activation of CP when reconstituted with rFXIII-A₂, rFXIII-B₂ subunit or the FXIII-A₂B₂ heterotetramer (p > 0.05 Fig. 2). The LP and AP showed reduced activation when FXIII-DP was reconstituted with the rFXIII-A₂ subunit, rFXIII-B₂ or the FXIII-A₂B₂ heterotetramer; however these differences were non-significant (Fig. 2a). A significant difference observed was in the rate of activation of LP of pool plasma, showing higher rate of activation compared to FXIII-DP. FXIII-DP reconstituted with rFXIII-B₂ with different concentrations of rFXIII-B₂ followed an uneven behavior. While reconstitution with 10 µg/ml rFXIII-B₂ did not show any significant effect on any of the pathways, FXIII-DP reconstituted with 5 and 20 µg/ml of rFXIII-B₂ had significantly raised activation levels for all three pathways (Fig. 2b). A significantly higher rate of activation of the AP was observed when CFH-DP was reconstituted with both rFXIII-A₂ and rFXIII-B₂ subunits individually (Fig. 2c). No significant difference was observed with addition of rFXIII-A₂B₂ (p > 0.05) as compared to the CFH-DP. The FXIII activity of CFH-DP was also significantly lower (27 ± 4% vs. 85 ± 8%; p < 0.0007) as compared to the pool plasma.

Complement activation upon transient expression of FXIII-B subunit in *SH-SY5Y* cell lines

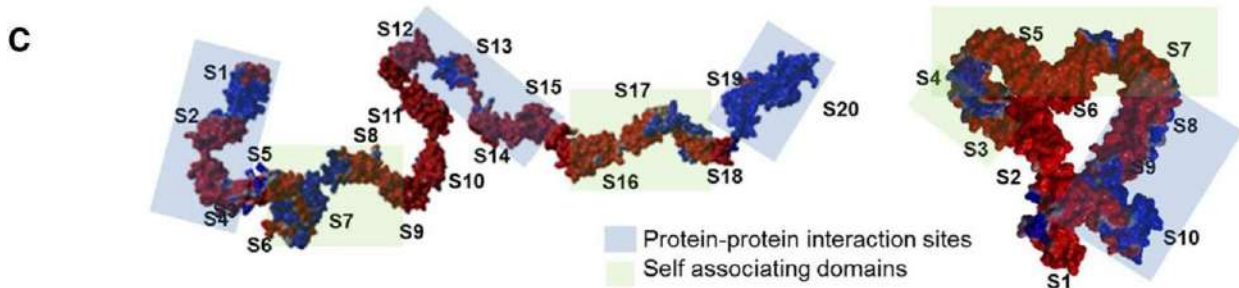
The levels of activation for all three complement pathways detected in the transiently expressed extracellular medium of *SH-SY5Y* cell lines were very low compared with pool plasma i.e. between 5 and 10% of the normal pool plasma. Compared with non-transfected cell line expression products, we observed that the LP showed significantly higher rate of activation (Fig. 3). The AP showed reduced activation, although the difference was non-significant (Fig. 3). No FXIII-B was detected in the harvested supernatants of non-transfected control in the western-blot (Fig. S1). We also did not detect any FXIII activity using the photometric assay in the harvested supernatants.



B

| FXIII B | S1 | S2 | S3 | S4 | S5 | S6 | S7 | S8 | S9 | S10 |
|----------|----|----|----|----|----|----|----|----|----|-----|
| Arg (+1) | 3 | 1 | 1 | 1 | 5 | 1 | 2 | 2 | 3 | 5 |
| Lys (+1) | 4 | 6 | 7 | 3 | 3 | 4 | 2 | 5 | 3 | 3 |
| His (+1) | 1 | 0 | 1 | 2 | 3 | 2 | 1 | 2 | 4 | 6 |
| Asp (-1) | 8 | 3 | 6 | 2 | 3 | 7 | 5 | 5 | 4 | 6 |
| Glu (-1) | 1 | 4 | 1 | 2 | 1 | 1 | 1 | 4 | 3 | 3 |
| | -1 | 0 | 2 | 2 | 7 | -1 | -1 | 0 | 3 | 5 |

| Factor H | S1 | S2 | S3 | S4 | S5 | S6 | S7 | S8 | S9 | S10 |
|----------|-----|-----|-----|-----|-----|-----|-----|-----|-----|-----|
| | | 3 | -3 | -2 | -1 | 3 | 2 | 5 | 1 | -5 |
| | S11 | S12 | S13 | S14 | S15 | S16 | S17 | S18 | S19 | S20 |
| | -1 | -6 | 5 | -4 | -4 | -1 | -1 | -3 | 0 | 8 |



D

CFHLinker: S1S2S3S4S5S6S7S8-9-S9S10S11S12S13S14S15S16S17S18S19-5-S20

F13BLinker: S1S2S3S4S5-5-S6S7S8-6-S9S10

Discussion

The Regulators of Complement Activation (RCA) gene cluster evolved from a series of gene duplication events, houses genes expressing complement system proteins as well as FXIII-B [32]. Even within the RCA gene cluster, a distinction can be made based on the point of divergence

during evolution between the proteins e.g. CFH and FXIII-B subunit belong to a common group distinct from C4b α or Cr1 protein [33]. Although this distinction between RCA proteins can be made based on the relative conservation of N-terminal sushi domains, the case of FXIII-B is ambiguous as some of its N-terminal domains show middling degrees of conservation [32]. Likewise, multi-domain assembly of

Fig. 1 Structural comparisons of Human Factor XIII-B and CFH. Computational approaches to delineate the structural similarities in FXIII-B and CFH in different orientations, on comparing FXIII-B full-atom model to CFH solution based structures. **a** Structural alignment of FXIII-B model with CFH model 1HAQ, 3GAU, 3GAV and 3GAW. (Green: CFH, Red: FXIII-B, aligned sushi domains are labelled red for FXIII-B). Lower panels represent the surface electrostatics of CFH for each of the four structures (Red: Negative, Blue:

Positive), at different solvent conditions. **b** Tabular representation of surface charges on each individual sushi domain present on CFH (adopted from Okemefuna et al. [23]), and FXIII-B for individual sushi domains based on presence of R, H, K, E, D amino acids, as calculated from the amino acid sequence. The sushi domains with surface glycosylation are within grey boxes in the table. **c** In the surface electrostatics map of CFH structure 1HAQ, the sushi domains binding to C3b and Heparin are shaded (blue, the CFH sushi domains responsible for self-assembly are shaded green. Corresponding to these domains, structurally aligned domains in FXIII-B are highlighted on FXIII-B model in similar colored shades). **d** Comparison of the length of inter-domain linkers present in CFH and FXIII-B, long linkers possibly responsible for self-folds and kinks are marked bold in black

sushi domains has given rise to both the CFH and FXIII-B proteins. A deeper look into their structural similarities reveal that although the sequence is ~60% conserved, structural alignment yields an almost 85% similarity between the two. This may be attributed to the conserved core fold of sushi domains. Structural analysis of full length solution based structures of CFH at increasing levels of NaCl, suggests high conformational flexibility for the protein [23]. It is reported that the fold-back structure of this 139 kDa protein involves non-covalent interactions based on variable surface charge densities (Acidic charge: CFH sushi domain S9, S12 and S15; Basic charge: CFH sushi domains S7, S13 and S20) depending on the solvent microenvironment that governs the orientation of the full length protein and its interaction with other proteins [24]. Structural alignment of the full length FXIII-B model with CFH structure demonstrates good alignment between the sushi domains that share similar charges (Acidic charge: FXIII-B sushi domains S1, S6 and S7; Basic charge: FXIII-B sushi domains S5, S9 and S10) indicating that the structural folds governing its interaction with other proteins, based on electrostatics are conserved between the two proteins. Another aspect determining overall fold and interaction interfaces in sushi domains containing proteins are the length and flexibility of inter-domain linkers. In CFH, long linkers are present between S8/S9 and S19/S20 facilitating the flexibility and overall fold, which are observed between S5/S6 and S8/9 in the FXIII-B model comparatively, most likely functioning similarly (Fig. 1) [23]. The high degree of structural similarity suggests that the FXIII-B subunit might be able to mimic CFH functionally in its absence or that such functions of FXIII-B have become vestigial, made redundant by more specifically evolved sushi domains of complement system. A reverse role of certain complement pathway proteins in coagulation

has been recently reported, however no involvement of sushi domains was identified [34–36]. However, our reconstitution experiments of FXIII-DP does not support any active physiological role of FXIII-B in any of the complement system pathways as no significant differences in the rate of activation was observed when the deficient plasma was reconstituted with various forms of the FXIII-B subunit (free FXIII-B and bound i.e. FXIII-A₂B₂) or for that matter even

its partner FXIII-A subunit. Interestingly, altered concentrations of rFXIII-B₂ resulting to higher AP activation indicate that it might still have a vestigial function that comes into light under non-physiological conditions (Fig. 2). However, we could not establish a consistent correlation between the rate of AP activation and FXIII-B₂ concentration since the rate of activation was similar for low (5 µg/ml) or high levels (20 µg/ml) of rFXIII-B₂ subunits. Transiently expression of FXIII-B₂ subunit in the cell line *SH-SY5Y* revealed significant differences in the LP (higher rate of activation). However, these differences are difficult to interpret physiologically since the endogenous complement activation observed here was much lower than physiological activation. When we directly checked the possibility of FXIII-B mimicking CFH functionally in CFH deficient plasma (i.e. representing a pathological condition) we observed a significantly higher rate of AP activation for free rFXIII-B₂ but no significant difference for the bound form i.e. FXIII-A₂B₂. This observation along with the changes observed when we used different concentrations of rFXIII-B₂ in FXIII-DP suggests that FXIII-B₂ (or free FXIII-B₂) might have a concentration dependent effect on the AP although this effect would not be observed under normal physiological conditions. Interestingly, the CFH-DP showed low FXIII activity of 23% when tested with a photometric assay. However, we cannot comment on whether this was as a result of the depletion process or if it reflects the true nature of the commercial CFH-DP since we tested only one batch of the same. Conclusively we can say that in pathological conditions FXIII-B might still be relevant functionally to the AP. Interestingly, genetic association of *F13B* gene polymorphisms with complement related problems like Acute Macular Degeneration (AMD) have been previously reported although there is no evidence of a functional association [37, 38]. However, our experiments did not detect any normal physiological role for FXIII-B₂ in the complement system. In free form plasma FXIII-B has been reported to be either dimeric or monomeric depending on the technique used to evaluate it [12, 39]. In reality it might well be that there exists equilibrium between the two states determined by the solvent concentration as has also been observed for CFH. Since it associates with FXIII-A in its dimeric form, it's likely that the monomeric form could have affinity for non-coagulation related proteins. Since the monomeric FXIII-B can adopt several different conformations that may contribute to pleiotropic roles for this protein,

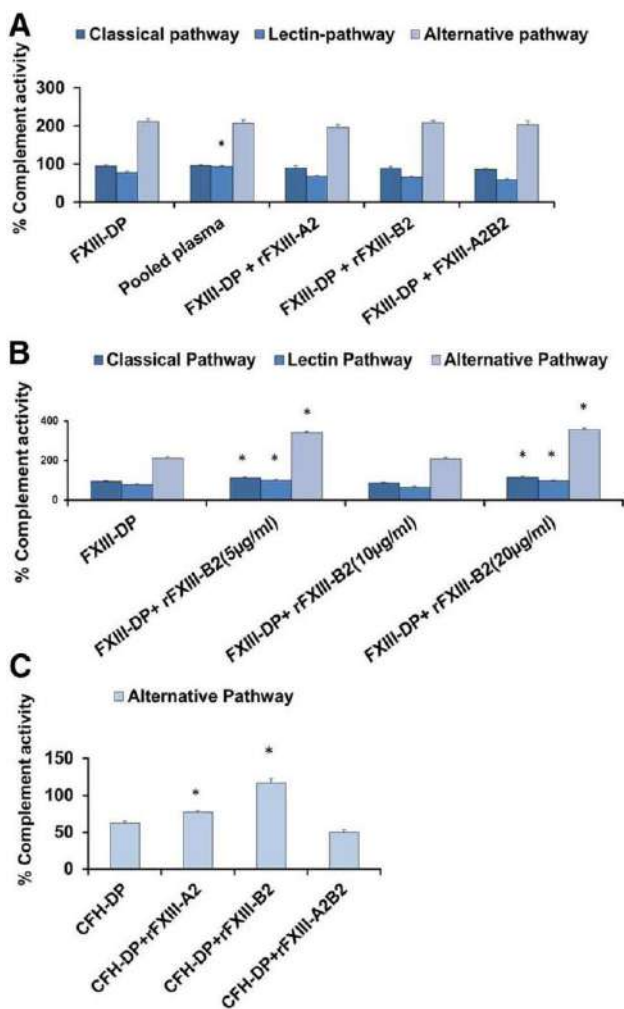


Fig. 2 Effect of FXIII and its subunits, on complement activation in FXIII deficient and CFH deficient background. Comparative bar-plot representations of the rate of complement activation, performed in (a). FXIII deficient plasma (FXIII-DP), healthy pool plasma (PP) and FXIII-DP when reconstituted with FXIII-A₂B₂ complex and each of its subunits individually. b The effect of increasing concentrations of FXIII-B subunit on rate of complement activation; performed in FXIII deficient plasma background. The reaction was spiked with 3 different concentrations of commercially available rFXIII-B₂ subunit. c Rate of alternative pathway activation after spiking CFH deficient plasma with individual FXIII subunits and also the complex. The three bars represent the rate of activation for the three complement pathways i.e. CP, LP and AP. The values for set of experiments a and b containing FXIII, were compared to values obtained in the deficient plasma without reconstitution (FXIII-DP) for all three separate pathways. A p value < 0.05 was considered significant and represent by an * in the graph. In experiment (c), the values for were compared with values obtained in the CFH deficient plasma without any reconstitution (CFH-DP). A p value < 0.05 was considered significant and is represented by an * in the graph

explaining its relative constitutive abundance in plasma. In future, a detailed evaluation of the status of FXIII-B subunit in the complement related deficiencies might help to establish a link in pathological scenarios like aHUS (Atypical

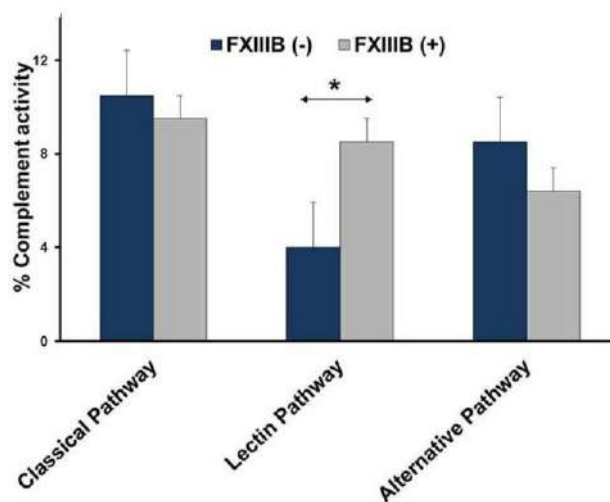


Fig. 3 Influence of FXIII-B on activation of Complement pathway in SHSY-5Y cell lines. Complement activation, as measured in extracellular fraction harvested from SHSY-5Y cell lines transfected with or without FXIII-B, 36 h post-transfection. A p value < 0.05 was considered significant and represent by an * in the graph

hemolytic uremic syndrome) something that is not ruled out in this study.

Author contributions AB and JO are the principle investigators of the study. MSA and SS performed the laboratory experiments. MSA, SS and AB analyzed the data, generated the images and co-wrote the article. AB, HY, VI and JO edited and revised the article. AB designed the study. None of the authors have any conflict of interest in the following work. The authors would like to acknowledge technical help from Sophie Lyonga.

Compliance with ethical standards

Conflict of interest Authors declare no conflict of interest.

Ethical approval This article does not contain any studies with animals performed by any of the authors.

References

- Amara U, Flierl MA, Rittirsch D et al (2010) Molecular intercommunication between the complement and coagulation systems. *J Immunol* 185(9):5628–5636. <https://doi.org/10.4049/jimmunol.0903678>
- Esmon CT (2004) The impact of the inflammatory response on coagulation. *Thromb Res* 114(5–6):321–327. <https://doi.org/10.1016/j.thromres.2004.06.028>
- Krisinger MJ, Goebeler V, Lu Z et al (2012) Thrombin generates previously unidentified C5 products that support the terminal complement activation pathway. *Blood* 120(8):1717–1725. <https://doi.org/10.1182/blood-2012-02-412080>
- Foley JH, Walton BL, Aleman MM et al (2016) Complement activation in arterial and venous thrombosis is mediated by plasmin.

- EBioMedicine 5:175–182. <https://doi.org/10.1016/j.ebiom.2016.02.011>
5. Markiewski MM, DeAngelis RA, Lambris JD (2008) Complexity of complement activation in sepsis. *J Cell Mol Med* 12(6a):2245–2254. <https://doi.org/10.1111/j.1582-4934.2008.00504.x>
 6. Jenny L, Dobó J, Gál P et al (2018) MASP-1 of the complement system enhances clot formation in a microvascular whole blood flow model. *PLoS ONE* 13(1):e0191292. <https://doi.org/10.1371/journal.pone.0191292>
 7. Adamiak M, Abdelbaset-Ismail A, Suszynska M et al (2017) Novel evidence that the mannan-binding lectin pathway of complement activation plays a pivotal role in triggering mobilization of hematopoietic stem/progenitor cells by activation of both the complement and coagulation cascades. *Leukemia* 31(1):262–265. <https://doi.org/10.1038/leu.2016.278>
 8. Gupta S, Biswas A, Akhter MS et al (2016) Revisiting the mechanism of coagulation factor XIII activation and regulation from a structure/functional perspective. *Sci Rep* 6(1):245. <https://doi.org/10.1038/srep30105>
 9. Biswas A, Thomas A, Bevans CG et al (2013) In vitro secretion deficits are common among human coagulation factor XIII subunit B missense mutants. Correlations with patient phenotypes and molecular models. *Human Mutation* 34(11):1490–1500. <https://doi.org/10.1002/humu.22391>
 10. Thomas A, Biswas A, Ivaskovic V et al (2015) Structural and functional influences of coagulation factor XIII subunit B heterozygous missense mutants. *Mol Genet Genomic Med* 3(4):258–271. <https://doi.org/10.1002/mgg3.138>
 11. Schroeder V, Kohler H (2016) Factor XIII: structure and function. *Semin Thromb Hemost* 42(04):422–428. <https://doi.org/10.1055/s-0036-1571341>
 12. Sourì M, Kaetsu H, Ichinose A (2008) Sushi domains in the B subunit of factor XIII responsible for oligomer assembly. *Biochemistry* 47(33):8656–8664. <https://doi.org/10.1021/bi8006143>
 13. Mezei ZA, Katona É, Kállai J et al (2017) Factor XIII levels and factor XIII B subunit polymorphisms in patients with venous thromboembolism. *Thromb Res* 158:93–97. <https://doi.org/10.1016/j.thromres.2017.08.018>
 14. Pitkänen HH, Jouppila A, Lemponen M et al (2017) Factor XIII deficiency enhances thrombin generation due to impaired fibrin polymerization - An effect corrected by Factor XIII replacement. *Thromb Res* 149:56–61. <https://doi.org/10.1016/j.thromres.2016.11.012>
 15. Deicke C, Chakrakodi B, Pils MC et al (2016) Local activation of coagulation factor XIII reduces systemic complications and improves the survival of mice after *Streptococcus pyogenes* M1 skin infection. *Int J Med Microbiol* 306(7):572–579. <https://doi.org/10.1016/j.ijmm.2016.06.001>
 16. Orosz ZZ, Katona É, Facskó A et al (2011) Factor XIII subunits in human tears; their highly elevated levels following penetrating keratoplasty. *Clin Chim Acta* 412(3–4):271–276. <https://doi.org/10.1016/j.cca.2010.10.017>
 17. Ariëns RA, Kohler HP, Mansfield MW et al (1999) Subunit antigen and activity levels of blood coagulation factor XIII in healthy individuals. Relation to sex, age, smoking, and hypertension. *Arterioscl Thromb Vasc Biol* 19(8):2012–2016
 18. Kopp A, Hebecker M, Svobodova E et al (2012) Factor H. A complement regulator in health and disease, and a mediator of cellular interactions. *Biomolecules* 2(1):46–75. <https://doi.org/10.3390/biom2010046>
 19. Rodriguez de Cordoba S, Rey-Campos J, Dykes DD et al (1988) Coagulation factor XIII B subunit is encoded by a gene linked to the regulator of complement activation (RCA) gene cluster in man. *Immunogenetics* 28(6):452–454
 20. Fagerberg L, Hallström BM, Oksvold P et al (2014) Analysis of the human tissue-specific expression by genome-wide integration of transcriptomics and antibody-based proteomics. *Mol Cell Proteom* 13(2):397–406. <https://doi.org/10.1074/mcp.M113.035600>
 21. Simon Á, Bagoly Z, Hevessy Z et al (2012) Expression of coagulation factor XIII subunit A in acute promyelocytic leukemia. *Cytometry* 82B(4):209–216. <https://doi.org/10.1002/cyto.b.21019>
 22. Thomas A, Gasque P, Vaudry D et al (2000) Expression of a complete and functional complement system by human neuronal cells in vitro. *Int Immunol* 12(7):1015–1023
 23. Okemefuna AI, Nan R, Gor J et al (2009) Electrostatic Interactions Contribute to the Folded-back Conformation of Wild Type Human Factor H. *J Mol Biol* 391(1):98–118. <https://doi.org/10.1016/j.jmb.2009.06.010>
 24. Aslam M, Perkins SJ (2001) Folded-back solution structure of monomeric factor H of human complement by synchrotron X-ray and neutron scattering, analytical ultracentrifugation and constrained molecular modelling. *J Mol Biol* 309(5):1117–1138. <https://doi.org/10.1006/jmbi.2001.4720>
 25. Moore BL, Kelley LA, Barber J et al (2013) High-quality protein backbone reconstruction from alpha carbons using Gaussian mixture models. *J Comput Chem* 34(22):1881–1889. <https://doi.org/10.1002/jcc.23330>
 26. Xu D, Jaroszewski L, Li Z et al (2014) AIDA: ab initio domain assembly server. *Nucleic Acids Res* 42(W1):W308–W313. <https://doi.org/10.1093/nar/gku369>
 27. Krieger E, Koraimann G, Vriend G (2002) Increasing the precision of comparative models with YASARA NOVA—a self-parameterizing force field. *Proteins* 47(3):393–402
 28. Krieger E, Vriend G (2014) YASARA View: molecular graphics for all devices—from smartphones to workstations. *Bioinformatics* 30(20):2981–2982. <https://doi.org/10.1093/bioinformatics/btu426>
 29. Katona E, Haramura G, Kárpáti L et al (2000) A simple, quick one-step ELISA assay for the determination of complex plasma factor XIII (A2B2). *Thromb Haemost* 83(2):268–273
 30. Katona EE, Ajzner E, Toth K et al (2001) Enzyme-linked immunosorbent assay for the determination of blood coagulation factor XIII A-subunit in plasma and in cell lysates. *J Immunol Methods* 258(1–2):127–135
 31. Lee KN, Birckbichler PJ, Patterson MK, JR (1988) Colorimetric assay of blood coagulation factor XIII in plasma. *Clin Chem* 34(5):906–910
 32. Krushkal J, Bat O, Gigli I (2000) Evolutionary relationships among proteins encoded by the regulator of complement activation gene cluster. *Mol Biol Evol* 17(11):1718–1730. <https://doi.org/10.1093/oxfordjournals.molbev.a026270>
 33. Reid KBM, Bentley DR, Campbell RD et al (1986) Complement system proteins which interact with C3b or C4b A superfamily of structurally related proteins. *Immunol Today* 7(7–8):230–234. [https://doi.org/10.1016/0167-5699\(86\)90110-6](https://doi.org/10.1016/0167-5699(86)90110-6)
 34. Müller-Calleja N, Ritter S, Hollerbach A et al (2018) Complement C5 but not C3 is expendable for tissue factor activation by cofactor-independent antiphospholipid antibodies. *Blood Adv* 2(9):979–986. <https://doi.org/10.1182/bloodadvances.2018017095>
 35. Skjeflo EW, Christiansen D, Fure H et al (2018) Staphylococcus aureus-induced complement activation promotes tissue factor-mediated coagulation. *J Thromb Haemost* 16(5):905–918. <https://doi.org/10.1111/jth.13979>
 36. Subramaniam S, Jurk K, Hobohm L et al (2017) Distinct contributions of complement factors to platelet activation and fibrin formation in venous thrombus development. *Blood* 129(16):2291–2302. <https://doi.org/10.1182/blood-2016-11-749879>
 37. Scheetz TE, Fingert JH, Wang K et al (2013) A genome-wide association study for primary open angle glaucoma and macular degeneration reveals novel loci. *PLoS ONE* 8(3):e58657. <https://doi.org/10.1371/journal.pone.0058657>

38. Hageman GS, Gehrs K, Lejnine S et al (2011) Clinical validation of a genetic model to estimate the risk of developing choroidal neovascular age-related macular degeneration. *Human Genom* 5(5):420–440
39. Schwartz ML, Pizzo SV, Hill RL et al (1973) Human Factor XIII from plasma and platelets. Molecular weights, subunit structures, proteolytic activation, and cross-linking of fibrinogen and fibrin. *J Biol Chem* 248(4):1395–1407

Publisher's Note Springer Nature remains neutral with regard to jurisdictional claims in published maps and institutional affiliations.

Chapter 5

Published Article

Disruption of Structural Disulfides of Coagulation FXIII-B Subunit; Functional Implications for a Rare Bleeding Disorder.

Sneha Singh, Mohammad Suhail Akhter, Johannes Dodt, Amit Sharma, Senthilvelrajan Kaniyappan, Hamideh Yadegari, Vytautas Ivaskevicius, Johannes Oldenburg and Arijit Biswas

A brief synopsis:

Continuing to exploration of novel roles and interacting partners of the FXIII-B subunit, chapter 5 is aimed at structural characterization of FXIII-B subunit disulfides. Since FXIII-B is filamentous in nature and bears 20 disulfide bonds, it makes it challenging to recombinantly express and study this molecule by traditional structural methods such as X-ray crystallography or NMR. As an alternative, in this chapter we rather tried to decipher first the roles of individual structural disulfides which are present of FXIII-B, to rule out how these may be affecting the mutational states of this protein, and its maturation at different levels; to . By inducing site-directed point mutations, we ablated each of the individual disulfide bond present in FXIII-B and the mutants were tested in-vitro for their rate of expression, secretion, stability and oligomerization by a combination of approaches. Furthermore, structural flexibility of these disulfides was tested by in-silico methods, on a FXIII-B monomer model (also generated in-silico). This chapter concludes that, a)all 20 disulfides are important for FXIII-B expression and secretion, b) disruption of FXIII-B structural disulfides leads to its intracellular retention in ER, c) even if secreted, the disulfide mutants fail to dimerize into FXIII-B₂, and show altered complexation, d) The FXIII-B Subunit disulfide bonds display variability in structural flexibility, but ablation of any of these bonds leads to a loss in stability. This chapter thus explains the dominant negative role of FXIII-B mutations in FXIII-deficiency, and how the structural cysteines of FXIII-B can act as one of the mutational hotspots in the heterozygous, mild-form of this rare bleeding disorder.

Int. J. Mol. Sci. 2019, 20(8), 1956; <https://doi.org/10.3390/ijms20081956>



Article

Disruption of Structural Disulfides of Coagulation FXIII-B Subunit; Functional Implications for a Rare Bleeding Disorder

Sneha Singh ¹, Mohammad Suhail Akhter ^{1,2}, Johannes Dodt ³, Amit Sharma ^{1,4},
Senthilvelrajan Kaniyappan ⁵, Hamideh Yadegari ¹, Vytautas Ivaskevicius ¹,
Johannes Oldenburg ¹ and Arijit Biswas ^{1,*}

¹ Institute of Experimental Haematology and Transfusion Medicine, University Clinic Bonn, 53127 Bonn, Germany; sneha.gupta@ukbonn.de (S.S.); suhailaiims@gmail.com (M.S.A.); sharmaaiims@gmail.com (A.S.); hamideh.yadegari@ukbonn.de (H.Y.); vytautas.ivaskevicius@ukbonn.de (V.I.); johannes.oldenburg@ukbonn.de (J.O.)

² College of Applied Medical Sciences, Jazan University, Jazan 82911, Saudi Arabia

³ Paul-Ehrlich-Institute, 63225 Langen, Germany; johannes.dodt@pei.de

⁴ Department of Hematology, All India Institute of Medical Sciences, New Delhi 110029, India

⁵ DZNE, German Center for Neurodegenerative Diseases, 53127 Bonn, Germany; Senthil.Kaniyappan@dzne.de

* Correspondence: arijit.biswas@ukb.uni-bonn.de; Tel.: +49-228-287-19428

Received: 2 April 2019; Accepted: 18 April 2019; Published: 22 April 2019



Abstract: Congenital FXIII deficiency is a rare bleeding disorder in which mutations are detected in *F13A1* and *F13B* genes that express the two subunits of coagulation FXIII, the catalytic FXIII-A, and protective FXIII-B. Mutations in FXIII-B subunit are considerably rarer compared to FXIII-A. Three mutations in the *F13B* gene have been reported on its structural disulfide bonds. In the present study, we investigate the structural and functional importance of all 20 structural disulfide bonds in FXIII-B subunit. All disulfide bonds were ablated by individually mutating one of its contributory cysteine's, and these variants were transiently expressed in *HEK293t* cell lines. The expression products were studied for stability, secretion, the effect on oligomeric state, and on FXIII-A activation. The structural flexibility of these disulfide bonds was studied using classical MD simulation performed on a FXIII-B subunit monomer model. All 20 FXIII-B were found to be important for the secretion and stability of the protein since ablation of any of these led to a secretion deficit. However, the degree of effect that the disruption of disulfide bond had on the protein differed between individual disulfide bonds reflecting a functional hierarchy/diversity within these disulfide bonds.

Keywords: coagulation Factor XIII; FXIII-B; disulfide bonds; FXIII deficiency

1. Introduction

Coagulation Factor XIII (FXIII) is a pro-transglutaminase that acts at the terminal stage of the blood coagulation cascade and is responsible for covalent cross-linking of pre-formed fibrin polymers making them resistant to premature fibrinolysis [1]. In plasma, FXIII exists as a zymogenic heterotetramer with non-covalently associated dimers of its catalytic FXIII-A and non-catalytic/carrier FXIII-B subunits. Thrombin activates this zymogenic complex by cleaving an N-terminal 37 amino acid long region on the FXIII-A subunit called the activation peptide (FXIII-AP). This cleavage is also accompanied by binding of calcium ions to FXIII-A, resulting in conformational changes that trigger the dissociation of the FXIII-B subunit as well as the opening up of the closed zymogenic dimeric form of the FXIII-A subunit into an open monomeric form of FXIII-A (FXIII_{Aa}) facilitating substrate access to its catalytic site

(a triad with a catalytic cysteine, i.e., Cys314 as its functional centre) [2]. Since this protein contributes to the stability of fibrin clots, inherited or acquired defects result in a bleeding predisposition [1]. The inherited form of FXIII deficiency is a rare coagulation disorder (one in one–four million) resulting from homozygous or compound heterozygous mutations in FXIII genes, and it usually causes a severe bleeding diathesis with umbilical cord bleeding as the most common symptom associated with this deficiency. More than 120 mutations have been detected in *F13A1* and *F13B* genes corresponding to the two subunits of FXIII since the first case was reported in 1962 by Duckert et al. [3–5]. More than 95% of the mutations in severe inherited FXIII deficiency occur in the *F13A1* gene (OMIM # 613225), but only a few mutations have been detected in the *F13B* gene (OMIM #613235) [5–12]. However, in the past decade, several reports from our group have indicated that the heterozygous form of this defect might also have clinical relevance as a mild form of FXIII deficiency, which we anticipate has a higher prevalence than severe inherited forms [13–15]. We have reported several mutations which were detected in individuals who suffer from inherited mild FXIII deficiency [14]. Many of these individuals are asymptomatic, but some also display unusual bleeding tendency when exposed to some kind of trauma. Interestingly, unlike the severe inherited form, in the mild form, the proportion of mutations detected in the FXIII-B subunit is far higher. Almost 20%–40% of the mutations detected in mild FXIII deficiency occur in *F13B* gene [5]. The catalytic FXIII-A subunit is a structurally and functionally well-characterized protein. Its partner FXIII-B subunit comparatively is a relatively unknown entity. There exists no biophysical structure for this protein, although based on its strong homology to complement factor H, several high-quality models of its repetitive sushi domains have been reported [16]. The FXIII-B protein is a traditionally secreted protein (bearing an N-terminal 20 amino acid long signal peptide) expressed in hepatocytes [17–19]. It associates with the FXIII-A subunit in the plasma to form the heterotetrameric complex. Since it is secreted in excess of FXIII-A subunit, it is also present in plasma in its unbound, free-form, which hints towards pleiotropic roles of this protein beyond coagulation [20]. Its circulating form had earlier been reported to be a monomer based on its sedimentation coefficient, although gel filtration results of FXIII-B expressed in insect cell lines indicate that it is a dimer [17]. Homology studies suggest that a monomer of FXIII-B subunit is composed of 10 repetitive sushi domains, held together by short peptide linkers. Sushi domains are also known as complement control modules since they also exist in complement system proteins like complement factor H (CFH) [21]. Functionally they act as chaperones to other catalytic proteins and regulate their functional states by binding to them. Each sushi domain has a conserved core structure with four consensus cysteine residues forming two disulfide bonds [22]. Therefore, a FXIII-B monomer will comprise of 20 disulfide bonds. The symmetrical arrangement of cysteine bond formation (abab pattern) in individual sushi domain gives specific intrinsic topology, thereby adopting a signature secondary structure, a β -sandwich type fold, and an overall globular shape. The disulfide bridges enable sushi domains to fold into a compact hydrophobic core enclosed by 3 + 2 beta-strands. Rigorous analysis of FXIII activation has revealed that the rate of activation of FXIII-A subunit is accelerated in the presence of FXIII-B subunit, which raises interest in its suggestive role in the regulation of FXIII-A mediated fibrin cross-linking [2,23]. Additionally, Soury et al., have suggested that FXIII-B mediates association of Fibrinogen, FXIII-A, and Thrombin, hence enhancing the cross-linking [23,24]. These developments in the last few years indicate that the role of FXIII-B in fibrin cross-linking extends beyond being a mere carrier/protective protein. Interestingly, three of the mutations detected in the FXIII-B subunit causing either severe or mild inherited FXIII deficiency, occur on the cysteines forming the structural disulfide bonds [5,13,14]. Transient expression of some of these mutations suggested pathomolecular influences on the core fold of the protein, consequently affecting its secretion. Disulfide bonds, structural or allosteric, play a major role in several coagulation proteins [25]. The disulfide bonds observed in FXIII-B are very likely structural, although no structural data exists for this subunit to confirm this assumption. The only structural data currently in literature comprises of electron microscopy studies which indicate the subunit to be filamentous in nature [26]. Even though the disulfide bonds present on each sushi domain of this subunit might be structural in nature, its relative

contribution to the functional aspects of the protein might differ. Some functional data exists of the involvement of select sushi domains of the FXIII-B subunit to its overall fold (its dimeric form) or in the interaction with partner FXIII-A subunit [17,27].

In the present study, we investigate the structural and functional relationship of these disulfide bonds to the overall functionality of the protein. We ablate these disulfide bonds by mutating one contributory cysteine at a time and transiently express the resulting variant in HEK293t cell lines in order to study their effect on stability/secretion of the protein. We also purified the expressed variants to study the impact of these mutants on their mutual dimerization and on the activation of the FXIII-A subunit. In the absence of a biophysical structure, we have generated a monomeric FXIII-B subunit model by assembling high quality threaded models of its individual sushi domains. The structural flexibility of the different disulfide bonds within this model is subsequently investigated using classical unbiased all-atomic molecular dynamic MD simulation. We observed that although mutating specific disulfide bonds have differing degrees of functional effect on the protein based on which domain they belong to, almost all of them uniformly hinder the global fold of the protein, resulting in secretion defects. This explains earlier similar observations for FXIII-B subunit mutations detected in FXIII deficiency [14,16].

2. Results

2.1. Disruption of FXIII-B Subunit Structural Disulfides Results in a Secretion Deficit

All 20 FXIII-B cysteine mutants were successfully expressed intracellularly, but only 8 of these (C118A, C153A, C180A, C267A, C274A, C396A, C454A, and C616A) were successfully secreted out of the cell at levels detectable by ELISA and Western blot (Figure 1A,B). Intracellularly, except for C302A, C524A, C553A, and C582A variants, all other mutants were detected at levels similar to or greater than the wild type. The eight mutants that were successfully secreted showed significantly lower secreted protein than the wild type (Figure 1A). Among the three variants reported so far on these disulfide bonds, only one was earlier shown to secrete any detectable amounts (~30–50% of wild type) of protein, i.e., C336F in earlier expression based studies (C316A based on earlier nomenclature) [14]. In our study, we have mutated the oppositely paired cysteine to the C336, i.e., C378 to an alanine. The variant in our study unlike the reported mutant C336F is not secreted at all. Since the expression methodology, as well as the evaluation strategy of this study, is exactly the same as the expression study on C336F, we believe that the type of substitution occurring on the particular cysteine does influence the fate of the protein even if both substitutions result in disruption of the same disulfide bond. Very clearly, the alanine substitution on the oppositely paired cysteine results in far greater misfolding compared to the C336F variant. Therefore, while C336F also disrupts the same disulfide bond, the protein variant does manage to fold itself and get secreted out, albeit with much lower efficiency than the wild type.

2.2. Disruption of FXIII-B Subunit Structural Disulfides Results Mainly in ER Accumulation

Subcellular distribution of the selected FXIII-B protein cysteine mutants evaluated by confocal microscopy showed significant intracellular retention when compared with wild-type FXIII-B protein (Figure 2A,B). The retention was primarily observed in ER (C59A, C91A, C118A, C153A, C180A, and C396A) with only two mutants showing higher detectable levels in trans-Golgi body (C59A and C91A) (Figure 2C). Classically secreted proteins usually attain their primary secretable folds in the ER, after which they are transported to the Golgi apparatus to be subsequently secreted. In the event of misfolding, exposed hydrophobic patches on the unfolded protein are detected by the quality control system of the cell, and these proteins are subsequently degraded via the ubiquitin response pathway. The two mutations i.e., C59A and C91A which show Golgi retention also show high retention in the ER (Figure 2B). These cysteine mutants possibly override the ER quality control system but then are returned back by Golgi through retrograde transport and subsequently degraded [28]. The C59A and C91A mutations, therefore, show no detectable secreted protein at all (Figure 2C). The remaining

mutants show accumulation in ER, but their levels in Golgi are similar to that of the wild type. This suggests that these cysteine mutants to some degree escape the ER-mediated stress response and the molecules that do make it to the Golgi are successfully secreted outside. These mutants, therefore, show low but detectable amounts of secreted protein. Clearly, disrupting different disulfide bonds affects the overall fold of the protein differently which then dictates their intracellular as well as extracellular fates. Our previous expression study on two of the reported cysteine variants also reflected this diversity, since the C25R mutant (C5R; earlier nomenclature) was observed to get strongly retained in ER and also showed no detectable secreted protein while the other C336F (C316F; earlier nomenclature) mutant was not significantly retained in either ER or Golgi and hence also showed low but detectable amount of secreted [13,14]. Another mutant, i.e., C450F (C430F; earlier nomenclature) reported and analyzed previously in BHK cell lines also showed strong retention in the ER by pulse-chase experiments and no secreted protein [6]. The C336F variant though also showed lower levels of intracellular distribution in both ER and Golgi unlike for almost all variants that we have studied which uniformly showed higher levels of intracellular retention than the wild type. As also explained in our earlier study this difference might originate from the fact that in the case of the C316F (C336F; current nomenclature used in this study), the mutation might have resulted in slower folding rates for the final protein.

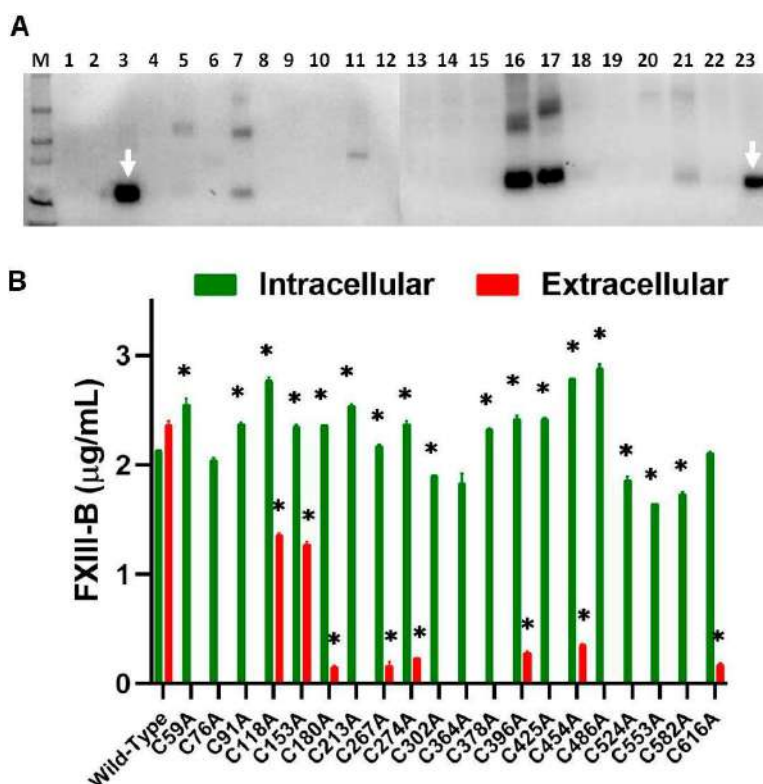


Figure 1. Transient expression of FXIII-B Cysteine mutants. **Panel A.** A conventional western blot of 10uL each of the wild type FXIII-B and 20 rFXIII-B cysteine mutants retained from the culture medium of transfected cells, probed against mouse to human FXIII-B antibody. **Lanes:** 1: Un-transfected control; 2: C76A; 3: Wild-Type; 4: C364A; 5: C396A; 6: C425A; 7: C454A; 8: C524A; 9: C553A; 10: C582A; 11: C616A; 12: C486A; 13: C378A; 14: C59A; 15: C91A; 16: C118A; 17: C153A; 18: C180A; 19: C213A; 20: C267A; 21: C274A; 22: C302A; and 23: rFXIII-B (Zedira, 75ng, positive control) White arrows represent the wild-type FXIII-B. **Panel B.** A comparative bar-plot representation of the antigenic levels of FXIII-B cysteine mutants versus the FXIII-B wild type evaluated on a quantitative sandwich ELISA based platform, detecting FXIII-B in 100µL of sample retained from transiently transfected cells. Green and red bars represent the intracellular and the extracellular fractions, respectively. A “*” symbol represents significance (p -value ≤ 0.05).

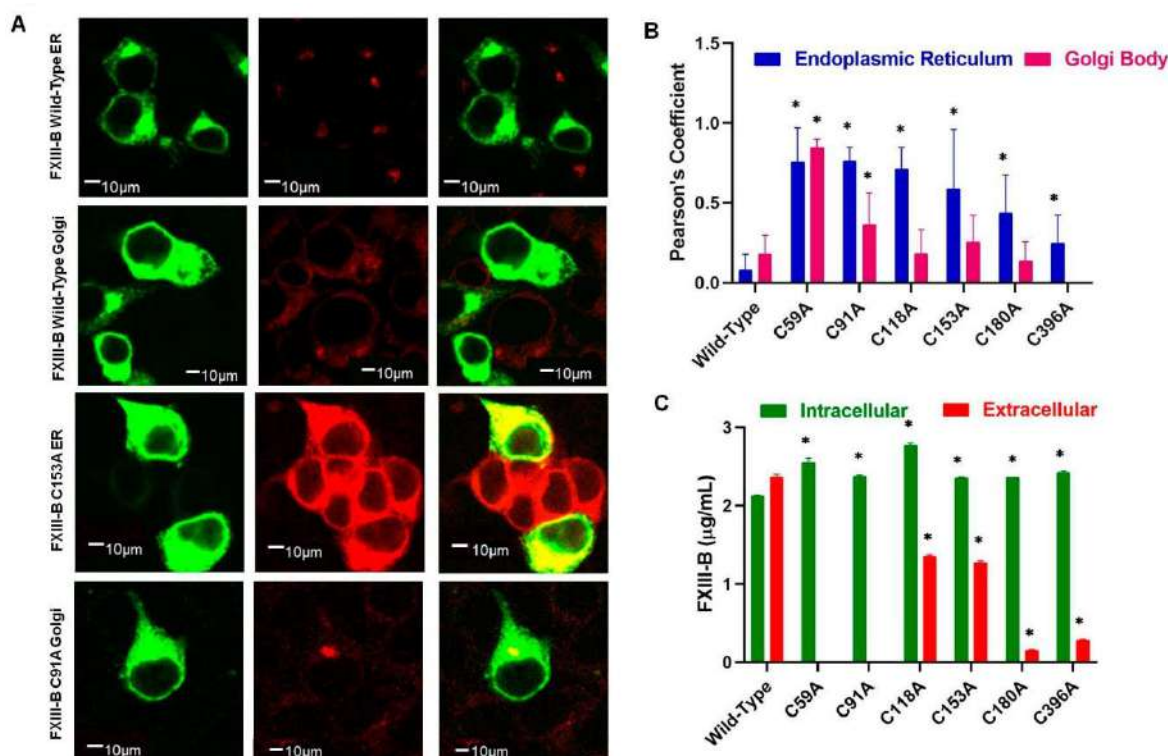


Figure 2. Effect of FXIII-B cysteine mutations on intracellular trafficking of FXIII-B protein. **Panel A.** Confocal microscopy tracking the subcellular localization of FXIII-B cysteine mutant proteins, via cell-specific markers; green (α FXIII-B), red (α -PDI (for endoplasmic reticulum) and α -TGN-46 (for trans-Golgi network)) with secondary antibodies conjugated with Alexa-488 and Alexa-555 respectively. Bars represent 10 μ m scale. **Panel B.** Bar-plot representation of Pearson's coefficient calculated as a measurement of the intensity of pixels, defining co-localization of FXIII-B within either endoplasmic reticulum (PDI), or trans-Golgi network (TGN-46). A "*" symbol represents significance (p -value < 0.05). **Panel C.** Bar plot representation of antigenic evaluation (ELISA) of select FXIII-B cysteine mutants which showed higher intracellular retention (on confocal immunostaining) when compared to wild-type. A "*" symbol represents significance (p -value < 0.05).

2.3. Secreted FXIII-B Cys-Mutants Show Altered Complexation States and Possible Dimer Disruption

Gel filtration runs for the recombinant wild type FXIII consistently showed two peaks, one of lower molecular weight (faster retention time) and the other of higher molecular weight (slower retention time). The high molecular weight peak with slower retention time was checked with Western blot and mass spectrometry and confirmed to contain FXIII-B subunits. No FXIII-B subunit was detected in the low molecular weight faster-retained peak. This peak, when tested with mass spectrometry, was confirmed to contain only albumin. Earlier studies with gel filtration runs conducted on FXIII-B purified from insect cell line also suggest FXIII-B to be dimeric with a single peak only although sedimentation studies contradict this evidence and instead suggest the FXIII-B be a monomer. The contradiction might reflect the flexibility of sushi domain-containing proteins to adopt different oligomeric states under different conditions as observed for CFH and that in fact for FXIII-B both monomeric and dimeric forms might be possible depending on their native physiological milieu. The Native PAGE runs for our recombinant wild type FXIII-B subunit also showed a single dimeric band. The gel filtration runs for the secreted cysteine mutants showed a different mobility pattern than the wild type. The C486A mutant showed two major peaks similar to the wild type but with faster mobility (lower retention times) and a small shoulder peak closer to the high molecular weight peak. This mutant might result in partial monomerization of the protein. Since this protein now has a free reactive cysteine, the monomeric form might interact with the albumin generating the altered

peak pattern. The other mutants except for C153A and C396A majorly showed only one major peak closer to the FXIII-B subunit peak observed in the wild type run but with slightly different mobility. Mutants C153A and C396A also showed one peak, but these were closer to the albumin peak detected in the wild type run. These peaks although closer to albumin peak detected in the wild type run had clearly different retention times than the albumin peak. These mutants most likely also behave like the C486A variant, with the difference that in these mutants the dimeric peak is completely non-existent since these mutants might completely disrupt the dimer and the resulting monomers with the reactive cysteines interact with albumin (possibly by forming a disulfide bond with another free cysteine on albumin) generating these altered patterns. Native PAGE of the mutants was also on similar lines showing altered band patterns than the wild type most likely suggestive of altered complexation states with albumin (Figure 3A). High molecular weight bands were observed for C153A and C118A mutants; mutants C274A and C454A showed low molecular weight bands, as compared to wild-type, hinting towards degradation, a few mutants (C180A and C267A) showed a smeary appearance also indicating degradation of the protein upon secretion. The variants C396A and C425A showed low levels but similar mobility as the wild-type protein. The mutants C180A and C302A showed paradoxical behavior on gel filtration columns and on Native PAGE. The mutant C180A was detected on Native PAGE gels, but was not retained in the gel filtration runs. This might reflect poor stability for this mutant which got degraded before gel filtration could be conducted. The mutant C302A, on the other hand, was detected in gel filtration runs but was non-detectable in the Native PAGE. This mutant might have a completely altered fold in the dimeric state thereby evading detection from antibodies in the Native PAGE. Almost all of the proteins after purification, showed levels close to baseline in these qualitative analyses when compared to wild-type, indicating early aggregation, low shelf-life, or degradation, even after successful secretion.

2.4. A Filamentous Monomer FXIII-B Subunit Model with Its N and C Terminals Aligned Close to Each Other

The final model of the FXIII-B subunit post equilibration shows a filamentous structure approximately 150 Å in length and 70 Å in width (Figure 4A). All cysteines in the simulation-equilibrated and the original assembled model were in the oxidized state. The N and C terminals of the structure are observed to interact with each other with a major twist in the middle region occupied by the S3, S4, and S5 domains. This twist and the N-C-terminal interaction appear to curtail the length of the monomer which otherwise would extend much longer. The initially assembled full-length model is quite different than the MD simulation-equilibrated model (Figure S1). This is evident from the huge change in conformation/RMSD (~23 Å) during the equilibration phase of the simulation (Figure S1). It is also clear from the length of the equilibration phase (~120 ns) that the original assembled model takes a long time to adopt an energetically stable monomeric state. While the N and C terminal ends of this monomer also align next to each other in the original assembled model, it differs from the simulation-equilibrated model significantly in form with the original model being significantly shorter than the equilibrated one (Figure S2). The C terminal region showed higher flexibility than the overall protein especially the S8, S9, and S10 domains (Figure S3). The simulation-equilibrated model shows distinct electrostatic patches around the S1, S3, S4, S7, and S8 sushi domains. We repeatedly emphasize the differences between the initially assembled model and the simulation-equilibrated final model because of the dichotomy over the dimeric state of the free FXIII-B subunit in the present literature. While initially understood to be a monomer from sedimentation coefficient studies, the free FXIII-B was later suggested to be a physiological dimer based on gel filtration chromatography performed with FXIII-B subunit expressed in insect cells [17,26]. This kind of variation in the oligomeric state is also observed in the closest homolog of FXIII-B, CFH [29]. While almost double the length of FXIII-B, CFH has also been observed in different solution states to exist in different oligomeric forms (i.e., dimer or monomer) [30]. One of the reasons proposed for the variation in conformation for these sushi domain containing proteins has been the variability in surface electrostatic patches exhibited by this domain under different solution states which promotes intra-subunit or inter-subunit interactions that

shift the tendency of these proteins to choose one or the other forms (i.e., monomer or dimer) [30]. The significant conformational difference between the assembled model and the simulation-equilibrated model of FXIII-B subunit suggests that this protein might exist in equilibrium between its respective states (monomer and dimer), with the local ionic environment dictating which of these states dominate.

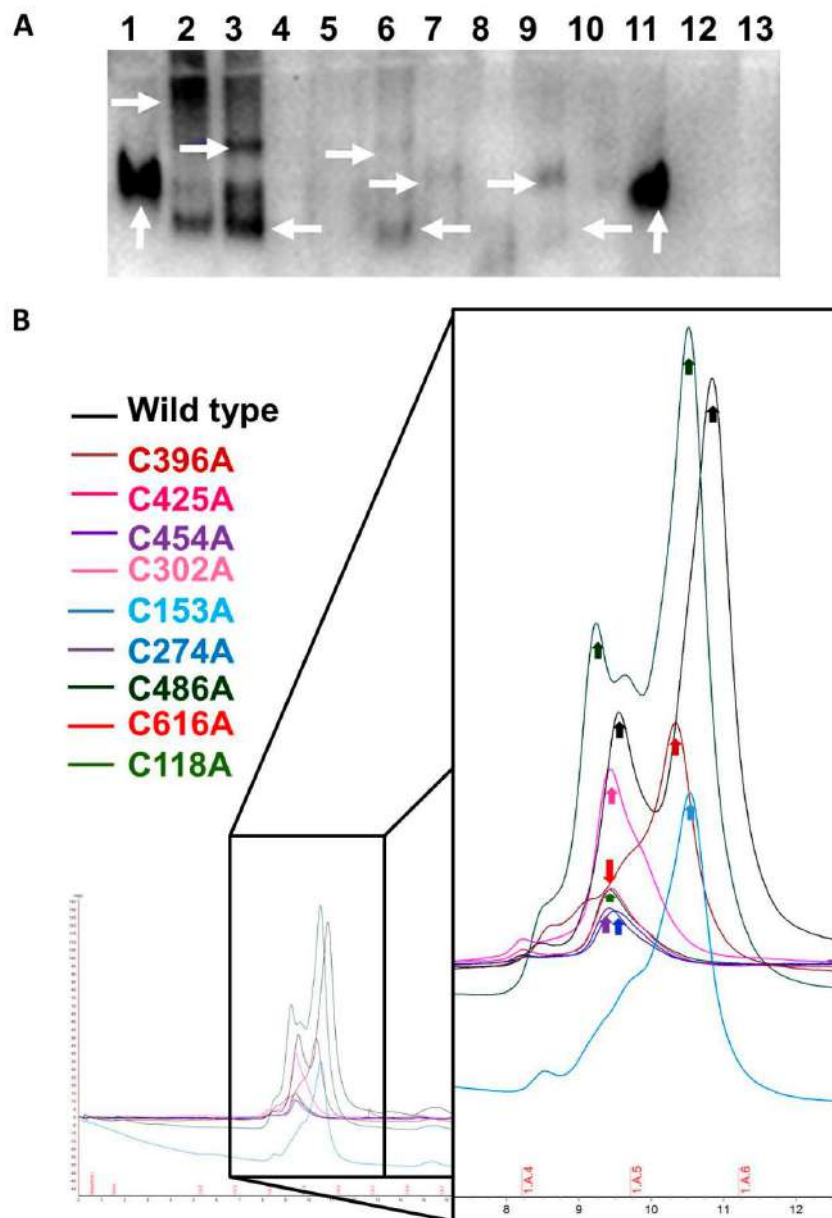


Figure 3. Altered complexation/Oligomerization of FXIII-B Cys mutants. **Panel A.** Western blot of rFXIII-B cysteine mutants after separation by native PAGE which were found to be secreted successfully (as detected by ELISA). Lanes: 1: Wild-Type; 2: C153A; 3: C118A; 4: C180A; 5: C267A; 6: C274A; 7: C396A; 8: C425A; 9: C454A; 10: C616A; and 11: rFXIII-B (Zedira, 75ng); 12: C302A. Vertical white arrows represent the Wild-type and rFXIII-B (Zedira GmbH, Darmstadt, Germany), whereas horizontal white arrows here indicate the diverse mobility of protein bands corresponding to FXIII-B (since the western blot has been probed with the mouse to human FXIII-B antibodies) **Panel B.** Gel-filtration chromatography of purified FXIII-B cysteine mutants. Color codes represent respective mutants indicated as inset in the figure. The x-axis denotes retention volume [ml], and the y-axis represents the amount of protein in mAU (UV-280nm).

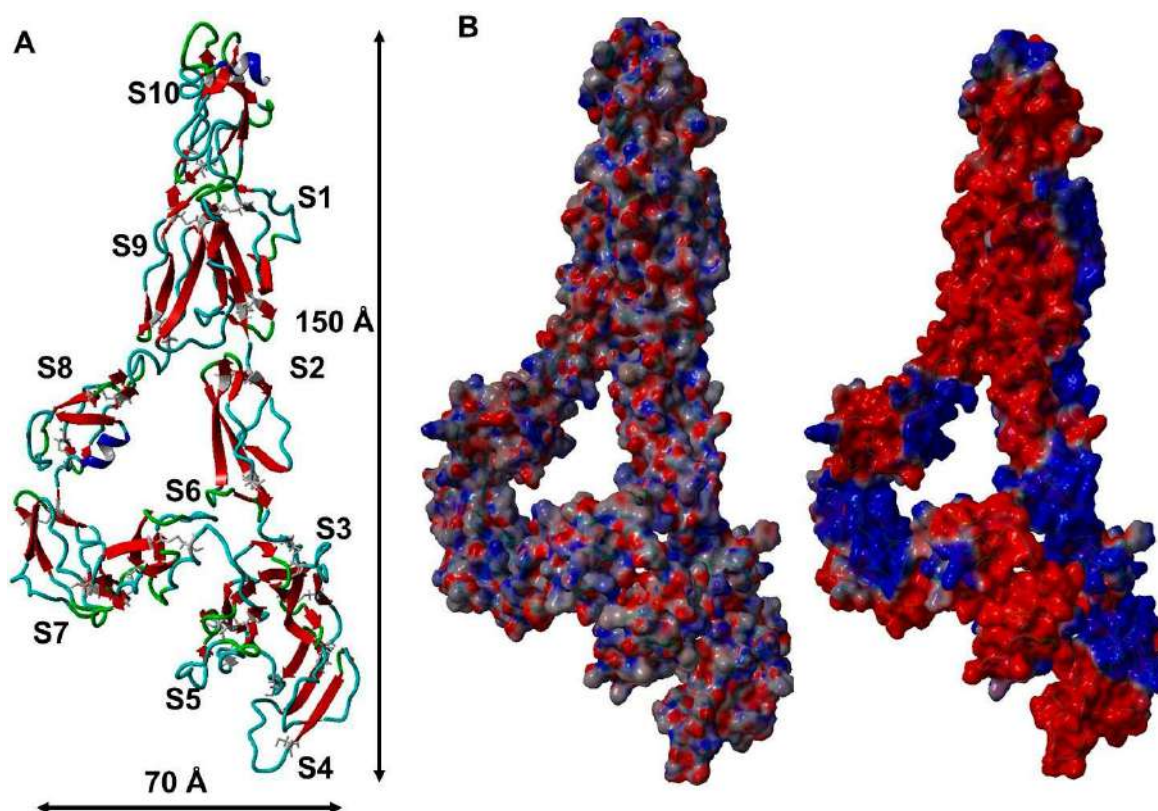


Figure 4. The FXIII-B subunit monomer model. **Panel A** shows the FXIII-B subunit monomer post-equilibrated model structure in ribbon format. The backbone is colored based on secondary structure. The disulfide-bonded cysteines are represented as grey colored stick forms. The individual sushi domains are numbered S1 to S10; N to C terminal. **Panel B** is the electrostatic surface representation of the FXIII-B subunit monomer model. The left side of Panel B shows the PBS styled depiction of surface electrostatics while the right side shows the PME styled depiction of surface electrostatic. Calculation and depiction for both forms of electrostatics were performed with macros embedded in YASARA. Red color indicates negative potential while blue represents positive potential.

2.5. The FXIII-B Subunit Disulfide Bonds Display Variability in Structural Flexibility, but Ablation of any of These Bonds Leads to a Loss in Stability

The disulfide bonds of the FXIII-B subunit monomer model displayed variability in bond length and dihedral energy during the production phase. The disulfide bonds showed bond length variability between 1.95–2.09 Å during their thermal motion which is typical of structural disulfide bonds [31]. The maximum bond length was observed for Cys153–Cys197 (2.06 ± 0.05 Å) of S3 sushi domain during the production phase (Figure 5A). All disulfide bonds were typically right handed and left handed spiral forms which is also typical of structural disulfide bonds. The dihedral energies (or dihedral strain energies) for C-terminal disulfide bonds of sushi domains S8, S9 and S10, i.e., Cys were observed to be the highest amongst all disulfide bonds and also showed a high degree of variability (22.07 ± 5.41 , 25.21 ± 5.01 , and 30.21 ± 16.26 kJ/mol, respectively) (Figure 5B). The change in free energy upon ablation of all disulfide bonds indicated a loss in stability with the highest loss in stability observed for the C180A variant present on S3 sushi domain (Figure 5C; $\Delta\Delta G = 0.73 \pm 0.11$).

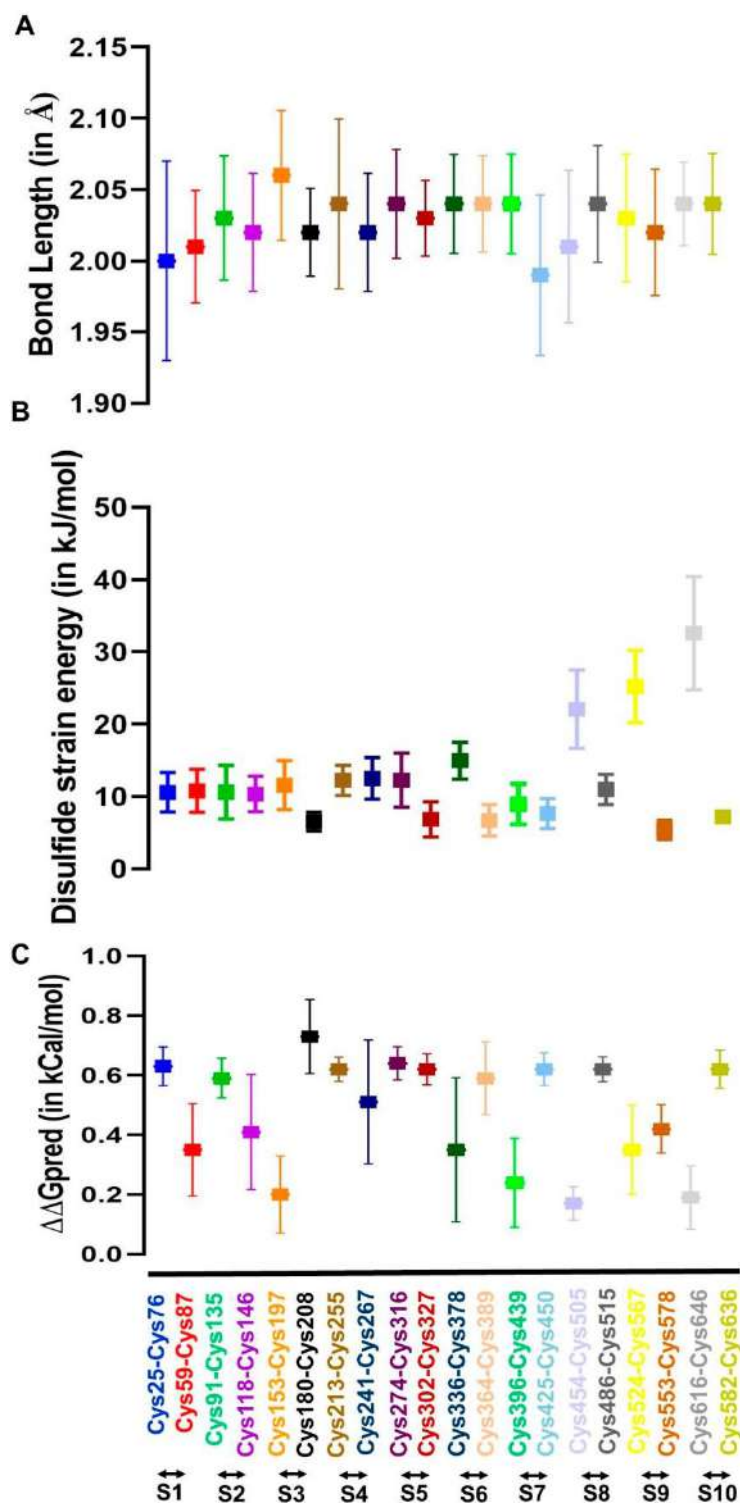


Figure 5. Evaluation of flexibility and stability of the disulfide bonds in the FXIII-B subunit monomer model. **Panel A** shows the variation in disulfide bond lengths during the simulation post equilibration of the FXIII-B subunit monomer model. **Panel B** shows the variation in disulfide strain energies of all disulfide bonds of the FXIII-B subunit monomer model during the MD simulation post-equilibration of the structure. **Panel C** shows the variability in free energy change when individual disulfide-bonded cysteines (the cysteines that have been mutated and expressed in this study) within the FXIII-B subunit monomer model are mutated to alanine. The evaluation was performed on several simulation trajectory structures (spaced at an interval of 20 ns) within the post-equilibrated simulation.

2.6. Disruption of Selected FXIII-B Disulfide Bonds can Affect the Rate of FXIII-Aa Generation

We had earlier demonstrated that spiking FXIII-B into FXIII-Aa generation assay could accelerate the generation of FXIII-Aa i.e., FXIII-A activation [2]. The recombinant wild type rFXIII-B subunit from this study also behaves similarly since we observe a jump of ~150% in the rate of FXIII-Aa generation/FXIII-A activation when the wild type recombinant was spiked into FXIII-Aa generation assay (rate of FXIII-Aa generation in the absence of FXIII-B: 151.05 Δ RFU/min; rate of FXIII-Aa generation when spiked with 10ng/mL of purified wild-type FXIII-B: 230.06 Δ RFU/min) (Figure 6) [2,23,32]. When spiked with mutants C118A, C274A, and C302A a milder effect on FXIII-A activation was observed when compared to spiking with the wild type rFXIII-B. Nevertheless, these three mutants still showed the rate of activation higher than the spiked sample. Spiking with mutants C396A and C454A show the same rate of FXIII-Aa generation as observed for the non FXIII-B spiked sample suggesting that these mutations completely abolish the accelerative effect of FXIII-B on FXIII-A activation. Spiking with C616A showed almost a similar effect on FXIII-Aa generation as that of the wild type, indicating that in spite of the disruption of the disulfide bond, the regulatory (accelerative) effect on FXIII-A is retained by this protein variant. Finally spiking with three mutants C153A, C180A and C486A contribute to a lowering of the rate of FXIII-Aa generation overall, i.e., even lower than that of non FXIII-B spiked sample. These mutants might be negatively regulating the activation of FXIII-A. Since only equal absolute amounts of each mutant, as well as wild type, were spiked into the assay, the observed effects can only be attributed to the functional effect of FXIII-B on the activation of FXIII-A and not to a quantitative effect, especially for the mutants. However, a major limitation of this aspect of our study is that we were not able to repeat this study multiple numbers of times to assign significance to the differences observed. This was especially owing to the poor overall yields and the degradation tendency for the mutants. However, the wild type FXIII-B was multiply spiked in the generation assay, and the differences observed with the mutations exceeded the variability observed for the wild type rFXIII-B.

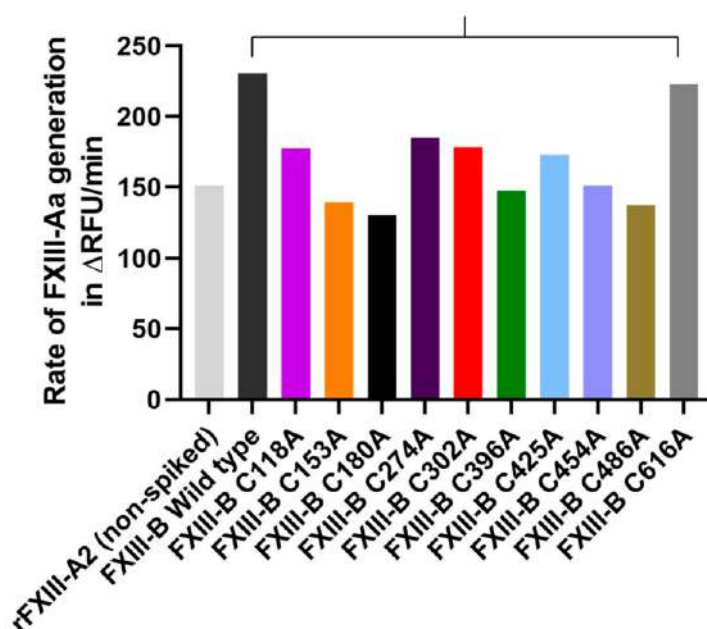


Figure 6. Effect of cysteine mutants on the rate of FXIII-Aa generation. This figure represents the comparative bar-plot representation of FXIII-Aa generation assay. The maximum rate of FXIII-Aa generation (μ) (in Δ RFU/min) upon spiking of FXIII-deficient plasma with 7 μ g/mL rFXIII-A₂ is represented in the x-axis, in the absence (grey bar), or presence (color-coded bars) of rFXIII-B₂ subunits or FXIII-B cysteine mutants (10 μ g/mL each).

3. Discussion

Disulfide bonds in the protein are primarily responsible for structural stability unless the nature of these disulfides is allosteric [33]. This is the reason why substitutive mutations resulting in their disruption often result in faulty proteins complicit in pathomolecular states. However, in proteins that contain multiple disulfide bonds, the effect of a single disulfide bond disruption might vary, depending on the position of that disulfide bond in the functional hierarchy of the protein. This means essentially that in multiple disulfide bonded proteins all disulfide bonds do not carry the same functional importance. The disulfide bonds themselves stabilize the domain/part of the protein that they are part of and by extension; their importance is contingent upon the role that the particular domain might play in the protein. Some domains/part of the protein might be rendered redundant during the course of evolution thereby also rendering the importance of the disulfides that they contain useless. Proteins containing multiple repetitive domains like sushi domain are examples in which functional hierarchy/diversity within disulfide bonds might exist. The FXIII-B subunit protein which is built from ten sushi domains, each of which contains two disulfide bonds displays such diversity. Mutations on these disulfide bonds have been reported in the two forms of congenital bleeding disorders associated with mutations in the FXIII-B subunit gene, i.e., the inherited severe FXIII deficiency and the mild FXIII deficiency [13,14]. The C430F (C450F; current nomenclature used in this study) mutation was detected in a 32 year old female patient with a bleeding tendency born of a consanguineous marriage [7,11]. The plasma of this patient showed no detectable levels of FXIII-B subunit. Additionally, FXIII-A subunit concentrate, when infused into this patient showed a significantly reduced half-life. The mutation C5R (C25R; current nomenclature used in this study) was detected in a female patient who reported bleeding symptoms post abdominal surgery. This patient showed simultaneous reduction of FXIII-A and FXIII-B subunit antigen levels, as well as of FXIII activity, below 50% of the normal, which is typical of mild FXIII deficiency. The mutation C316F (C336F; current nomenclature used in this study), was detected in two individuals, one male and one female, who reported epistaxis and hematoma in the neck post brain surgery, respectively. No antigenic levels were performed for these patients, however FXIII activity was demonstrated to be in the mild-FXIII deficiency range (20–60%). Our earlier investigations had shown that these mutations, although occurring on structural disulfides will have different degrees of severity of impact on the secreted protein [13]. Our current directed mutational investigation further substantiates this fact. When we disrupt the FXIII-B disulfide bonds one at a time, the effect on the secreted protein varies from mutant to mutant. A majority (12 out of 20) of them are non-secreting mutants, the ones showing secreted amounts of protein do so in significantly diminished amounts except for two mutations C118A and C153A which show close to 50% of the wild type protein (Figure 1). However, an overwhelmingly uniform observation made for all the mutants, secreted or not was their intracellular accumulation. All mutants showed intracellular accumulation and more specifically/commonly accumulation in the ER (Figure 2). Therefore, we conclude that mutating any structural disulfide bond within FXIII-B subunit would result in a secretion deficit. The mutants that were successfully secreted were observed to show an altered complexation pattern in gel filtration runs as well as with Native PAGE. Therefore, the disruption of the specific disulfide bonds either result in alteration of FXIII-B's physiological dimeric state or the presence of a reactive cysteine (the reduced cysteine partnering the mutated cysteine) results in the interaction of the mutant FXIII-B with other neighboring proteins (through new putative disulfide bonds). Amongst the successfully secreted mutants, half of them retained their accelerative effect of the rate of FXIII-A activation/FXIII-Aa generation (as observed for wild type FXIII-B) in spite of their low amounts (Figure 6). The fact that FXIII-B subunit can positively regulate (accelerate) the activation of FXIII-A subunit has already been reported in the recent past [2,23]. The remaining half showed either a complete abolition of this effect or a negative effect on the rate of FXIII-A activation/FXIII-Aa generation. Mutating specific FXIII-B cysteine's (check results and Figure 6) could, therefore, abolish the proteins regulatory effect on FXIII-A subunit or might even affect it negatively. However, in the context of the current experimentation performed, we cannot offer a mechanism by which these mutations might affect interaction/regulation

with/of FXIII-A subunit since this would require additional quantitative binding studies. Structurally, based on our analysis of the FXIII-B monomer model, differential structural flexibility of disulfide bonds across the FXIII-B subunit is a critical factor in determining its native fold as well as its putative interactions during dimerization/interaction with other proteins. The dihedral energies of the disulfide bonds (or disulfide strain energies) were particularly on the higher end and more variable towards the C-terminal of FXIII-B subunit. Therefore, the disulfide bonds at the C-terminal of the FXIII-B subunit appear to control the overall global flexibility of FXIII-B. The FXIII-B monomer model clearly shows distinct electrostatic patches which could play an important role in its dimerization or interaction with other proteins like the FXIII-A subunit (Figure 4). The global effect of disruption of individual disulfide bonds is likely mediated by the effect that this has on a) the local structural flexibility b) neighboring electrostatic patches. Consistent with our observations made from the expression of the cysteine mutants, the *in silico* analysis of these disulfide bonds also shows variability in effect on overall stability (free energy; $\Delta\Delta G$) (Figure 5C). To summarize, we conclude that all 20 FXIII-B subunit disulfide bonds are important to the structural stability, secretion, and function of the protein. However, these disulfide bonds do show structural and functional diversity as gauged from the variable effects we observed when we mutated them individually. In the inherited severe form of FXIII deficiency in which mutations in FXIII-B subunit are even rarer; it is difficult to conceive of detecting more cysteine mutants. Rather these cysteine mutants might exist in more preponderance in the inherited mild form of FXIII deficiency or heterozygous FXIII deficiency. Even in a heterozygous state, cysteine mutations can conceivably have a dominant negative effect, because, as observed in our study, the release of a reactive cysteine can open up the mutated variant to different interactions with another of its own subunit (during folding) or other proteins leading to change in complexation states (also observed in our study). This makes these disulfide bonds potential mutational hotspots in the mild form of this rare bleeding disorder.

4. Materials and Methods

4.1. Cell Lines and Cell Culture

The human HEK293t cell line was purchased from DSMZ German Collection of Microorganisms and Cell Cultures, (Braunschweig, Germany). All cells were cultured in high glucose DMEM (Life Technologies Europe BV, Bleiswijk, Netherlands), supplemented with 10% v/v FBS (Invitrogen), 1% v/v penicillin-streptomycin antibiotics and 0.1% v/v Fungizone (Life Technologies Europe BV, Bleiswijk, Netherlands), at 37 degrees in 5% CO₂ incubator. All experiments were performed on sub-cultured cells in the logarithmic phase (below passage 20).

4.2. Cloning and Expression of FXIII-B Cysteine to Alanine Mutants

Human *F13B* cDNA (ORF length 1986 bp) was inserted into the cloning site of pEZ-M01 vector (used as Wild type construct for all the following experiments). Site-directed mutagenesis was performed on the aforementioned construct, using GeneArt Site-directed mutagenesis system (Life Technologies, Carlsbad, CA, USA). Mutagenesis was performed with the aim of disrupting individual cysteine bonds present in every sushi domain (FXIII-B C59A, FXIII-B C76A, FXIII-B C91A, FXIII-B C118A, FXIII-B C153A, FXIII-B C180A, FXIII-B C213A, FXIII-B C267A, FXIII-B C274A, FXIII-B C302A, FXIII-B C364A, FXIII-B C378A, FXIII-B C396A, FXIII-B C425A, FXIII-B C454A, FXIII-B C486A, FXIII-B C524A, FXIII-B C553A, FXIII-B C582A, and FXIII-B C616A). All primers were synthesized by MWG Eurofins (MWG Eurofins GmbH, Ebersberg, Germany). All plasmid construct clones were completely sequenced and verified for the correct incorporation of mutation *in-house*. Wild type *F13B* cDNA and mutated DNA were transfected into mammalian HEK293T cells for transient expression. Briefly, 2.7×10^5 cells were transfected with 3 μ g of plasmid DNA along with 6 μ l of transfection reagent Lipofectamine 2000 (Invitrogen) following the manufacturer's protocol. The culture was harvested 48 h post-transfection. FXIII-B being a secretory protein, the culture medium (supernatant) was collected,

and centrifuged at 1000 g, for 5 min at 4 degrees. Additionally, to analyze intracellular contents, cellular lysis was performed using mammalian M-PER reagent (Thermo Fischer Scientific, Rockford, IL, USA) following the manufacturer's protocol. Cellular lysate was centrifuged at 13000 g, for 10 min at 4 degrees. Both intracellular and extracellular fractions were stored at -80 degrees until further use. The samples were verified for the antigenic presence of FXIII-B protein by ELISA and Western blot analysis.

4.3. Antigenic Quantification of FXIII-B Cysteine Mutants

FXIII-B antigen levels were determined, upon wild-type/mutants FXIII-B were quantified in culture supernatants (extracellular secreted FXIII-B) and cell lysates (intracellular FXIII-B) using the Technozym FXIII-B:Ag Sub ELISA kit (Technoclon GmbH, Vienna, Austria) according to the manufacturer's instructions. The standard assay detection limit was $0.95 \mu\text{g/mL}$; lower antigen concentrations to $0.009 \mu\text{g/mL}$ (sensitivity) were determined according to the manufacturer's dilution protocol. FXIII-B levels from normal pooled plasma and from high/low controls from the kit were measured as controls.

4.4. Western Blot Analyses

For antigenic estimation in extracellularly secreted FXIII-B protein in cysteine mutants, western blot was performed using $10 \mu\text{L}$ of crude supernatant. Briefly, an equal volume of total crude protein corresponding to Wild-type (positive control), Un-transfected control (negative control), and 20 cysteine mutants were separated on 4%–16% gradient SDS-PAGE (Bio-Rad Laboratories, Hercules CA, USA). Resolved proteins were transferred to PVDF membrane at 80V for 90 min in cold-room. The membrane was blocked for 1 h at room temperature in blocking reagent (3% w/v BSA in PBS with 0.05% Tween-20). Subsequently, after a wash with PBS-Tween-20 (0.05%), the membrane was incubated for 1 h at room temperature in Primary antibody (250ng/mL) (mouse-anti human FXIII-B monoclonal antibody, in-house generated in association with Eurogentec Deutschland GmbH, Cologne, Germany) with mild shaking. After washing thrice in PBS-Tween (0.05%), the membrane was incubated for 1 h at room temperature in HRP tagged Secondary antibody (50ng/mL) (Goat Anti-mouse IgG (H+L) Secondary antibody, HRP; Thermo Fischer Scientific, Carlsbad, CA, USA). Finally, the membrane was washed thrice in PBS-Tween 20, and PBS, respectively. Chemiluminescent signal quantification, Image acquisition (ChemiDoc MP, Bio-Rad) and densitometric evaluation of signal were performed on Image lab Software (Bio-Rad) version 4.1.

4.5. Confocal Immunofluorescence of Expressed FXIII-B Protein and its Cysteine Mutants

The HEK293t cells, transiently transfected for expression of FXIII-B protein, were subjected to immunofluorescence analyses to evaluate intracellular trafficking of wild-type vs. cysteine mutants of rFXIII-B protein. The mutants that exhibited no extracellular secretion and high intracellular retention as compared to wild-type in ELISA assessments were tested further. Briefly, 24 h post-transfection HEK-293T cells (grown on glass coverslips) were fixed using 4% (w/v) PFA in PBS, followed by blocking with 0.1% (v/v) Triton-X 100 in PBS azide supplemented with 10% (v/v) FBS, and immunostaining with first and secondary antibodies for 2 h and 1 h, respectively. Trafficking analyses were performed via cell-specific markers; FXIII-B subunit (mouse monoclonal IgG, in-house generated in association with Eurogentec, Belgium) and the cell compartments ER (IgG rabbit polyclonal anti-calnexin; Abcam, England) and Golgi (anti-TGN46 antibody produced in rabbit; Sigma-Aldrich, Saint Louis, MO, USA) Signal detection was performed using an IgG Alexa Fluor 488 conjugated goat anti-mouse IgG (H+L) secondary antibody (Life technologies, Carlsbad, CA, USA) against the FXIII-B subunit and an IgG Alexa Fluor 594 conjugated goat anti-rabbit IgG (H+L) secondary antibody (Life technologies, Carlsbad, CA, USA) against the ER and Golgi compartment. The coverslips were mounted onto microscope slides with Vectashield antifade mounting medium (Vector Labs, Burlingame, CA, USA) and analyzed with the Olympus Fluo View FV1000 or Leica SL confocal microscope. The comparative degree of colocalization for wild type versus mutants was calculated as mean Pearson's correlation coefficient

in ImageJ software. A minimum number of $n = 10$ regions of interests were extracted from the micrographs to calculate the degree of colocalization.

4.6. Native-PAGE-blot Analysis of Expressed FXIII-B Protein and its Cysteine Mutants

In order to track the oligomeric state of successfully secreted FXIII-B cysteine mutants (detected by conventional western blot and ELISA), non-denaturing Native-PAGE was performed (Life Technologies Europe BV, Bleiswijk, Netherlands) as per manufacturer's guidelines (only for the mutants reflecting wider bands in Western blots above) (Figure 3A). Briefly, samples were prepared using the BN Sample buffer (Life Technologies Europe BV, Bleiswijk, Netherlands). After electrophoretic separation, the gel was placed in 2X NuPAGE Transfer buffer (Life Technologies, Carlsbad, CA, USA) for 10 min at RT. Subsequently, protein transfer to PVDF membrane was performed at 60V for 90 min in cold-room, followed by blotting (as Western blot procedure mentioned above).

4.7. Purification of Wild Type FXIII-B and its Cysteine Mutants

Secreted protein harvested post transfection of HEK293T cells, was concentrated 15-20 times, using Amicon ultra-filters (Cut-off 30,000Da, Merck, Darmstadt, Germany) and was subjected to immuno-affinity based purification using the Thermo Scientific Pierce Co-IP kit (Pierce Biotechnology, Rockford, IL, USA) following the manufacturer's protocol. Briefly, mouse monoclonal antibodies against human FXIII-B (generated in-house in association with Eurogentec Deutschland GmbH, Cologne, Germany) were immobilized to Amino-Link plus coupling resin, for 2 h at room temperature. The resin was then washed and incubated with transfected HEK293T cellular medium concentrates (with the detected antigenic presence of FXIII-B protein (Figure 3A)) overnight in cold-room. Next day, the resin was washed, and protein bound to anti-FXIII-B antibody was eluted. Eluted protein was further subjected to gel filtration chromatography, to ensure its purity and to characterize the oligomeric association of secreted protein upon mutation in comparison to wild-type (Figure 3B). Gel filtration chromatography was performed on Äkta Pure protein purifier system, using Superdex®200 Increase column (GE healthcare UK Ltd, England, UK). All purifications were performed in a cold room, on a column pre-equilibrated with PBS, pH 7.4 (flow rate 400 μ L/min). The comparative oligomeric state of wild-type versus mutant proteins was calculated on the basis of peak retention time for each mutant vs. wild-type FXIII-B.

4.8. In Silico Analysis of FXIII-B Subunit Disulfide Bonds

In the absence of a biophysical structure for the FXIII-B subunit, we generated a full-length monomer model of the FXIII-B subunit. The model was built by assembling previously reported high quality threaded models of all ten FXIII-B subunit sushi domains on the AIDA domain assembly server (<http://aida.godziklab.org/>) (accessed on November 19th, 2018). in default mode, i.e., without any constraint [16,34]. The model was initially subjected to 500 ps of refinement MD simulation using the macro md_refine embedded in YASARA [35,36]. This macro uses YAMBER3 force field parameters in YASARA in order to remove steric clashes and improve rotamer geometry [37]. The structure with the lowest energy in the simulation trajectory was chosen for conducting further simulations. This structure was then subjected to all-atom unrestrained MD simulation using the md_sim macro embedded in YASARA. Briefly, a simulation cell with periodic boundaries and 20 Å minimum distances to protein atoms was employed with explicit solvent. The AMBER03 force field, NPT ensemble was used with long range PME potential and a cut-off of 7.86 Å [38]. Hydrogen bond networks were optimized using the method of Hooft and co-workers [39]. The simulation cell was filled with water at a density of 0.997 g/mL and a maximum sum of all bumps per water of 1.0 Å. The simulation cell net charge was neutralized with a final 0.9% (wt/vol) NaCl concentration. The entire system was energy minimized by steepest descent to remove conformation stress within the structure, followed by simulated annealing minimization until convergence was achieved. The MD simulation was performed at a temperature of 298 K. Simulation was run for ~500 ns (including the time needed to equilibrate). Electrostatic surface

potential was calculated and graphically depicted using the Adaptive Poisson-Boltzmann Solver integrated within YASARA [35]. The structural flexibility of the FXIII-B subunit disulfide bonds in the monomer model was analyzed on simulation trajectory snapshots captured per 250 ps in the production phase (i.e., post-equilibration). Each of these snapshots was converted to PDB format before submission to the Disulfide Bond Dihedral Angle Energy Server (<https://services.mbi.ucla.edu/disulfide/>) (accessed on February 7th, 2019). for evaluation of the disulfide bonds. This server calculates the dihedral angles of all disulfide bonds found in the uploaded structure PDB file. Based on these angles, dihedral energy (disulfide strain energy) is calculated according to an empirical formula first defined by Katz et al. [40]. In addition to disulfide strain energies, disulfide bond length variations for all uploaded structures were also evaluated on this server. The change in free energy (i.e., loss or gain of stability) for each disulfide bond was calculated on the MAESTROweb server (<https://biwww.che.sbg.ac.at/maestro/web/maestro>) ((accessed on February 7th, 2019).) by uploading the PDB file of the final simulation snapshot in the production phase (i.e., equilibrated structure) [41]. This server predicts the change in free energy ($\Delta\Delta G$) values along with a corresponding prediction quality measure for a single or list of mutations corresponding to the uploaded structure is specified. Positive $\Delta\Delta G$ values indicate loss of stability, while negative indicate a gain of stability. The prediction quality measure varies between 0 and 1, with values approaching 1 indicating a reliable prediction.

4.9. Effect of Spiking Wild Type FXIII-B and Its Cysteine Variants into the FXIII-Aa Generation Assay

FXIII-Aa generation was triggered by tissue factor/phospholipids (TF/PL), and FXIII-A isopeptidase activity was measured using the fluorogenic substrate A101 (Zedira GmbH, Darmstadt, Germany) in a Safire microtiter plate reader (Tecan, Crailsheim, Germany). Twenty microliters FXIII-deficient plasma (deficient for FXIII-A₂ and FXIII-B₂; Haemochrom Diagnostica GmbH, Essen, Germany) spiked with rFXIII-A₂ (7 µg/mL), and purified rFXIII-B₂-mutants (10 µg/mL) were incubated with 55 µL reagent solution (5 µL 100 mM glycine methyl ester, 5 µL 2 mM fluorogenic FXIII-A substrate, 10 µL phospholipids (Rossix, Mölndal, Sweden) diluted 1:10 in HBS, and 35 µL HBS (20 mM Hepes, 150 mM NaCl)/0.1% serum albumin pH 7.5. After pre-incubation of the mixture for 5 min, the reaction was started with 20 µL Innovin (recombinant TF, Dade Behring, Marburg, Germany) 1:1400 diluted in HBS, 50 mM CaCl₂ pH 7.5. Fluorescence was measured over 1 h at $\lambda_{ex} = 330$ nm and $\lambda_{em} = 430$ nm in kinetic mode two-times per minute. Data were analyzed based on growth-curve analyses, with the slope of the curve (μ) representing the growth rate [32]. Data were fitted using R-package “grofit”, based on the dose-response relationship [42]. Non-parametric spline estimation was done to fit the data, and to obtain characteristic parameters lag phase tlag, maximal growth rate μ , Area under curve A, and maximal time to peak tmax) derived from a single growth curve.

5. Statistical Analyses

Comparisons of means were performed using a non-parametric Mann-Whitney's t-test. All statistical analyses were performed in Graphpad Prism (Version 8.0.2). Details for curve fitting for FXIII-Aa generation assay are provided under the method section of FXIII-Aa generation assay.

Supplementary Materials: Supplementary materials can be found at <http://www.mdpi.com/1422-0067/20/8/1956/s1>.

Author Contributions: A.B. conceived and designed the project. S.S., M.S.A. and A.S. performed the expression analysis. J.D. performed generation assays. S.S. and S.K. performed protein purification. S.S. and H.Y. did the confocal microscopy. A.B. performed the in silico analyses. S.S. and A.B. co-wrote the manuscript. V.I. and J.O. read and edited the manuscript. All authors critically reviewed the manuscript.

Funding: This research received no external funding.

Acknowledgments: Authors would like to thank ISTH Reach the world fellowship for position of Amit Sharma, who worked as guest scientist from AIIMS, India in this project.

Conflicts of Interest: The authors declare no conflict of interest.

References

1. Biswas, A.; Ivaskevicius, V.; Thomas, A.; Oldenburg, J. Coagulation factor XIII deficiency. Diagnosis, prevalence and management of inherited and acquired forms. *Hamostaseologie* **2014**, *34*, 160–166. [[PubMed](#)]
2. Gupta, S.; Biswas, A.; Akhter, M.S.; Krettler, C.; Reinhart, C.; Dodt, J.; Reuter, A.; Philippou, H.; Ivaskevicius, V.; Oldenburg, J. Revisiting the mechanism of coagulation factor XIII activation and regulation from a structure/functional perspective. *Sci. Rep.* **2016**, *6*, 30105.
3. Duckert, F.; Jung, E.; Shmerling, D.H. A hitherto undescribed congenital haemorrhagic diathesis probably due to fibrin stabilizing factor deficiency. *Thromb. et Diath. Haemorrh.* **1960**, *5*, 179–186. [[CrossRef](#)]
4. Seitz, R.; Duckert, F.; Lopaciuk, S.; Muszbek, L.; Rodeghiero, F.; Seligsohn, U. ETRO Working Party on Factor XIII questionnaire on congenital factor XIII deficiency in Europe: Status and perspectives. Study Group. *Semin. Thromb. and Hemost.* **1996**, *22*, 415–418. [[CrossRef](#)]
5. Biswas, A.; Ivaskevicius, V.; Seitz, R.; Thomas, A.; Oldenburg, J. An update of the mutation profile of Factor 13 A and B genes. *Blood Rev.* **2011**, *25*, 193–204. [[CrossRef](#)] [[PubMed](#)]
6. Hashiguchi, T.; Ichinose, A. Molecular and cellular basis of deficiency of the b subunit for factor XIII secondary to a Cys430-Phe mutation in the seventh Sushi domain. *J. Clin. Investig.* **1995**, *95*, 1002–1008. [[CrossRef](#)]
7. Hashiguchi, T.; Saito, M.; Morishita, E.; Matsuda, T.; Ichinose, A. Two genetic defects in a patient with complete deficiency of the b-subunit for coagulation factor XIII. *Blood* **1993**, *82*, 145–150. [[PubMed](#)]
8. Izumi, T.; Hashiguchi, T.; Castaman, G.; Tosetto, A.; Rodeghiero, F.; Girolami, A.; Ichinose, A. Type I factor XIII deficiency is caused by a genetic defect of its b subunit: Insertion of triplet AAC in exon III leads to premature termination in the second Sushi domain. *Blood* **1996**, *87*, 2769–2774.
9. Souri, M.; Izumi, T.; Higashi, Y.; Girolami, A.; Ichinose, A. A founder effect is proposed for factor XIII B subunit deficiency caused by the insertion of triplet AAC in exon III encoding the second Sushi domain. *Thromb. Haemost.* **1998**, *80*, 211–213. [[CrossRef](#)]
10. Wada, H.; Souri, M.; Matsumoto, R.; Sugihara, T.; Ichinose, A. Alloantibodies against the B subunit of plasma factor XIII developed in its congenital deficiency. *Thromb. Haemost.* **2013**, *109*, 661–668. [[PubMed](#)]
11. Saito, M.; Asakura, H.; Yoshida, T.; Ito, K.; Okafuji, K.; Matsuda, T. A familial factor XIII subunit B deficiency. *Br. J. Haematol.* **1990**, *74*, 290–294. [[CrossRef](#)] [[PubMed](#)]
12. Tahlan, A.; Ahluwalia, J. Factor XIII: Congenital deficiency factor XIII, acquired deficiency, factor XIII A-subunit, and factor XIII B-subunit. *Arch. Pathol. Lab. Med.* **2014**, *138*, 278–281. [[CrossRef](#)] [[PubMed](#)]
13. Ivaskevicius, V.; Biswas, A.; Loreth, R.; Schroeder, V.; Ohlenforst, S.; Rott, H.; Krause, M.; Kohler, H.-P.; Scharrer, I.; Oldenburg, J. Mutations affecting disulphide bonds contribute to a fairly common prevalence of F13B gene defects: Results of a genetic study in 14 families with factor XIII B deficiency. *Haemophilia* **2010**, *16*, 675–682.
14. Thomas, A.; Biswas, A.; Ivaskevicius, V.; Oldenburg, J. Structural and functional influences of coagulation factor XIII subunit B heterozygous missense mutants. *Mol. Genet. Genom. Med.* **2015**, *3*, 258–271. [[CrossRef](#)]
15. Ivaskevicius, V.; Windyga, J.; Baran, B.; Schroeder, V.; Junen, J.; Bykowska, K.; Seifried, E.; Kohler, H.P.; Oldenburg, J. Phenotype-genotype correlation in eight Polish patients with inherited Factor XIII deficiency: Identification of three novel mutations. *Haemophilia* **2007**, *13*, 649–657. [[CrossRef](#)]
16. Biswas, A.; Thomas, A.; Bevans, C.G.; Ivaskevicius, V.; Oldenburg, J. In vitro secretion deficits are common among human coagulation factor XIII subunit B missense mutants: Correlations with patient phenotypes and molecular models. *Hum. Mutat.* **2013**, *34*, 1490–1500. [[CrossRef](#)] [[PubMed](#)]
17. Souri, M.; Kaetsu, H.; Ichinose, A. Sushi domains in the B subunit of factor XIII responsible for oligomer assembly. *Biochemistry* **2008**, *47*, 8656–8664. [[CrossRef](#)]
18. Schroeder, V.; Kohler, H.P. Factor XIII: Structure and Function. *Semin. Thromb. Hemost.* **2016**, *42*, 422–428.
19. Nagy, J.A.; Henriksson, P.; McDonagh, J. Biosynthesis of factor XIII B subunit by human hepatoma cell lines. *Blood* **1986**, *68*, 1272–1279.
20. Komaromi, I.; Bagoly, Z.; Muszbek, L. Factor XIII: Novel structural and functional aspects. *J. Thromb. Haemost. JTH* **2011**, *9*, 9–20. [[CrossRef](#)]
21. Venter, J.C.; Adams, M.D.; Myers, E.W.; Li, P.W.; Mural, R.J.; Sutton, G.G.; Smith, H.O.; Yandell, M.; Evans, C.A.; Holt, R.A.; et al. The sequence of the human genome. *Science (New York, N.Y.)* **2001**, *291*, 1304–1351. [[CrossRef](#)]
22. Norman, D.G.; Barlow, P.N.; Baron, M.; Day, A.J.; Sim, R.B.; Campbell, I.D. Three-dimensional structure of a complement control protein module in solution. *J. Mol. Biol.* **1991**, *219*, 717–725. [[CrossRef](#)]

23. Souri, M.; Osaki, T.; Ichinose, A. The Non-catalytic B Subunit of Coagulation Factor XIII Accelerates Fibrin Cross-linking. *J. Biol. Chem.* **2015**, *290*, 12027–12039. [[CrossRef](#)]
24. Byrnes, J.R.; Wilson, C.; Boutelle, A.M.; Brandner, C.B.; Flick, M.J.; Philippou, H.; Wolberg, A.S. The interaction between fibrinogen and zymogen FXIII-A2B2 is mediated by fibrinogen residues gamma390-396 and the FXIII-B subunits. *Blood* **2016**, *128*, 1969–1978. [[CrossRef](#)]
25. HOGG, P.J. Contribution of allosteric disulfide bonds to regulation of hemostasis. *J. Thromb. Haemost.* **2009**, *7*, 13–16. [[CrossRef](#)]
26. Carrell, N.A.; Erickson, H.P.; McDonagh, J. Electron microscopy and hydrodynamic properties of factor XIII subunits. *J. of Biol. Chem.* **1989**, *264*, 551–556.
27. Katona, E.; Penzes, K.; Csapo, A.; Fazakas, F.; Udvardy, M.L.; Bagoly, Z.; Orosz, Z.Z.; Muszbek, L. Interaction of factor XIII subunits. *Blood* **2014**, *123*, 1757–1763. [[CrossRef](#)]
28. Geva, Y.; Schuldiner, M. The back and forth of cargo exit from the endoplasmic reticulum. *Curr. Biol.* **2014**, *24*, 130–136. [[CrossRef](#)]
29. Aslam, M.; Perkins, S.J. Folded-back solution structure of monomeric factor H of human complement by synchrotron X-ray and neutron scattering, analytical ultracentrifugation and constrained molecular modelling. *J. Mol. Biol.* **2001**, *309*, 1117–1138. [[CrossRef](#)]
30. Okemefuna, A.I.; Nan, R.; Gor, J.; Perkins, S.J. Electrostatic interactions contribute to the folded-back conformation of wild type human factor H. *J. Mol. Biol.* **2009**, *391*, 98–118. [[CrossRef](#)]
31. Sevier, C.S.; Kaiser, C.A. Formation and transfer of disulphide bonds in living cells. *Nature reviews. Mol. Cell Biol.* **2002**, *3*, 836–847.
32. Dodt, J.; Volkers, P.; Seitz, R. Factor XIIIa generation assay: A tool for studying factor XIII function in plasma. *Anal. Biochem.* **2013**, *439*, 145–151. [[CrossRef](#)]
33. Chiu, J.; Hogg, P.J. Allosteric disulfides: Sophisticated molecular structures enabling flexible protein regulation. *J. Biol. Chem.* **2019**, *294*, 2949–2960. [[CrossRef](#)]
34. Xu, D.; Jaroszewski, L.; Li, Z.; Godzik, A. AIDA: Ab initio domain assembly server. *Nucleic Acids Res.* **2014**, *42*, W308–W313. [[CrossRef](#)]
35. Krieger, E.; Vriend, G. YASARA View - molecular graphics for all devices - from smartphones to workstations. *Bioinformatics (Oxford, England)* **2014**, *30*, 2981–2982. [[CrossRef](#)]
36. Krieger, E.; Koraimann, G.; Vriend, G. Increasing the precision of comparative models with YASARA NOVA—a self-parameterizing force field. *Proteins* **2002**, *47*, 393–402. [[CrossRef](#)]
37. Krieger, E.; Darden, T.; Nabuurs, S.B.; Finkelstein, A.; Vriend, G. Making optimal use of empirical energy functions: Force-field parameterization in crystal space. *Proteins* **2004**, *57*, 678–683. [[CrossRef](#)]
38. Duan, Y.; Wu, C.; Chowdhury, S.; Lee, M.C.; Xiong, G.; Zhang, W.; Yang, R.; Cieplak, P.; Luo, R.; Lee, T.; et al. A point-charge force field for molecular mechanics simulations of proteins based on condensed-phase quantum mechanical calculations: Amber Force Field. *J. Comput. Chem.* **2003**, *24*, 1999–2012. [[CrossRef](#)]
39. Hooft, R.W.; Vriend, G.; Sander, C.; Abola, E.E. Errors in protein structures. *Nature* **1996**, *381*, 272. [[CrossRef](#)]
40. Katz, B.A.; Kosiakoff, A. The crystallographically determined structures of atypical strained disulfides engineered into subtilisin. *J. Biol. Chem.* **1986**, *261*, 15480–15485.
41. Laimer, J.; Hofer, H.; Fritz, M.; Wegenkittl, S.; Lackner, P. MAESTRO—multi agent stability prediction upon point mutations. *BMC Bioinform.* **2015**, *16*, 116. [[CrossRef](#)] [[PubMed](#)]
42. Kahm, M.; Hasenbrink, G.; Lichtenberg-Fraté, H.; Ludwig, J.; Kschischo, M. grofit: Fitting Biological Growth Curves with R. *J. Stat. Softw.* **2010**, *33*, 7–10.



© 2019 by the authors. Licensee MDPI, Basel, Switzerland. This article is an open access article distributed under the terms and conditions of the Creative Commons Attribution (CC BY) license (<http://creativecommons.org/licenses/by/4.0/>).

Chapter 6

Accepted Article

The plasma Factor XIII heterotetrameric complex structure: unexpected unequal pairing within a symmetric complex

Sneha Singh, Alexis Nazabal, Senthilvelrajan Kanniyappan, Jean-Luc Pellequer, Alisa S. Wolberg, Diana Imhof, Johannes Oldenburg & Arijit Biswas

A brief synopsis:

Recollecting the conclusions derived from the former chapters as well as the recent findings on FXIII reported by other research groups, this chapter aimed at deriving the first full-atom structural model of FXIII-A₂B₂ heterotetramer complex, as found in plasma. As much is known both structurally, and functionally about the individual subunits so far by the former studies; in this chapter we aim at the plasma FXIII complex, its complex interface, subunit assembly, activation and ultimately how this complex interface can act as a potential driver of unexplained FXIII-deficient states ranging from mild to severe FXIII deficiency. The structural model of FXIII complex presented in this chapter demonstrates; a) How integrative hybrid approaches are useful for structural characterization of native plasma complexes; b) There exists an unequal pairing among FXIII-B subunit monomers to FXIII-A₂ dimer, forming FXIII-A₂B₂ complex; that influences both the association and activation of plasma FXIII; c) Thermodynamic patterns corresponding to subunit interaction and complex activation reveal that both the events are step-wise processes. This chapter hence provides the first atomic basis on which putative inhibitors can be designed and tested. The ideas on assembly and disassembly of the complex would require further biochemical validation but represent interesting starting points for research into the conformational changes occurring during these events.

Biomolecules. 2019 Dec; 9(12): 765. doi: 10.3390/biom9120765

Article

The Plasma Factor XIII Heterotetrameric Complex Structure: Unexpected Unequal Pairing within a Symmetric Complex

Sneha Singh ¹, Alexis Nazabal ², Senthilvelrajan Kaniyappan ³, Jean-Luc Pellequer ⁴ 
 Alisa S. Wolberg ⁵ , Diana Imhof ⁶, Johannes Oldenburg ¹ and Arijit Biswas ^{1,*} 

¹ Institute of Experimental Hematology and Transfusion medicine, University Hospital of Bonn, Sigmund-Freud Street 25, 53127 Bonn, Germany; Sneha.Gupta@ukbonn.de (S.S.); Johannes.Oldenburg@ukbonn.de (J.O.)

² CovalX, Schützengasse 2, CH-8001 Zürich, Switzerland; alexis.nazabal@covalx.com

³ German Center for Neurodegenerative Diseases (DZNE), Sigmund-Freud-Str. 27, 53127 Bonn, Germany; Senthil.Kaniyappan@dzne.de

⁴ Univ. Grenoble Alpes, CEA, CNRS, IBS, F-38000 Grenoble, France; jean-luc.pellequer@ibs.fr

⁵ Department of Pathology and Laboratory Medicine and UNC Blood Research Center, University of North Carolina at Chapel Hill, 8018A Mary Ellen Jones Building, Chapel Hill, NC 27599-7035, USA; alisa_wolberg@med.unc.edu

⁶ Pharmaceutical Biochemistry and Bioanalytics, Pharmaceutical Institute, University of Bonn, An der Immenburg 4, 53121 Bonn, Germany; dimhof@uni-bonn.de

* Correspondence: arijit.biswas@ukb.uni-bonn.de; Tel.: +49-228-2871-9428; Fax: +49-228-2871-6087 Received:

25 October 2019; Accepted: 19 November 2019; Published: 21 November 2019



Abstract: Factor XIII (FXIII) is a predominant determinant of clot stability, strength, and composition. Plasma FXIII circulates as a pro-transglutaminase with two catalytic A subunits and two carrier-protective B subunits in a heterotetramer (FXIII-A₂B₂). FXIII-A₂ and -B₂ subunits are synthesized separately and then assembled in plasma. Following proteolytic activation by thrombin and calcium-mediated dissociation of the B subunits, activated FXIII (FXIIIa) covalently cross links fibrin, promoting clot stability. The zymogen and active states of the FXIII-A subunits have been structurally characterized; however, the structure of FXIII-B subunits and the FXIII-A₂B₂ complex have remained elusive. Using integrative hybrid approaches including atomic force microscopy, cross-linking mass spectrometry, and computational approaches, we have constructed the first all-atom model of the FXIII-A₂B₂ complex. We also used molecular dynamics simulations in combination with isothermal titration calorimetry to characterize FXIII-A₂B₂ assembly, activation, and dissociation. Our data reveal unequal pairing of individual subunit monomers in an otherwise symmetric complex, and suggest this unusual structure is critical for both assembly and activation of this complex. Our findings enhance understanding of mechanisms associating FXIII-A₂B₂ mutations with disease and have important implications for the rational design of molecules to alter FXIII assembly or activity to reduce bleeding and thrombotic complications.

Keywords: coagulation factor XIII complex; threaded modeling; cross-linking mass spectrometry; HADDOCK flexible docking; molecular dynamics simulation; atomic force microscopy; isothermal titration calorimetry

1. Introduction

Plasma coagulation factor XIII (FXIII) circulates as a heterotetramer composed of two catalytic FXIII-A subunits tightly-associated (10^{-7} – 10^{-9} M) with two carrier/regulatory FXIII-B subunits

(FXIII-A₂B₂) [1,2]. During coagulation, proteolytic activation by thrombin and calcium-mediated dissociation of FXIII-B subunit generates activated FXIII-A (FXIIIa) that covalently cross links fibrin, promoting clot stability [3]. Deficiency in plasma FXIII antigen or activity is associated with mild-to-severe bleeding [3]. The structure of the catalytic FXIII-A subunits is well-characterized, consisting of an activation peptide (FXIII-AP, residues 1–37) followed by four distinct domains: β -sandwich (residues 38–183), central core (residues 184–515), β -barrel-1 (residues 516–627), and β -barrel-2 (residues 628–731) [4]. Both zymogen and activated forms of FXIII-A have been crystallized [4,5], revealing a compact structure of zymogen FXIII-A₂, but an open, extended conformation of activated FXIIIa. Despite the essential regulatory role of FXIII-B, structural information on this molecule is sparse. Sequence homology with complement proteins suggest each FXIII-B subunit is composed of ten sushi domains, each containing ~60 amino acid residues and two disulfide bonds [6]. Although sedimentation analysis initially suggested FXIII-B is a monomer, more recent data suggest FXIII-B circulates as a dimer [6,7]. Sushi domains 4 and 9 (S4 and S9) are thought to mediate FXIII-B₂ dimerization, whereas S1 and S2 are thought to promote interactions with the FXIII-A subunits [1,6]. The size and complexity of FXIII-A₂B₂ make it difficult to characterize by traditional methods such as X-ray crystallography or NMR. Apart from a partial all-atom model generated with minimal experimental data [8], there is no detailed model for the FXIII-B₂ dimer or the FXIII-A₂B₂ complex. Consequently, knowledge of the structural interface between FXIII-B subunits or the FXIII-A₂B₂ heterotetramer is incomplete. Structural resolution of plasma FXIII-A₂B₂ and its transition to activated FXIIIa is essential for defining implications of missense FXIII mutations, as well as the development of potential FXIII(a) inhibitors for treating bleeding and thrombotic complications associated with abnormal clot stabilization.

Integrative/hybrid (IH) approaches are useful for dissecting the structural architecture of complexes that escape traditional structural determination techniques [9,10]. These approaches integrate biochemical and computed data to yield structural information on macromolecular complexes. For example, IH has revealed detailed molecular conformational states of glucagon receptor [11] and the chromatin remodeling complex [12], and recently a combination of structural methods with atomic force microscopy (AFM) has provided key information on factor Va bound to activated protein C [13]. Since FXIII-A₂B₂ has not been amenable to traditional structural analysis, we addressed this gap using a bootstrapped IH approach. We first used atomic force microscopy to define the macromolecular structure of the FXIII subunits individually and as a complex, and chemical cross-linking and mass spectrometry (XL-MS) to define residues in the FXIII-A₂B₂ inter-subunit interface. We then used these data as structural constraints to assemble, first, a monomeric FXIII-B subunit model followed by an all-atom structural model of the FXIII-A₂B₂ complex. We then overlaid these putative models on surface topographic atomic force micrographs of FXIII-A₂B₂ to produce a complete macromolecular structure [10]. Finally, we integrated molecular simulations from the all-atom model with ITC (isothermal titration calorimetry) to interrogate conformational thermodynamics during FXIII-A₂B₂ assembly, activation, and subunit disassociation. Our data indicate FXIII-A₂B₂ assembles with unexpected unequal pairing within an otherwise symmetric complex, and suggest this conformation is essential for FXIII function. These findings provide the first molecular structure of this important coagulation protein.

2. Materials and Methods

Software, databases, and webservers used in this study are listed in Supplementary Table S1.

PDB co-ordinates for one of the simulation snapshots of the complex model taken from the production phase of the simulation trajectory is provided as a supplementary file. Detailed methodology can be found in the Supplementary Methods.

2.1. FXIII-A and FXIII-B Subunit, Cloning Expression, and Purification

Cloning expression and purification of rFXIII-A (recombinant FXIII-A) subunit was performed as described by Gupta et al., 2016 [8] (Supplementary Figure S2a). Human FXIII-B cDNA, inserted into the cloning site of pReciever-M01 mammalian expression vector, was transfected into HEK293t cells, as per previously reported protocol [16]. Secreted protein harvested post-transfection was concentrated and subjected to immunoaffinity purification using the Thermo Scientific Pierce Co-IP kit (Pierce Biotechnology, USA) (Supplementary Figure S2b).

2.2. Purification of FXIII-A₂B₂ Complex

FibrogamminP (CSL Behring, Germany) reconstituted in water was run on a Superdex 200 increase 10/300 column Äkta Pure system (GE healthcare, Germany) equilibrated with 20 mM Tris and 100 mM NaCl, at pH 7.4. The peak corresponding to FXIII-A₂B₂ (320 Kda) was repurified in triplicate, until a highly pure, single, homogenous, monodispersed peak was obtained with no excipients (Supplementary Figure S2c). The eluted peak was concentrated and quantified for further downstream applications.

2.3. Atomic Force Microscopy (AFM) of FXIII

Surface topology of recombinant FXIII-A₂ (rFXIII-A₂ expressed and purified in-house), recombinant FXIII-B₂ (rFXIII-B₂ expressed and purified in-house), and FXIII-A₂B₂ (purified from FibrogamminP, CSL Behring, Marburg, Germany) was analyzed individually using high-resolution AFM. Briefly, samples suspended in PBS pH 7.4 (1–2 mM) were placed on a freshly-cleaved mica and allowed to adsorb (15 min). Non-adherent proteins were removed by washing twice with imaging buffer (10 mM Tris-HCl, 50 mM KCl, pH 7.4). Samples were imaged in oscillation mode in liquid (imaging buffer) as described by [17] and acquired using a Nanoscope III microscope.

2.4. XL-MS of FXIII-A₂B₂ Heterotetramer Complex

One μ L of 3.12 μ g/mL purified FXIII-A₂B₂ was mixed with 1 μ L of a matrix of re-crystallized sinapinic acid (10 mg/mL) in acetonitrile/water (1:1, *v/v*), trifluoroacetic acid (TFA) 0.1% (K200 MALDI Kit; CovalX, Zurich, Switzerland). After mixing, 1 μ L of each sample was spotted on the MALDI plate. After crystallization at room temperature, the plate was introduced in the MALDI mass spectrometer (Ultraflex III MALDI ToF, Bruker Daltonik GmbH, Bremen, Germany) equipped with HM2 high-mass detection (CovalX, Zurich, Switzerland) and analyzed immediately in high-mass MALDI mode. MS data were analyzed using Complex Tracker analysis software (CovalX, Zurich, Switzerland). For characterization and peptide mass fingerprinting, the purified FXIII-A₂B₂ complex was subjected to ASP-N, trypsin, chymotrypsin, elastase, and thermolysin proteolysis, followed by nLC-LTQ Orbitrap MS/MS analysis (formic acid 1% added to the final solution after digestion) (Supplementary Figure S3). Purified FXIII-A₂B₂ (1.25 μ M) was cross linked with 2 μ L of DSS (d0d12) reagent (Creative Molecules Inc., Canada) at room temperature for 3 h, prior to digestion. Nano-LC chromatography was performed using an Ultimate 3000 (Dionex, IL, USA) system in-line with an LTQ Orbitrap XL mass spectrometer (ThermoFischer Scientific, IL, USA). Acquired data were analyzed by XQuest version 2.0 and Stavrox version 2.1. The FXIII-B intra-subunit and FXIII-A-FXIII-B inter-subunit cross-linked peptides and residues are presented in Supplementary Tables S2 and S3.

2.5. Generation of the FXIII-B Subunit Model

FXIII-B intra-subunit XL-MS cross-linked residues were matched to residue contact prediction data to generate constrained models of FXIII-B monomers on the AIDA server (<http://aida.godziklab.org/>) [18] (Supplementary Figures S4 and S5). Sushi domains were based on previously-generated high-quality threaded models from I-TASSER [19] (<https://zhanglab.ccmb.med.umich.edu/I-TASSER/>) (Supplementary Figure S6a–S6j). We also assembled a FXIII-B subunit monomer model (Supplementary

Figure S5) in default mode, i.e., without constraints and docked this model symmetrically (M-Z docking server [20]) to model unbound FXIII-B₂ dimer.

2.6. Generation of the FXIII-A₂B₂ All-Atom Model

Inter-subunit, XL-MS-directed docking of all FXIII-B monomer conformations on the FXIII-A₂ crystal structure (PDB ID: 1f13) was performed using the HADDOCK expert interface webserver (<http://milou.science.uu.nl/services/HADDOCK2.2/>) [21]. Since this webserver allows for only bi-molecular docking, whereas the in-silico model involves three proteins (FXIII-B monomer and FXIII-A₂ dimer), we treated the dimer as a single molecule by renumbering the residues of each FXIII-A monomer in continuum. We based structural constraints for modeling and docking FXIII-B monomer on FXIII-A₂ on inter- and intra-subunit cross-linked residues (Supplementary Tables S2 and S3). Docking constraints (n = 64) required that all residues belong to detected cross-linked peptides that can form side chain contacts (Supplementary Table S4) to cover the FXIII-A₂/FXIII-B trimer surface. Moreover, FXIII-A₂/FXIII-B contact residues were assigned constant lower and upper limit distances of 3 and 24 Å, respectively [22]. We then manually constructed the resulting docked trimer into a tetramer with bilateral symmetry.

2.7. Molecular Dynamics Simulations of the FXIII-A₂B₂ Heterotetramer Models

Stability of the top-scoring FXIII-A₂B₂ complex (best HADDOCK scores amongst the major docking clusters, Supplementary Figure S7) from the HADDOCK [23] server was assessed using all-atom molecular dynamics (MD) simulations (YASARA Structure suite 17.4.17 platform [21,23,24] with the embedded md_sim macro) [25,26]. A steered molecular dynamics (SMD) simulation was separately performed on the MD-equilibrated model 1 to dissociate the FXIII-B₂ subunit dimer from the FXIII-A₂ dimer. The SMD was performed with md_runsteered macro embedded in YASARA, with minor modifications in the steering force (applied acceleration, 100 pm/ps²). Analyses of simulation variables, model quality, and model characteristics are detailed in Supplementary material. All subsequent structural analyses were performed on the MD-equilibrated complex model 1.

2.8. Modeling Transition States between the First FXIII-A₂: FXIII-B₂ Contacts and the Final FXIII-A₂B₂ Complex

To generate a model of the initial contact between dimeric FXIII-A₂ and FXIII-B₂, we docked the crystal structure of FXIII-A₂ dimer with the dimeric model of unbound FXIII-B₂ on the Z-dock rigid docking server [27]. We considered the highest scoring complex as the initial contact structure and the FXIII-A₂B₂ complex model 1 generated on HADDOCK [21,23,24] as the final structure, and submitted these to the MINACTION path server (<http://lorenz.dynstr.pasteur.fr/suny/submit.php?id0=minactionpath#submit>) to generate C_α-backbone models of the transition-states between these two structures [28]. Once a large number of coarse-grained intermediates were generated, we converted 8 intermediates to full atom models, as described [4].

2.9. Fitting and Docking Atomic Protein Structures on AFM Surface Topographs

We docked three-dimensional heterotetramer coordinates within the AFM-derived topographic surface (envelope) using the AFM-Assembly protocol [29,30]. We defined the docking score as the number of atoms from the protein structure in the favorable layer, and translated this score into pseudo-energy values, where the best score corresponds to the lowest energy. We ran docking protocols on HADDOCK top-scored FXIII complex models, as well as on the crystal structure of FXIII-A₂ and the models of unbound FXIII-B₂. For each docking simulation, we retained the top 10⁵ potential solutions and further analyzed the top 10 to produce the minimum docking energy, average energy of the top 10 docking solutions, root-mean-square deviation (RMSD) of the top 3 docking solutions, and shift of the best docking solution from the center of the docking grid.

2.10. ITC-Based Thermodynamic Profiling of the Assembly and Dissociation of the FXIII-A₂B₂ Heterotetramer Complex

Finally, we directly measured thermodynamic changes during complex assembly and disassembly of the FXIII-A₂B₂ heterotetramer using ITC on a MicroCal200 microcalorimeter (Malvern Panalyticals, Malvern, UK). To examine FXIII subunit association, we titrated 2.5 μM of rFXIII-A₂ (cell) against 25 μM rFXIII-B (syringe). We analyzed the resulting isotherms using Origin 7.0 (Originlab) and fitted the data using **Affinimeter** and a custom model based on stepwise association of the subunits, FS ↔ MA + A1 ↔ MA₂, where FS is free species, M is FXIII-A₂ in cell, and A is FXIII-B from syringe. To examine FXIII-A₂B₂ complex disassembly, we titrated 1.25 mM FXIII-A₂B₂ in the cell (13.8 U Thrombin; Sigma-Aldrich Chemie GmbH, Taufkirchen, Germany) against 25 mM CaCl₂ in the syringe. We performed blank experiments to account for the heat of dilution. We first analyzed data for a single set of binding models using Origin software, to observe binding as a global fit. We then calculated heat capacity changes for each injection based on algorithms within the Origin software and stoichiometric equilibria model (described below) in **Affinimeter** (<https://www.affinimeter.com>) and iterated between these until no further significant improvement in fit was observed. Data were fit using the custom design model and hypothetical equation M1 + A1 ↔ M1A1 + A1 ↔ M1A2 + A1 ↔ M1A3, where M is FXIII-A₂B₂ and A is calcium ion.

3. Results

3.1. AFM Topographs Indicates Complex Formation Restricts the Conformational Flexibility of FXIII-B

AFM analysis of the FXIII-A₂B₂ complex revealed that each isolated surface height signal had a bi-partite appearance (Supplementary Figure S8) comprised of a clearly compact part (FXIII-A subunit) from which filamentous signals (FXIII-B subunit) extended in different directions (Figure 1). The maximum height observed in the topographic images (raw) for the FXIII-A₂B₂ complex was 5.9 nm for whole field, which was lower than those recorded for either the FXIII-A₂ subunit (9.5 nm) or the FXIII-B₂ subunit (19.2 nm) (Figure 1, Supplementary Figure S8). This demonstrates that the association of FXIII-B₂ with FXIII-A₂ restricts the conformational flexibility of free FXIII-B₂ subunit making it more compact. In the surface topographic images only, part of the dispersed flexible region, i.e., the FXIII-B subunit is visible peeking out from underneath the compact part, i.e., the FXIII-A subunit. This can be explained by an overall negative charge carried by FXIII-A₂ dimer surface, which relies on positive electrostatic patches on the FXIII-B subunit to adhere to the mica surface in a complexed state (Figure 1). The differences in height might be attributed to adsorption effects on the structure of the protein [31,32]. Wrapping of FXIII-B subunits around FXIII-A₂ dimer occurred from one side, giving the molecule a bi-partite appearance, suggesting partial asymmetry in the complex.

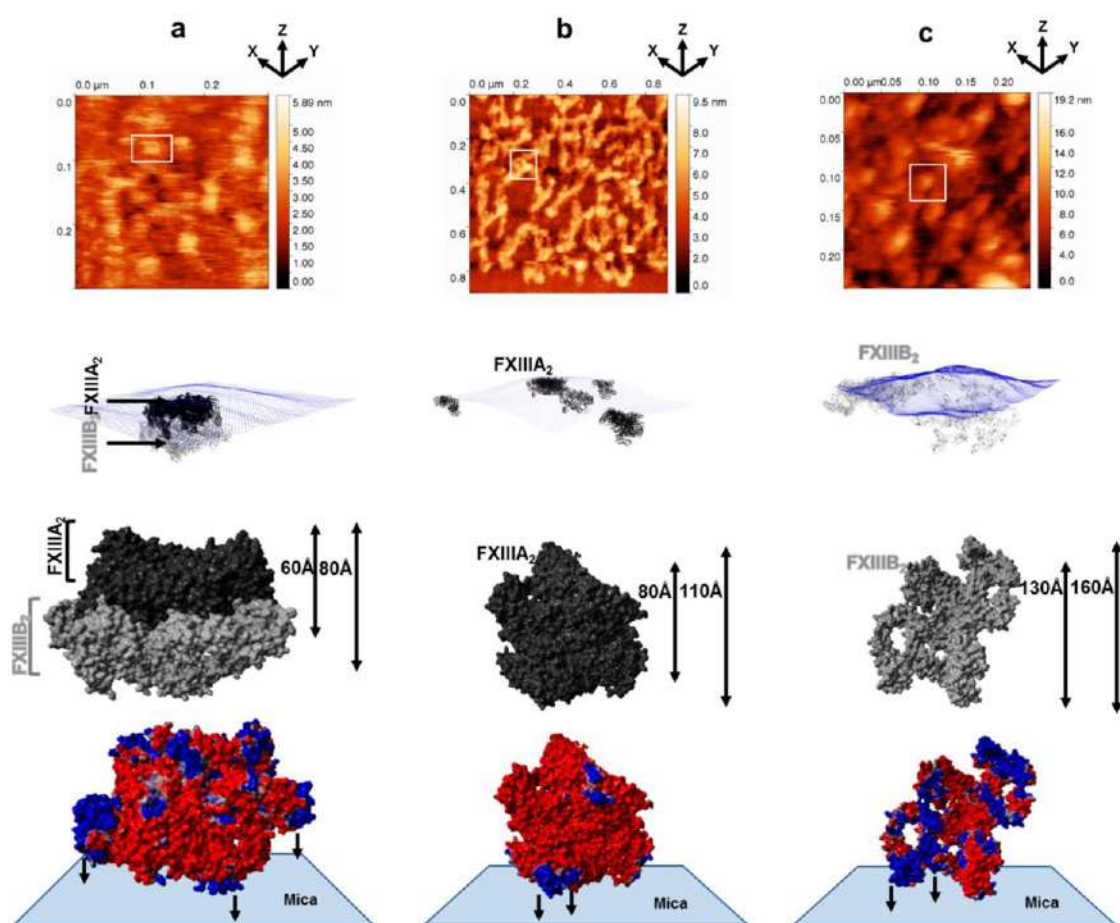


Figure 1. Conformational state of factor XIII (FXIII) complex, FXIII-A, and FXIII-B subunits by atomic force microscopy (AFM). Figure 1 is split row wise into panels a, b, and c running top to bottom. (a) goes top to bottom in the following order for the AFM- and AFM-based docking of the best FXIII-A₂B₂ complex model, i.e., the topmost image is the raw AFM image with the docking pose of one of the crops below it. In the docking pose, the topography is depicted as blue dots while the different docked complexes (of model one only) are depicted in black (FXIII-A₂) and gray (FXIII-B₂) ribbon format. Below the docking pose is a molecular surface-based representation of FXIII-A₂B₂ complex as it would be viewed in one of the many poses it would adopt while adhering to the mica in the AFM instrument. The minimum and maximum heights that this pose is likely to have, are indicated to the right. The FXIII-A and FXIII-B subunits are depicted in black and gray color, respectively. The lowermost image is PME electrostatic surface structural representation of the same pose depicted in alignment with the hypothetical mica surface to which it adheres. (b,c) panels follow the same trend as (a), only they represent the FXIII-A dimeric crystal structure and the dimeric unbound FXIII-B model, respectively.

3.2. Cross-Links in the FXIII-A₂B₂ Complex Interface Expose Reverse, N-to C-Terminal Symmetry between FXIII-A and FXIII-B Subunits

We then used XL-MS to identify inter- and intra-molecular contacts within the FXIII-A₂B₂ complex. This analysis generated 358 total peptides, with an overall coverage of 80% for FXIII-A and 91% for FXIII-B. The cross-linked FXIII-A₂B₂ heterotetramer (MW 319.950 kDa) had 34 cross-linked peptides located within the heterotetramer interface (Supplementary Table S3). Inter-subunit cross-links were detected between residues from the FXIII-A C-terminal barrel domains and the FXIII-B N-terminal S1, S2, and S3 sushi domains, whereas residues in the FXIII-A N-terminal β-sandwich domain were cross linked to residues from the FXIII-B C-terminal S6, S7, S8, and S9 sushi domains (Figure 2a). The FXIII-A catalytic core region was cross linked to FXIII-B sushi domains S3, S4, S5, S7, S8, and S9. Intra-subunit

cross-links with the FXIII-B₂ dimer interface largely involved residues in the N-terminal sushi domains (S1-S4), but fewer cross-linkings within sushi domains S6, S7, and S8 (Figure 2b, Supplementary Table S3). These findings differ from those previously reported for inter- and intra-subunit interactions within the FXIII-A₂B₂ complex [1,6].

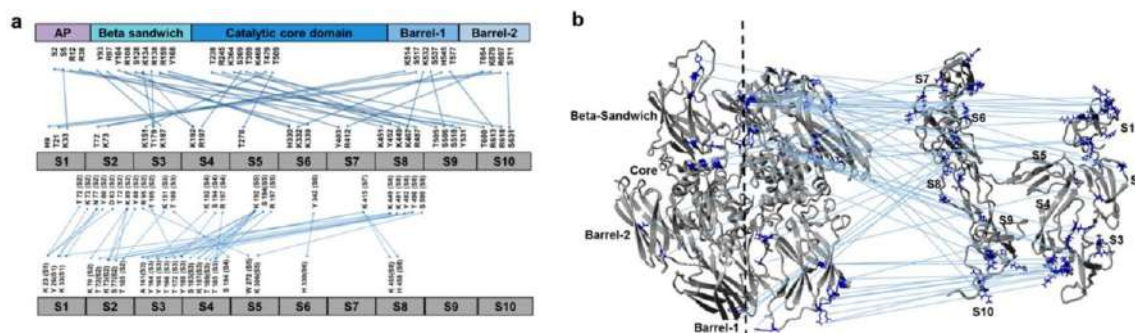


Figure 2. Cross-linking and mass spectrometry (XL-MS) derived cross-linking residues of FXIII complex reveals an N-to C-terminal symmetry. (a) shows the domain-wise distribution of both FXIII-B monomer model docking to FXIII-A₂ crystal structure, distance constraints (upper part of image), and monomer FXIII-B model assembly, distance constraints (lower part of image), that were generated from the XL-MS cross-linking information of the purified FXIII-A₂B₂ heterotetramer complex (Supplementary Tables S2 and S3). (b) shows a structural description of the information shown in (a). The crystal structure of the FXIII-A subunit dimer and the monomer model of the FXIII-B subunit have been illustrated in ribbon format.

3.3. Molecular Docking Reveals a Stoichiometrically-Symmetrical, Bi-Partite, FXIII-A₂B₂ Complex

To understand the origin of the reverse symmetry of the FXIII-A₂B₂ complex observed in the XL-MS data, we used molecular docking to model FXIII-A₂B₂ assembly. Of five potential models of FXIII-B monomer (Supplementary Figure S5), only two gave successfully docked clusters with FXIII-A₂; of these, we selected the topmost model (Supplementary Figure S9, chosen based on HADDOCK scores) of the top-most docking cluster as our model of choice based on agreement with structural information from AFM. This model (model 1) also illustrated a symmetric bi-partite structure, in which FXIII-A subunits are compact, and FXIII-B subunits are more dispersed and flexible (Figure 3a). Following equilibration, backbone RMSD/total energy charts (Figure 3b) indicated this model of FXIII-A₂B₂ showed good stability and was stereochemically validated (Supplementary Figure S10). Discrepancies in validation were like those observed for standard complex crystal structures. The FXIII-B N-terminal sushi domains (S1, S2, and S3 domains) extended into flexible arms (Figure 3c), although each FXIII-B monomer showed different flexibility and secondary structure following the simulation (Figure 3d,e, Supplementary video S1). We observed two distinct positively-charged electrostatic patches (two one each monomer, four in all) on FXIII-B (Figure 3f,g), which may represent potential fibrinogen interaction interfaces [33], since these would create excellent complementarity with the negatively charged regions within the currently-proposed FXIII-B interaction site on fibrinogen [33–37].

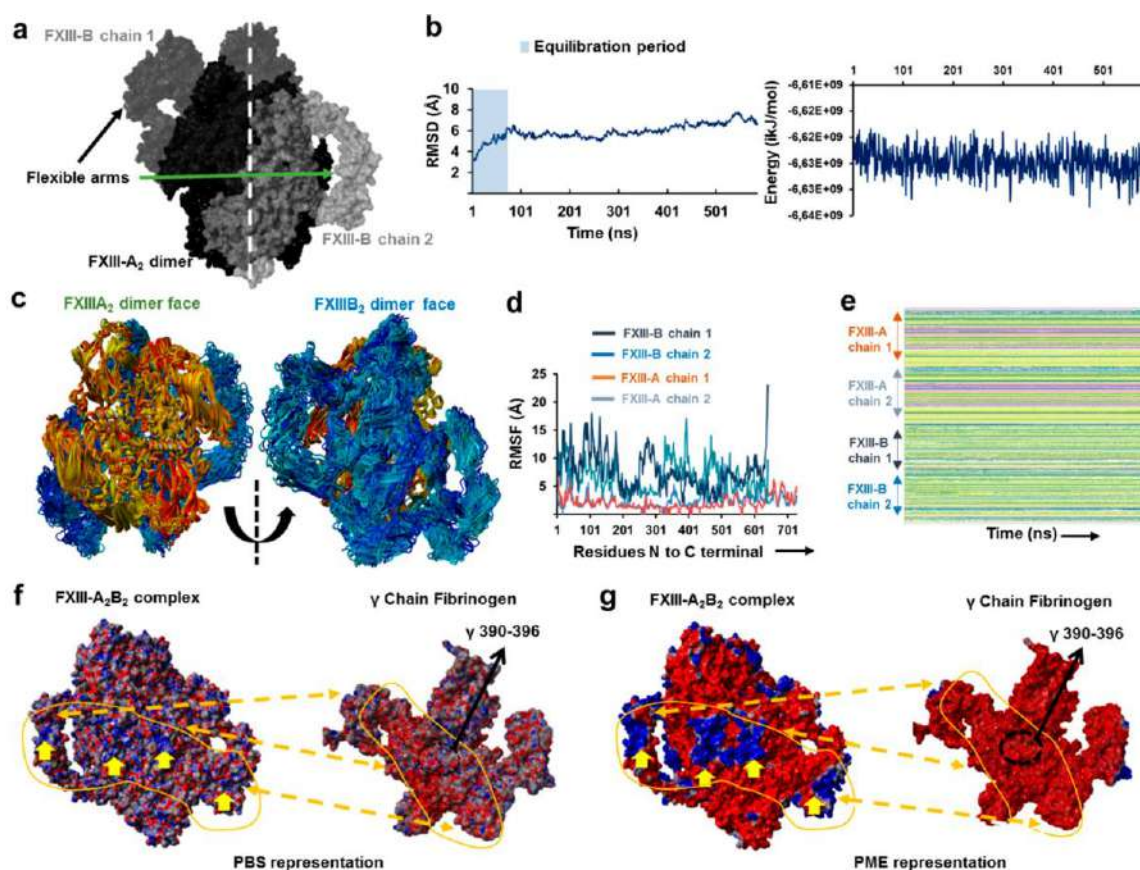


Figure 3. The all-atom structure of the FXIII-A₂B₂ complex. (a) is the symmetrical representation of the best modeled all-atom structure of the FXIII-A₂B₂ complex. The structure has been depicted by its molecular surface in different shades of black and gray for the individual chains of FXIII-A and FXIII-B subunits. (b) shows the C- α backbone RMSD and the total energy graphs for the MD simulation conducted on the FXIII-A₂B₂ complex structure model. (c) are aligned simulation snapshots from the MD simulation conducted on FXIII-A₂B₂ complex structure represented with FXIII-A subunit face (left) and the FXIII-B subunit face (right). The snapshots of FXIII-A and FXIII-B subunits are depicted in ribbon format with colors ranging between yellow-red and cyan-blue for either subunit, respectively. (d) shows the graph representing RMSF for the FXIII-A₂B₂ complex structure MD simulation, with individual chains represented by different color as mentioned in the inset. (e) represents the secondary structure profile of individual chains of FXIII-A and FXIII-B subunits for the FXIII-A₂B₂ complex structure MD simulation. (f) is the PBS-based electrostatic surface representation of the FXIII-A₂B₂ complex structure (left) and γ chain of fibrinogen (right) taken from fibrinogen crystal structure (PDB ID: 3GHG). Red color indicates negative surface electrostatic potential, whereas blue represents positive potential. Indicated positive electrostatic patches on the FXIII-A₂B₂ complex structure are likely to interact with negatively charge bearing regions in and around the FXIII interaction site of fibrinogen γ chain (the specific residues are numbered and indicated with a black arrow). (g) is the same view as (f) but electrostatic surface representation has been done with the PME method. The prominent electrostatic patches on the FXIII-B subunit are marked with yellow arrows in (f,g). The complementary electrostatic regions between FXIII and fibrinogen γ chain have been marked with dotted arrows and continuous uneven lines covering the shape of the region in (f,g).

3.4. Molecular Docking into the AFM Topographs Identifies the Best Model Representative of the Native FXIII Complex

To rule out false positive conformational models of the FXIII-A₂B₂ complex, we docked the two FXIII-A₂B₂ modeled structures onto the AFM topography image. According to the docking scores (AFM dock), FXIII-A₂B₂ complex model 1 had globally better scores than complex model 2 for the

10 selected docked regions of the AFM images (Figure 4). Each isolated surface height signal had a bi-partite appearance (Supplementary Figure S8) comprised of a compact part (FXIII-A₂) from which filamentous signals (FXIII-B) extended in different directions. The AFM topographs were in line with the complex model 1 appearance. The complex model 1, therefore, represents the native conformation of FXIII complex.

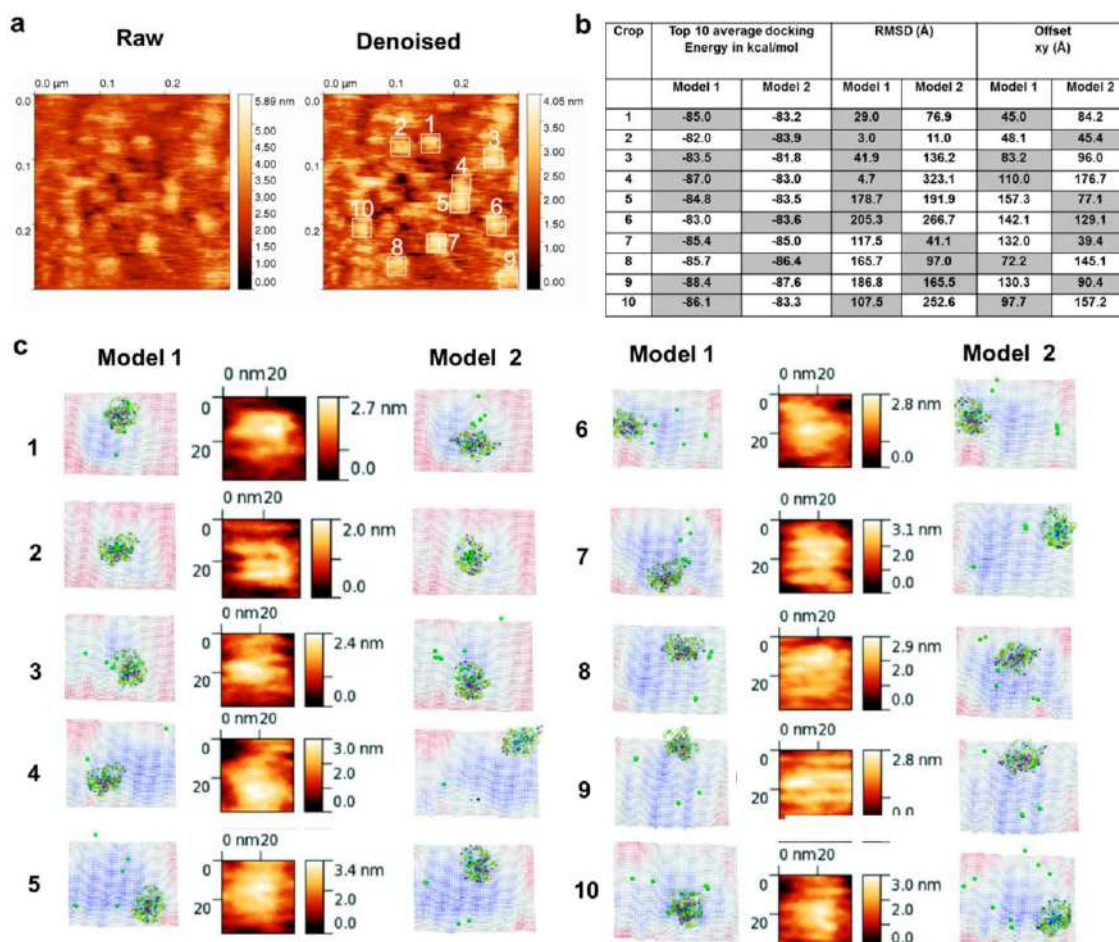


Figure 4. AFM based docking of FXIII complex models reveals model 1 as the best complex. (a) shows the raw and denoised AFM topographic images for the purified FXIII-A₂B₂ complex. The height scales are depicted to their right. The denoised image also shows in white lined squares the crops on the topographic surface to which docking of the two best models (HADDOCK scores) of the FXIII-A₂B₂ complex were performed on the DockAFM pipeline [30]. (b) is a table presenting the comparative scores obtained from the docking of the two FXIII-A₂B₂ complex model structures on the ten AFM image crops depicted in (a). The xy (offset) represents the shift of the docked model structure (model 1 and model 2) from the center of the topographic surface. The most favorable structure is chosen as that having the smallest shift from the center. (c) shows side-by-side the best docking pose for the two FXIII-A₂B₂ complex model structures on each of the ten crops side by side to a close-up topographic view of the crop itself. The topography of the docked pose is inverted, i.e., looking from below the surface. The color of the topography (blue to red) is the height in Z (red is low and blue is high). The structures of the two models are depicted in ribbon format.

3.5. Unequal Pairing within the Bi-Partite FXIII-A₂B₂ Complex Influences Dissociation of Subunits during FXIII Activation

Analysis of the final model 1 of the FXIII-A₂B₂ complex indicated inequality in binding of individual FXIII-B monomers to the FXIII-A₂ dimer (Figure 5a), as well as comparative differences in

analysis. The transition state analysis of the heterotetramer assembly shows that the association of dimeric subunits to form a complex is asymmetric, two-step binding, where FXIII-B monomer first strongly associates with FXIII-A₂ dimer, stabilizing a transient state FXIII-A₂B'B (where B' represents the unbound monomer). This complex then forms the FXIII-A₂B₂ complex where all subunits interact in totality (Figure 5d). These data show that the two-step asymmetrical binding most likely results in unequal pairing between the monomers within the complex.

3.7. Thermodynamic Patterns Underlying FXIII-A₂B₂ Complex Assembly and Dissociation Suggest Stepwise Models for Both Events

Finally, having investigated the complex assembly and disassembly (during activation) events at a structural level, we performed ITC for the same events to explain the operant thermodynamic variables. ITC enabled us to (a) examine the thermal changes corresponding to protein interface interactions upon binding and (b) correlate the thermal motions derived from activation-induced disassembly of the complex to the structural dynamics of individual subunits obtained by the model analyses. The first set of ITC experiments were performed to illustrate the thermal mechanics underlying the binding of FXIII subunits. When fitted with one set of binding sites, data measuring association of FXIII-A₂ and FXIII-B₂ yielded a K_d of 66.7 nM. A sequential two-step binding model based on hints from the unequally paired FXIII-A₂B₂ complex model 1 suggested that the first binding event of FXIII-B₂ to FXIII-A₂ is an enthalpically-favorable exothermic reaction ($\Delta H = -226.25$ kJ/mol), however, yields a conformationally-restricted state with positive, unfavorable entropy ($-T\Delta S > 0$) and K_d of 1.5 nM. The second binding event (MA \leftrightarrow MA₂) is also enthalpically favorable ($\Delta H = -360$ kJ/mol) with unfavorable entropic changes ($-T\Delta S > 0$), but a comparably weaker K_d of 4.3 μ M, due to the spatial restriction faced by the second monomer upon interaction (Figure 6). These thermodynamic patterns agree with our transition state analysis suggesting a two-step binding assembly, the latter being of low affinity, leading to heterotetramer assembly.

To analyze the dissociation of the complex upon activation, we also interrogated calcium binding to the thrombin-cleaved FXIII-A₂B₂ complex. On the basis of the stoichiometric equilibrium model (Figure 7a) post-fitting, the first calcium binding event (set at K_d 100 μ M [39–41]) showed an entropically-driven, negative-T ΔS , and unfavorable, endothermic ΔH (4.78 kJ/mol) pattern. The second event, corresponding to K_d of 1 mM, had highly negative -T ΔS , and endothermic ΔH (150.70 kJ/mol) behavior. In contrast, the third event, corresponding to K_d of 1.94 μ M, had a highly positive -T ΔS and exothermic ΔH (-154.42 kJ/mol) (Figure 7) heat change. Experiments assessing thrombin- and calcium-mediated dissociation of FXIII-A₂B₂ suggested the events proceeded stepwise. (i) Calcium binds to FXIII-A₂ in the heterotetramer complex. (ii) The calcium-bound heterodimer separates (i.e., FXIII-AB). Given heat signatures (Figure 7d) obtained for event 2 ($\Delta H > 0$, $-T\Delta S > 0$), we propose that the system maintains thermal equilibrium by first dissociating into a transient FXIII-AB heterodimer. This step combats the unfavorable enthalpy of A/A or B/B subunits suggested by the in silico pseudo-binding energy calculated for our complex model 1 (Figure 5c). (iii) The FXIII-AB heterodimer separates into individual, free subunits. During this event, unfavorable conformational entropies are counteracted by favorable enthalpic changes, which explain the final disruption of FXIII-AB heterodimer into calcium saturated, activated and open FXIII-A * monomer [31]). At the conditions used (T = 30 °C), all three events were spontaneous ($\Delta G < 0$). The flipping patterns of enthalpy and entropy in the sub-events that occur during dissociation of the complex suggests the role of bulk solvent coming into play, along with calcium saturation of FXIII-A that is responsible for stepwise disassembly of the complex [42–44]. Collectively, our thermodynamic data support the premise that FXIII undergoes two unique stepwise modes of complex assembly and disassembly in plasma (Supplementary Figure S11).

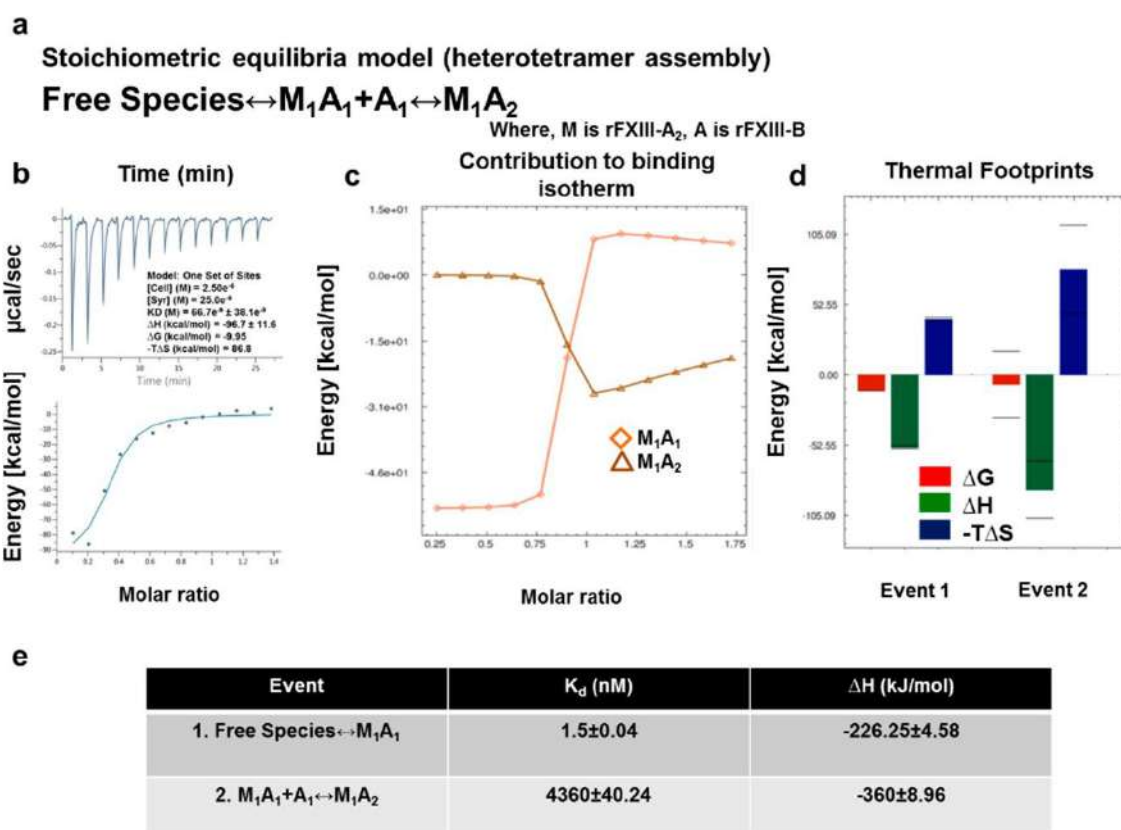


Figure 6. In-solution associations of FXIII subunits studied by ITC. (a) is the equation depicting the stoichiometric binding equilibrium model, followed for the analysis of data derived from ITC (model was generated in **Affinimeter** using model builder approach). (b) represents the titration of 2.5 μ M rFXIII-A₂ (in cell), with 25 μ M FXIII-B subunits (in syringe). The upper image of this panel is the raw data depicting the heat change upon each injection; the lower image in this panel is the normalized data, with integrated heat change plotted against the concentration ratio of rFXIII-B vs. rFXIII-A₂ (blank controls not shown). A solid black line represents the corresponding fit obtained in Origin software using one-set of binding mode. (c,d) are based on **Affinimeter** analyses depicting the contribution of individual reactants of the equation (a) towards the isotherm. The heat signatures depicting the free energy changes, changes in enthalpy, and entropy in the two events explained in (a), respectively. (e) is a table explaining the two thermodynamic events, and their corresponding dissociation constants (K_d) and changes in enthalpy (ΔH).

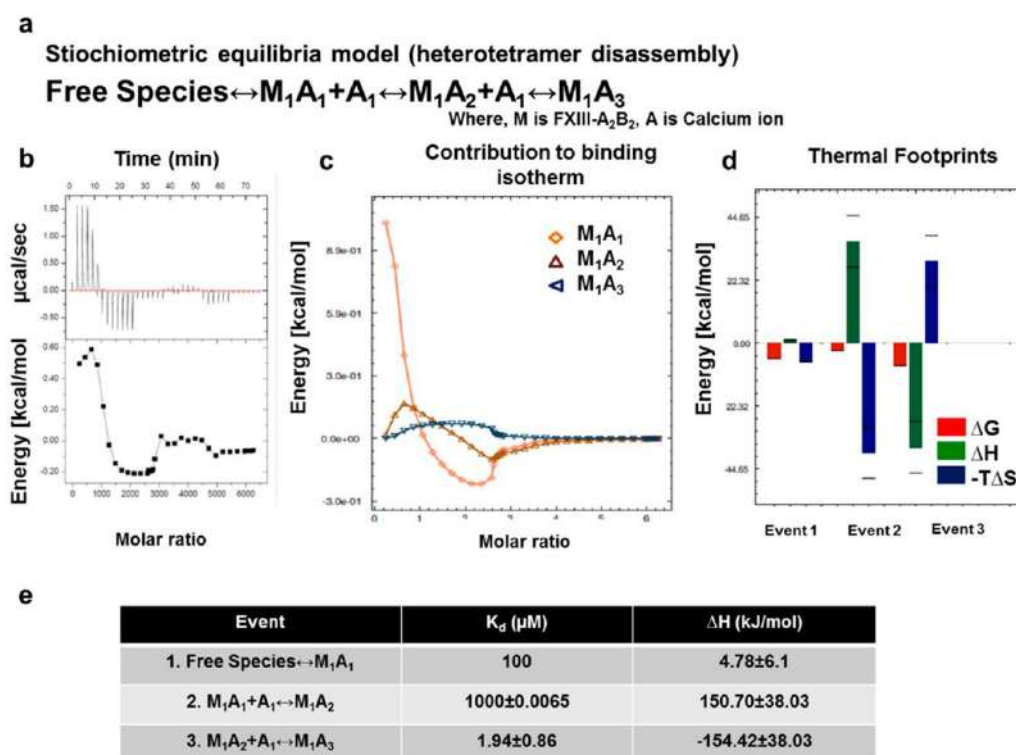


Figure 7. In-solution dissociation of FXIII complex in the presence of thrombin and calcium studied by ITC. (a) is the equation depicting the stoichiometric binding equilibrium model followed for the analysis of data derived from ITC (model was generated in **Affinimeter** using model builder approach). (b) represents the titration of 1.25 mM FXIII-A₂B₂, with 25 mM CaCl₂. Upper image of this panel is the ORIGIN raw data depicting the heat change upon each injection and the lower image in this panel is the normalized data, with integrated heat change plotted against the concentration ratio of CaCl₂ vs. FXIII. A solid black line represents the corresponding fit obtained in Origin software using one-set of binding mode. (blank controls not shown) (c,d) are based on **Affinimeter** analyses depicting the contribution of individual reactants of equation (a) towards the isotherm. The heat signatures depicting the free energy changes, changes in enthalpy, and entropy in the two events explained in Figure 6a, respectively. (e) is a table explaining the three thermodynamic events, and their corresponding dissociation constants (K_d) and changes in enthalpy (ΔH).

4. Discussion

4.1. IH Approaches Reveal a Unique FXIII Complex Structure

The FXIII complex has always presented a structural functional challenge to researchers owing to its dynamic nature and association with various other proteins such as fibrinogen in its physiological and biochemical life cycle. The interpretation of pathomolecular mechanisms is further limited by the absence of an all atom basis for this complex, as well as the development of drugs and inhibitors to bind both complexed and isolated FXIII-A [45–48]. Indirect evidence, in the context of interdomain interactions, exists but does not have a visual and structural basis [1]. The final structure of the FXIII-A₂B₂ complex model derived in this study fills this gap. Notably, our model presents a new picture of the complex that differs from the current paradigm in several important ways [1,6]. First, our model suggests FXIII-B subunit N-terminal sushi domains are relatively free, with positive surface electrostatic patches, indicating a potential role of this flexible region in interactions with other proteins like fibrinogen [30,31,33]. These interactions would be especially relevant when evaluating the effect of FXIII or fibrinogen surface mutations that disrupt or disorder their mutual complex. In addition, reports have suggested the N-terminal region of FXIII-B interacts with the

FXIII-A subunit [1]. This observation could also be a secondary allosteric effect observed during the competitive binding studies performed, since both our all-atom structure, as well as the XL-MS analysis, suggest increased density of interdomain interactions at the C-terminal end of FXIII-B. The recent report by Proptopopova et al. [49], based primarily on AFM studies in air, suggests partial wrapping of B subunits around central core of FXIII-A₂. Our study registers similar observations, but we propose a different orientation possibility for individual subunits within the complex. Differences between our interpretations might be due to the surface properties of the following: (a) complex; (b) the HOPG/mica surface; (c) sample preparation; or (d) imaging in air or buffer, which affects the overall behavior of the molecule under the microscope [32,50]. The association analyses by ITC reveal that the binding of individual subunits is strong ($\sim 10^{-9}$ M, single set of binding mode) but differs by a factor of 10 from the latest report ($\sim 10^{-10}$ M) in which one of the subunits was immobilized, unlike our solution-based label-free evaluation [1]. Interestingly, our heterotetramer model 2 generated from the flexible docking (which was observed to be stable over an MD simulation run for >100 ns) matches the previous literature on FXIII-A. The FXIII-B interactions, i.e., the C-terminal sushi domains of this model were observed to be free and the S1 and S2 sushi domains were observed to be partially interacting with the FXIII-B subunit (Supplementary Figure S9). Nevertheless, this model was eliminated from being the best representation, since it showed lower scores when matched to the AFM images of the heterotetramer (Figure 4). However, because of the similarity observed for the model 2 with previous literature, we do not completely deny that another conformational pose of the heterotetramer, one similar to the model 2, could actually be a more correct representative. Future studies involving cryo-EM-based exercises could shed more light in this regard.

4.2. Assembly of FXIII-A₂B₂ is a Two-Step Process Aided by the Conformational Flexibility of FXIII-B Subunit

Assembly of the FXIII-A₂B₂ complex in plasma and its subsequent activation and disassembly are well known phenomenon. However, the thermodynamic variables underlying these events have not been investigated in detail, especially in the context of the conformational changes that occur during these processes. Published data address only the thermolability of individual domains of FXIII-A subunit [51]. In contrast to transglutaminase-2 (TG2), a near homologue of FXIII-A which has been thoroughly investigated in the thermodynamic aspect [52], detailed data for the FXIII complex is not available. Our ITC experiments performed in-solution balance our structural investigation into FXIII oligomeric association and disassembly upon activation by identifying subtle changes in thermodynamic parameters that fit into our structural models. The thermodynamic study of FXIII complex assembly was performed by titrating both subunits against each other. Stepwise association of the two FXIII-B subunits onto FXIII-A dimer, also depicted by the in-silico transition state models, suggests the conformation adopted by the transient transition state FXIII-A₂BB' supports final complex association (Figure 5d). The heat signatures observed in our study show that desolvation of the inter-subunit interface leading to the stabilization of non-covalent contacts across the interface is a gradual two-step event aided by the conformational flexibility of FXIII-B subunits. While the globular FXIII-A structure remains relatively static, the flexible FXIII-B monomers twist and bend to individually accommodate the FXIII-A monomers. This two-step, unequal, asymmetrical assembly, further supported by the significantly different binding energies for the two events observed in our ITC profile (Figure 6), is the underlying cause for an unequally paired complex. This analysis is additionally supported by our AFM-based observations, in which the free form of FXIII-B is flexible and long but once associated with the FXIII-A, becomes more compact. Regardless of this association, even complex-bound FXIII-B retains some flexibility, especially at its N-terminal regions, as observed from the thermal motions of the complex model simulation (Supplementary video S1). These observations also suggest that the FXIII-B subunit undergoes a significant conformational change during its transition from a free molecule to a bound one.

4.3. Unequal Pairing within the FXIII Complex May Generate a Transient FXIII-AB Species during the Activation Induced Complex Disassembly

We studied FXIII complex disassembly by saturating thrombin-cleaved FXIII-A₂B₂ with increasing concentrations of calcium in an ITC platform. The thermodynamic driving forces responsible for complex activation indicate the role of solvation energies [43] that release the subunits in the presence of calcium ions (Figure 7). Here, the transition of the zymogenic heterotetramer to active, open, monomeric FXIII-A* involves formation of a transient FXIII-AB heterodimer in which FXIII-A subunits are incompletely saturated with calcium and are still loosely bound to one of the FXIII-B monomers. Our thermodynamic analyses indicate how low-entropy interfacial water molecules [42,53,54] assist in disrupting the tetrameric interface in FXIII-A₂B₂, aiding the entropic compensations that act against unfavorable enthalpies. The relevance of this model of dissociation becomes clearer when examining the nature of unequal pairing within the complex. Unequal pairing of individual FXIII-B monomers, especially at the C-terminal hinge region of FXIII-A (residues 500–520) (Supplementary Figure S12a, Supplementary videos S3 and S4), is favorable since it enables bulk solvent to sneak past the interface between loosely bound B monomer and A subunits (Supplementary Figure S12b), aiding dissociation to perform timed activation. This flexible hinge region is critical for the movement of FXIII-A barrel domains, enabling its activation and giving rise to its open extended conformation [8]. Equally strong binding of both FXIII-B subunit monomers to FXIII-A₂ would be energetically expensive, also yielding possibly slower activation and subunit dissociation. However, this observation does not suggest the complex breaks down into a trimer (FXIII-A₂B) and a monomer (FXIII-B), as is also observed in our SMD for separation of FXIII-B₂ from FXIII-A₂. Notably, bulk solvent and water does not play a role during the separation in the SMD (Supplementary video S2), unlike a physiological scenario in which it is an active participant. Bulk solvent/water permeates interfaces between all subunits, bringing a semblance of symmetry to the disruption and disassembly process in the physiological environment. Nevertheless, we can conclude that the process of dissociation is strong enough to separate FXIII-A monomers from each other (Supplementary video S2 and Supplementary Figure S13), providing further support that the activated FXIII-A molecule is a monomer [31]. Given the binding affinity of the FXIII subunits and their conformational motions, FXIII mutations that affect interface residues or conformational flexibility are likely to undermine complex assembly, resulting in either loosely or too tightly bound complex. A tightly bound complex can trap the oligomer in less flexible states and alter rates of activation, whereas a loosely held complex can be susceptible to spontaneous disassembly. The models of assembly and disassembly during activation of FXIII complex implicated by our study are particularly relevant in the context of the structural data and thermodynamics for research pharmacologists interested in generating inhibitors and drugs directed against the complex. The steps detailed in these events, especially in the thermodynamic context, can be objectively addressed to virtually and actually screen for inhibitors as has been done for TG2, FXIII's homologue [55].

4.4. Is Complex Interface a Potential Underlying Driver of Unexplained Heterozygous FXIII Mutations Observed in Mild FXIII Deficiency?

The catalytic FXIII-A subunit bears a special place in the transglutaminase (TGase) family as it is the only member that exists in a complexed form (FXIII-A₂B₂). Consequently, interfacial residues within the complex are under selective pressure, wherein mutations at these residues might be associated with a broad range of factor deficit (mild to severe FXIII deficiency). Inspection of recently reported missense mutations of F13A1 genes (p.His342Tyr, p.Asp405His, p.Gly411Cys, p.Gln416Arg, p.Leu539Pro, p.Arg540Gln, p.Gln601Lys, and p.Arg611His) [56–59] suggests these mutations lie on the interface rim [60] where they may be involved in FXIII-A and FXIII-B subunit interactions. Similarly, FXIII-B missense mutations (p.Cys336Phe, p.Val401Glu, p.Pro428Ser, and p.Cys430Phe) [61,62], also map to interfacial patches. Notably, a majority of these mutations were reported in the heterozygous state from mild FXIII deficiency patients. Since inherited FXIII deficiency is an autosomal recessive

disorder, the dominant negative effect of heterozygous FXIII gene mutations might be explained by their pathomolecular influence on the complex interface.

5. Conclusions

To summarize, our study presents not only a new view of the FXIII complex, but also proposes new mechanisms to explain FXIII complex association and disassembly. The structure provides a basis on which FXIII mutations (particularly those thought to affect the FXIII molecular interface) can be probed to define their pathomolecular mechanisms. Furthermore, our model provides the first atomic basis on which putative inhibitors can be designed and tested. Our models present interesting starting points for research into conformational changes occurring during FXIII complex assembly and disassembly. Further biochemical validation of hypotheses stemming from these models is warranted. In addition, the AFM-based analysis only presents a partial surface view of the structure, and therefore we plan to further refine the structure by matching it to cryo-EM based images of the FXIII_A₂B₂ complex.

Supplementary Materials: The following are available online at <http://www.mdpi.com/2218-273X/9/12/765/s1>.

Author Contributions: A.B. conceived and designed the project; S.S. performed the protein expression, purification, and ITC; A.N. performed and analyzed XL-MS; S.S. and S.K. performed AFM; J.-L.P. performed AFM dock analyses; A.B. performed all the in-silico analyses; S.S. and A.B. analyzed the data and co-wrote the manuscript; A.S.W., D.L., and J.O. read and edited the manuscript. All authors critically reviewed the manuscript.

Funding: This research was funded by the CSL Behring, grant number- N-045.0180.

Conflicts of Interest: Authors declare no conflict of interest.

References

1. Katona, E.; Péntzes, K.; Csapó, A.; Fazakas, F.; Udvardy, M.L.; Bagoly, Z.; Orosz, Z.Z.; Muszbek, L. Interaction of factor XIII subunits. *Blood* **2014**, *123*, 1757–1763. [[CrossRef](#)] [[PubMed](#)]
2. Radek, J.T.; Jeong, J.M.; Wilson, J.; Lorand, L. Association of the A subunits of recombinant placental factor XIII with the native carrier B subunits from human plasma. *Biochemistry* **1993**, *32*, 3527–3534. [[CrossRef](#)] [[PubMed](#)]
3. Biswas, A.; Ivaskevicius, V.; Thomas, A.; Oldenburg, J. Coagulation factor XIII deficiency. Diagnosis, prevalence and management of inherited and acquired forms. *Hamostaseologie* **2014**, *34*, 160–166. [[CrossRef](#)] [[PubMed](#)]
4. Stieler, M.; Weber, J.; Hils, M.; Kolb, P.; Heine, A.; Büchold, C.; Pasternack, R.; Klebe, G. Structure of active coagulation factor XIII triggered by calcium binding: Basis for the design of next-generation anticoagulants. *Angew. Chem. Int. Ed. Engl.* **2013**, *52*, 11930–11934. [[CrossRef](#)]
5. Fox, B.A.; Yee, V.C.; Pedersen, L.C.; Le Trong, I.; Bishop, P.D.; Stenkamp, R.E.; Teller, D.C. Identification of the calcium binding site and a novel ytterbium site in blood coagulation factor XIII by x-ray crystallography. *J. Biol. Chem.* **1999**, *274*, 4917–4923. [[CrossRef](#)]
6. Souri, M.; Kaetsu, H.; Ichinose, A. Sushi domains in the B subunit of factor XIII responsible for oligomer assembly. *Biochemistry* **2008**, *47*, 8656–8664. [[CrossRef](#)]
7. Seelig, G.F.; Folk, J.E. Noncatalytic subunits of human blood plasma coagulation factor XIII. Preparation and partial characterization of modified forms. *J. Biol. Chem.* **1980**, *255*, 8881–8886.
8. Gupta, S.; Biswas, A.; Akhter, M.S.; Krettler, C.; Reinhart, C.; Dodt, J.; Reuter, A.; Philippou, H.; Ivaskevicius, V.; Oldenburg, J. Revisiting the mechanism of coagulation factor XIII activation and regulation from a structure/functional perspective. *Sci. Rep.* **2016**, *6*, 30105. [[CrossRef](#)]
9. Bullock, J.M.A.; Sen, N.; Thalassinou, K.; Topf, M. Modeling Protein Complexes Using Restraints from Crosslinking Mass Spectrometry. *Structure* **2018**, *26*, 1015–1024. [[CrossRef](#)]
10. Zheng, J.; Corzo, C.; Chang, M.R.; Shang, J.; Lam, V.Q.; Brust, R.; Blayo, A.-L.; Bruning, J.B.; Kamenecka, T.M.; Kojetin, D.J.; et al. Chemical Crosslinking Mass Spectrometry Reveals the Conformational Landscape of the Activation Helix of PPAR γ ; a Model for Ligand-Dependent Antagonism. *Structure* **2018**, *26*, 1431–1439.e6. [[CrossRef](#)]

11. Yang, L.; Yang, D.; de Graaf, C.; Moeller, A.; West, G.M.; Dharmarajan, V.; Wang, C.; Siu, F.Y.; Song, G.; Reedtz-Runge, S.; et al. Conformational states of the full-length glucagon receptor. *Nat. Commun.* **2015**, *6*, 7859. [[CrossRef](#)][[PubMed](#)]
12. Zhang, X.; Wang, X.; Zhang, Z.; Cai, G. Structure and Functional Interactions of INO80 Actin/Arp Module. *J. Mol. Cell Biol.* **2018**. [[CrossRef](#)] [[PubMed](#)]
13. Chaves, R.C.; Dahmane, S.; Odorico, M.; Nicolaes, G.A.F.; Pellequer, J.-L. Factor Va alternative conformation reconstruction using atomic force microscopy. *Thromb. Haemost.* **2014**, *112*, 1167–1173. [[CrossRef](#)] [[PubMed](#)]
14. Doerr, A. A home for integrative structural models. *Nat. Methods* **2018**, *15*, 409. [[CrossRef](#)]
15. Burley, S.K.; Kurisu, G.; Markley, J.L.; Nakamura, H.; Velankar, S.; Berman, H.M.; Sali, A.; Schwede, T.; Trehwella, J. PDB-Dev: A Prototype System for Depositing Integrative/Hybrid Structural Models. *Structure* **2017**, *25*, 1317–1318. [[CrossRef](#)]
16. Thomas, A.; Biswas, A.; Ivaskevicius, V.; Oldenburg, J. Structural and functional influences of coagulation factor XIII subunit B heterozygous missense mutants. *Mol. Genet. Genom. Med.* **2015**, *3*, 258–271. [[CrossRef](#)]
17. Kaniyappan, S.; Chandupatla, R.R.; Mandelkow, E. Purification and Characterization of Low-n Tau Oligomers. *Methods Mol. Biol.* **2018**, *1779*, 99–111. [[CrossRef](#)]
18. Xu, D.; Jaroszewski, L.; Li, Z.; Godzik, A. AIDA: Ab initio domain assembly server. *Nucleic Acids Res.* **2014**, *42*, W308–W313. [[CrossRef](#)]
19. Yang, J.; Yan, R.; Roy, A.; Xu, D.; Poisson, J.; Zhang, Y. The I-TASSER Suite: Protein structure and function prediction. *Nat. Methods* **2015**, *12*, 7–8. [[CrossRef](#)]
20. Pierce, B.; Tong, W.; Weng, Z. M-ZDOCK: A grid-based approach for Cn symmetric multimer docking. *Bioinformatics* **2005**, *21*, 1472–1478. [[CrossRef](#)]
21. van Zundert, G.C.P.; Rodrigues, J.P.G.L.M.; Trellet, M.; Schmitz, C.; Kastiris, P.L.; Karaca, E.; Melquiond, A.S.J.; van Dijk, M.; de Vries, S.J.; Bonvin, A.M.J.J. The HADDOCK2.2 Web Server: User-Friendly Integrative Modeling of Biomolecular Complexes. *J. Mol. Biol.* **2016**, *428*, 720–725. [[CrossRef](#)]
22. Mattson, G.; Conklin, E.; Desai, S.; Nielander, G.; Savage, M.D.; Morgensen, S. A practical approach to crosslinking. *Mol. Biol. Rep.* **1993**, *17*, 167–183. [[CrossRef](#)]
23. Bonvin, A.M.J.J.; Karaca, E.; Kastiris, P.L.; Rodrigues, J.P.G.L.M. Defining distance restraints in HADDOCK. *Nat. Protoc.* **2018**, *13*, 1503. [[CrossRef](#)]
24. de Vries, S.J.; van Dijk, M.; Bonvin, A.M.J.J. The HADDOCK web server for data-driven biomolecular docking. *Nat. Protoc.* **2010**, *5*, 883–897. [[CrossRef](#)]
25. Krieger, E.; Vriend, G. YASARA View – Molecular graphics for all devices – From smartphones to workstations. *Bioinformatics* **2014**, *30*, 2981–2982. [[CrossRef](#)]
26. Krieger, E.; Koraimann, G.; Vriend, G. Increasing the precision of comparative models with YASARA NOVA—a self-parameterizing force field. *Proteins* **2002**, *47*, 393–402. [[CrossRef](#)]
27. Pierce, B.G.; Wiehe, K.; Hwang, H.; Kim, B.-H.; Vreven, T.; Weng, Z. ZDOCK server: Interactive docking prediction of protein-protein complexes and symmetric multimers. *Bioinformatics* **2014**, *30*, 1771–1773. [[CrossRef](#)]
28. Franklin, J.; Koehl, P.; Doniach, S.; Delarue, M. MinActionPath: Maximum likelihood trajectory for large-scale structural transitions in a coarse-grained locally harmonic energy landscape. *Nucleic Acids Res.* **2007**, *35*, W477–W482. [[CrossRef](#)]
29. Chaves, R.C.; Teulon, J.-M.; Odorico, M.; Parot, P.; Chen, S.-W.W.; Pellequer, J.-L. Conformational dynamics of individual antibodies using computational docking and AFM. *J. Mol. Recognit.* **2013**, *26*, 596–604. [[CrossRef](#)]
30. Chaves, R.C.; Pellequer, J.-L. DockAFM: Benchmarking protein structures by docking under AFM topographs. *Bioinformatics* **2013**, *29*, 3230–3231. [[CrossRef](#)]
31. Anokhin, B.A.; Stribinskis, V.; Dean, W.L.; Maurer, M.C. Activation of factor XIII is accompanied by a change in oligomerization state. *FEBS J.* **2017**, *284*, 3849–3861. [[CrossRef](#)] [[PubMed](#)]
32. Godon, C.; Teulon, J.-M.; Odorico, M.; Basset, C.; Meillan, M.; Vellutini, L.; Chen, S.-W.W.; Pellequer, J.-L. Conditions to minimize soft single biomolecule deformation when imaging with atomic force microscopy. *J. Struct. Biol.* **2017**, *197*, 322–329. [[CrossRef](#)] [[PubMed](#)]
33. Souiri, M.; Osaki, T.; Ichinose, A. The Non-catalytic B Subunit of Coagulation Factor XIII Accelerates Fibrin Cross-linking. *J. Biol. Chem.* **2015**, *290*, 12027–12039. [[CrossRef](#)] [[PubMed](#)]

34. Byrnes, J.R.; Wilson, C.; Boutelle, A.M.; Brandner, C.B.; Flick, M.J.; Philippou, H.; Wolberg, A.S. The interaction between fibrinogen and zymogen FXIII-A2B2 is mediated by fibrinogen residues gamma390-396 and the FXIII-B subunits. *Blood* **2016**, *128*, 1969–1978. [[CrossRef](#)]
35. Kohler, H.P. Interaction between FXIII and fibrinogen. *Blood* **2013**, *121*, 1931–1932. [[CrossRef](#)] [[PubMed](#)]
36. Smith, K.A.; Pease, R.J.; Avery, C.A.; Brown, J.M.; Adamson, P.J.; Cooke, E.J.; Neergaard-Petersen, S.; Cordell, P.A.; Ariens, R.A.S.; Fishwick, C.W.G.; et al. The activation peptide cleft exposed by thrombin cleavage of FXIII-A(2) contains a recognition site for the fibrinogen alpha chain. *Blood* **2013**, *121*, 2117–2126. [[CrossRef](#)]
37. Wolberg, A.S. Fibrinogen and factor XIII: Newly recognized roles in venous thrombus formation and composition. *Curr. Opin. Hematol.* **2018**, *25*, 358–364. [[CrossRef](#)]
38. Xue, L.C.; Rodrigues, J.P.; Kastritis, P.L.; Bonvin, A.M.; Vangone, A. PRODIGY: A web server for predicting the binding affinity of protein-protein complexes. *Bioinformatics* **2016**, *32*, 3676–3678. [[CrossRef](#)]
39. Hitomi, K.; Kojima, S.; Fesus, L.; Máté, À. Demény, Ilma Korponay-Szabo, and Laszlo Fésüs. In *Chapter 1; Structure of Transglutaminases: Unique Features Serve Diverse Functions*; Hitomi, K., Kojima, S., Fesus, L., Eds.; Springer: Tokyo, Japan, 2015. [[CrossRef](#)]
40. Kristiansen, G.K.; Andersen, M.D. Reversible activation of cellular factor XIII by calcium. *J. Biol. Chem.* **2011**, *286*, 9833–9839. [[CrossRef](#)]
41. Ambrus, A.; Bányai, I.; Weiss, M.S.; Hilgenfeld, R.; Keresztesy, Z.; Muszbek, L.; Fésüs, L. Calcium binding of transglutaminases: A ⁴³Ca NMR study combined with surface polarity analysis. *J. Biomol. Struct. Dyn.* **2001**, *19*, 59–74. [[CrossRef](#)]
42. Dragan, A.I.; Read, C.M.; Crane-Robinson, C. Enthalpy-entropy compensation: The role of solvation. *Eur. Biophys. J.* **2017**, *46*, 301–308. [[CrossRef](#)] [[PubMed](#)]
43. Olsson, T.S.G.; Ladbury, J.E.; Pitt, W.R.; Williams, M.A. Extent of enthalpy-entropy compensation in protein-ligand interactions. *Protein Sci.* **2011**, *20*, 1607–1618. [[CrossRef](#)] [[PubMed](#)]
44. Benfield, A.P.; Teresk, M.G.; Plake, H.R.; DeLorbe, J.E.; Millsbaugh, L.E.; Martin, S.F. Ligand Preorganization May Be Accompanied by Entropic Penalties in Protein-Ligand Interactions. *Angew. Chem. Int. Ed.* **2006**, *45*, 6830–6835. [[CrossRef](#)] [[PubMed](#)]
45. Al-Horani, R.A.; Karuturi, R.; Lee, M.; Afosah, D.K.; Desai, U.R. Allosteric Inhibition of Factor XIIIa. Non-Saccharide Glycosaminoglycan Mimetics, but Not Glycosaminoglycans, Exhibit Promising Inhibition Profile. *PLoS ONE* **2016**, *11*, e0160189. [[CrossRef](#)]
46. Avery, C.A.; Pease, R.J.; Smith, K.; Boothby, M.; Buckley, H.M.; Grant, P.J.; Fishwick, C.W.G. (±) cis-Bisamido epoxides: A novel series of potent FXIII-A inhibitors. *Eur. J. Med. Chem.* **2015**, *98*, 49–53. [[CrossRef](#)]
47. Badarau, E.; Collighan, R.J.; Griffin, M. Recent advances in the development of tissue transglutaminase (TG2) inhibitors. *Amino Acids* **2013**, *44*, 119–127. [[CrossRef](#)]
48. Novakovic, J.; Wodzinska, J.; Tesoro, A.; Thiessen, J.J.; Spino, M. Pharmacokinetic studies of a novel 1,2,4-thiadiazole derivative, inhibitor of Factor XIIIa, in the rabbit by a validated HPLC method. *J. Pharm. Biomed. Anal.* **2005**, *38*, 293–297. [[CrossRef](#)]
49. Protopopova, A.D.; Ramirez, A.; Klinov, D.V.; Litvinov, R.I.; Weisel, J.W. Factor XIII topology: Organization of B subunits and changes with activation studied with single-molecule atomic force microscopy. *J. Thromb. Haemost.* **2019**, *17*, 737–748. [[CrossRef](#)]
50. Chang, C.-E.A.; McLaughlin, W.A.; Baron, R.; Wang, W.; McCammon, J.A. Entropic contributions and the influence of the hydrophobic environment in promiscuous protein-protein association. *Proc. Natl. Acad. Sci. USA* **2008**, *105*, 7456–7461. [[CrossRef](#)]
51. Kurochkin, I.V.; Procyk, R.; Bishop, P.D.; Yee, V.C.; Teller, D.C.; Ingham, K.C.; Medved, L.V. Domain structure, stability and domain-domain interactions in recombinant factor XIII. *J. Mol. Biol.* **1995**, *248*, 414–430. [[CrossRef](#)]
52. Kanchan, K.; Ergülen, E.; Király, R.; Simon-Vecsei, Z.; Fuxreiter, M.; Fésüs, L. Identification of a specific one amino acid change in recombinant human transglutaminase 2 that regulates its activity and calcium sensitivity. *Biochem. J.* **2013**, *455*, 261–272. [[CrossRef](#)]
53. Gopal, S.M.; Klumpers, F.; Herrmann, C.; Schäfer, L.V. Solvent effects on ligand binding to a serine protease. *Phys. Chem. Chem. Phys.* **2017**, *19*, 10753–10766. [[CrossRef](#)]
54. Ben-Amotz, D. Water-Mediated Hydrophobic Interactions. *Annu. Rev. Phys. Chem.* **2016**, *67*, 617–638. [[CrossRef](#)]

55. Song, M.; Hwang, H.; Im, C.Y.; Kim, S.-Y. Recent Progress in the Development of Transglutaminase 2 (TGase2) Inhibitors. *J. Med. Chem.* **2017**, *60*, 554–567. [[CrossRef](#)]
56. Ivaškevičius, V.; Biswas, A.; Garly, M.-L.; Oldenburg, J. Comparison of F13A1 gene mutations in 73 patients treated with recombinant FXIII-A2. *Haemophilia* **2017**, *23*, e194–e203. [[CrossRef](#)]
57. Thomas, A.; Biswas, A.; Dodt, J.; Philippou, H.; Hethershaw, E.; Ensikat, H.J.; Ivaskevicius, V.; Oldenburg, J. Coagulation Factor XIII A Subunit Missense Mutations Affect Structure and Function at the Various Steps of Factor XIII Action. *Hum. Mutat.* **2016**, *37*, 1030–1041. [[CrossRef](#)]
58. Biswas, A.; Ivaskevicius, V.; Thomas, A.; Varvenne, M.; Brand, B.; Rott, H.; Haussels, I.; Ruehl, H.; Scholz, U.; Klamroth, R.; et al. Eight novel F13A1 gene missense mutations in patients with mild FXIII deficiency: In silico analysis suggests changes in FXIII-A subunit structure/function. *Ann. Hematol.* **2014**, *93*, 1665–1676. [[CrossRef](#)]
59. Ivaskevicius, V.; Biswas, A.; Bevans, C.; Schroeder, V.; Kohler, H.P.; Rott, H.; Halimeh, S.; Petrides, P.E.; Lenk, H.; Krause, M.; et al. Identification of eight novel coagulation factor XIII subunit A mutations: Implied consequences for structure and function. *Haematologica* **2010**, *95*, 956–962. [[CrossRef](#)]
60. David, A.; Sternberg, M.J.E. The Contribution of Missense Mutations in Core and Rim Residues of Protein-Protein Interfaces to Human Disease. *J. Mol. Biol.* **2015**, *427*, 2886–2898. [[CrossRef](#)]
61. Ivaskevicius, V.; Biswas, A.; Loreth, R.; Schroeder, V.; Ohlenforst, S.; Rott, H.; Krause, M.; Kohler, H.-P.; Scharrer, I.; Oldenburg, J. Mutations affecting disulphide bonds contribute to a fairly common prevalence of F13B gene defects: Results of a genetic study in 14 families with factor XIII B deficiency. *Haemophilia* **2010**, *16*, 675–682. [[CrossRef](#)]
62. Hashiguchi, T.; Ichinose, A. Molecular and cellular basis of deficiency of the b subunit for factor XIII secondary to a Cys430-Phe mutation in the seventh Sushi domain. *J. Clin. Investig.* **1995**, *95*, 1002–1008. [[CrossRef](#)]



© 2019 by the authors. Licensee MDPI, Basel, Switzerland. This article is an open access article distributed under the terms and conditions of the Creative Commons Attribution (CC BY) license (<http://creativecommons.org/licenses/by/4.0/>).